Mesozoic to Early Tertiary tectonic- sedimentary evolution of the Northern Neotethys Ocean: evidence from the Beysehir-Hoyran-Hadim Nappes, Southern Turkey

Theo Andrew

Thesis submitted for the degree of Doctor of Philosophy

University of Edinburgh

2002

I declare that this thesis has been written by myself and is the result of my own research, except where contributions have been stated and duly acknowledged.

Theo Andrew

“The sun sets on the western mountain. The cliff thrusts forward, suspended in space.
See the ocean in its vastness and the sky in its immensity.”

From the T’ai Chi classics, unknown author.

Abstract

The Beysehir-Hoyran-Hadim Nappes crop out over 700km, from east to west in the Pisidian and Central Taurus Mountains of southern Turkey. During this study, field obsevations of lithological, structural and sedimentological features are combined with igneous geochemical data derived from samples collected to help redefine a series of tectono-stratigraphic units and also determine the origin of the Beysehir-Hoyran-Hadim Nappes.

Above a regionally autochthonous Tauride carbonate platform, the Beysehir-Hoyran Nappes begin with Ophiolitic Melange, consisting of blocks of neritic and pelagic limestone, basalt, serpentinite, radiolarian chert and, in places, amphibolite-grade metamorphic sole-type rocks, together set in a highly sheared siltstone and mudstone matrix. Locally, large slices of serpentinized harzburgite are incorporated in the melange. The peridotite sheets include lenses of chromitite and dunite and are cut by a series of dolerite dykes. The higher thrust sheets in the Hadim area begin with the Korualan Unit; a thrust sheet (ca. 400m thick) of mainly redeposited carbonates, quartzose sandstones and mudstones of Mid-Late Triassic age, interpreted as a proximal slope/base-of-slope succession. Regionally above is the Huglu-type Unit; a thrust sheet (ca. 1 km thick) of Mid-Late Triassic intermediate-acidic extrusives, volcaniclastics and minor pelagic carbonates, interpreted as a continental rift. Post-rift subsidence in this thrust sheet is recorded by thin (<100m thick) Upper Triassic-Upper Cretaceous pelagic carbonate and radiolarian chert, depositionally above. The uppermost thrust sheet, the Boyali Tepe-type Unit, comprises broken formation and melange, including Jurassic shallow-water carbonate, Ammonitico Rosso condensed pelagic limestone, radiolarian chert and Upper Cretaceous pelagic limestone, representing a Bahaman-type carbonate platform which subsided in Early Jurassic time. Anastomosing zones of tectonic-sedimentary melange separate these higher units.

The Beysehir-Hoyran Nappes document Triassic rifting and Jurassic-Cretaceous passive margin subsidence bordering the Northern Neotethyan Ocean. The Late Cretaceous harzburgitic ophiolite probably formed above a northerly dipping subduction zone within the Neotethyan ocean basin. Ophiolitic melange formed along the leading edge of the overiding plate. The ophiolite was emplaced southwards onto the northern margin of the Tauride platform in latest Cretaceous time, probably during collision of the passive margin with a trench. The nappe pile and underlying platform (Hadim Nappe) were thrust ca. 150km further south in Late Eocene time during regional continental collision and suture zone tightening.

Several alternative palaeo-tectonic models are considered and tested in the light of data presented from this study. Assuming ‘in-sequence’ thrusting, the Beysehir-Hoyran Nappes restore to a location north of a northerly Neotethyan spreading axis. More probably, they originated near the south margin of the northern Neotethys, but reached their position by ‘out-of-sequence thrusting’. Formation within a localised southerly strand of the northern Neotethys (Inner Tauride ocean) is more probable than within the main Neotethys further north. Wider implications for the Tethyan ocean as a whole and several other orogenic belts are also considered.

Acknowledgements

Over the last four years I have had the pleasure of meeting and working with a great deal of people who have made the process of producing this 'labour of love' a lot easier. Thankyou Alastair Robertson for all the considerable time and effort you have given over the course of this project. Your enthusiasm for all things (apart from a big e-mail folder!) is a joy to see and a source of inspiration.

I suppose the chain of events that brought me to Edinburgh started one day back in Leicester with an innocent suggestion from Allan Collins……

The Tethyan Research Group (past, present and future!) during my time here have been a constant source of inspiration, in particular the 1998-2002 vintage; Khalil Al-Riyami, Nikos Kourampas, Noah Jaffey, Matthew Clark, Mat Hard'n'fast, and Sam Rice.

Timur Üstaomer, Ulvican and family, Ali Ünlügenç, Ömer Faruk Çelik are all thanked for being more than just friendly faces in foreign places. The fieldwork in Turkey could not have been done without your help. Taniel Danelian generously helped out with all things radiolarian and Olivier Monod kindly provided hard to find literature which proved to be crucial in the end. Nik Glazebrook provided much needed expert fieldwork assistance during the second field season.

The PhD studentship was kindly sponsored by the Natural Environment Research Council, the Caledonian Brewery, and during the last few months the City of Edinburgh Council and the Diagenesis Research Group. The third and final field season was made possible only by the generosity of the University of Edinburgh who kindly supported fieldwork costs.

Technical assistance at Edinburgh University was expertly supplied by Geoff Angell, Dodie James, Shane Voss , Justin McNeil, Mike Hall and Yvonne Cooper.

Whilst demonstrating on numerous memorable fieldtrips (in particular Cyprus, Whitby & Inchnadamph) I have benefited from various words of wisdom; some related to this project, some about geoscience and some about life in general. In particular, ENKC, JRU, SLH, RAS, RSH and Peder Aspen all had sensible things to say. Also many thanks to John Dixon and Katy Hardacre for reading through early drafts of various chapters.

Big thanks to all the people who have brightened my days during my time in Edinburgh and who I am proud to call my friends. In no particular order; John Braisby, for sharing a big flat and many good times. May there be many more round the corner! Rich Hesketh, for not only being there at the end, but being a much needed source of distraction. Lets face it- slime volleyball IS much more fun than writing up. Matthew Clark, again, for being there from the start and sharing much of this amazing adventure with me. Colonel Mustard, for the rainy day rides home. Pete McFadzean, for keeping it westside baby. For real….Ruth Gilpin for all the black cab moments, "TAXI FOR GILPIN!". Emily Good, for amongst other things teaching me how to do crosswords during countless coffee breaks. Andrew Cavanagh, for showing me that there is another way. Gavin England, for his antipodean humour and 'thirst' for the good life. Ira Ojala for all the 'zoomhey'; whatever it means! Chris Byrne, for sharing a little flat and putting up with me during the last few months, and finally, Anna Hultman, for knowing how to make me smile :-)

The biggest thankyou is reserved for my family; June, Peter and big bruv Piers for their unconditional love and support.

Chapter 1

1. INTRODUCTION

1.1 Rationale

During the last few decades much work has been carried out in the Eastern Mediterranean region, notably in Greece, Turkey, Cyprus and Syria. These regions display exceptional preservation of units documenting a variety of processes, including rifting, sea floor spreading, subduction and collision, which makes this region critical to advance detailed understanding of plate tectonic processes. Previous work has mainly focused on the south-Tethyan regions (e.g. Antalya Complex; Waldron, 1984; Mamonia Complex, Swarbrick, 1980). Only recently has attention turned towards the northern Tethyan ocean basins and margins (e.g. Lycian Nappes, Collins & Robertson, 1999; Ulukisla Basin, Clark, 2002). Northern Neotethys was probably the main strand of the Tethyan Ocean during the Mesozoic (Sengör & Yilmaz l981; Robertson & Dixon, 1984); thus, its southern margin is a critical part of the Tethyan system.

Many emplaced continental margins are structurally complex and have experienced multiple deformation events. Attempts to restore such margins depend critically on whether in-sequence ('piggy-back') thrusting can be assumed. For example, in Tethyan regions, most reconstructions have assumed in-sequence thrusting (e.g. Othris, Greece; Smith *et al*. l979; Pindos, Greece; Fleury l980, Degnan & Robertson l998, Antalya, SW Turkey; Robertson l993). However, out-of-sequence thrusting has been shown to play a role in some emplaced continental margins (e.g. Oman; Searle *et al*. l990). Here, the example of the regionally extensive Mesozoic Beysehir-Hoyran Nappes within the central Taurus Mountains, S Turkey (Figs. 1.1 and 1.2) is considered. This thesis reconstructs their tectonic evolution and palaeogeography based on new sedimentological, structural and igneous geochemical data, combined with integration of existing tectono-stratigraphical information. Alternative in-sequence versus out-of-sequence thrust reconstructions are considered with implications for comparable emplaced continental margins elsewhere.

1.2 Regional and tectonic setting

The Beysehir-Hoyran-Hadim (B-H-H) Nappes are a regional-scale unit within the Central and Pisidian Taurus Mountains of southern Turkey, and crop out for over 700km laterally, from the Eastern Mediterranean coast near Silifke to Dinar in the northwest (Figs. 1.1 and 1.2). The nappes derive their name from important geographical features; i.e. Lake Beysehir in the centre of the region, Lake Hoyran in the west and the town of Hadim in the east.

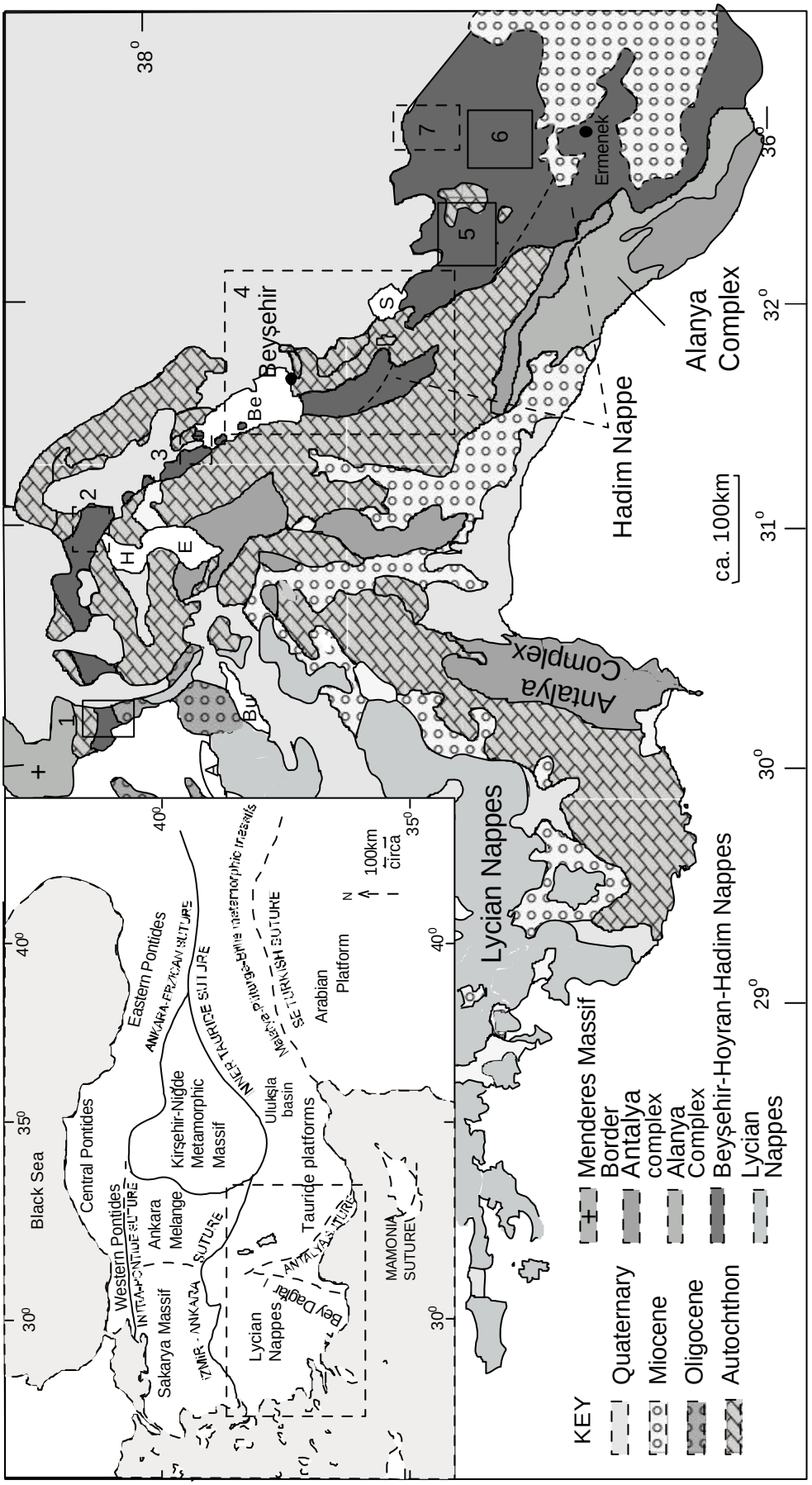

Fig. 1.1 Map showing the main tectonostratigraphic sub-divisions of southwest Turkey. Modified from Gutnic *et al* (1979). Inset is a tectonic map showing the main suture zones and tectonic units of Turkey. Also shown is the position of the main field areas; 1,Dinar; 2, Kumdanli; 3, Sarkikaraagaç; 4, Beysehir; 5, Hadim; 6, Ermenek; 7, Karaman. Lakes are shown as; A, Açi; Be, Beysehir; Bu, Burdur; E, Egirdir; H, Hoyran; S, Suglu.

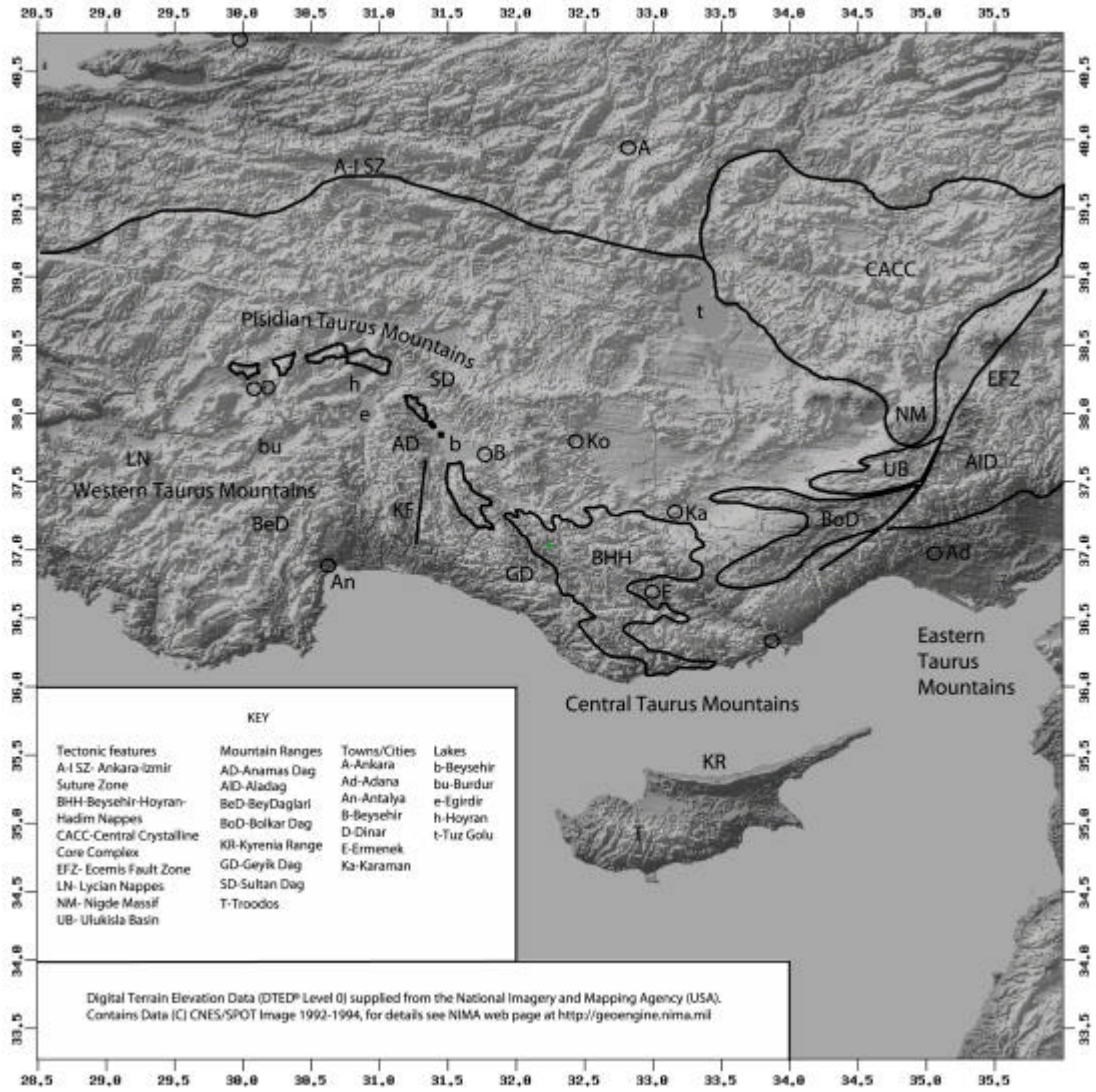

Fig. 1.2 Digital Terrain Elevation Model of southern Turkey and Cyprus, with overlain interpretations of main tectonic and geographic features relevant to this study. Digital Terrain Elevation Data (DTED®) Level 0 from the National Imagery and Mapping Agency (NIMA). Elevation post spacing is 30 arc second (nominally one kilometre).

The Hadim Nappe lies beneath the Beysehir ophiolites and consists of Late Palaeozoic-Mesozoic carbonate platform and marginal units. The Beysehir-Hoyran Nappes include Mesozoic carbonate platform, deep-sea and ophiolitic units and, together with the Hadim Nappe, were seen as part of a vast unit (Bozkir Nappes; Özgül & Arpat 1973), including the Lycian Nappes to the west, that were thrust from a northerly Tethyan ocean basin onto the Anatolide/Tauride carbonate platform to the south in latest Cretaceous time (Şengör & Yilmaz 1981, Tekeli 1981; Robertson & Dixon 1984, Dercourt *et al*. 1986, 1992, Stampfli, 2000). An outline appreciation of the Mesozoic Tethyan tectonic evolution in the Eastern Mediterranean region is a prerequisite to understand the regional context of the B-H Nappes. The following introduces the reader to the regional tectonic setting.

1.2.1 Tethys ocean

The first mention of a Tethyan ocean dates back to the late 19th century, when Neumayr (1885) suggested an ancient equatorial seaway separated Eurasia and Gondwana taking account of Jurassic ammonite faunas. The ocean remained unnamed until Suess (1893) introduced the term Tethys, after the Greek Titan of the same name. In Greek mythology Tethys was the personification of the fertile ocean, who married her brother Oceanus and gave birth to the springs, lakes and rivers of the world. The idea of the Tethyan ocean was refined by Wegener (1924), Carey (1958) and Wilson (1963), who theorised that Tethys was initiated in the Late Palaeozoic as a westwards narrowing gulf of Pangea, now commonly known as Palaeotethys (Laubscher & Bernoulli, 1977; Hsü & Bernoulli, 1978; Stöcklin, 1974; Sengör, 1979). This ocean basin is believed to have closed in post-Triassic time (Smith, 1971; Dewey *et al.*, 1973) creating new oceanic basins to the south, collectively known as Neotethys (Laubscher & Bernoulli, 1977; Sengör, 1979). Continental blocks from this oceanic gulf form not only Turkey, but also constitute most of southern Europe, northern Africa, the Middle East and Asia (Fig. 1.3).

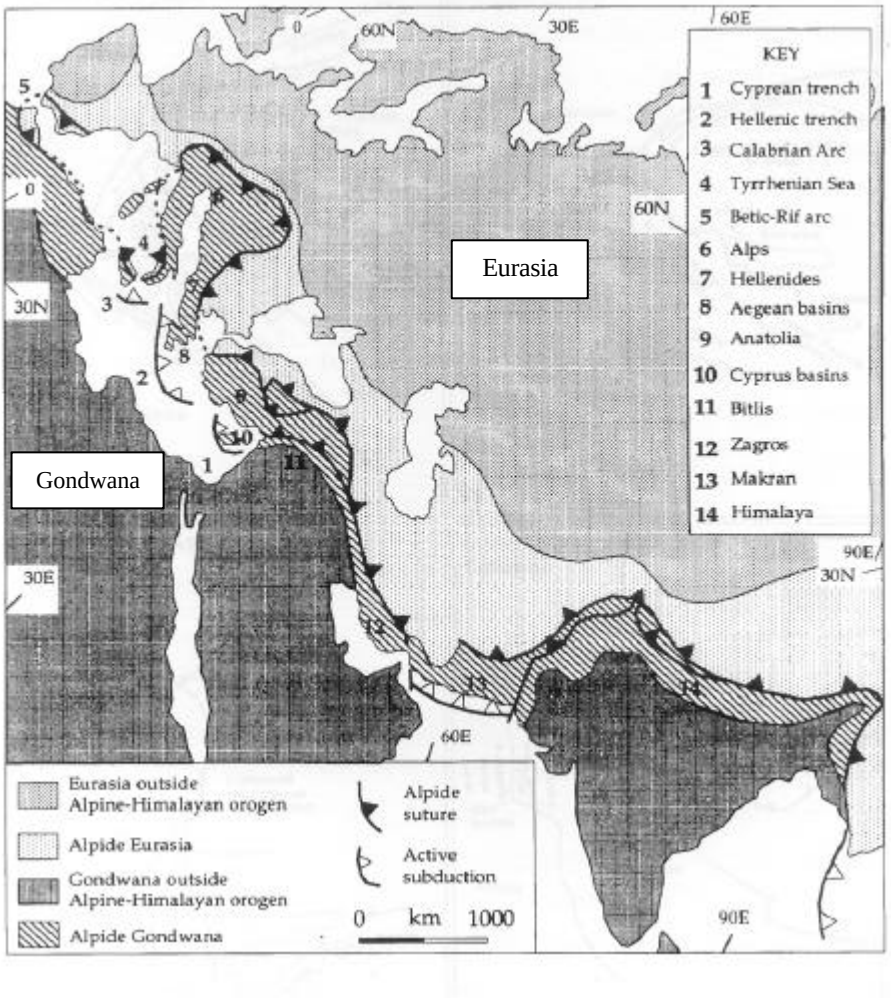

Fig. 1.3 Outline tectonic map of the Alpine-Himalayan orogenic belt (after Payne, 1989).

The only widely accepted distinction between the terms Palaeotethys and Neotethys is the presence of Palaeozoic versus Mesozoic oceanic crust (Robertson *et al*, 1996; and references therein). Uncertainty about the evolution of Palaeotethys and Neotethys in the eastern Mediterranean region has reflected in three main models being proposed for the formation of this part of the orogenic belt; namely, a single evolving Tethys model (Robertson & Dixon, 1984; Robertson *et al.,* 1991; Stampfli *et al.,* 1991); a single Mesozoic Tethys model (Dercourt *et al.,* 1986, 1993); and a southwards-subduction model (Sengör & Yilmaz, 1981; Sengör *et al.,* 1984). A general consensus has yet to be reached, and is unlikely to until much more regional work, such as this study, has been carried out.

1.2.2 Single evolving Tethys model (Robertson & Dixon, 1984; Robertson *et al.,* 1991; Stampfli *et al.,* 1991)

This model, as shown in Fig. 1.4, infers that a long-lived Tethyan ocean existed continuously from Late Palaeozoic time throughout the Mesozoic and into the Tertiary. The dominant influence affecting Tethys during this time was the episodic northwards subduction of oceanic crust beneath Eurasia and the associated northerly-drift of continental fragments rifted from Gondwana. During the Mesozoic, the south Tethyan area was marked by interconnected oceanic strands that were interspersed with microcontinents. Ophiolites formed during times of regional convergence mainly by spreading above subduction zones in both northerly and southerly oceanic basins. Emplacement of these ophiolites, which occurred in the Jurassic in Greece and during the Late Cretaceous in Cyprus and Turkish areas, is thought to be mainly related to the collision of crustal units with subduction trenches.

1.2.3 Single Mesozoic Tethys model (Dercourt *et al.,* 1986, 1993)

In this model (Fig. 1.5), a single oceanic basin existed throughout Triassic and Jurassic time situated to the north of Gondwanan-related units. Dominantly northwards-subduction is inferred, as for Model A. Spreading during the Cretaceous rifted the Gondwanan margin and formed a series of microcontinents within a small ocean basin. During regional plate divergence, Jurassic and Cretaceous ophiolites were formed at a single mid-ocean ridge within this northern basin. A single source for all the eastern Mediterranean ophiolites (e.g. the Ankara-Izmir and Vourinos suture zones) is derived from earlier reconstructions by Ricou *et al* (1979, 1984), with the inference that most ophiolites are far-travelled (e.g. the Antalya and Pindos ophiolites).

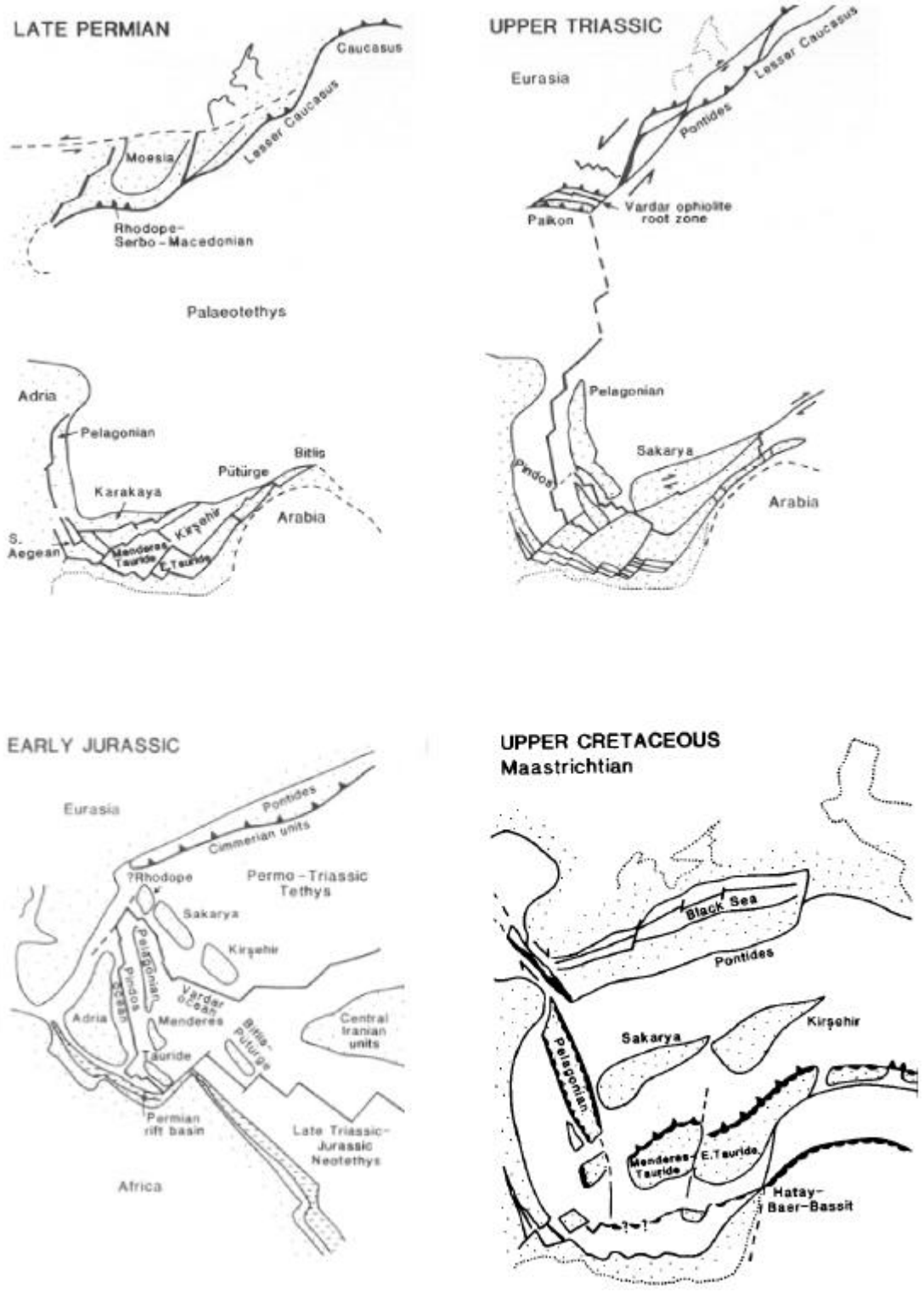

Fig. 1.4 Model A: Single evolving Tethys model (Robertson & Dixon, 1984; Robertson *et al.*, 1991)

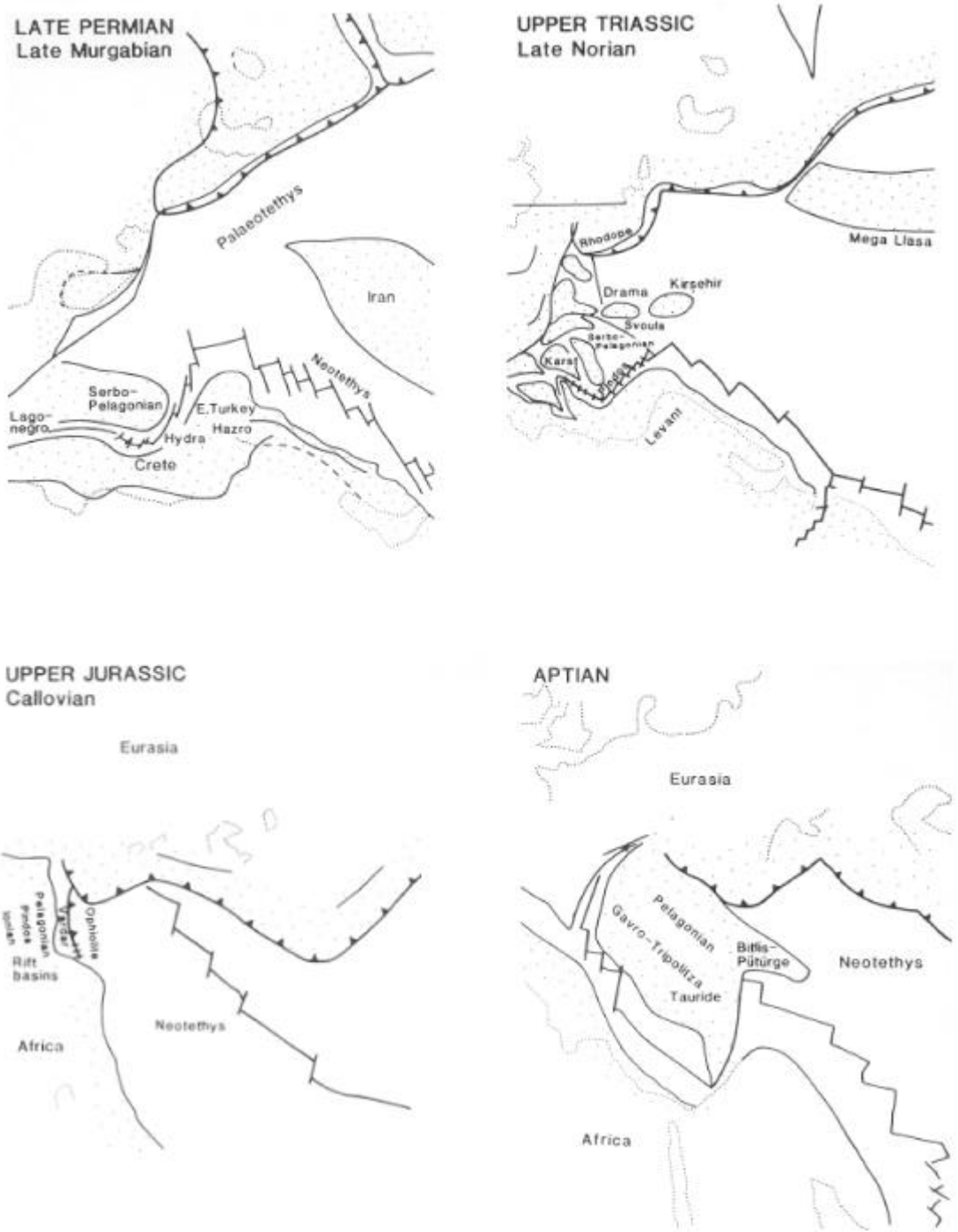

Fig. 1.5 Model B: Single Mesozoic Tethys model (Dercourt *et al.*, 1986, 1993)

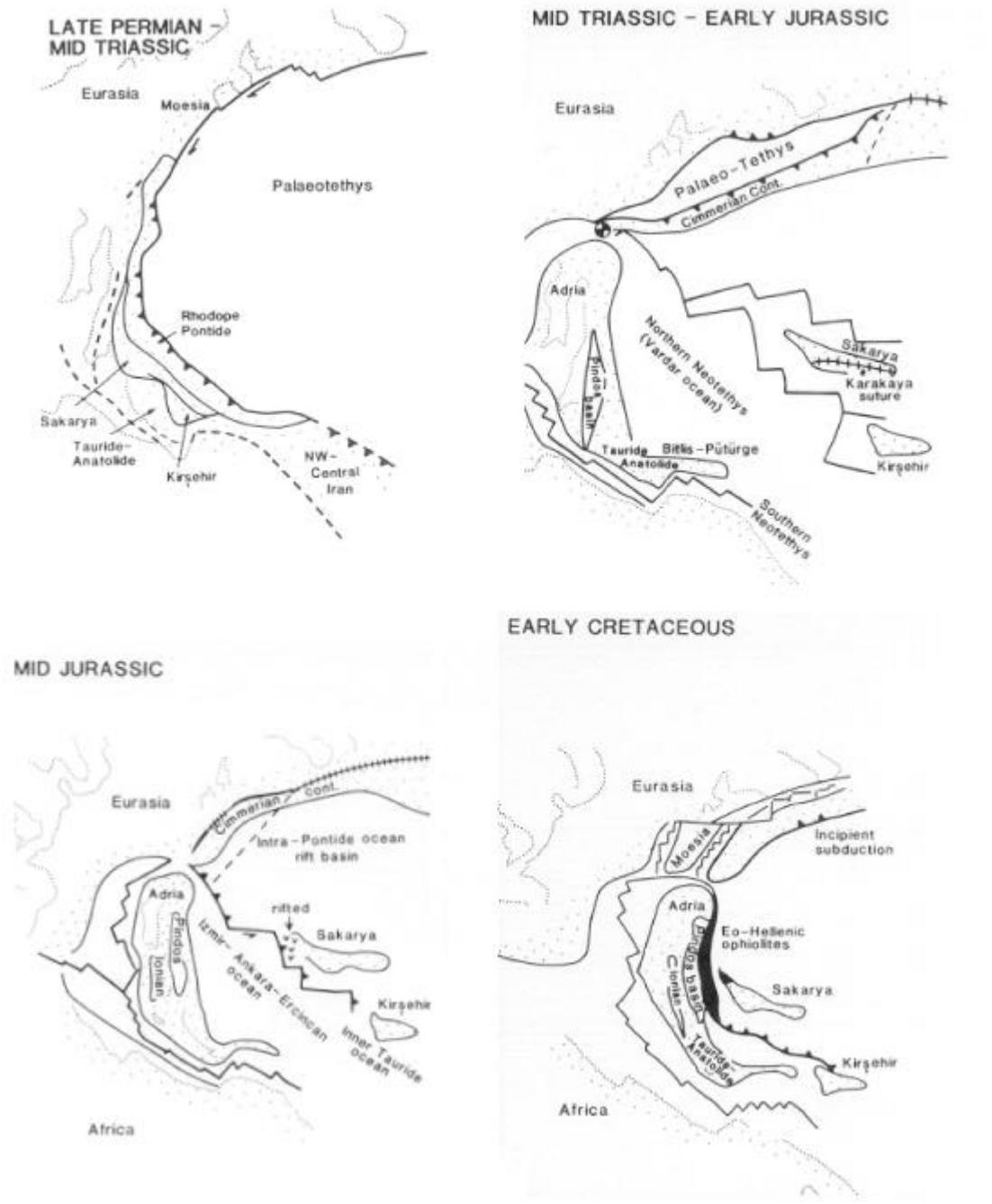

Fig. 1.6 Model C: Southwards-subduction model (Sengör & Yilmaz, 1981; Sengör *et al.*, 1984).

1.2.4 Southwards subduction model (Sengör & Yilmaz, 1981; Sengör *et al.,* 1984).

In this model, during Late Palaeozoic time the southern margin of Eurasia was passive with southwards-subduction being accommodated along the northern margin of Gondwana (Fig. 1.6). This closure of Palaeotethys initiated Triassic back-arc basin formation and rifting of the Gondwanan margin to form the Cimmerian microcontinent, which subsequently drifted northwards to collide with the passive Eurasian margin in Late Triassic time. To accommodate this, in the south new oceanic basins formed in back-arc settings (e.g. Karakaya and Neotethys). Late Cretaceous ophiolite obduction occurred in a number of oceanic basins that finally sutured during Tertiary time.

It is widely accepted that local problems exist with all three of these models. However, only Model A explains four key points that appear to be geologically well established: i.e. dominantly northward-subduction in the north; multiple ocean basins from Triassic onwards in the south; supra-subduction spreading of the major ophiolites; and emplacement from both northerly and southerly Mesozoic ocean basins (Robertson, *et al*., 1996). The validity of each of the regional models is not assumed in advance and are subsequently tested in the light of data presented in this thesis (Section 8.2).

This thesis is concerned with the evolution of the northern Tauride margin and associated Neotethyan ocean to the south of the Sakarya continent and Kirsehir block (Figs. 1.2 and 1.4), the eastern part of which is also known as the Inner Tauride Ocean (Oktay, 1973; Görür *et al*., 1984). The northern Menderes-Tauride passive margin and oceanic units to the west of this area are preserved as the allochthonous Lycian Nappes, which were thrust from the Izmir-Ankara suture zone onto the Menderes-Tauride microcontinent during final closure in the Early Tertiary (Collins, 1997; Collins & Robertson, 1998). The area to the east of the Beysehir-Hoyran ocean basin was subducted without trace during this episode; however, the preserved Lower Tertiary Ulukisla Basin records the final evolution of the Neotethys (Inner Tauride Ocean) in this region (Clark, 2002, Clark & Robertson, in press). The southern margin of the Tauride microcontinent is now preserved as imbricate thrust units within the Antalya and Alanya Complexes of southern Turkey (Robertson & Woodcock, 1982), and the Mamonia Complex of Cyprus (Swarbrick, 1980).

1.3 Project methods

This is a fieldwork-based project, including five months of field studies spread over three field seasons in the Central Taurus mountains of Turkey. Fieldwork techniques included measuring of sedimentary logs, gathering of structural and sedimentological data, sample collection, field descriptions of key features and detailed mapping, where applicable. Good quality geological maps exist for certain areas meaning large-scale remapping was mostly not required, however, each map had to be field checked during reconnaissance.

Since their discovery by Blumenthal (1947, 1951, 1956, 1960/63), the regional tectono-stratigraphy of the Beysehir-Hoyran Nappes was established by Monod (l977) and by Özgül (l976, l997). In addition, various parts of the Beysehir-Hoyran Nappes and related relatively autochthonous units were studied by a number of workers, including Haude (1969), Koçyigit (l976), Gutnic (l977), Gutnic *et al*. (1968, 1979), Gökdeniz (l981) and Demirkol (l984). More recently part of the area was re-mapped by the Turkish geological survey, i.e. Maden Tetkik ve Arama (MTA 1997, Senel *et al*. 1998). However, this mainly local work resulted in a general lack of consistency between areas as local names were often used in the stratigraphic nomenclature. Consequently, the B-H-H Nappes as a whole were generally poorly understood and not properly integrated into Tethyan-wide tectonic synthesis. During the course of this project, along-strike variation versus similarity were investigated and documented, following careful fieldwork area selection. Ideally, to achieve these aims a multitude of detailed tectonostratigraphic cross sections would be required; however, in view of the vast outcrop size of the nappes (Fig. 1.7), several key areas only could be investigated (Fig. 1.1); from west to east as follows: Dinar, Kumdanli, Sarkikaraagaç, Beysehir, Hadim, Ermenek and Karaman. The previous stratigraphic frameworks were tested and where possible utilised and incorporated into a new regional tectono-stratigraphy.

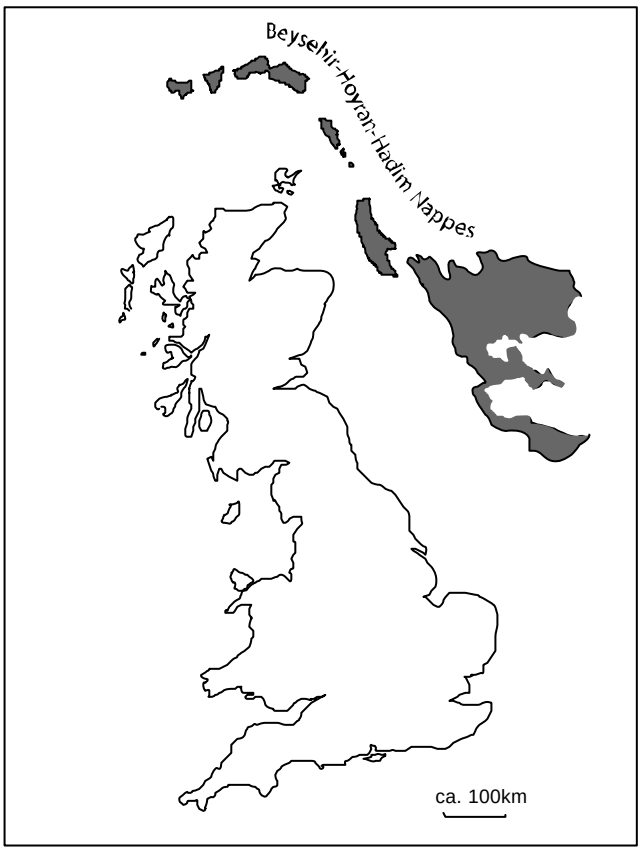

Fig. 1.7 Size comparison of the B-H-H Nappes with mainland Britain.

Samples collected in the field were studied using a variety of laboratory-based techniques. Field-based observations and sedimentary logs were backed up with detailed hand-specimen and thin section analysis, where appropriate, to provide relevant facies and environmental information. Furthermore, representative suites of volcanic and ophiolitic peridotite samples were analysed using whole rock x-ray fluorescence (XRF) to shed light on the geochemical nature and likely tectonic settings of genesis. The samples analysed come from basinal and ophiolitic units within the B-H Nappes. More detailed analysis of the peridotite samples was carried out using the University of Edinburgh electron microprobe to help infer the setting of ophiolite genesis. A study of radiolaria (siliceous microfauna) within selected key pelagic sequences was undertaken with the help of Dr. Taniel Danelian of the Laboratoire de Micropaléontologie, Université Pierre & Marie Curie (Paris VI), with the aim of tightening the stratigraphic control and documenting radiolarian fauna present.

1.4 Thesis organisation

In order to prove a regional coherency of the B-H-H Nappes it is vital to systematically discuss the tectono-stratigraphy from each area separately, even though this method introduces a lot of overlap. The chapters are individually as self-contained as possible, with each tectono-stratigraphy chapter introducing the previous work pertinent to this study, before giving a discussion of the regional lithological succession. New work undertaken by this study is clearly identified and integrated into a revised tectono-stratigraphic scheme presented in each chapter. Interpretation of each succession is not discussed in these chapters to cut down on repetition that could otherwise arise. After this introduction in **Chapter 1**, **Chapter 2** considers the type area near Lake Beysehir and allows the reader to familiarise with the tectono-stratigraphy of the B-H-H Nappes and autochthonous units as a whole. **Chapter 3** then documents the facies variants seen in the Pisidian Taurides in the northwest. **Chapters 4 and 5** document the along-strike continuation of the nappes in the Hadim area and in the Ermenek-Karaman area respectively. **Chapter 6** is a self-contained geochemistry chapter, presenting new data from this study. **Chapter 7** establishes that there is a regional tectono-stratigraphic coherency across the B-H-H Nappes as a whole and provides an interpretation of the likely tectonic settings for each allochthonous unit. This forms the basis of overall tectonic reconstructions and structural analysis presented in **Chapter 8**. Also, a number of alternative palaeotectonic models are proposed and tested in the light of data presented here. The thesis closes in **Chapter 9** with a brief summary of conclusions and a preferred model of tectonic evolution for the B-H Nappes. The methodology of radiolarian extraction used in this study, species identification, age determinations and selected plates illustrating the radiolarian fauna are presented in **Appendix 1**. XRF preparation techniques and data are shown in **Appendix 2**, whilst electron microprobe techniques and data are presented in **Appendix 3**. A published manuscript derived from work undertaken in this study is included in **Appendix 4** for the benefit of the reader who would like a concise discussion of the main themes involved in this thesis.

1.5 Pronunciation of the Turkish language

Within this thesis all localities, and therefore, tectono-stratigraphic units are referred to by their full Turkish names. The modern Turkish language uses a Latin-based alphabet with pronunciation similar to the English language. However, the pronunciation values of Turkish letters never change the way they frequently do in English: a letter or combination of letters always represents the same sound in Turkish. Some of these values are the same as they are in English but many are not and quite a few are misleading. Here are the main differences;

a/A: The "a" in "father".
ay/AY: The "y" n "sky"; the "igh" in "light"; the "uy" in "buy".
c/C: The "j" and "dg" in "judge".
ç/Ç: The "ch" in "church".
e/E: The "e" in "get".
ey/EY: The "a" in "plate"; the "ei" n "eight"; the "ay" in "say".
g/G: Always follows a vowel, which it lengthens. It is not otherwise pronounced.
i/I: The "u" in "minute
i/I: The "i" in "sit"
iy/IY: The "ee" in "tree"; the "ea" in "sea".
ö/Ö: Similar to the German pronunciation.
s/S: The "sh" in "shoe" and "cash".
ü/Ü: Similar to the German pronunciation

1.5.1 Place names

ak: white
bey :old arabic word for ‘sir’
bozkir: pale grey/steppe
bucak: corner or angle
çay: stream
dag/daglari: mountain/mountain range
dere: stream or valley
deniz: sea
dinar: ancient persian gold coin
dipsiz: bottomless
göl/gölü: lake
hadim: eunuch
kara: black or land
köy: village
kizil: red
kisla: barracks
sehir: town
sü: water
tepe: hill
ulu: great

1.6 A brief note on terminology

Throughout this thesis the terms 'melange' and 'broken formation' are often used. Many different authors have different criteria for the definition of the term melange, often with a specific implication for the formation process. To avoid any confusion arising from such differences, this thesis follows the definition of a melange as defined in Raymond (1984);

"…..a melange is here defined as a body of rock mappable at a scale of 1:24000 or smaller and characterised both by the lack of internal continuity of contacts or strata and by the inclusion of fragments and blocks of all sizes, both exotic and native, embedded in a fragmented matrix of finer-grained material".

This thesis also uses the definition of 'broken formation', thus;

"…..*formations broken by faults, but which retain substantial continuity of contacts and internal stratigraphic units, are called broken formation. No distinction is made between units deformed by gravity-induced fracturing and those with tectonically-induced features*."

Importantly, the criteria of matrix composition and fabric are not implicit in the definitions of the terms. Furthermore, as both sedimentary and tectonic processes may play a role in the melange/ broken formation genesis, no genetic significance is implied by the term (Raymond, 1984). However, during this thesis the term 'Ophiolitic Melange' is specifically used to describe a discrete tectonostratigraphic unit composed predominantly of melange containing ophiolitic lithologies; thus, the term Ophiolitic Melange' does not infer a specific lithology (e.g. serpentinite), but rather a number of related lithologies which together define a tectonostratigraphic unit.

The specific definition of a 'debris flow' varies significantly in the literature from:

" ….a flowing mixture of debris and water having sediment concentrations greater than 60% by volume or 80% by weight" (Vallance and Scott, 1997).

"…..debris flow motion is vitally influenced by both solid and fluid forces, thus, distinguishing debris flows from related phenomena such as rock avalanches and sediment-laden water floods" (Iverson *et al*., 1981).

For simplicity, the definition by Iverson *et al.* (1981) is preferred. The term 'debris flow' is used here to describe any extremely poorly sorted clastic lithology, with a moderate to high percentage of fine-grained matrix material (i.e. a matrix supported texture), that is inferred to have been deposited from a rich sediment laden source, without implying an initial sediment:water ratio.

Chapter 2

2. TECTONOSTRATIGRAPHY OF THE BEYSEHIR REGION

The aim of this chapter is to introduce the reader to the tectonostratigraphy of the Beysehir-Hoyran-Hadim (B-H-H) Nappes and the autochthon in the Beysehir region itself. The sedimentology, structure and tectonic interpretations will be dealt with in later chapters. Much of this chapter, specifically the parts concentrating on the Palaeozoic-Mesozoic succession of the Autochthon and the Hadim Nappe, is essentially a literature survey, which provides background to the original studies, emphasised in the text, carried out on the Early Tertiary autochthonous sequence and the B-H Nappes during this work.

2.1 Previous work

Geological work in this region is long established. The earliest reports date back to the 19^{th} century when W.J Hamilton mentioned Neogene sedimentary rocks that lie in the depression between Beysehir and Bozkir (Hamilton, 1836). Initial mapping and regional correlations were carried out by Blumenthal between 1941 and 1960. The most relevant work by Blumenthal to this study was a 1/200,000 scale summary map of the Beysehir-Seydisehir region (Blumenthal, 1947). Much of the focus of previous studies was on the autochthonous rocks and not the B-H-H Nappes themselves. Part of this interest relates to the occurrence of commercially viable bauxite in the carbonate platform close to the town of Seydisehir. The quantity of bauxite is estimated as c. $50x10^6$ tonnes (Wippern, 1962).

The most relevant work for this study was carried out by Olivier Monod in the Beysehir region; he carried out research for his Doctoral degree at the University Paris Sud d'Orsay (Monod, 1977). Monod mapped the Beysehir area, producing a colour map at 1:10,000 scale. His work involved litho-tectonic studies, and palaeontological dating of fossiliferous units. This study in the Beysehir region follows on from Monod's work, which first defined the tectonostratigraphical units, in order to place the B-H-H Nappes into a regional geological context. During the course of this study Monod's tectonostratigraphical scheme and geological map (Fig. 2.1) were field checked and revised where necessary.

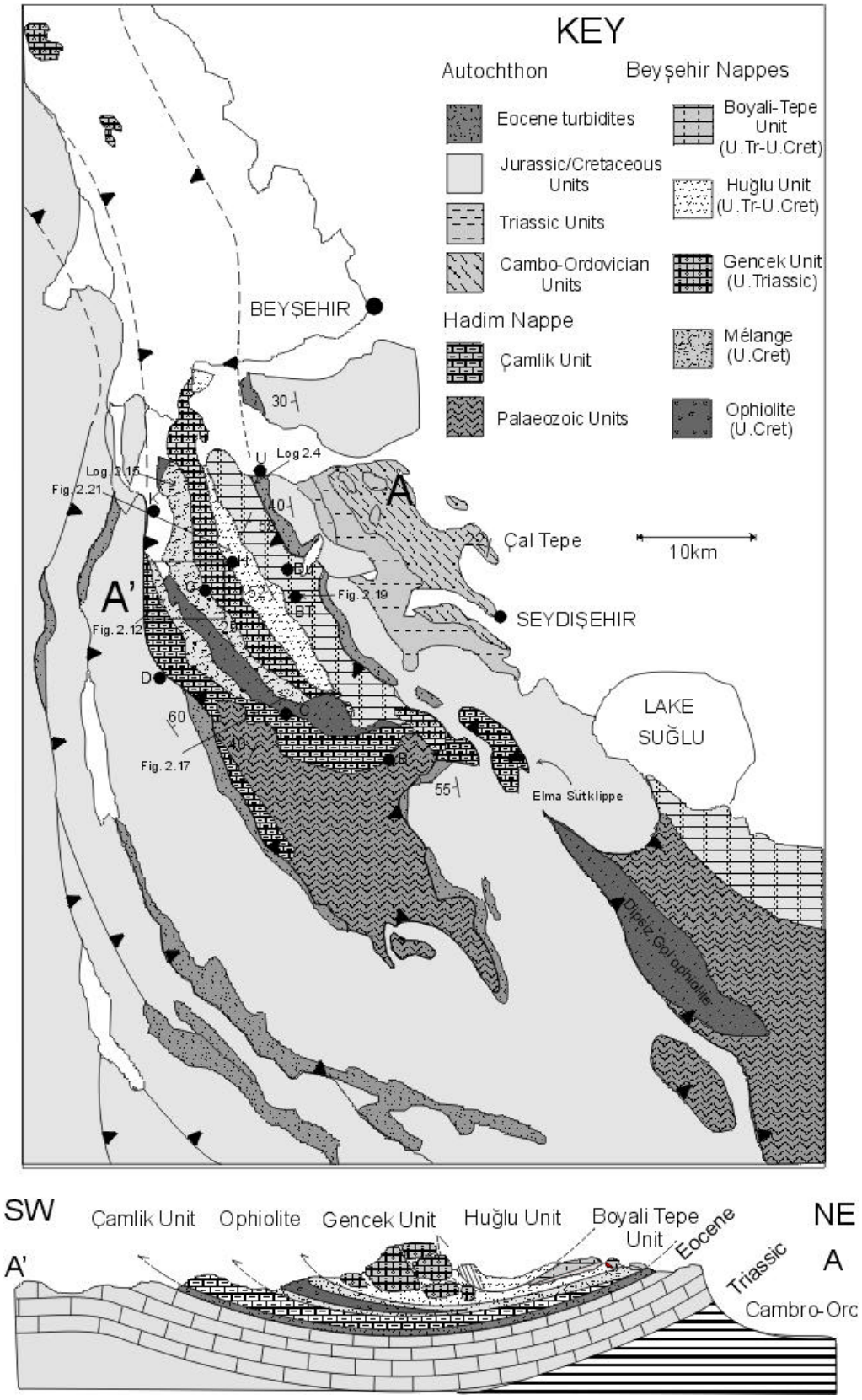

Fig 2.1 (previous page) Geological map and cross section of the Beysehir area (after Monod, 1977). For location see Fig. 1.1. Localities mentioned in text marked as follows; BT, Boyali Tepe; C, Çamlik; D, Derebucak; Du, Durak; G, Gencek; H, Huglu; K, Kayabasi; U, Üzümlü.

2.2 Introduction

The main outcrop of the B-H-H Nappes lies to the south of Lake Beysehir, from which the Nappes derived their name (Figure 2.1). In their type area the B-H-H Nappes consist of a series of NW-SE trending thrust sheets, predominantly carbonate sediments, volcanics and ophiolite-related lithologies which were thrust from the NE to the SW over regionally autochthonous carbonate platform basement, termed the Geyik Dag (Monod, 1977; Özgül, l976). The B-H-H thrust system in this area is represented by two main subdivisions, named the Hadim and Beysehir Nappes, respectively. Five thrust sheets are recognised; their age ranges are shown in Table 2.1.

The Hadim Nappe, which is the lowest and largest tectonic unit, consists of a complete stratigraphic succession from the Palaeozoic through the Mesozoic. Previously it has been considered þara-autochthonous'; i.e. relatively unmoved (Monod, 1977; Gutnic *et al*., 1979). However, it seems the amount of displacement has been underestimated, as discussed in Chapter 8, and this unit is here considered as fully allochthonous.

Overlying the Hadim Nappe is the Beysehir Nappe. This consists of four tectonostratigraphic units stacked with a synformal geometry (Figure 2.1). An extensive thrust sheet of serpentinised harzburgite and associated ophiolitic melange occupies the lowest structural position. This is overlain by carbonate-dominated thrust sheets, known as the Gencek and Boyali-Tepe units, which occur at a similar structural level on both limbs of the synform. The highest position in the stack is represented by the Huglu unit, which consists of volcanics, subordinate clastics and a pelagic carbonate cover.

	Unit Name	Age Range
Hadim Nappe	Bademli Unit	Devonian to L.Jurassic
	Camlik Unit	L.Jurassic to U.Cretaceous
Beysehir Nappe	Ophiolite + Melange	U.Cretaceous
	Gencek Unit	U.Triassic to U.Cretaceous
	Boyali-Tepe Unit	U.Triassic to U.Cretaceous
	Huglu Unit	M.Triassic to U.Cretaceous

Table 2.1 Age ranges of the B-H-H nappes in the Beysehir area.

2.3 Regional Autochthon (Geyik Dag Unit)

The allochthonous Neotethyan units of the B-H-H Nappes were emplaced over the less deformed Mesozoic carbonate platform units and their Pre-Cambrian-Palaeozoic basement, traditionally known

as the Geyik Dagi Unit. (Özgül & Arpat, 1973). In southern Turkey the autochthon consists of a collage of sutured platform units of various sizes. The main autochthonous units that are encountered in the Beysehir region are the Anamas Dag, the Akseki carbonate platform and the Sultan Dag (Fig. 2.1).

To the west of Lake Beysehir lies the Anamas Dag, which consists of Upper Triassic shallow marine sandstones, overlain by a thick sucession of Lower Jurassic to Upper Cretaceous carbonates, which comprise the highest peaks in this range. A small intra-platform basin separated the Anamas Dag carbonate platform from the more extensive Karacahisar platform to the south (Waldron, 1984; Robertson, 1993). The regional-scale Akseki carbonate platform extends many hundreds of kilometres to the east. To the north of Lake Beysehir the autochthon comprises the Sultan Dag Mountains, predominantly Precambrian-Palaeozoic basement. This autochthonous block extends to the south-east and outcrops in this study area between the towns of Beysehir and Seydisehir, as discussed below.

2.3.1 Autochthonous Palaeozoic basement.

The autochthonous Palaeozoic basement in the Beysehir-Seydisehir region is essentially the south-eastwards extension of the Sultan Dag from the more northerly Pisidian Taurus region. In this area it is represented by three main formations, as shown in Figure 2.2: the Lower Cambrian Çal Tepe Formation, the Mid-Cambrian Seydisehir Schists Formation and the Ordovician Sobova Formation (Dean & Monod, 1970; Monod, 1977).

2.3.1.1 Çal Tepe Formation (Lower-Mid Cambrian)

The type section of the Cambrian sequence in the Beysehir region crops out approximately 8 km north of Seydisehir. The formation draws its name from the NW-SE trending range of hills that rise above the plains which characterise the typical topography further north around Seydisehir. The formation can be split into three mappable units, as shown in Figure 2.3 (Dean & Monod, 1970; Monod, 1977). The basal 50m is represented by massive grey unstratified dolomite with little or no distinguishing features. Overlying this is the main carbonate succession which consists of black partly dolomitised limestone at the base, overlain by well-bedded mudstones and packstones. Rare echinoderm and trilobite fragments can be found along with sponge spicules and intraformational breccias. Up-section, the facies changes to a more well-bedded grainstone/packstone lithology with crinoid and trilobite fragments. Towards the top, silt horizons become more abundant before being overlain by 40m of red nodular limestone, similar in appearance to the Mesozoic 'Ammonitico Rosso' facies.

The base of this Formation is more or less unfossiliferous; however, above the dolomitic unit a fauna consisting of *Protolenidae* trilobite remains indicate an Early Cambrian age. The upper red nodular limestone has abundant trilobite remains which suggests a Mid-Cambrian age (Monod, 1977).

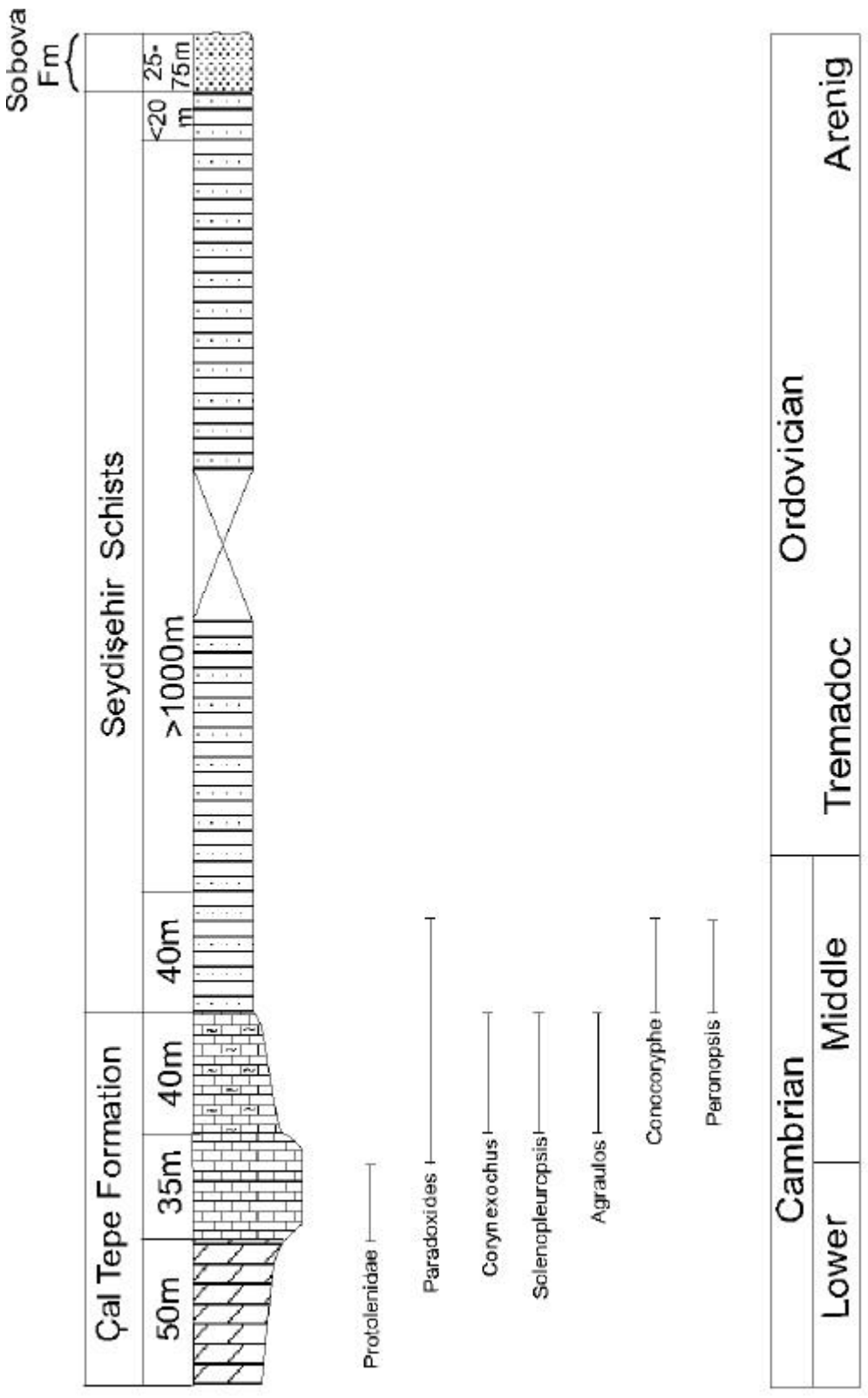

Fig.2.2 Lower Palaeozoic stratigraphy of the Beysehir Autochthon (Monod, 1977). Trilobite age ranges included for reference (Dean & Monod, 1970).

2.3.1.2 Seydisehir Formation (Mid Cambrian-Ordovician)

The outcrop of this formation forms the plain between Çal Tepe, near Seydisehir, and the foothills of the Taurus Mountains to the southwest. The total thickness is hard to determine because of its faulted nature. However, two excellent sections at the base and top of the formation allow three main subdivisions to be made, as shown in Figure 2.2 (Monod, 1977). The Seydisehir Formation overlies the Çal Tepe carbonates with a normal contact. The basal c.40m is characterised by grey micaceous mudstones, altered to a yellow colour, interbedded with rare calcareous beds which contain Mid-Cambrian *Paradoxoides.* trilobite fragments (Monod, 1977). This is overlain by well-bedded red/green silty mudstone with interbedded lenses of red nodular limestone similar in appearance to the upper part of the Çal Tepe Formation. Fauna, e.g. small inarticulated brachiopods, conodonts and trilobite fragments, extracted from these interbeds suggest a Lower Ordovician age (Monod, 1967).

The main body of the Seydisehir Formation consists of >1000m of interbedded fine-grained mudstones and sandy quartzites. Sedimentary features, such as flute casts, load casts and ripple marks can also be seen in places (Dean & Monod, 1970; Monod, 1977).

The top of the Formation is represented by approximately 20m of green mudstone interbedded with more sandy horizons and subordinate fossiliferous lenticles, containing a small fauna of brachiopods including *Alimbella* sp., *Hesperethis* sp. and *Scaphorthis* sp. (Monod, 1977). This formation is widespread throughout the whole Taurus range and south-eastern Turkey (Dean and Monod, 1990).

2.3.1.3 Sobova Formation (Late Arenig)

This unit describes the range of lithologies which overlies the Seydisehir shales but underlies the regional Mesozoic unconformity (Monod 1977). Its outcrop is restricted to a couple of localities; hence, for the purposes of this study it is of limited significance. An Upper Arenig age was previously assigned to this Formation from a trilobite fauna of *Agerina sp., Carolinites sp., Ilaenus sp., Niobe sp. and Symphysurus sp.* (Dean & Monod, 1970).

2.3.2 Autochthonous Mesozoic units

The transgressive Mesozoic sequence of the Geyik Dagi Unit unconformably overlies the Lower Palaeozoic basement and consists dominantly of platform-type carbonates, except Upper Triassic-Lower Jurassic clastics (Fig 2.3).

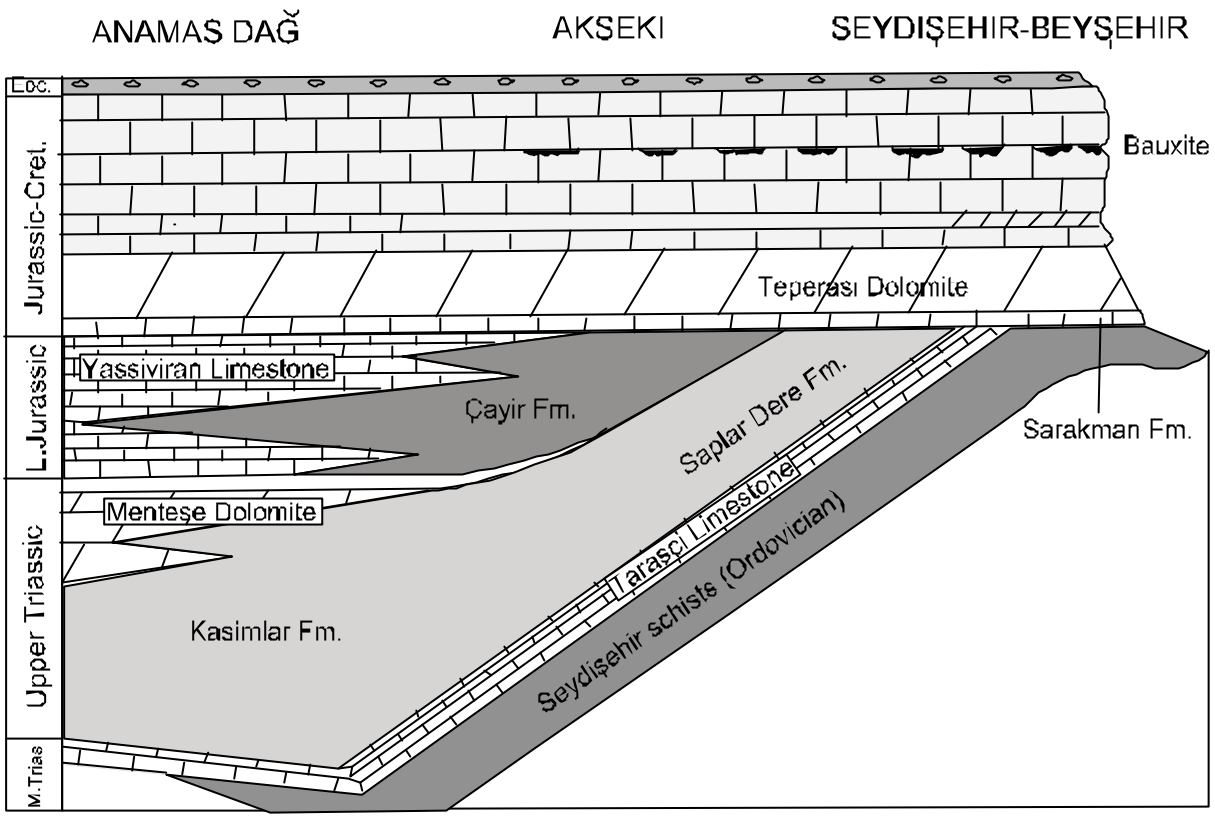

Fig.2.3 Rock relations diagram of the Mesozoic Autochthon in the Beysehir area (redrafted from Gutnic *et al*,1979).

2.3.2.1 Triassic

In the internal parts of the central Taurus mountains, the Mesozoic sequence of the Geyik Dag Unit begins with a thick Mid-Jurassic carbonate sequence (Özgül, 1976). Around Beysehir-Seydisehir this transgressive sequence starts with Anisian carbonates. These, in turn, are overlain by Carnian plant-bearing and turbiditic sandstones (Monod, 1977). Further west in the Anamas Dag these Upper Triassic sandstones become much thicker and show lateral and vertical transitions into Upper Triassic dolomites and reefal limestones (Gutnic *et al*, 1979; Waldron, 1984). The uppermost Triassic and Lower Jurassic is characterised by terrestrial red sandstones and conglomerates (Çayir Formation; Gutnic *et al*, 1979; Monod and Akay, 1984) in the Anamas Dag and Akseki platform.

2.3.2.2 Jurassic – Late Cretaceous

The Çayir Formation reaches 200m thick in the more western parts, but is not present towards the east in the Autochthon (e.g. Beysehir). A regional unconformity exists above the Triassic units. In the Beysehir-Seydisehir area the Lower Palaeozoic basement and transgressive Mid-Upper Triassic is overlain by Mid-Jurassic limestones (Monod, 1977). The remainder of the succession is dominated by

a thick (>1000m) carbonate succession extending through the Cretaceous to the Early Tertiary. This succession consists dominantly of grainstones and wackestones with little or no distinguishing fauna. A series of stratigraphic gaps and bauxite horizons are apparent in the latest Cretaceous succession in the Seydisehir area, suggesting a period of emergence of the autochthon (Monod, 1977; Özgül, 1984).

2.3.2.3 Late Cretaceous -Tertiary

The Upper Cretaceous (Maastrichtian) – Palaeocene succession consists predominantly of bioclastic packstones and grainstones interbedded with calcareous mudstones (Monod, 1977). The thickness of this interval varies from >80m just south of Lake Beysehir (Dikmen Tepe) to >20m in the vicinity of Tarasçi (15km further south). This unit is depositionally overlain by Lower-Mid Eocene Nummulitic limestone, which reaches up to 20m thick (Fig.2.5). These limestones are capped by a thin red hardground in the Üzümlü and Tarasçi areas (Monod, 1977).

The top of the carbonate succession is overlain by calcareous sandstone and siltstone turbidites of Upper Lutetian age (Mid Eocene), as determined from the benthic foraminifera *Asterocyclina stellatus* (Monod, 1977). As this Early Tertiary sequence could reveal details of the emplacement history of the B-H Nappes, this critical sequence was field checked and remeasured. Figure 2.4 shows a log through the Late Cretaceous-Early Tertiary Autochtonous sequence measured at the type locality 2km SSE of Üzümlü village. The Mid-Eocene clastic unit is well bedded on a cm-scale and displays sharp contacts with interbedded fissile mud beds (Fig.2.6). Groove casts are commonly seen on the underside of the more sandy members. The uppermost unit of the autochthon is a polygenetic debris flow, which varies in thickness from 150m (Tepearasi- Fig. 2.1) to >20m (south of Derebucak-Fig. 2.1). Clast size is extremely variable, from >1m to <1cm. Common clast lithologies include radiolarian chert, tuff, volcanic clasts and limestone.

This unit is well exposed in a number of localities, notably in the Derebucak and Üzümlü areas (Fig.2.1), but it has been subjected to extensive localised shearing, primarily due to the overthrusting of the B-H-H Nappes, which obscures much of the original sedimentary features. A more in depth discussion of the tectonic fabrics and kinematics is given in Section 8.1.2. However, where the local shear strain is low the original texture of the lithology can be determined. One such locality is found to the south of Derebucak village. Recent construction of a reservoir dam has excavated a large section through this unit. Large phacoids, up to 15m long and 5m thick, consisting of coarse-grained clastics are tectonically interleaved with lenses of finer grained sediments. Lithologically, the coarser sediment comprises clast-supported, limestone-dominated breccia, which is texturally very immature (see Fig.2.7). Clast size varies from >20cm to<1cm. The larger clasts appear to be dominated by more exotic lithologies, such as radiolarian chert and altered volcanics, similar to those encountered in the B-H-H Nappes situated directly above. The phacoids of finer grained sediment are composed of massive sandsone, which varies in grain size from coarse to fine. Diffuse stratification is defined by fining-upward sequences (Fig. 2.8). Clast composition of the sandstone is similar to the breccia, which suggests they were sourced from the same area.

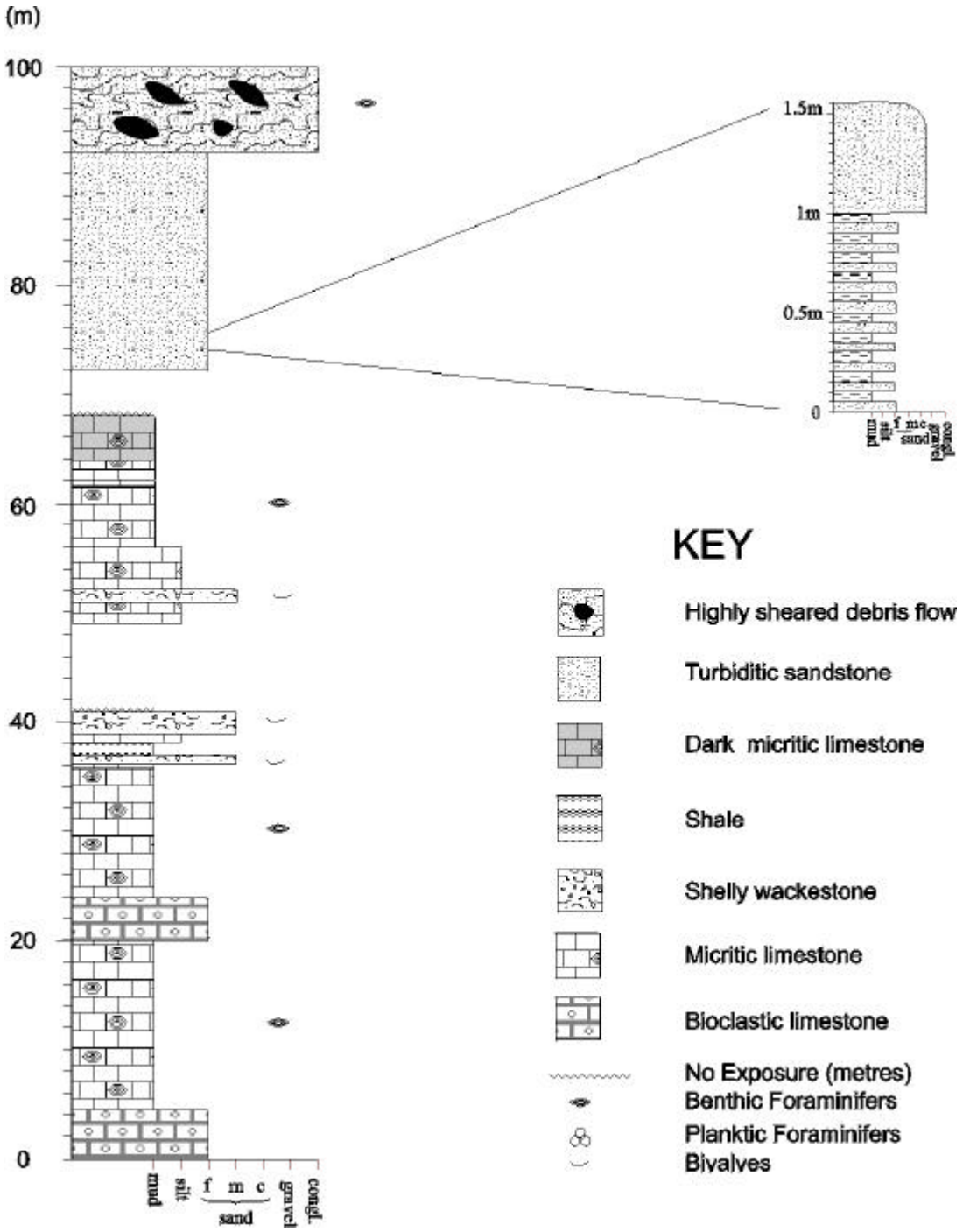

Fig.2.4 Log through the Late Cretaceous- Early Tertiary succession at the top of the Autochthonous carbonate platform (measured by the trackside 2km south-east of Üzümlü village, see Fig. 2.1).

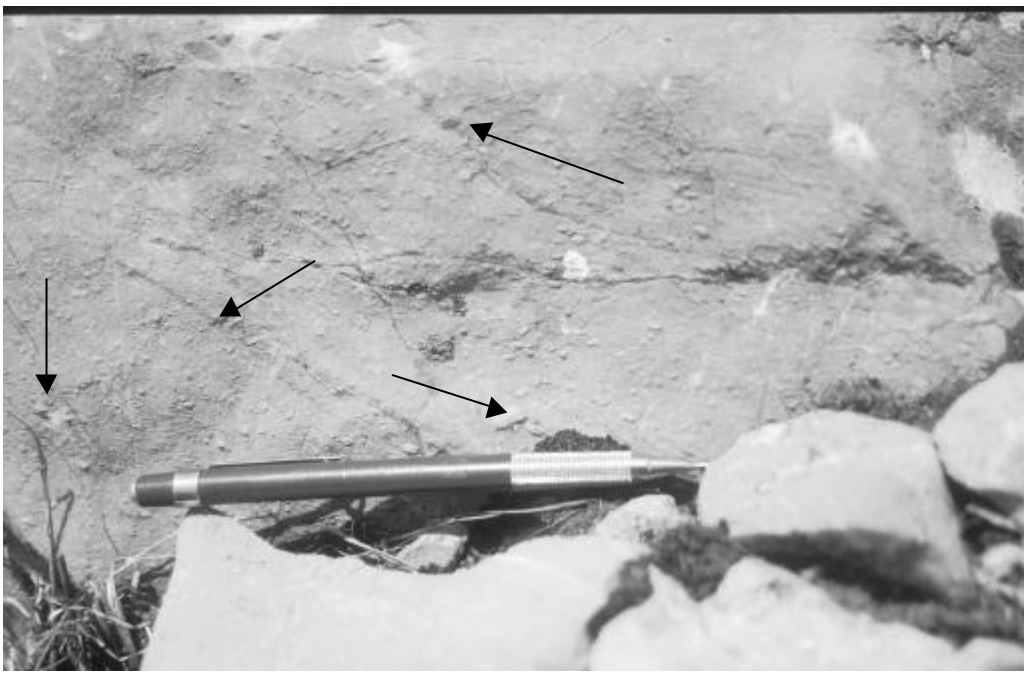

Fig. 2.5 Mid-Eocene Nummulitic limestone at the Üzümlü locality. Nummulites are highlighted by arrows.

Fig.2.6 Mid-Eocene turbidites at the Üzümlü locality. Hammer left of the middle is ca. 30cm long.

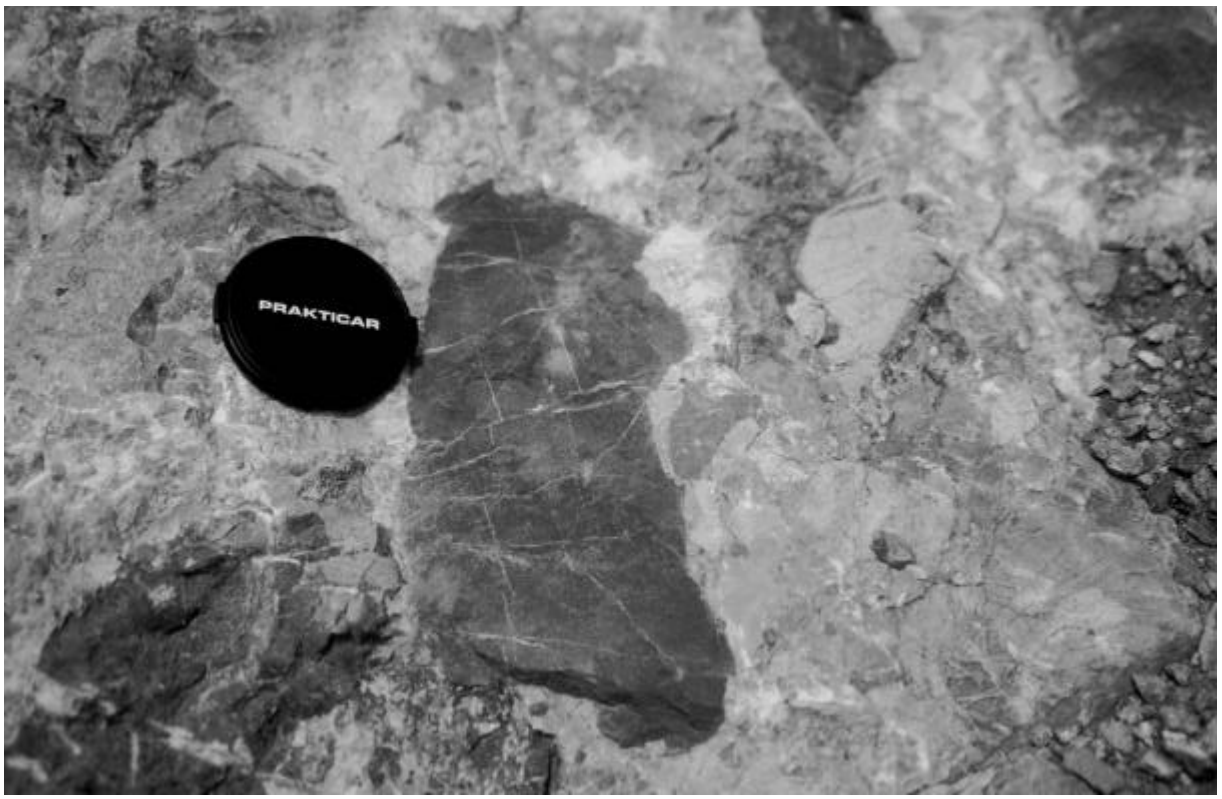

Fig. 2.7 Coarse polymict breccia at the top of the Autochthonous succession 3km to the southeast of Derebucak (see Fig.2.1 for location).

Fig. 2.8 Normal grading in finer-grained sediment 3km to the southeast of Derebucak (see Fig.2.1).

2.4 Allochthonous Hadim Nappe

The Hadim Nappe is the lowest structural unit of the B-H-H Nappes and is found exclusively in the south of the study area (Fig.2.1). It has a broad, synformal geometry (Fig.2.1), except in the southern regions of the allochthon where the thrust sheet forms a recumbent antiform overturned to the west. The basis of the classification of the Hadim Nappe, as used here, is the subdivision proposed by Monod (1977). The Hadim nappe can be divided into two units: the Devonian to Lower Jurassic Bademli unit and the Lower Jurassic to Upper Cretaceous Çamlik unit.

2.4.1 Palaeozoic Bademli unit

As described by Monod (1977), the Bademli unit of the Hadim Nappe consists of Devonian schists and quartzites, Carboniferous shales and carbonates, Permian limestone, Lower Triassic carbonates and Lower Jurassic siliciclastic sediments (Fig 2.9). The lowermost units of the Hadim Nappe have no formal name, but are identified by descriptive teminology in the literature.

2.4.1.1 Devonian schists and quartzites

The best described locality for the Palaeozoic Hadim Nappe units is in the area around Bademli (Fig.2.1). A succession of shales and quartzites, interbedded with lenses of black carbonate, crop out to the south of the village. The carbonate layers contain abundant coralline debris and brachiopods, including Mid-Upper Devonian age *Cyrtospirifer*, *Platyspirifer*, *Zdimir*, *Schizophoria* and *Reticularia*, and rare trilobite fragments of the Lower Devonian *Phacops* genera. A lower contact is not observed, but a minimum thickness of 100m is measured (Monod, 1977).

2.4.1.2 Carboniferous shales, carbonates and quartzites.

The underlying Devonian succession passes conformably into approximately 50m of shales and black sandstones, with rare interbeds of limestone containing brachiopods *Inlatia* and *Ovatia* of Early Carboniferous age. Overlying this is a 100m-thick well-bedded neritic carbonate succession, the base of which is sandy. Up-section the siliciclastic content decreases and the dominant lithology consists of calcarenite and carbonate grainstone. Interbeds of oosparite, sandy limestone and quartzite occur, which have yielded the benthic foraminifer *Archaediscidae* of Early Carboniferous age, at the very top of this succession. The Late Carboniferous is represented by massive granular dolomite, with thin intercalations of quartzite and limestone, overlain by pink nodular limestone rich in disarticulated brachiopods and algae (Monod, 1977).

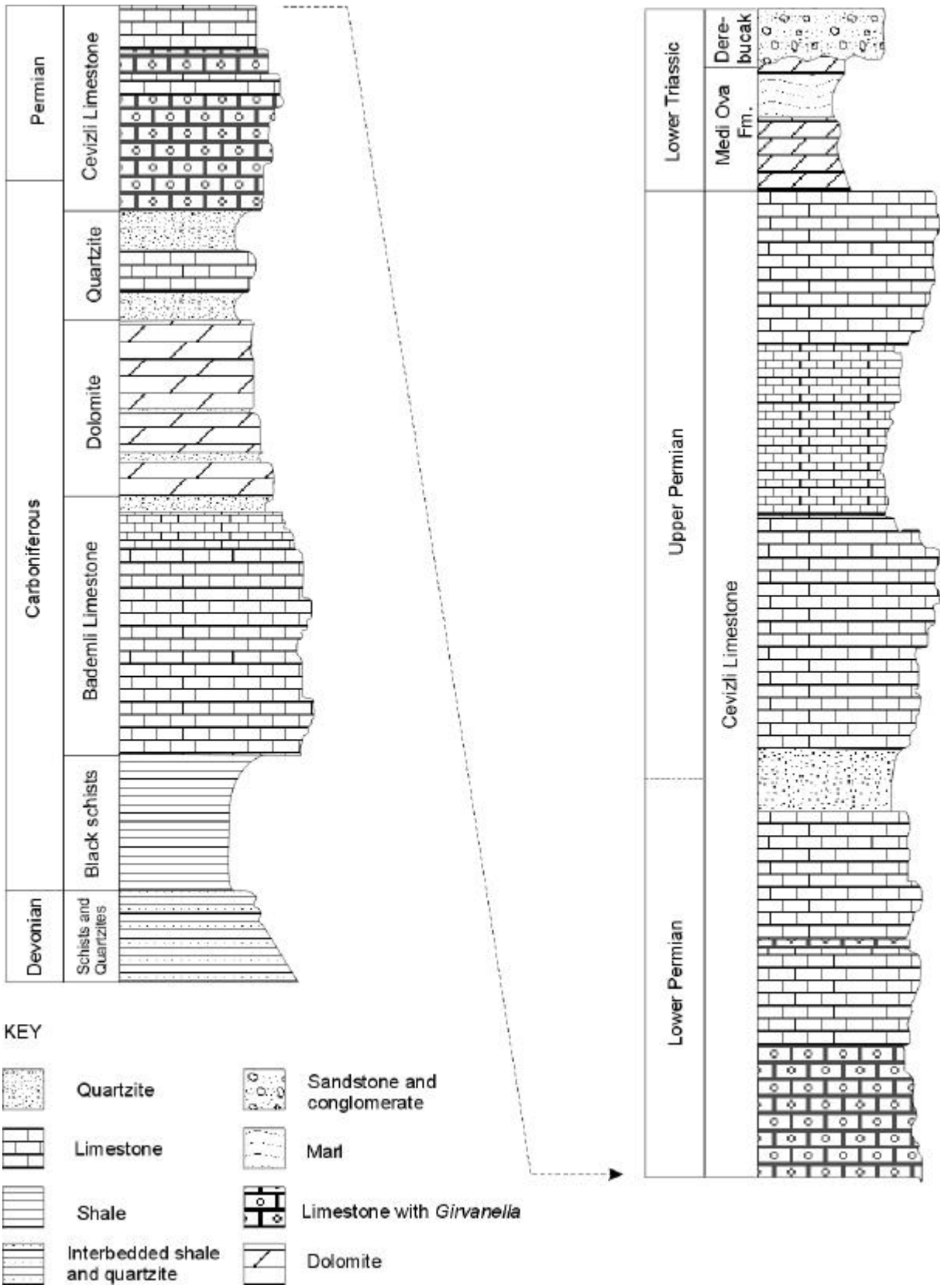

Fig. 2.9 Stratigraphy of the Palaeozoic Bademli Unit of the Hadim Nappe (field checked from Monod 1977). Scale is 1cm:25cm.

2.4.1.3 Permian limestone (Cevizli Limestone)

The succession of overlying Permian limestone to the north of Bademli village starts with Upper Carboniferous to Early Permian pink nodular limestones, which contain abundant oncoids and pisoids. The benthic foraminifera, *Fusilina* is commonly found forming the nucleus of many oncoids. These sediments pass upwards into c. 50 metres of bioclastic packstone and oolitic grainstone. Further up section the succession returns to red nodular limestone with abundant microbial mats and a diverse, fragmented shelly fauna. The remainder of the Lower Permian succession is characterised by foraminiferal packstones and grey bioclastic limestones formed from fragmented bivalves and gastropods interstratified with microbial mats (Monod, 1977).

The interval between the Early and Late Permian is marked by siliciclastic sedimentation, represented by c.40m of white unfossiliferous quartzite. Carbonate deposition resumed in the Mid- Late Permian (Kazanian to Tatarian) with well-stratified, thickly bedded dark grey limestone. Up-section interbeds of shale become more common. The latest Permian is characterised by massive to thick-bedded dark grey limestone, with interbeds of finely laminated micritic limestone interpreted as algal boundstones (Monod, 1977). Intraformational breccias commonly occur in the uppermost 50m of the section to the north of Bademli (Fig. 2.10).

2.4.1.4 Lower Triassic carbonates (Medi Ova Formation)

The penultimate interval of the Bademli unit is a succession of marls and limestones conformably overlying the Palaeozoic sequence. The thickness of the formation varies from approximately 200m in the type section to completely cut out by the overlying Lower Jurassic unconformity elsewhere (e.g. at Derebucak village or west of Bademli village; Fig.2.1).

The base of the Medi Ova Formation conformably overlies the Permian limestones and consists of well-bedded dolomite. This grades up-section into thinly bedded nodular marls, with a fauna of brachiopods (cf. *Unionites*) and gastropods (cf. *Natiria costata*), alternating with beds of wackestone, recrystallised oosparites and calcareous sandstone (Monod, 1977).

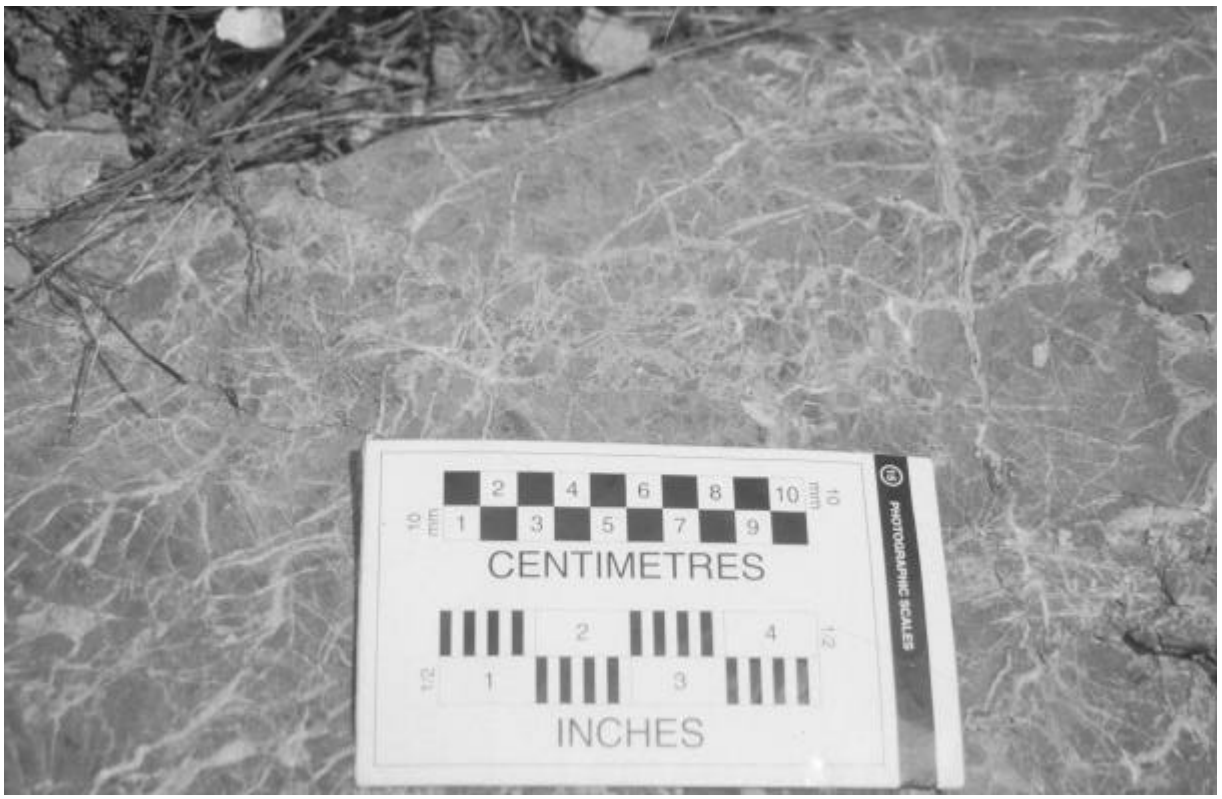

Fig.2.10 Intraformational breccias in the Permian Cevizli Limestone north of Bademli village.

2.4.1.5 Lower Jurassic siliciclastics (Derebucak Formation)

Unconformably overlying the Palaeozoic and early Mesozoic units of the Hadim Nappe is a succession of red siliciclastic sedimentary rocks. A representative section is hard to define due to extensive lateral facies variation throughout the formation, although a number of lithologies recur in most outcrops.

To the south-west of Bademli village a section through the unit consists of predominantly red, well-sorted micaceous sandstone intercalated with thin-bedded siltstone, whereas in a section to the south-west of Derebucak, the formation is more conglomeratic. It consists predominantly of poorly sorted, well-rounded clasts of limestone (including Permian *Fusilinid* limestone, micritic limestone, rare neritic and redeposited limestone), quartzite, sandstone, chert (predominantly black), shale, rare altered silicic volcanics and low-grade metamorphosed clastics (e.g. mica schist), all set in a sandy matrix. It is apparent that the most abundant clasts types within the formation are derived from the subjacent basement, e.g Medi Ova Formation and Cevizli limestone.

Owing to its unfossiliferous nature, a precise age is unobtainable for the Derebucak Formation. However, a maximum age of Early Triassic can be inferred from the age of the underlying Medi Ova

Formation. Also, large agglutinated foraminifera (Lituolidae cf. *Haurania*), from sandy limestones at the summit of the formation indicate a minimum age of mid Early Jurassic (Gutnic *et al*, 1979). It is worth noting that the contact with the Medi Ova Formation is unconformable; therefore, the lowermost age possible for the Derebucak conglomerates is not reliable.

Similar Upper Triassic-Lower Jurassic coarse, red oligomict clastic sediments can be correlated across the Taurus Mountain belt and into the Hellenides (Chios). Collectively this range of sediments have been termed the Çayir Formation (Monod and Akay, 1984).

2.4.2 Lower Jurassic-Upper Cretaceous Çamlik Unit

The Çamlik Unit is the topmost unit of the Hadim Nappe and represents a carbonate cover extending over most of the Mesozoic time. A transitional facies of sandy limestone and dolomite conformably overlies the terrestrial Derebucak Formation, whilst the majority of the Çamlik Unit consists of a succession of neritic limestone c.500m thick.

The Çamlik Unit forms a narrow series of mountains in the frontal regions of the allochthon (40km long with a maximum width of 4km), which trend NW-SE north of Derebucak to Çamlik village. They then bear west to Bademli and the Elma Süt klippe (ca. 10km south of Seydisehir; Fig.2.1). Due to the synclinal shape of the B-H-H Nappes, small outcrops are located in the northwestern limb near Ugurlu (Fig.2.1). The highest peak in the chain reaches an elevation of 2083m (Imeçali Tepe).

2.4.2.1 Lower Jurassic transitional units

The base of the Çamlik Unit conformably overlies the sandstones and conglomerates of the Derebucak conglomerate. A laterally variable transition zone exists for the lowermost ca. 100m. In the vicinity of Bademli, from Medi Ova in the west up to Imeçali Tepe and the Elma Süt klippe (fig.2.1), the red sandstones of the Derebucak Formation gradually pass into calcareous sandstones with a fauna of small bivalves. The overlying succession, i.e. Gölcük Yayla Formation, consists predominantly of well-bedded packstone-grainstone, intercalated with beds of sandstone and silty marl. The limestone beds yield a rich fauna of variably oriented bivalves and gastropods. Encrusting algae, ooids, small benthic foraminifera and rare calcareous algae are present within this facies. Numerous fragments of *Palaeodasycladus* sp. algal assemblages indicate a mid-Early Jurassic age (Monod, 1977). Further west in the environs of Derebucak village the Gölcük Yayla Formation is not present. The same stratigraphical horizon, i.e. above the Derebucak conglomerates but below the main body of the neritic limestones of the Çamlik Unit, is represented by a dolomitic succession. The dominant lithology consists of massive-thick bedded dolomitic grainstones and packstones, with abundant bivalve fragments, ooids and encrusting *Girvanelles* algae (Monod, 1977). The age of the facies has not been directly established, but given its similar stratigraphical and sedimentological nature a comparable age as its lateral equivalent can be assumed. This dolomitic succession is limited to the Derebucak valley, with an outcrop area of ca. 10km in length; therefore, it is only of local significance.

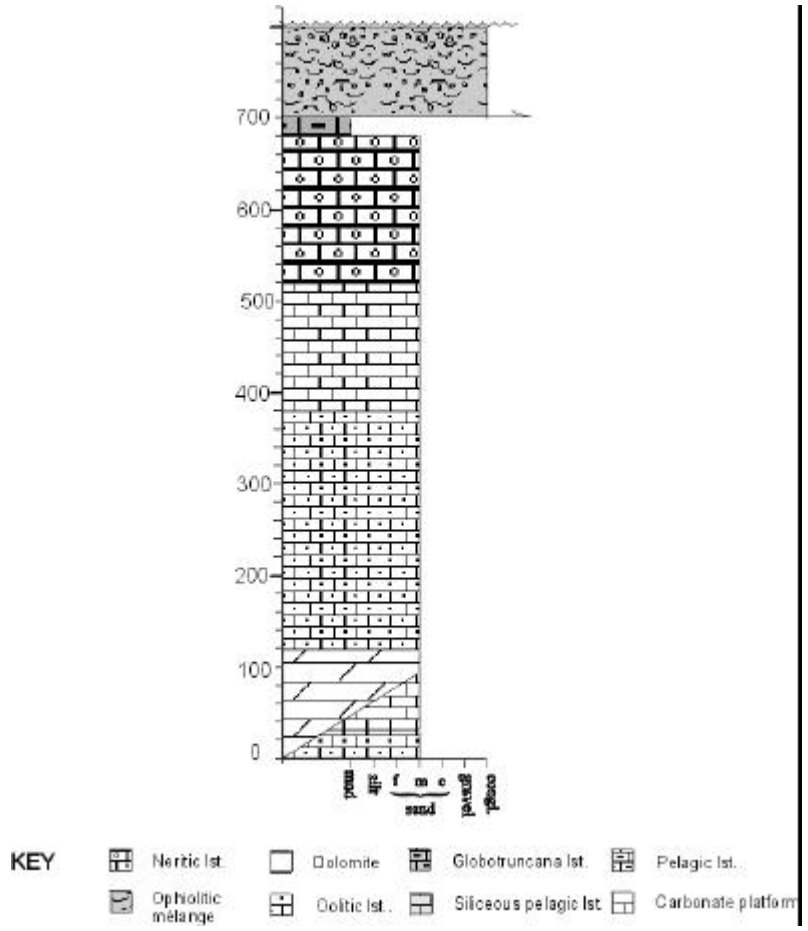

Fig.2.11 Composite log of the Çamlik Unit (field checked from Monod, 1977).

2.4.2.2 Mid Jurassic-Upper Cretaceous neritic limestone

The Çamlik Unit continues with a dominantly neritic limestone succession (ca. 500m thick), forming an elevated topography where it crops out. Traditionally, the base of this unit was distinguished from the subjacent units by a lack of terrigenous sediment. The limestones of the Çamlik Unit were subjected to intense karstification and neotectonic faulting making a single type section inappropriate to illustrate the succession as a whole. However, a composite section can be established, as shown in Fig. 2.11.

Two main facies dominate the lower section (ca. 100m) of the Çamlik Unit: 1) pisolitic grainstones and 2) black limestone. The pisolitic grainstones contain abundant bioclasts, such as fragments of bivalves, gastropods, calcareous algae and agglutinated benthic foraminifera, including *Lituolidae* cf. *Haurania* and *Nautiloculina*, set in a sparite cement (Monod, 1977). The second lithotype consists of intercalated bioclastic packstones and vuggy wackestone, both with abundant disarticulated shelly fauna, especially bivalves.

Above this is a thick succession, ca. 200m, of oosparite, with abundant bioclasts, including fragmented crinoid ossicles. Locally intraformational breccias are abundant, comprising clasts of oosparite-micrite.

The next identifiable sequence overlying the oolitic member is a succession of well-bedded micritic limestones (wackestones). Rare bioclasts are found in this facies, including *Calpionellids* and encrusting algae, e.g. *Clypeines jurassica*, the latter of which indicates an Upper Jurassic-Lower Cretaceous age for this section of the succession (Monod, 1977; Gutnic *et al*., 1979).

The penultimate facies of the Çamlik Unit is a thick succession, ca. 150m, of thick-bedded bioclastic calcarenites and breccias. Important bioclasts include fragmented rudist corals and Orbitoides. Determinations from these fauna indicate a Late Cretaceous age (Monod, 1977).

The summit of this unit records an abrupt change in sedimentation from neritic limestones to a thin succession of red/white-coloured, well-bedded micrite, ca. 10-30m. The representative section, seen only locally in, and close to, the Elmasüt klippe, consists of homogenous micritic limestone, interbedded at the top with coarse calciturbidites composed exclusively of neritic limestone clasts. Pelagic fauna found within the micritic lithology include the Maastrichtian pelagic foraminifera *Globotruncana arca*, *G. linnei*, *G. tricarinata* and *G. flexuosa*. (Monod, 1977).

2.5 Ophiolite and Ophiolitic Mélange

In the Beysehir area, the Hadim Nappe is overthrust by Upper Cretaceous Ophiolitic Melange and a dismembered ophiolite, comprising serpentinised peridotite and amphibolite. The main outcrop of Ophiolitic Mélange follows the general NW-SE trend of the B-H-H Nappes (Fig.2.1), forming an intermontane valley, betwixt the mountainous topography created by erosion of the thick carbonate thrust sheets (Çamlik and Gencek Units). Additional thin slivers of sedimentary melange infill an anatomising fracture network within, and separating, the higher thrust sheets. The principal outcrop of ophiolitic rock occurs as imbricated thrust sheets within the main body of the Ophiolitic Melange (Fig.2.13). However, ophiolite-related rocks are also found as small blocks within the melange towards the trailing edge of the allochthon, e.g. in the vicinity of Durak village (Fig 2.1).

The following sections describe the litho-stratigraphy of the Ophiolitic Mélange and ophiolite as a whole. Discussion of the geochemistry and formation of these units is given in Chapters 6 & 7.

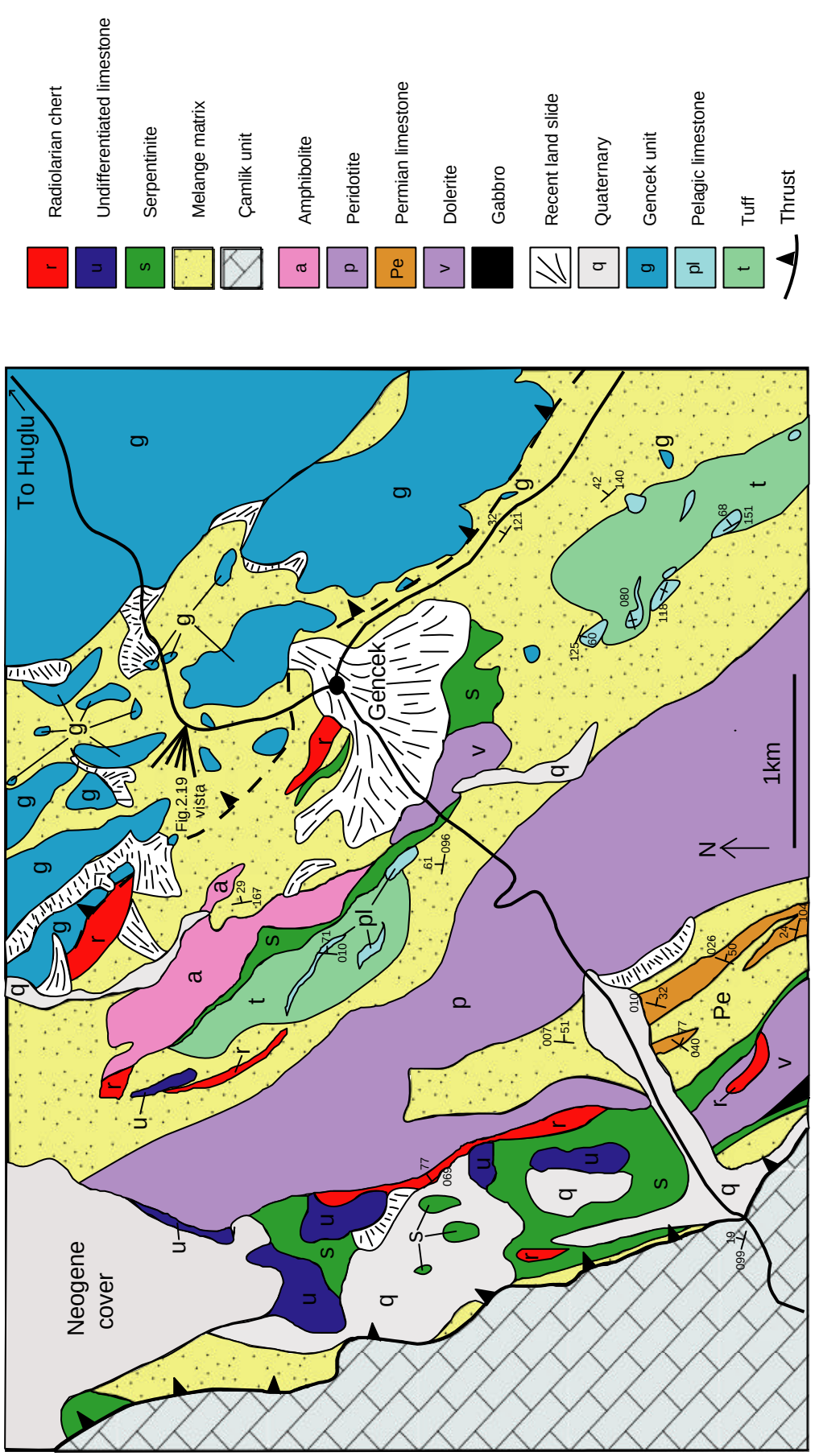

Fig.2.12 Geological map of the Ophiolitic Melange near Gencek village (field checked and redrafted from Monod, 1977). See Fig. 2.1for location.

2.5.1 Ophiolitic Mélange

Although generally poorly exposed, the thrust between the underlying Hadim Nappe and the Ophiolitic Melange is sharp, unlike the upper contact, which is gradational to broken formation. The area in the vicinity of Gencek (Fig.2.1) is excellent to study the different lithologies and their inter-relationships within the heterogeneous melange. Detailed mapping in this area shows inclusions within the melange have a crude NW alignment and there is a general stratification in the matrix (Figs.2.12, 2.14).

2.5.2 Melange Matrix

In zones of high shear strain, generally in the lower regions of the melange beneath the peridotite thrust sheet, the matrix comprises tectonically brecciated (>m scale) inclusions, e.g. chert, lava and serpentinite, and incompetent, highly sheared, olive-coloured, scaly clay/mudstone. An intense anatomising shear fabric has destroyed any remnants of original sedimentary structures.

Where the local shear strain is low, as above the peridotite thrust sheet, the matrix of the melange commonly exhibits a clastic fabric, comprising crudely stratified, well-sorted fine to medium-grained sandstone which is conglomeratic in places, e.g. N27 [844388]. In some localities, however, this stratification is extremely well developed and the melange matrix consists of calc-turbidites, e.g. N27 [856386]. The matrix consists predominantly of detrital quartz, redeposited limestone, radiolarian chert and ophiolitic-derived material, found in varying degrees of abundance depending on the location (Fig.2.13).

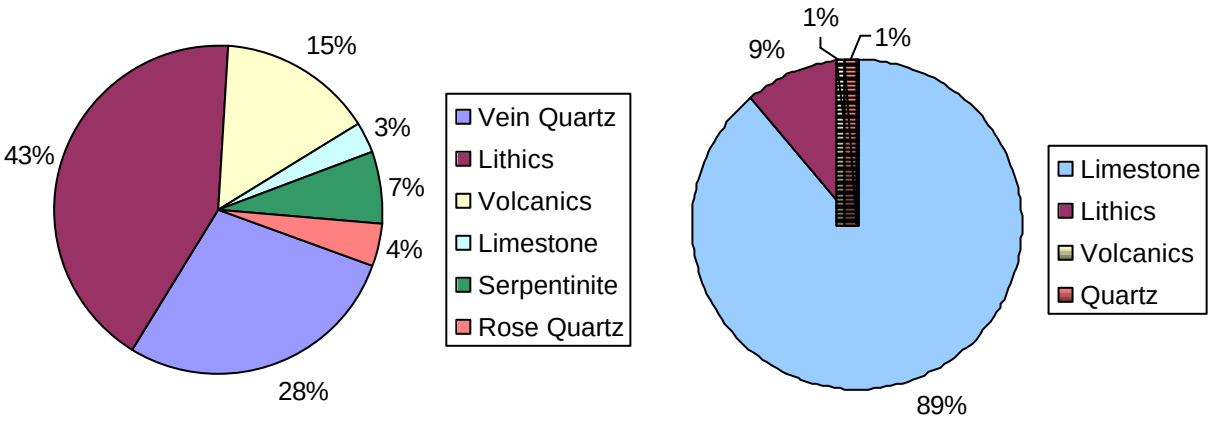

Fig. 2.13 Pie charts showing clast composition of conglomerate at two different points in the Melange matrix.

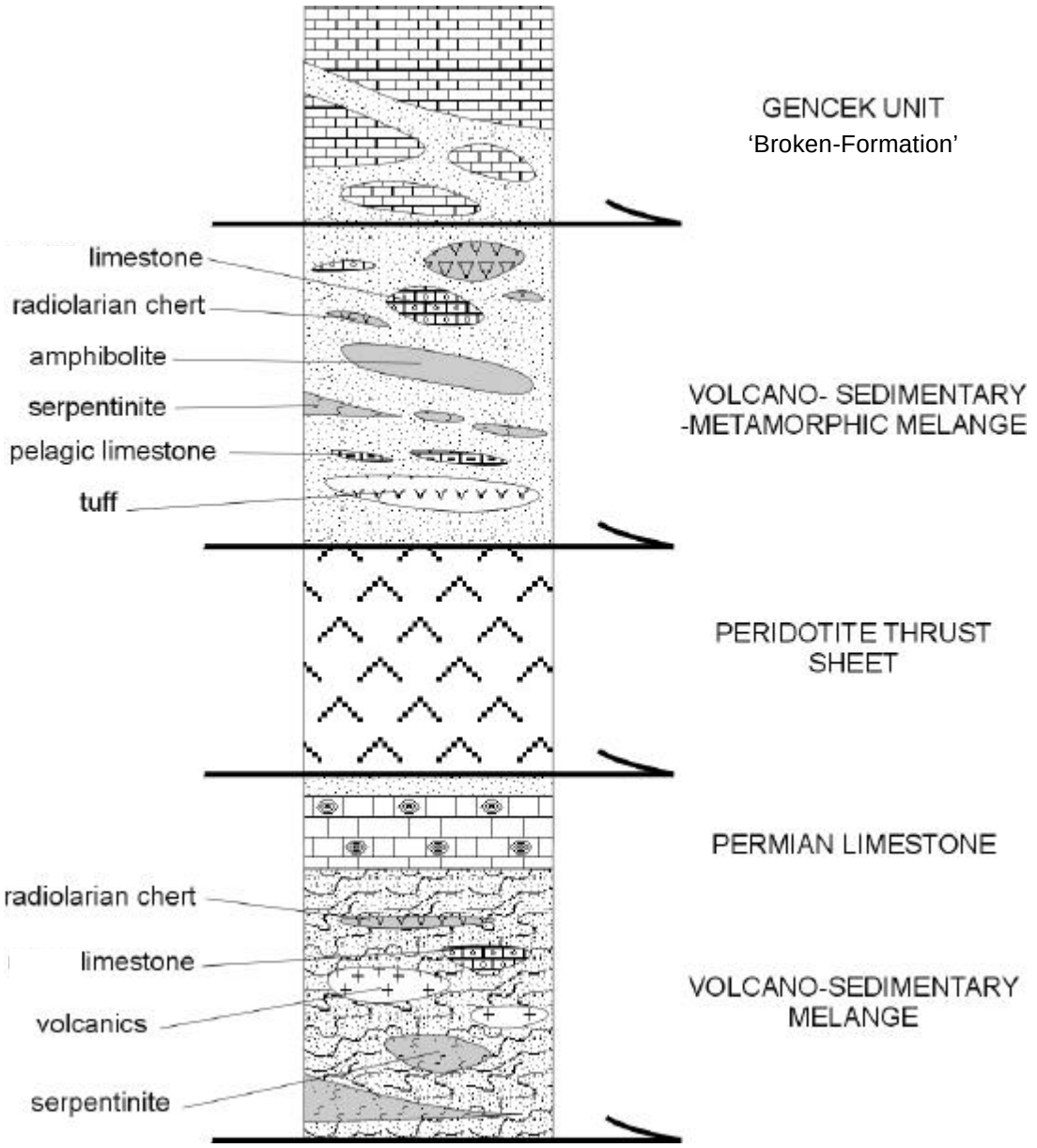

Fig. 2.14 Rock relations diagram showing composition of the Ophiolitic Melange in the Beysehir area (not to scale).

2.5.3 Melange inclusions

The melange is heterogeneous with various different lithologies incorperated from a number of different tectonic settings. These lithologies include serpentinite, pelagic limestone, radiolarian chert, basalt, dolerite, tuff, Palaeozoic limestone, redeposited limestone, amphibolite, gabbro and volcanic

debris flow deposits. A thrust sheet, ca. 500m thick, of serpentinised peridotite constitutes the single most voluminous ophiolite lithology in the melange.

On an outcrop scale, small equant blocks in the Ophiolitic Melange exhibit a random orientation and distribution; however when a larger area is considered, the bigger (ca. 1km), elongate thrust-bound, blocks are seen to possess continuity along strike, and consequently, a crude stratigraphy is apparent (Fig.2.14). A brief summary of the major sedimentary lithology types is given below.

2.5.3.1 Limestone Inclusions

Limestone is by far the most common type of lithology found as blocks within the melange. Various depositional settings are represented by the diverse carbonate facies seen, including pelagic, neritic and redeposited limestones.

The top of the Ophiolitic Melange passes gradationally into the overlying Gencek limestone, which consists of a 'broken formation' of Triassic neritic carbonate. The vast proportion of white recrystallised neritic limestone in the upper part of the melange can be correlated with the Gencek 'broken formation' (described in more detail in section 2.6.1).

Detailed mapping of the mélange shows that at a slightly lower stratigraphical position, tectonically imbricated blocks (metre-kilometre scale) of interbedded red pelagic limestone, redeposited limestone and chert are dispersed throughout the melange (Fig.2.12). The blocks consistently exhibit continuity along strike for virtually the entire length of the melange for more than 25km. Each of the blocks has a comparable stratigraphy. Figure 2.15 shows a measured section through one of these limestone blocks, from a locality 3km northeast of Kayabasi (Fig 2.1). The dominant lithology is well-bedded pelagic nodular mudstone, with abundant bedded chert intercalations, replacement chert nodules and stylolitic horizons. Towards the top of the sequence thin beds of white redeposited limestone are seen. The succession is topped by radiolarian chert that is manganese-rich in places. Typically the chert interbeds within the sequence are highly fractured and recrystallised destroying much of the original texture. Reconnaisance shows that ribbon radiolarian chert at the top of the sequence is much better developed elsewhere. A good locality to see this lithology is 15km SW of Beysehir on the road to Huglu village, situated structurally on the north-eastern limb of the Beysehir syncline (Fig 2.1). Here the road section cuts through ca. 10m of extremely well-bedded ribbon radiolarian chert. The sequence is highly folded into small tight isoclinal folds, generally overturned towards the south.

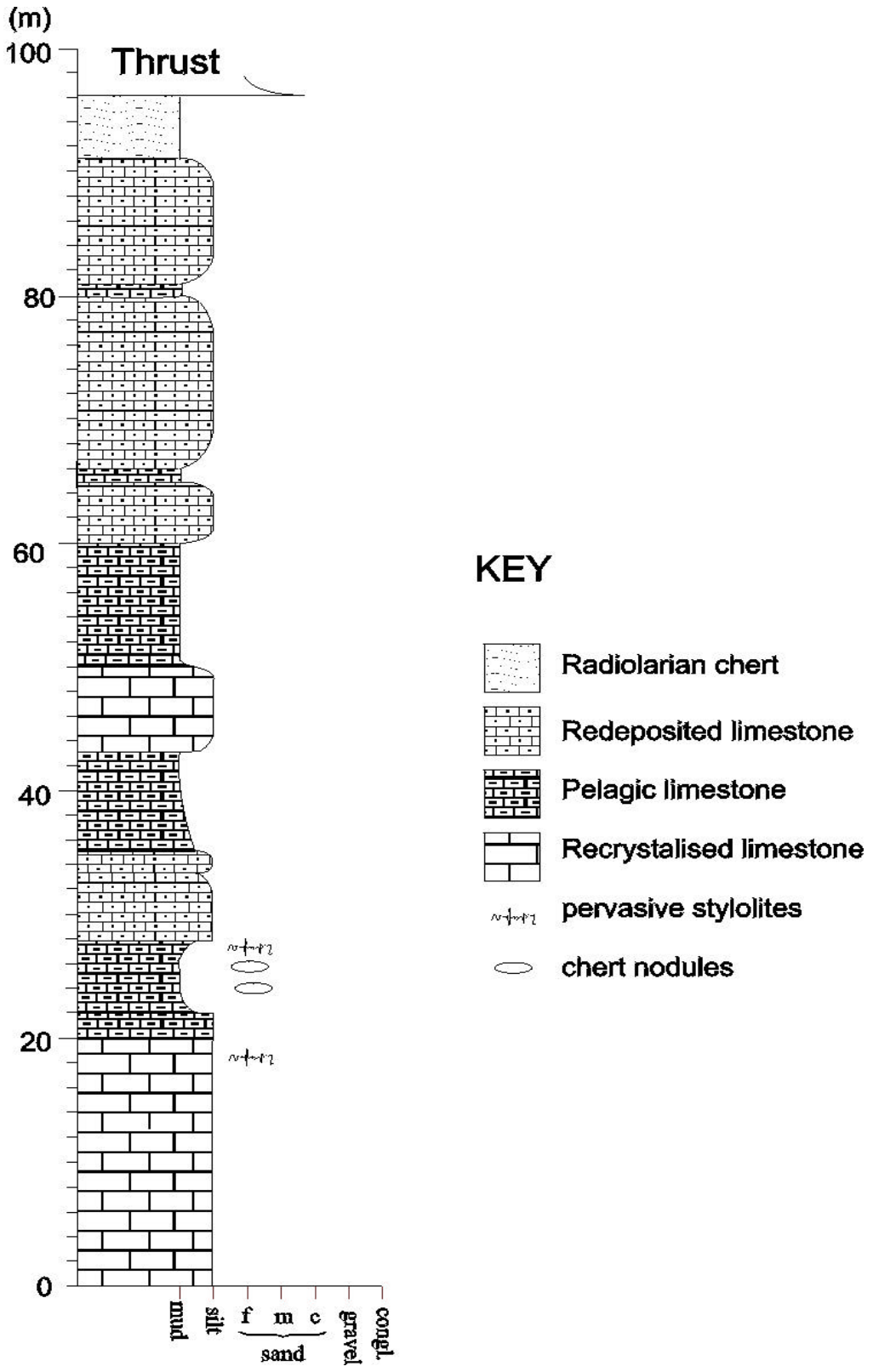

Fig.2.15 Redeposited limestone facies found as blocks in melange. Log measured 3km to the northeast of Kayabasi village (see Fig. 2.1 for location).

2.5.3.2 Volcano-sedimentary- metamorphic rock melange.

Beneath the limestone-rich horizon in the melange is a volcano-sedimentary sub-unit, locally incorporating amphibolite-facies metamorphic rocks. Common lithologies within the melange at this stratigraphic horizon include large blocks (>10m) of serpentinite, dolerite, pillow lavas, radiolarian chert, tuff, pelagic limestone and volcanic debris flow deposits. Basaltic inclusions are commonly aphanitic, highly sheared and heavily altered to chlorite and epidote. An original pillow geometry can be seen locally, often with relict interstitial sediment between the pillow necks, for example in the north-eastern limb of the Beysehir syncline, c.a 2km south of Durak village (Fig.2.16). A number of samples were collected from this locality for geochemical analysis (Section 6.2).

Fig.2.16 Highly sheared and altered pillow lavas in the Ophiolitic Melange near Durak village (Fig. 2.1).

In two specific areas, tectonic lenses (>10m) of serpentinite and amphibolite occur together as discrete blocks above the main body of the ophiolite. One such locality is shown in Fig.2.12. Here the lithology consists of amphibolite displaying well-developed banding of quartz/feldspar-rich layers and layers of amphibole altered to epidote. Subordinate biotite is also present in the more mafic bands showing alignment with the dominant fabric. This banding is cut by thin ductile shear zones (<1cm), isolating zones of low-strain phacoids, which possess a granoblastic texture. This deformation is not coeval with the deformation seen in the melange, which suggests multiple stages of deformation prior

to inclusion in the melange. Also present in the mélange at this horizon are other rare metamorphic assemblages, such as gneiss and quartzite (Monod, 1977).

At a similar structural level in the melange are a series of thrust slices of interbedded tuff and volcaniclastic sediment capped by pelagic limestone. This succession is identical to the Huglu Unit of the higher thrust sheets (discussed in more detail in section 2.6) and the two can be correlated (Monod, 1977).

2.5.3.3 Peridotite thrust sheet

The largest ophiolite body consists of a ca. 500m-thick thrust sheet of peridotite, forming an elongate outcrop, 30km long and 2-3km wide, from Kayabasi to Çamlik (Fig. 2.1) and culminating in the massive dome-shaped Kizil Dag (1977m). Lithologically, it consists of dominantly serpentinised harzburgite, with bands and lenses of dunite, pyroxenite and chromite. The harzburgite varies from fresh up to 70% alteration to serpentinite. It exhibits the characteristics of many ultramafic tectonites, including a tectonic fabric created by aligned olivine crystals.

Locally, the peridotite has an ultramafic cumulate texture, which is seen at one locality to the north of Kayabasi (Fig.2.1). Here, a pervasive banding is defined by alternating layers of highly serpentinised dunite with dispersed chromite (ca. 10cm) and chromite (1-2cm). A primary magmatic origin (cumulate texture) for the banding has been inferred (Monod, 1977). A number of samples of peridotite were collected for geochemical analysis (Section 6.3).

A suite of generally east-northeast striking dolerite dykes, ranging from 10cm to 5m wide, cut the peridotite. The dykes are mainly isolated, but in some cases occur as swarms (Monod, 1977; Dilek *et al*, 1999). A representative dyke of this type exhibits well-developed chilled margins with aphanitic to sub-aphanitic textures in the centre. Minerals in this groundmass include augite, plagioclase and amphibole. Commonly the groundmass is slightly altered to chlorite. Rare pyroxenite and microgabbroic dykes can also be found within the peridotite. All of the dykes found crosscutting the ophiolite do not continue into the melange; therefore they must have been intruded before the formation of the mélange.

2.5.3.4 Permian Fusilinid limestone

One of the most enigmatic units in the Ophiolitic Melange is a series of small slices of Permian limestone located directly beneath the main body of the ophiolite, only known locally ca. 3km to the SW of Gencek village near the road to Derebucak (Fig. 2.12). The largest of the elongate lensoidal slices reaches 2km long, with a width of several hundred metres. Lithologically, the slices consist of packstones-wackestones, with Palaeozoic encrusting algae and Upper Permian *Fusilinid* foraminifera.

The presence of the foraminifera *Neoschwagerinids* sp., *Polydiexodina* and *Sumatrina* sp. suggest that the slices are from a more northerly biofacies than the Permian limestone in the Hadim Nappe, which are of a southerly origin (Altiner *et al*., 2000). These slices of Permian limestone in the melange can therefore be correlated with other Upper Permian outer platform or platform margin deposits of the Tauride belt (e.g. in the Sultan Dag or Bolkar Dag) (Altiner *et al*., 2000).

2.5.3.5 Basal Ophiolitic Melange

The base of the melange is characterised by abundant inclusions of ophiolitic lithologies set in a highly sheared matrix. Common lithologies found as blocks in the melange include serpentinite, pillow lava and other volcanic rocks, chert, neritic limestone and rare gabbro.

This sub-unit of the mélange is well-exposed ca. 1km NW of Çamlik village. Fig.2.17 shows a representative section through part of the melange (Konya sheet N27 [790359]). Little altered volcanic rocks were collected from this locality for geochemical analysis (Section 6.2).

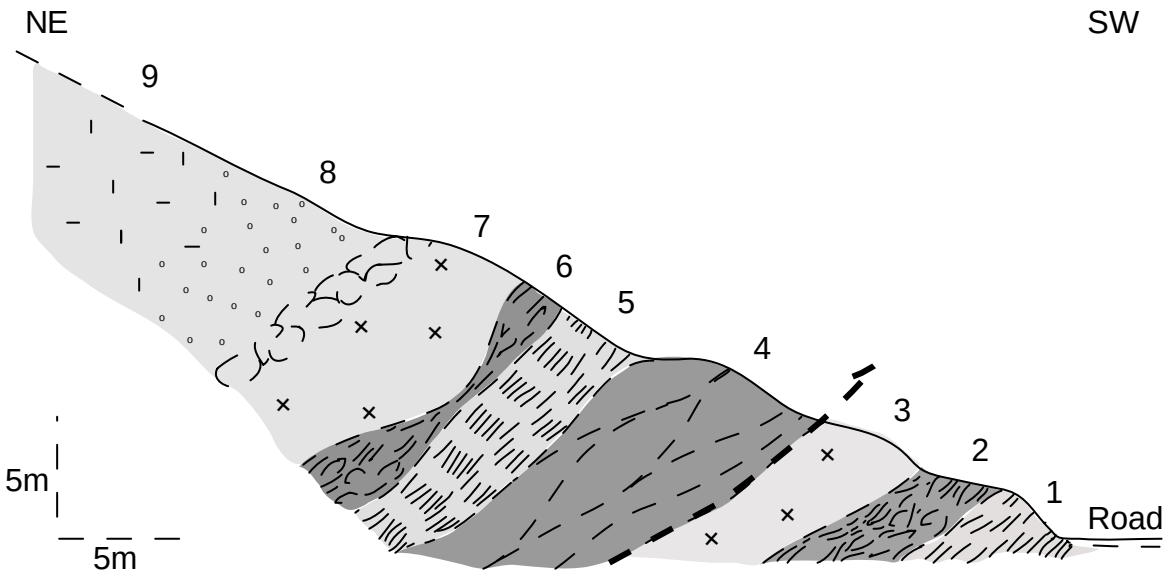

Fig.2.17 Cross section through the Ophiolitic Mélange 1km NW of Çamlik village.

1. Well-bedded, red/green radiolarian chert, highly sheared into phacoids.
2. Coarse basaltic breccia, highly sheared in schistose, mica-rich matrix.
3. Massive aphanitic basalt, with patchy calcareous cement.
4. Tectonised lava and serpentinite.
5. Red radiolarian chert.
6. Sheared volcanic breccia.
7. Massive aphanitic basalt, heavily altered to chlorite and epidote. Poorly developed pillow lava forms on top surface. (e.g. Sample TA62)
8. Amygoidal basalt, sub-aphanitic groundmass. Vesicles infilled with carbonate.
9. Feldspar porphry with aphanitic groundmass. Plagioclase phenocrysts 1-2cm in long section, randomly oriented.

2.6 Allochthonous Beysehir Nappes

The Beysehir Nappes form the highest thrust sheets in this area. Unlike the Palaeozoic Hadim Nappe, they comprise exclusively Mesozoic units. Previous studies (e.g. Monod, 1977) classified these thrust sheets as normal coherent sequences, whereas this study shows that they should be thought of as broken formation (Section 1.6). Three main subdivisions are present, as below;

2.6.1 Upper Triassic Gencek Unit

The Gencek Unit forms a mountainous ridge, extending ca. 30km from the SW corner of Lake Beysehir, trending south-east to Kizil Dag (near Çamlik), along the axial trace of the Beysehir syncline (Fig. 2.1). Some of the highest summits found in the B-H-H Nappes are formed of this unit, for example Zekeriya Ak Dag (2135m) and Yülük Tepe (2166m).

The Gencek unit consists of Triassic massive white neritic limestone, which has been tectonically emplaced onto the underlying ophiolite and melange. Unlike the other units of the B-H Nappes no Jurassic-Cretaceous cover sequence has been identified. The most striking features of the Gencek unit is its remarkable lack of stratification and its structural disruption. It is primarily for these reasons that a complete section could not be measured through this unit.

The Gencek unit is characterised by unstratified cemented bioclastic packstone and oolitic grainstones. Bioclasts include bryozoan fragments, coralline fragments, algae and shelly fauna, such as bivalves, gastropods and brachiopods. The most important macrofauna within the unit is the large bivalve Megalodon, specifically *Conchodon infraliasicus* which indicates a Rhaetian age (Monod, 1977). The Gencek unit is structurally disrupted and forms dm-km sized blocks (i.e. broken formation) set in a sandy matrix of the uppermost part of the ophiolitic mélange (Fig.2.18). The dominant structural trend of anatomising bounding fracture surfaces is approximately NW-SE (normal to the transport direction).

2.6.2 Upper Triassic-Upper Cretaceous Boyali Tepe Unit

The Boyali-Tepe unit lies at a similar structural level as the Gencek unit and forms the most northeasterly unit of the B-H Nappes in the Beysehir area (Fig.2.1). Its consists of a stratigraphically inverted broken formation of Upper Triassic neritic carbonate, with a Lower Jurassic-Upper Cretaceous condensed, pelagic carbonate cover sequence (Monod, 1977). During this study the Boyali Tepe Unit was field checked and new logs were measured as described below. Even though the succession has been structurally disrupted local sequences can be measured, such as the type locality at Boyali Tepe from where the unit draws its name (Konya sheet [N27 796475]). Figure 2.19 shows a measured section of this locality.

The Boyali Tepe succession begins with approximately 300m of well-bedded, fine-grained carbonate packstone-wackestones, with abundant bioclastic material such as disarticulated bivalves, gastropods,

bryozoans and encrusting algae. The presence of the foraminifer *Involutina* indicates a Rhaetian age (Monod, 1977). Late-stage dolomitisation affects some of the Boyali Tepe unit. The lower contact is tectonic, hence the stratigraphic base of the unit is unknown. Within the uppermost two metres of the top of the neritic unit, intercalations of pink pelagic micritic limestone become more abundant until the lithology changes sharply to Ammonitico Rosso-type pink nodular pelagic limestone. The boundary between the two lithologies is marked by a thin (<10cm) matrix-supported limestone breccia, consisting of semi-rounded neritic limestone clasts, on average >5cm, set in a fine muddy matrix. The overlying succession consists of 14m of pink nodular limestone. Lithologically, this comprises extremely well-bedded (on average 10cm thickness) muddy micritic limestone, separated by shale-rich stylolitic horizons. These contacts are extremely irregular, contributing to the nodular appearance of the outcrop.

Previous studies have extracted a fauna of ammonites, found within the basal section of this stratigraphic horizon, including *Denkmannia* cf. *elegans*, *Mercaticeras mercati*, ?*Hildates (Murleyiceras)* cf. *murleyi*, *Dactilioceras* sp., *Phylloceras* gr. *nilsoni*, *Phylloceras* sp. and *Lytoceras* sp. (Monod, 1977). The preservation of the ammonite assemblage is poor making it difficult to determine a zonal age; however, the fauna suggest a Lower to Middle Toarcian age (Gutnic *et al*., 1970; Monod, 1977). The relatively unfossiliferous upper section does not permit dating using macro-fossils.

The final metre of the Ammonitico Rosso facies is characterised by a transition zone of interbedded mudstone and recrystallised, replacement chert before passing into a ribbon-radiolarian chert interval of 5 to 10m. This thickness is approximate due to the poor outcrop. Preliminary biostratigraphical work carried out during this study on a number of samples collected from this horizon indicates an Oxfordian to Early Hauterivian fauna (T. Danelian, pers. com, 2001). Radiolarians were extracted from samples collected from the top, middle and base of this unit and imaged using a Phillips SEM at the University of Edinburgh. The methodology of sample preparation and images are shown in Appendix 1.

The radiolarian chert of the type section is overlain by 7m of cherty, pelagic limestone. The lower 3m is marked by a transition zone of interbedded grey, micritic mudstone and nodular chert, which has commonly coalesced into laterally pervasive secondary bedding up to 20cm thick (Fig.2.20). This grades into massive, grey micritic mudstone. Fine stylolites cut the lithology on a cm-scale creating a fine nodular appearance. Small chert nodules, 1-2cm in long section, are aligned preferentially giving the impression of bedding. Dating of the succession by pelagic foraminifera (e.g. *Globotruncana* sp.) indicates an age ranging from Albian-Cenomanian to Coniacian-Santonian (Monod, 1977).

The top of the Boyali Tepe Unit is marked by a poorly exposed radiolarian chert horizon and a well-developed chert/volcanic breccia (Fig.2.21). Where exposed, the breccia is unstratified and comprises poorly sorted, angular, clasts of variable nature set in a sandy matrix. Clast sizes range from <1cm to >30cm and consist dominantly of recrystallised chert and altered basalt. Subordinate neritic limestone clasts are also present in smaller numbers.

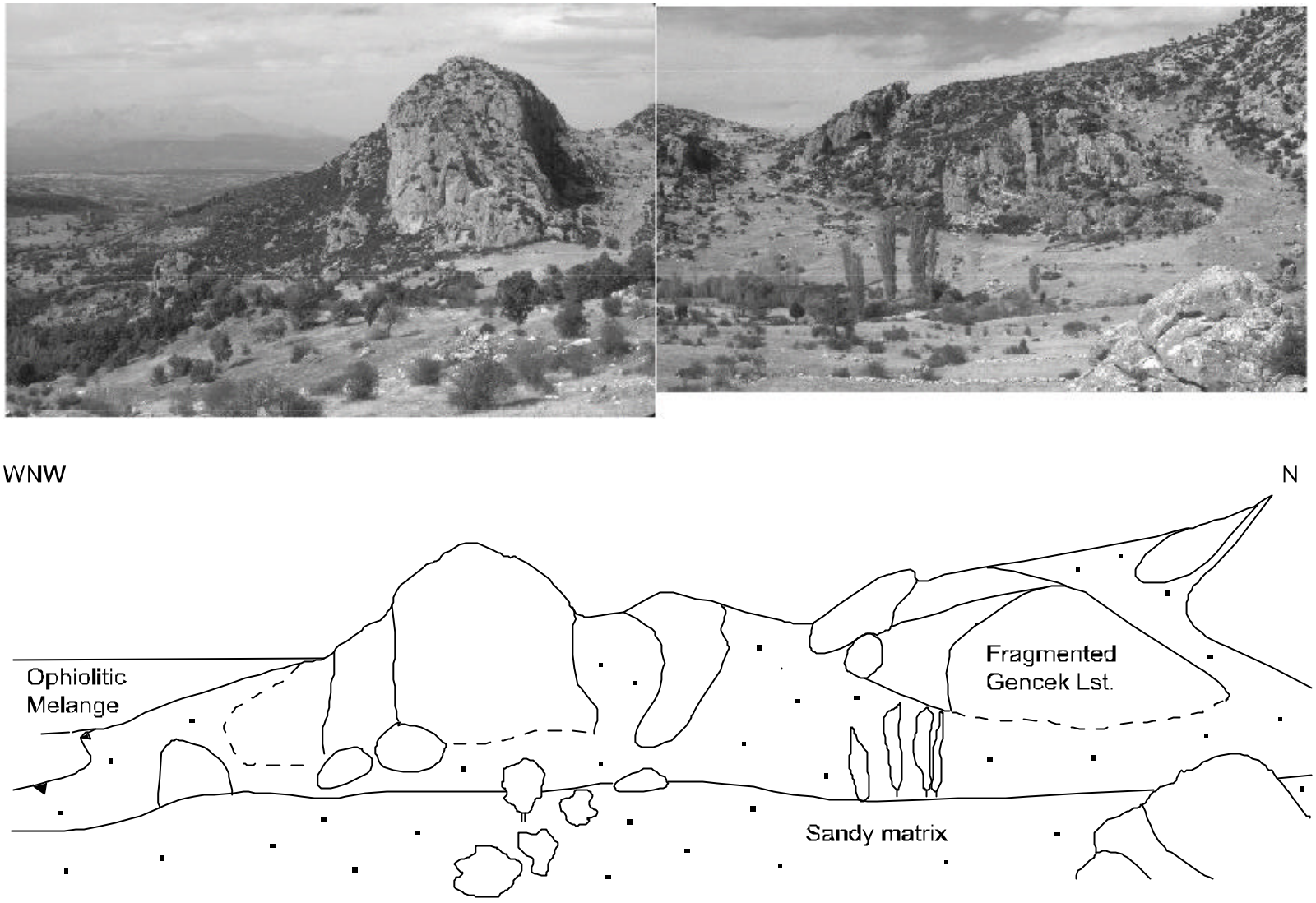

Fig.2.18 Interpreted field sketch of large blocks of the Gencek Unit broken formation overlying and grading into the Ophiolitic Melange (for location see Fig. 2.12.

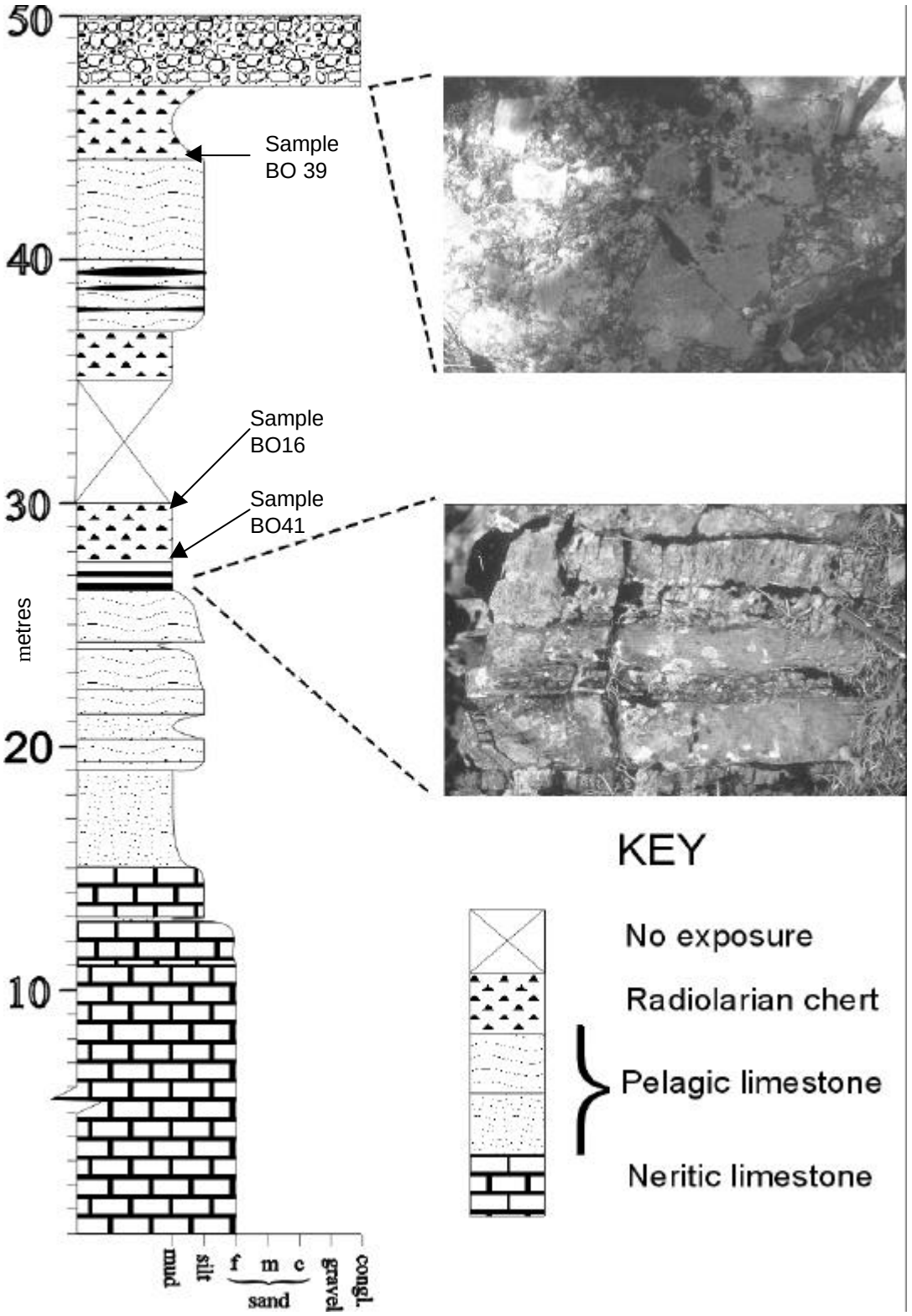

Fig.2.19 Measured log of the Boyali Tepe section. The upper inset shows the volcano-sedimentary breccia at top of Boyali Tepe section, whilst the lower inset shows interbedded pelagic limestone and chert. Sample numbers of radiolarian chert specimens collected is shown (Appendix 1). For location of log see Fig. 2.1.

2.6.3 Triassic-Upper Cretaceous Huglu Unit

The Huglu Unit forms the uppermost thrust sheet of the B-H Nappes in the Beysehir area. It consists of a thick sequence (~1000m) of distinctive green volcano-sedimentary lithologies, capped by a condensed sequence of pelagic limestone, as shown in Fig.2.20 (Monod, 1977). The unit is named after the type section area in the vicinity of Huglu village (Konya sheet N27 [745488]; Fig.2.1).

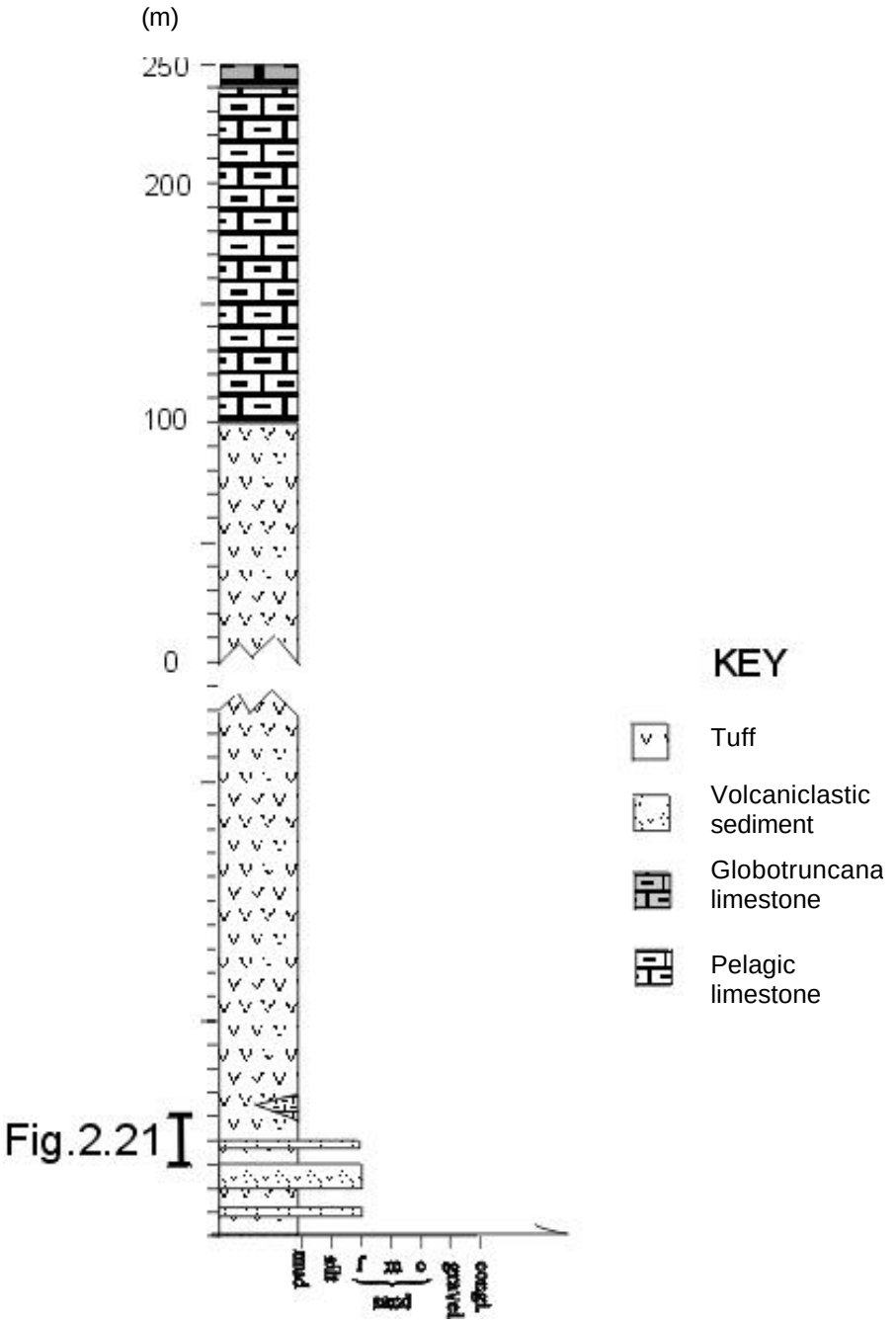

Fig.2.20 Generalised stratigraphy of Huglu Unit (field checked and redrafted from Monod, 1977).

2.6.3.1 Lower volcano-sedimentary unit

The lowermost volcano-sedimentary sub-unit crops out parallel to the strike of the B-H Nappes between the Gencek and Boyali Tepe units (Fig.2.1). The type section of this sub-unit is in the roadcutting approximately 1km north of Huglu towards Beysehir. Fig.2.21 shows a representative log through part of the volcano-sedimentary succession in the type section.

The bottom of the section is characterised by volcanic-rich debris flow deposits. The most common clasts are highly altered (chloritised) siliceous volcanic rocks and less common neritic limestone. Most of the succession is dominated by bottle-green to khaki-coloured tuff, which is well bedded, extremely fine grained and shows a distinctive conchoidal fracture. In thin section they display a hypocrystalline aphanitic texture. The groundmass comprises <75% microcrystalline quartz and feldspar with <5% glassy patches. Commonly, the samples possess a microporphyritic texture of equant, euhedral quartz and felspar microphenocrysts. Less common (<1%) are spherical glass rimmed devitrification spots and anhedral accessory opaque minerals. All of the samples are heavily affected by chloritisation.

Locally intercalated with the tuff is a suite of siliceous, aphanitic volcanic rocks. Patchy devitrification spots are commonly seen on fresh surfaces. In thin section these extrusive rocks possess a cryptocrystalline-microcrystalline groundmass, with an intergranular texture of dominantly feldspar and quartz, with subordinate heavily altered pyroxene (augite?). Extensive chloritisation (up to 75%) helps to give the rock its distinctive green colour. Section 6.1 discusses he petrological and geochemical characteristics of a number of samples collected from the Huglu type section.

Field work shows that interbedded with the volcanogenic succession are localised clastic and volcaniclastic sequences. Fig.2.21 illustrates one such sequence of massive mudstones, cross-bedded redeposited limestones and rare coarse-grained arkosic sandstones measured in this study towards the base of the Huglu type section.

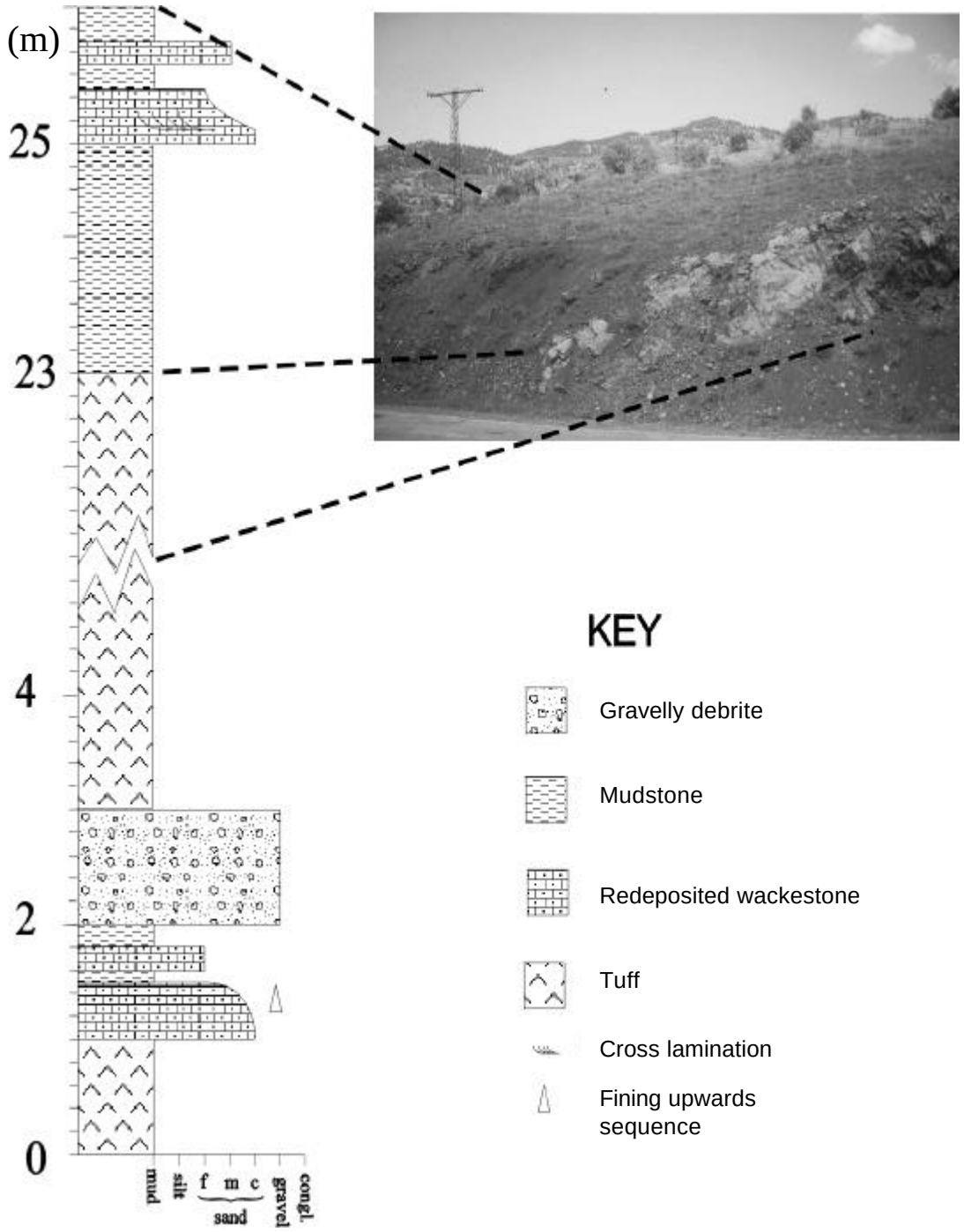

Fig.2.21 Log measured through clastic sequence in the Huglu Unit (see Fig.2.1 for location).

2.6.3.2 Upper pelagic limestone unit

Lying in normal stratigraphic contact with the underlying volcano-sedimentary unit is a thin succession (~100m) of pelagic limestone (Fig. 2.20). This sub-unit forms a linear ridge striking NW-SE, which crops out directly SW of Huglu village (Konya sheet N27 [743485]; Fig.2.1). At this location both the upper and lower contacts are seen clearly. The lower normal contact is approximately at the base of the break of slope. The upper contact is obscured by scree but can be inferred to be tectonic as it passes into the sandy matrix of the Gencek Unit broken formation. The most common lithology of this unit consists of well-bedded micritic limestone with dominantly pelagic fauna, e.g. Ammonites and the pelagic bivalve *Daonella*, indicating an Anisian-Ladinian age (Monod, 1977).

The upper part of this succession is siliceous with abundant chert nodules and beds. The uppermost section forming the summit of the ridge consists of red nodular pelagic limestone and contains a fauna of small pelagic foraminifera including *Globotruncana coronata, G. sigali, G. lapparenti, G. cf. Shneegansi* which indicate a Coniacian-Senonian Upper Cretaceous age (Monod, 1977).

Reconnaisance during this study shows that local variation is common. Along the south shore of Lake Beysehir (Fig.2.1) the upper pelagic limestone of the Huglu Unit crops out. Here the sequence is imbricated, but complete local sequences can be measured, which consist of pelagic limestone, chert, redeposited limestone with intercalations of sandstone and mudstone. Although the section is similar there is a lot more redeposited limestone in this sequence.

2.7 Summary

The region to the south of Lake Beysehir is the type area for the Beysehir-Hoyran-Hadim Nappes; thus, understanding the tectonostratigraphy is critical for comparisons with other areas. Figure 2.22 summarises the lithostratigraphy of the main units in the Beysehir area. In addition, some of the major findings from this chapter are summarised below:

1. The lowermost exposed part of the autochthon comprises Cambrian limestones and Ordovician shales. These are unconformably overlain by Upper Triassic siliciclastic sediments (e.g. the Çayir Formation) and Mid-Jurassic transgressive limestones. The main succession of the thick Tauride carbonate platform sequence conformably lies above. The uppermost part of the autochthon is represented by Early Tertiary siliciclastic sediments and debris flows, which are locally highly sheared by the overthrusting of the B-H-H Nappes above.

2. The Late Palaeozoic-Mesozoic Hadim Nappe is the lowest unit of the B-H-H Nappes, and shares a similar Mesozoic stratigraphy to the main Tauride carbonate platform below.

3. The ophiolite comprises thrust slices of serpentinised harzburgite, including lenses of chromitite and dunite, which are cut by a series of dolerite dykes. Blocks of amphibolite-grade metamorphic sole-type lithologies are locally found in the melange.

4. The Ophiolitic Melange comprises blocks of neritic and pelagic limestone, basalt, serpentinite and radiolarian chert, all set in a highly sheared silt and mudstone matrix. Kilometre-scale thrust slices of Permian limestone (dissimilar to the Hadim Nappe) are locally found beneath the ophiolite in the melange.

5. The Gencek Unit broken formation comprises large (km-scale) blocks of Late Triassic massive neritic limestone set in tectono-sedimentary melange.

6. The Boyali Tepe unit also begins with Late Triassic neritic limestone, then passes into Early Jurassic nodular limestone, Upper Jurassic-Lower Cretaceous radiolarian chert and Cretaceous pelagic limestone. The top of the unit is characterised by chert and volcanic debris flows. This unit is consistently stratigraphically inverted.

7. The bipartate Huglu unit begins with Mid-Triassic volcanic lithologies, overlain by a condensed sequence of pelagic limestones, which spans Late Triassic to Upper Cretaceous time.

8. The higher thrust (e.g. the Gencek, Boyali Tepe and Huglu Units) sheets comprise latest Cretaceous 'broken formation' and are included in tectono-sedimentary melange matrix.

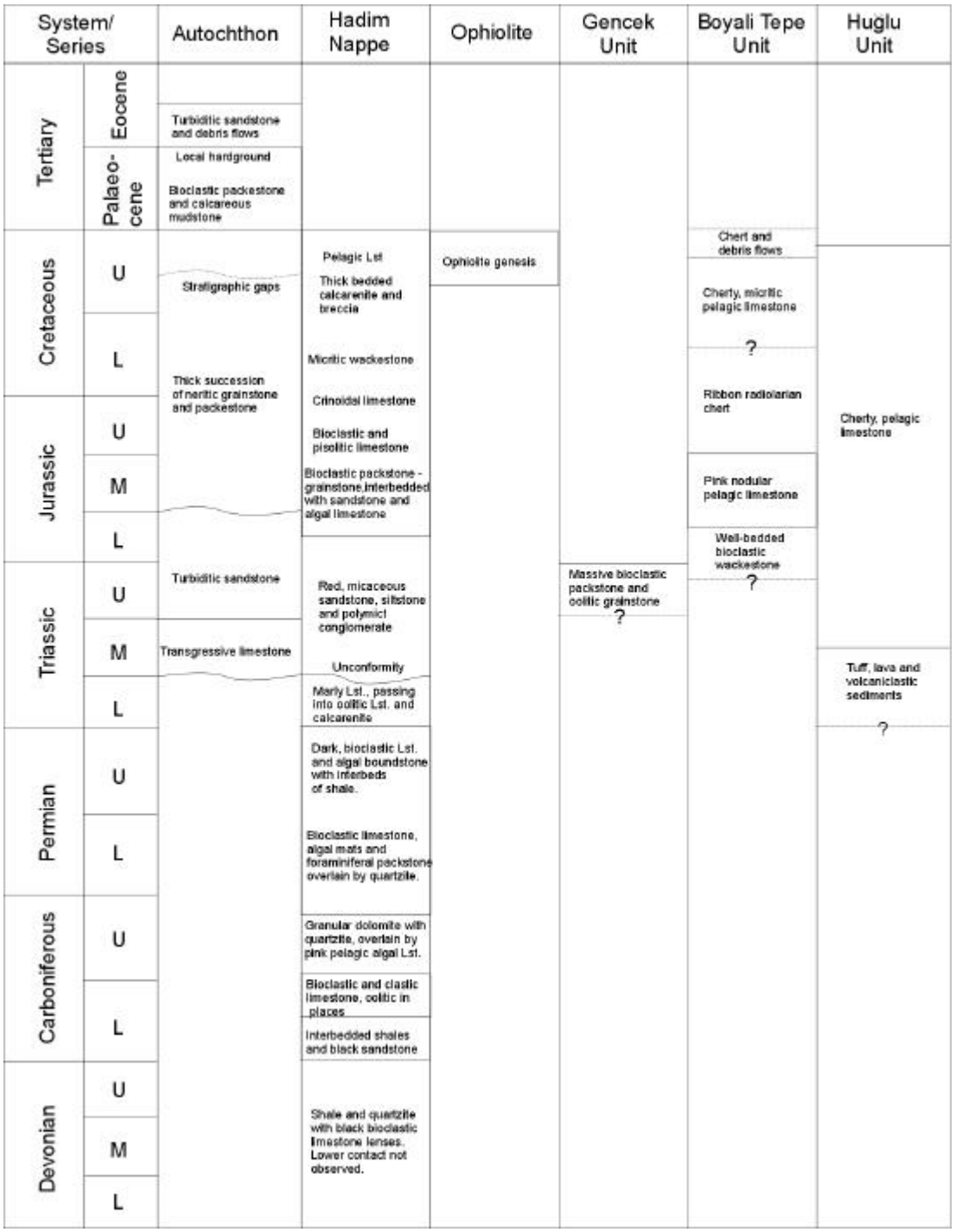

Fig. 2.22 Late Palaeozoic to Early Tertiary lithostratigraphic summary of the Beysehir area (age data from Monod, 1977).

Chapter 3

3. TECTONOSTRATIGRAPHY OF THE B-H NAPPES IN THE PISIDIAN TAURIDES

This chapter examines the extension of the B-H Nappes from the Beysehir area into the Pisidian Taurus Mountains to the northwest. The focus is on the tectonostratigraphy to enable a regional correlation. As before, much of the original work carried out in this study concentrates on the allochthonous B-H Nappes and the uppermost Early Tertiary history of the Autochthon, which provides information on the emplacement record of the Nappes. Consequently, the Lower Palaeozoic-Mesozoic history of the Autochthon should be treated as an in depth literature review, which was checked during fieldwork. The Upper Cretaceous to Early Tertiary autochthonous succession and the B-H Nappes are investigated, with new logs measured and presented here.

In total, three sections were chosen to illustrate the B-H Nappes in this region; 1) Sarkikaraagaç area (north of Lake Beysehir), 2) Kumdanli area (north of Lake Hoyran) and 3) Dinar area (Fig.3.1). Due to their tectonostratigraphic similarities, the Sarkikaraagaç and Kumdanli areas will be dealt with together to avoid unnecessary repetition.

3.1 Previous work

Various researchers have worked in the three outcrop areas of this study. In the Sarkikaraagaç region, north of Lake Beysehir, initial detailed mapping was carried out by Kelter (1968). This was refined by the Maden Tektik ve Arama Genel Müdürlügü (M.T.A). The area was remapped at 1:25,000 scale (Öztürk *et al*, 1981) and compiled into a regional 1:100,000 sheet of the Isparta area (Senel, 1997). More recently, work has been carried out on the geochemistry of the Kizildag ophiolite (Elitok, 2000).

The earliest relevant work in the Kumdanli area was the publication of the Ankara sheet 1:500,000 scale geological map (Erentöz *et al.,* 1963), which was followed up with detailed 1:25,000 mapping and stratigraphical work in the region directly to the north of Hoyran Lake and the in the Sultan Dag mountains (Demirkol, 1977, 1981, 1984; Koçyigit, 1983, 1984).

In the Dinar region, to the far west of the study area, the most useful previous work was carried out by Marcel Gutnic as part of his research for his Doctoral degree at the University Paris Sud d'Orsay. Tragically, Marcel died before he finished writing up his results, but the principal extracts of his notebooks were compiled by Olivier Monod into a comprehensive thesis on the geology to the north of Isparta (Gutnic, 1977). Recent work has concentrated on the autochthonous Late Precambrian Sandikli Basement Complex (Göncüoglu & Gürsu, 2001).

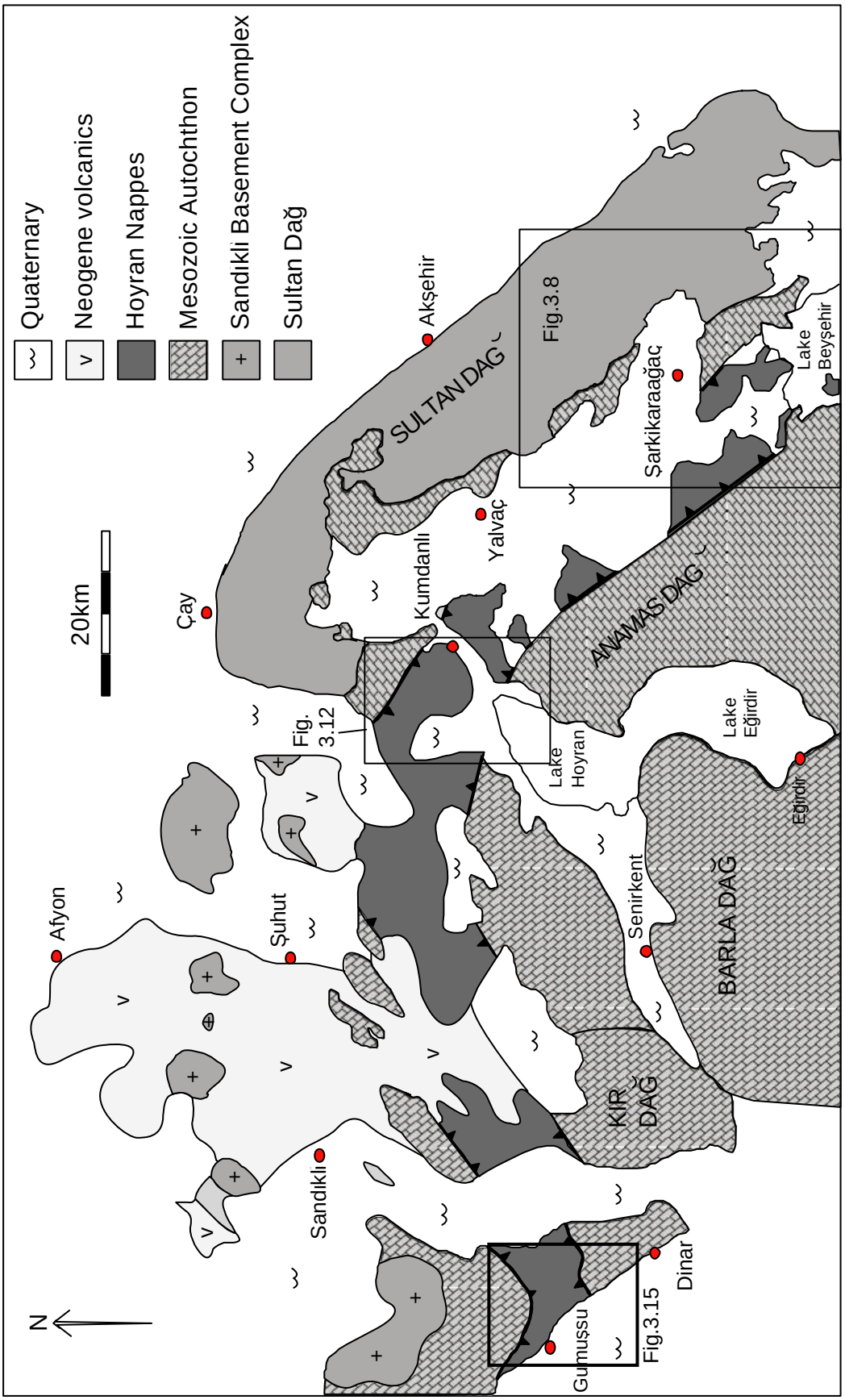

Fig 3.1 Geological map of the Pisidian Taurides showing the major tectonostratigraphical units pertinent to this study. (redrafted from Gutnic, 1977, Monod, 1977 and Gutnic *et al*., 1979). For location see Fig. 1.1.

3.2 Tectonostratigraphy of the western Pisidian Taurides: Sarkikaraagaç and Kumdanli areas.

The B-H Nappes extend northwards under Lake Beysehir and crop out on the northern shore as a narrow (<10km) NNW-SSE trending synformal thrust pile of ophiolitic rocks, melange and neritic carbonate. The Nappes follow the trend of the Sultan Dag northwards towards the Yalvaç plain where they are covered by younger Neogene and Quaternary sediments. To the northeast of Hoyran Lake the B-H Nappes re-emerge and bend to strike E-W towards Dinar (Fig. 3.1).

Three main tectonstratigraphical units comprise the B-H Nappes in these areas, as shown in Table 3.1 below. In the Sarkikaraagaç area, Ophiolitic Melange and slices of coherent ophiolite have been thrust directly onto the regional autochthon, which comprises the Sultan Dag in the east and the Anamas Dag in the west. The uppermost unit consists of a fragmented thrust sheet of Triassic massive neritic carbonate. In the Kumdanli area the tectonostratigraphic situation is similar, with Ophiolitic Melange and Upper Triassic-Lower Jurassic neritic carbonates tectonically emplaced onto the same autochthonous unit. The only major difference is the absence of large coherent ophiolite thrust sheets, as seen near Sarkikaraagaç.

<table>
<tr><th></th><th>B-H Nappes</th><th>Autochthon</th></tr>
<tr><td rowspan="3">Sarkikaraagaç area</td><td>Kizildag Ophiolite</td><td rowspan="5">In East:
Sultan Dag

In West:
Anamas Dag</td></tr>
<tr><td>Ophiolitic Mélange</td></tr>
<tr><td>U.Tr-L.Jr. neritic carbonate</td></tr>
<tr><td rowspan="2">Kumdanli area</td><td>Ophiolitic Mélange</td></tr>
<tr><td>U.Tr-L.Jr. neritic carbonate</td></tr>
</table>

Table 3.1 Summary of the tectonostratigraphy in the Sarkikaraagaç area and Kumdanli areas.

3.2.1 Regional Autochthon

To the north of Lake Beysehir, the B-H Nappes were tectonically emplaced onto an autochthon that is similar to that seen in the Beysehir area. Essentially the nappes lie on the boundary between two distinct autochthonous units; in the east the Sultan Dag and in the west the Anamas Dag. The Sultan Dag comprises Late Precambrian sedimentary rocks trangressively overlain by Mesozoic carbonate rocks, which can be directly correlated with the succession in the Beysehir area (Monod, 1977; Gutnic *et al*,

1979). The Anamas Dag exhibit a succession similar to the Akseki platform and represents the westerly part of the Geyik Dag autochthonous succession in the Taurus Mountains (Özgül, 1976).

3.2.1.1 The Sultan Dag autochthon north of Lake Beysehir (Sarkikaraagaç area)

In the Sarkikaraagaç area, the Sultan Dag autochthonous series begins with limestones of the Çal Tepe Formation, with a gradual transition into the Seydisehir Formation (Fig.3.2). The Lower Palaeozoic sequence seen to the north of Lake Beysehir is identical to that seen in the Beysehir-Seydisehir area, as detailed in Chapter 2.3.1 (Kelter, 1968; Monod, 1977). Mid-Triassic sandstones of the Pinarbasi Formation and Upper Anisian-Ladinian limestones of the Tarasçi Formation crop out above a regional unconformity at the top of the Lower Palaeozoic sequence (see Chapter 2.3.2.1).

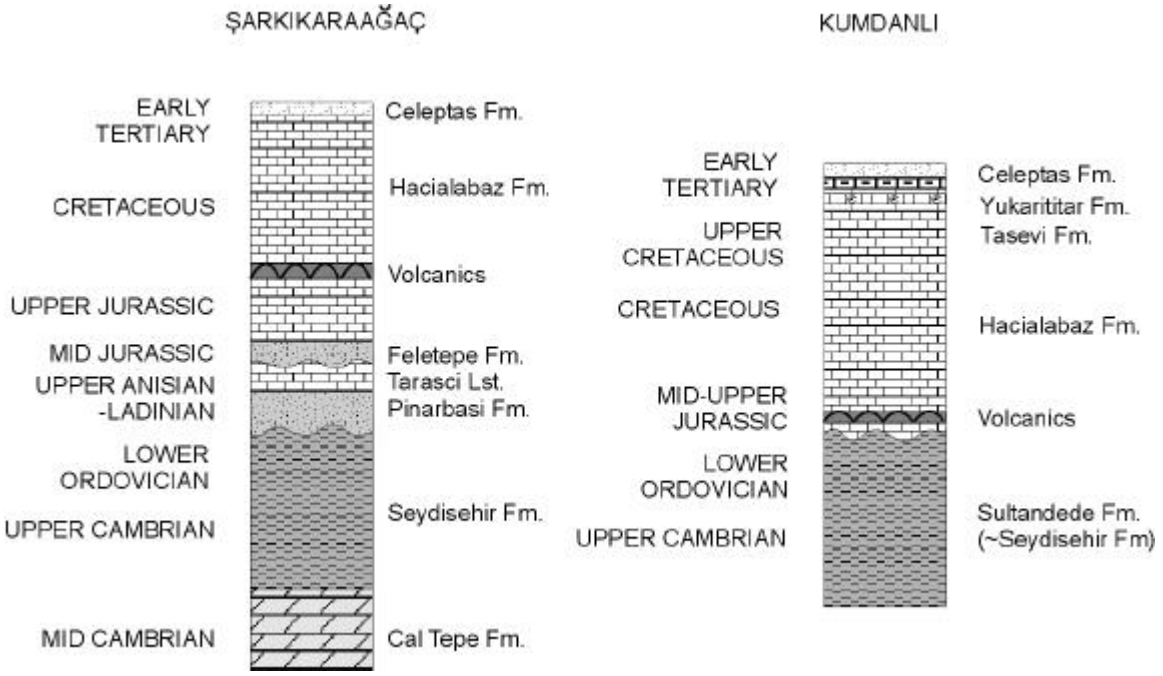

Figure 3.2 Tectonostratigraphy of the Sultan Dag autochthonous sequence in the Pididian Taurides.

A second unconformity that can be correlated with the Beysehir area exists at the top of the Triassic sequence and the Jurassic Feletepe Formation (Fig.3.2). This relatively thin (0-50m) transgressive sequence consists of intercalated conglomerate, siltstone, sandstone and oolitic-pisolitic limestone and is considered to be the extension of the Mid-Jurassic Sarakman Formation as seen in the Beysehir area (Monod, 1977; Senel, 1997). However, a fauna of *Kurnubia* sp., *Valvulina* sp., *Lituolidae* and *Pfenderininae* cf. *formulara* suggests a slightly younger Lower Jurassic?-Mid-Jurassic age (Öztürk *et al*, 1981). This transgressive sequence is overlain by a thick (ca.550m) Upper Jurassic-Lower Tertiary carbonate platform succession known as the Hacialabaz Formation (Demirkol, 1977). Unlike the Beysehir

area, a suite of doleritic sills have been intruded into the lowermost levels of this unit (Haude, 1968; Desprairies & Gutnic, 1970; Gutnic, 1977; Monod, 1977; Koçyigit, 1984). In this study area, the sills crop out near Felepinar village in carbonates of Mid-Upper Jurassic age (Monod, 1977; Koçyigit, 1984). The top of the autochthonous carbonate sequence is represented by Lower Tertiary flysch (Celeptas Formation). These upper units are better developed to the north of Lake Hoyran; hence, to avoid repetition they will be described together with the Kumdanli area.

3.2.1.2 The Sultan Dag autochthon northeast of Lake Hoyran (Kumdanli area)

The Sultan Dag autochthonous succession in this region is extremely similar to that seen further south in the Sarkikaraagaç and Beysehir areas. The lowermost unit is the Sultandede Formation, which comprises a thick sequence (ca.550m) of low-grade metamorphosed, intercalated sandstone, greywacke and phyllite with lenses of coarse recrystallised limestone (Demirkol, 1977, 1984). The unit is highly deformed and possesses a well-developed foliation and commonly forms tight disharmonic recumbent, to overturned, folds (Demirkol, 1984). The Sultandede Formation is relatively unfossiliferous and consequently is undated; however, it can be directly correlated with the Seydisehir Formation (Chapter 2.3.1.2), which is of Middle Cambrian to Ordovician age (Monod, 1977; Demirkol, 1984).

The Lower Palaeozoic Sultandede Formation is then unconformably overlain by the Upper Jurassic-Cretaceous Hacialabaz Formation. It is worth noting that the Triassic and Lower Jurassic units seen further south (i.e. the Pinarbasi, Tarasçi and Feletepe Formations) are not present in this area. Further east in the type area of the Sultan Dag, the Lower Palaeozoic succession extends through the Ordovician and includes units of Devonian and Permian ages (Demirkol, 1984). These, however, do not crop out in the chosen study area.

The Hacialabaz Formation is a 550m-thick carbonate sequence (which is equivalent to the lesser known Hoyran Group in terminology; Koçyigit, 1984) generally consisting of dark grey/blue, thin to thick bedded, locally massive and recrystallised, oobiosparite, biomicrite and biosparite with local dolomite lenses (Demirkol, 1981,1984). This conformably passes into ca. 50m of Cenomanian-Maastrichtian pelagic limestone, with different local terminologies (Tasevi and Gölcük Formations; Demirkol, 1981, 1984). The traditional view is that this is then overlain by 70-900m(?) of Upper Palaeocene-Lower Eocene biomicrite, i.e. the Yukaritirtar Formation, followed by 50m-1100m(?) of sandy turbidites, the Celeptas/Dereköy Formation of Mid-Eocene (Lutetian) age (Demirkol, 1981, 1984; Koçyigit, 1983, 1984). New logs were measured through the Upper Cretaceous-Middle Eocene sequence of the autochthon with the aim of resolving these conflicting data. Part of the reason for discrepancies reported by different workers for the thicknesses of these upper units is that the lithologies show rapid lateral and vertical facies changes. Three sections were chosen (Fig.3.3); one to the north of Kumdanli, the second to the north of Celeptas and the third 0.5km to the south of Yukaritirtar village (the type section for the Yukaritirtar Formation).

North Kumdanli section (Fig. 3.3)

The first log of the section (Log 177) begins with grey coloured biomicrite of the Tasevi Formation, containing the Upper Cretaceous pelagic foraminifer *Globotruncana* sp., the absence of which was used to identify the beginning of the Lower Palaeocene Yukaritirtar Formation. At this locality it comprises 94m of well-bedded grey biomicrite, with an abundant fauna of benthic foraminifera (including *Nummulites* sp., *Miliolidae* and *Discocyclina* sp.) intercalated with beds, generally <0.5m but up to 2m thick, of fine-coarse sand sized, redeposited grainstone and packstone. Some horizons of biomicrite, especially towards the top of the section, are partially recrystallised and have abundant replacement chert nodules. The top of the Yukaritirtar Formation is represented by a change to red/pink coloured pelagic biomicrite and silty limestone, an interval 11m thick. This is overlain by 11m of turbiditic fine-grained sandstone and pink mudstone, belonging to the Celeptas Formation, before passing into a 3m-thick horizon of slumped sediments. Pink coloured biomicrite has been deformed into sub metre-scale isoclinal, recumbent soft sediment folds, generally facing to the east and overturned to the west (Figs.3.4 and 3.5). The succession passes back into 17m of fine-grained sandy turbidites, as evidenced by sedimentary structures such as normal grading and sole marks. The top of the Celeptas Formation consists of more sandy material containing randomly oriented metre-scale blocks of pelagic limestone, which contain a fauna of the pelagic foraminifera *Globotruncana* sp.

North Celeptas section (Fig. 3.3)

This log begins near the top of the Yukaritirtar Formation because in the field it was hard to determine the precise contact (owing to the absence of the pelagic foraminifera *Globotruncana* sp.) with the underlying Maastrichtian Tasevi Formation. A section, 5m thick, of grey extremely well-bedded biomicrite with abundant radiolaria, interbedded with fine granular redeposited limestone beds then grades conformably into 11m of pink shaley/silty limestone of the upper unit of the Yukaritirtar Formation. A faulted contact with minimal displacement separates the Celeptas Formation, which consists of extremely well-bedded, medium grained sandstone and pink shaley limestone turbidites at this locality. The sequence continues for 9m before passing into a 2-3m slumped horizon, which has erosive contacts with the lowermost unit. This horizon consists exclusively of pink muddy limestone plastically deformed into metre-scale recumbent soft-sediment folds. The fold data, when plotted on stereonets as poles to the axial surface indicate a northeasterly vergence direction (Fig.3.5). Normal sedimentation resumes above, with 15m of thinly bedded fine sandstone, mudstone and debris flow deposits. Large blocks up to 10m in size are included in this sandy matrix. The blocks consist exclusively of variably oriented Upper Cretaceous *Globotruncana* limestone and intensely slumped pink pelagic limestone, similar to those lithologies further down the succession.

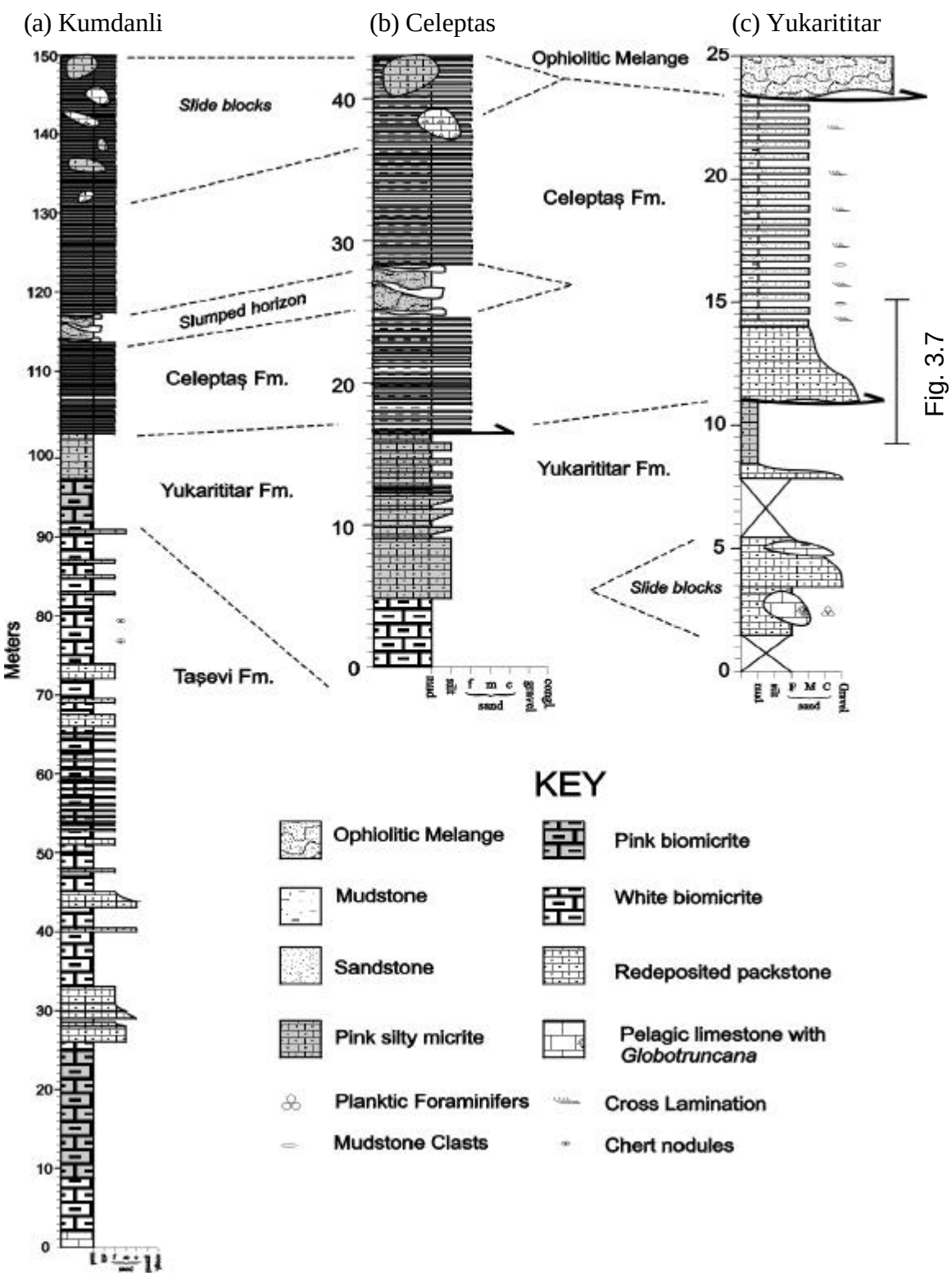

Fig.3.3 Measured logs through the top of the autochthonous carbonate platform sequence (see Fig. 3.12 for location)

Fig. 3.4 Field photograph and line drawing showing soft-sediment slump folds within the Celeptas Formation. Photograph taken of fallen block 26m upsection on the Celeptas measured section (Fig. 3.3). Hammer is 30cm long.

Yukarititar measured section (Fig. 3.3)

This section also starts halfway up the Yukaritirtar Formation because of the difficulties with identifying in the field the contact with the underlying Tasevi Formation. The measured log begins with well-bedded grey biomicrite before passing into ca.20m of normally graded coarse-fine packstone-wackesone with lenses of limestone conglomerate. Incorporated within this lithology are large blocks, up to 10m in size, of Upper Cretaceous pelagic limestone with the pelagic foraminifera *Globotruncana* sp. At the top of this local sequence thin beds of grey micritic limestone yield a fauna, including *Nummulites* sp., *Discocyclina* sp. and ?*Globigerina* sp.?, before passing into 2.5m of well-bedded pink micritic pelagic limestone. The sequence then passes into 3m of normally graded coarse-fine grained, redeposited packstone with what appears to be an erosive lower contact. However, this contact is deceptive as it is a minor thrust décollment, with a top to the NW sense of displacement (Fig.3.7). The evidence for this interpretation is the angular discordance that exists between the beds above and below the décollment and the shear fabrics locally developed below and along the décollment. The Celeptas Formation rests conformably on top and consists of 9.5m of cm-dm beds of coarse-fine grained packstone, sandstone and mudstone turbidites. Sedimentary structures are abundant in this horizon, including load structures on basal surfaces, mudstone rip-up clasts, normal grading and low angle cross lamination in the more coarse grained beds. Palaeocurrent data collected from these beds indicates a general northwesterly flow (Fig.3.6). The section ends with Ophiolitic Melange resting on top with a low-angle thrust contact.

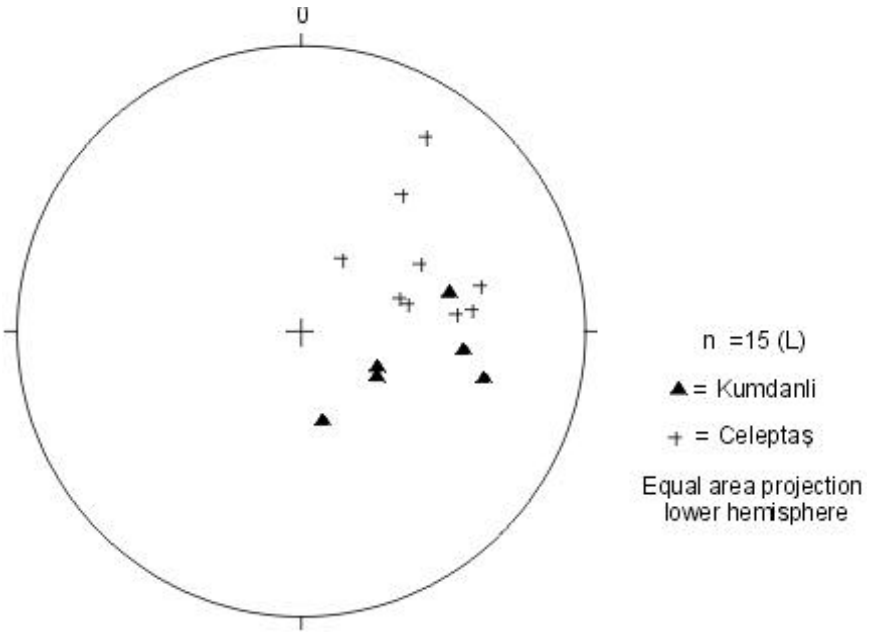

Figure 3.5 Poles to planes of axial surfaces (i.e. vergence) collected from soft-sediment slumps within the Early Tertiary sequence at Kumdanli and Celeptas. Data are uncorrected for post-Eocene rotation.

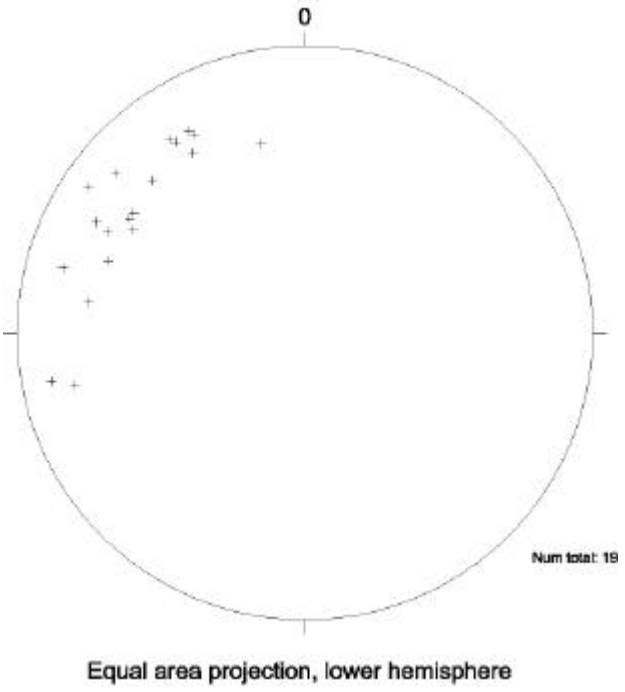

Fig.3.6 Palaeocurrent data (cross laminations) from the Celeptas Formation, collected near Yukarititar village (see Fig.3.3 and 3.12)

Fig.3.7 Field photograph and line drawing of boundary between the Celeptas and Yukarititar Formations. See Figures 3.3 and 3.12 for location. Prominent redeposited packstone bed in photo is ca. 11m upsection on Log 176 (Fig. 3.3). The lower boundary of this bed is a minor shear décollement as evidenced by C-S shear fabrics and cross cutting relationships.

3.2.1.3 The Anamas Dag autochthon in the Sarkikaraagaç area

In the eastern Pisidian Taurus Mountains the B-H Nappes overlap the boundary between the two autochthonous series: the Sultan Dag (described in chapters 3.2.1.1 and 3.2.1.2) and the Anamas Dag in the west. The exact nature of this boundary is unclear, but the slight differences between the stratigraphy are widely believed to reflect a palaeogeographical difference (e.g. Robertson & Dixon, 1984 and references therein). For the purposes of this study, the Anamas Dag can be considered the extension of the Akseki platform in the southeast, which has previously been discussed in Chapter 2.3. To avoid repetition the reader is referred to this chapter and Fig 2.3 for an outline of the stratigraphy.

As in the Beysehir area, the Palaeocene-Lower Eocene top of the carbonate platform succession passes into a Mid-Eocene turbidite sequence termed the Gölgeli Formation, which has been subsequently dated by M. Görmüs through the identification of the following microfossil assemblages: *Nummulites* cf. *Milleodut*, *Nummulites* sp., *Discocyclina* sp., *Assilina* cf. *Exponens*, *Globigerina* sp., *Europertia magna* and *Smountina* sp. (Elitok, 2000, 2002).

3.2.2 Allochthonous Units

In this eastern Pisidian Taurus area, the allochthonous B-H Nappes were emplaced directly onto the uppermost level of the autochthon. The following sections discuss the main features of the Nappes in these areas.

3.2.2.1 The B-H Nappes in the Sarkikaraagaç region (Fig.3.8)

Figure 3.8 shows a geological map of the B-H Nappes to the north of Lake Beysehir. Like the extension of the units to the south, the Nappes have a broadly synformal geometry. The lowermost unit at the bottom of the thrust pile consists of coherent thrust sheets of ophiolite-related lithologies, the main outcrops of which form Kizildag (1903m) to the south of Sarkikaraagaç town and the eastern foothills of the Anamas Dag (ranging from 1963-1421m). Together, these two main outcrops are known as the Kizildag ophiolite (Elitok, 2000). The contact to the east is obscured by Quaternary alluvium, but is inferred to be tectonic, with the Kizildag ophiolite having been emplaced onto the Sultan Dag autochthon. The contact to the west with the Anamas Dag is now neotectonic in origin. The Kizildag ophiolite forms the northeasterly hanging wall of a dextral oblique fault array (Senel *et al*., 1997), the extension of which continues along the western margin of Lake Beysehir. During the course of this study these allochthonous units were investigated with the following findings.

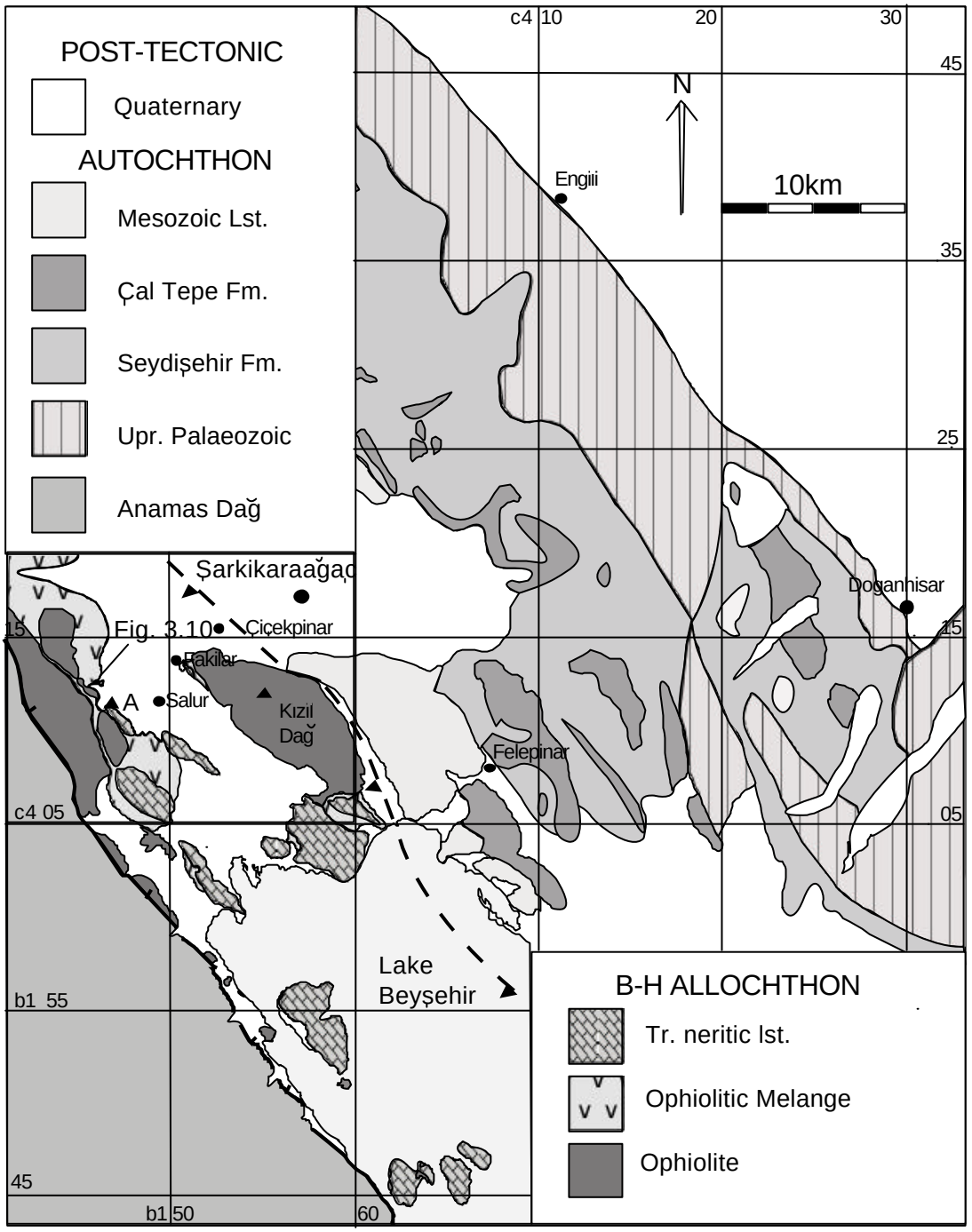

Fig.3.8 Geological map of the Sarkikaraagaç area north of Lake Beysehir. Adapted from Monod (1977), Senel (1997) and authors own mapping (boxed area around Salur village). A, Agilkaya Tepe. For location see Fig. 3.1.

3.2.2.1.1 Kizildag ophiolite

The Kizildag ophiolite consists of two main units; 1) a lower sub-ophiolitic metamorphic assemblage (ca.150m thick), and 2) an upper ca. 800m thick peridotite thrust sheet. The reported type section for the sub-ophiolitic metamorphic sole is to the north of Yenicekale village (Fig. 3.8), 15km due west of Sarkikaraagaç (Elitok, 2000). At this locality lithologies within the metamorphic sole include amphibolite, gneissic amphibolite, amphibole schist, quartzite, dolerite, calcschist and serpentinite. Other lithologies were also incorporated as blocks from the underlying sedimentary sequence.

The upper part of the Kizildag ophiolite is predominantly harzburgitic peridotite, which is variably serpentinised. Locally, in the highest levels of the ophiolite the peridotite has a dunitic composition with small chromite pods. In the eastern part of the Kizildag ophiolite pyroxenite dykes and small-scale altered gabbroic intrusions are also found locally (Elitok, 2000). Isolated dolerite dykes cut the ophiolite, a number of which are affected by calcic metasomatism (rhodingitisation). A more in-depth look at the igneous geochemistry of these ophiolitic rocks is given in Section 6.3.

3.2.2.1.2 Ophiolitic Mélange

In the Sarkikaraagaç area, Ophiolitic Melange lies above the ophiolite and comprises a number of exotic lithologies as blocks set in a moderate to highly sheared fine-grained matrix. Good sections through the mélange are not abundant; hence, it is hard to give a detailed account of all the lithologies present. One locality 4km west of Salur village, however, shows a well-developed section through the sequence which illustrates the wide range of lithologies incorporated in the melange (Fig.3.10). The chosen section arbitrarily begins with a large block, ca.150m in size, of gabbro, locally pegmatic in places and then continues through ca.200m of melange matrix and smaller exotic inclusions to the next large ophiolitic block; which comprises a ca.300m thick imbricated thrust sheet of sheeted dykes. A number of samples were collected for geochemical analysis, the results of which are presented in Section 6.3.4. The melange matrix of the chosen section consists of moderately-highly sheared volcaniclastic sandstone and olive/brown mudstone throughout. Shear fabrics within this matrix are extremely variable, but strike generally with a NW-NE trend with a high dip towards the east.

Even though no coherent sequence of condensed pelagic limestone and chert (e.g the upper section of the Boyali-Tepe Unit) exists as a coherent unit in this area, isolated blocks do exist in the melange as seen in the section above. Another locality where this type of succession is seen near Fakilar village (Fig.3.9). Here a ridge of limestone runs NW-SE to the east of the village which consists of a thin thrust slice, approximately 100m thick, of neritic carbonate overlain by a condensed pelagic sequence of pink nodular limestones (Fig.3.9)

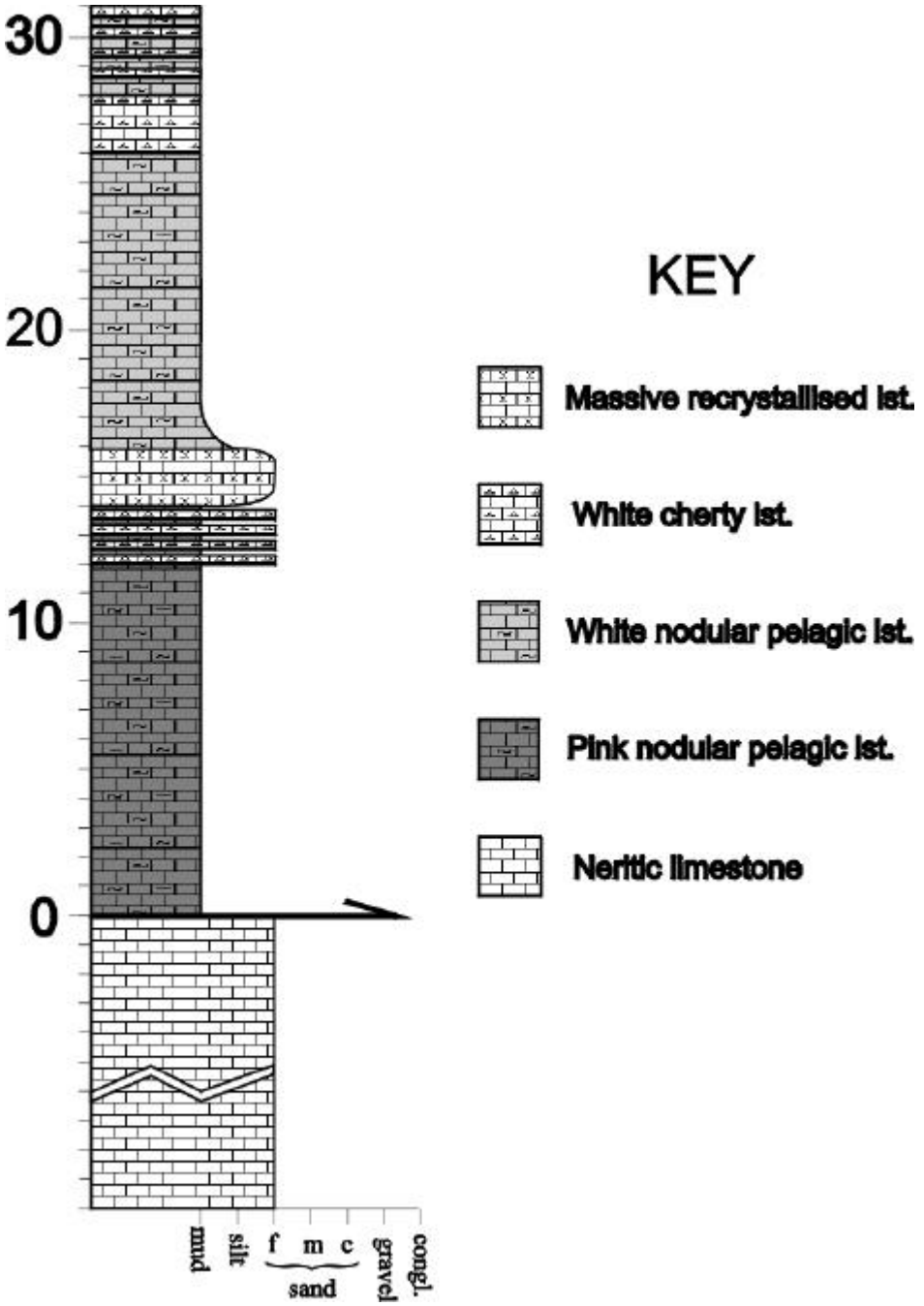

Fig.3.9 Measured log through Ammonitico Rosso sequence at Fakilar village.

Fig.3.10 Sketch section through the Ophiolitic Melange west of Salur village.

3.2.2.1.2 Triassic neritic carbonate thrust sheet

The uppermost levels of the B-H Nappes in this area are occupied by a thrust sheet predominantly composed of Upper Triassic neritic carbonate. The contact with the underlying units is well preserved in a small quarry, ca.2.5km to the west of Salur village on the northern side of Agilkaya Tepe (Fig.3.8). At this locality massive white recrystallised neritic packstone-wackestone has been thrusted onto the Ophiolitic Melange. The basal contact is marked by a 5m-thick tectonic breccia, comprising m-sized, extremely poorly sorted, angular clasts of limestone (fragmented *in situ)*, before passing into the melange proper. Upper Triassic age (Fig.3.11).

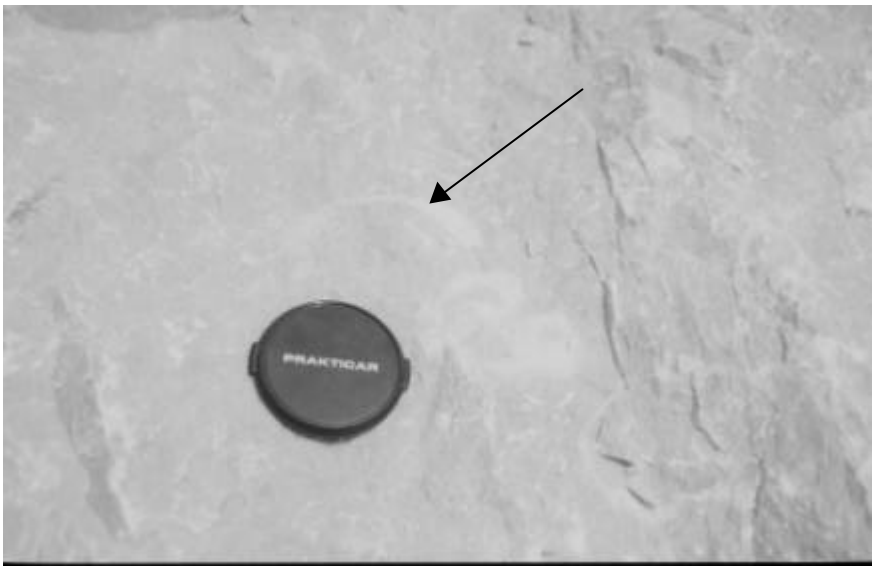

Fig.3.11 Field photograph showing *Megalodons* in Triassic neritic carbonate. Photograph is of fallen block in quarry ca. 2.5km west of Salur village. Arrow indicates shell.

Previously, this unit was correlated with the Gencek Unit (Chapter 2.6.1) of the Beysehir area (Monod, 1977; Gutnic *et al*, 1979) and the Domuz Dag Unit of the Lycian Nappes (Senel *et al*., 1997). The view favoured here is that this unit represents the northerly extension of the Gencek Unit, because all aspects of this lithology are identical and a direct correlation between the Lycian Nappes and the B-H Nappes (two similar but separate Nappe systems in their own right) is an oversimplification of the regional tectonics. A more detailed discussion of regional tectonostratigraphic correlation is given in Section 7.1.

3.2.2.2 The B-H Nappes in the Kumdanli region (north of Lake Hoyran)

The Kumdanli region is tectonostratigraphically the most simplistic area with only two subdivisions of allochthon (e.g. Demirkol, 1984). Like the B-H Nappes elsewhere, they exhibit a synformal geometry. The lowermost unit consists of Ophiolitic Melange emplaced onto the local autochthon, the Sultan Dag. This is overlain by a thrust sheet of Triassic neritic carbonate, known locally as the Kumdanli limestone (Demirkol, 1981). These allochthonous units were investigated with the major findings as follows:

3.2.2.2.1 Ophiolitic Melange

The lowest structural position in the Kumdanli area is occupied by the Ophiolitic Melange. Unlike the Sarkikaraagaç area, no coherent thick slices of ophiolite-related rocks are present. A thickness of the melange is hard to determine because no complete section through the poorly exposed sequence exists and extensive neotectonic faulting adds to the complexity; however, a thickness of ca. 500m is estimated. Earlier work on the lithologies incorporated into the melange concentrated on identifying the larger (km-scale) mappable blocks (e.g. the Aydogmus Limestone: Jurassic neritic limestone, Kuzutasi Limestone: Maastrichtian pelagic limestone and Derebag radiolarite units of Demirkol, 1981). Consequently, equally important numerous smaller blocks in the melange were previously disregarded.

The melange matrix generally consists of highly sheared chocolate brown mudstone, although locally a much coarser nature is seen. For example, 3km east of Armutlu village at Kuzutasi Tepe the melange matrix consists of coarse chert/volcaniclastic debris flow deposits with blocks of oolitic packstone, chert and vesicular basalt floating in the matrix. Various exotic lithologies are incorporated into the melange including debris flow deposits, neritic limestone, radiolarian chert, pink pelagic limestone, nodular pelagic limestone, serpentinite (Fig.3.13), diabase, gabbro and cherty sandstone.

As in the Sarkikaraagaç region, no coherent sequence of condensed pelagic limestone and chert exists above the melange (i.e the Boyali Tepe Unit of the Beysehir area). However, similar lithologies are incorporated into the melange as blocks, a good example of which is located 1.5km to the NW of Kumdanli village. At this locality a large block, ca.80m thick, of coarse limestone talus breccia is entrained in the Ophiolitic Melange. Elements within the block are predominantly composed of angular to semi-rounded clasts of white neritic limestone, pink pelagic limestone and chert. Minor sedimentary reworking forms lenses of locally derived laminated mudstone and grit (Fig.3.14).

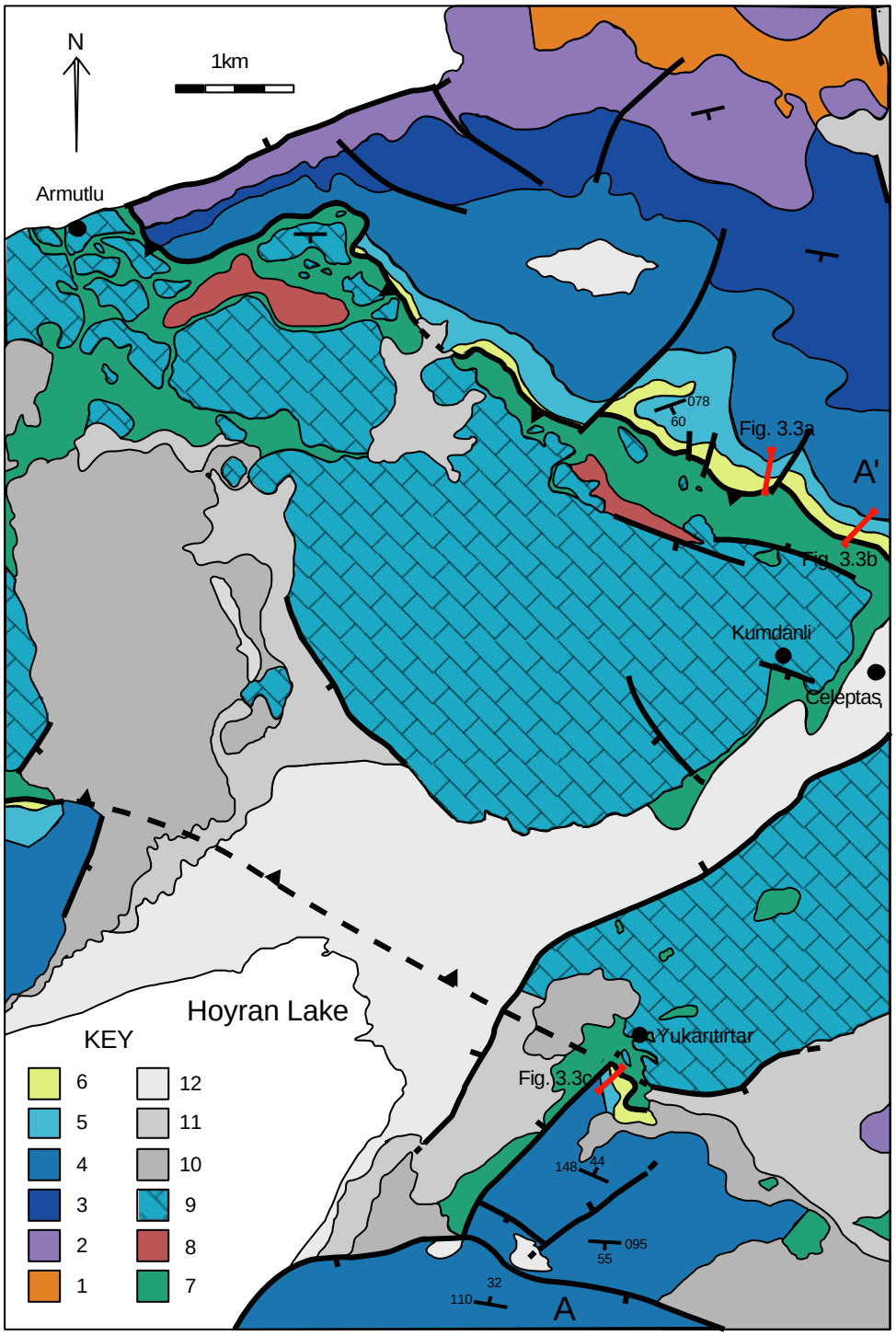

Fig.3.12 Geological map of the Kumdanli area (field checked and redrafted from Demirkol, 1984). **1**, Sultandede Fm; **2**, Hacialabaz Fm; **3**, Tasevi Fm; **4**, Gölcük Fm; **5**, Yukarititar Fm; **6**, Celeptas Fm; **7**, Ophiolitic Melange; **8**, Radiolarian chert; **9**, U. Triassic neritic limestone; **10**, Miocene cover; **12**, Pliocene cover; **12**, Quaternary alluvium.

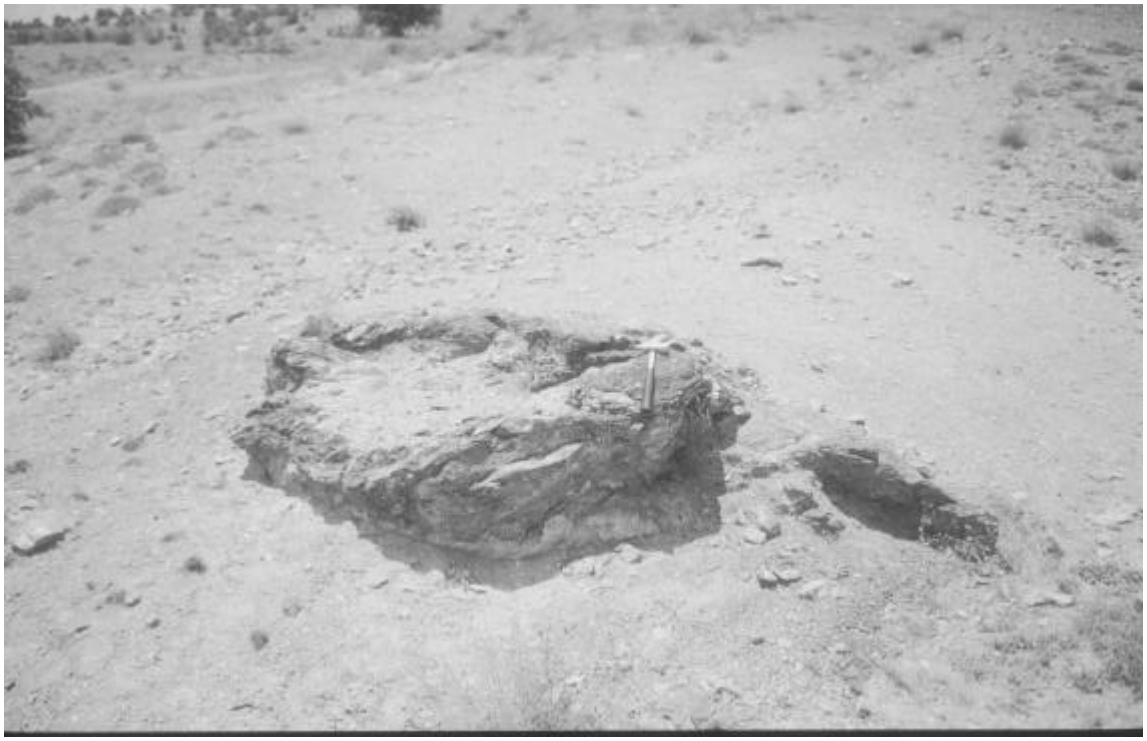

Fig.3.13 Serpentinite block in negative weathering Ophiolitic Melange, near Armutlu village. Hammer is 30cm long.

Fig.3.14 Limestone breccia with affinities to the Boyali Tepe Unit in Ophiolitic Melange, ca. 1.5km NW of Kumdanli.

3.2.2.2.2 Upper Triassic-Lower Jurassic neritic limestone thrust sheet: the Kumdanli limestone

Structurally overlying the Ophiolitic Melange is a carbonate thrust sheet, locally known as the Kumdanli limestone. It is a grey-white neritic limestone, that is generally massive and recrystallised, but regularly jointed and locally dolomitised. A fauna of *Involutina sinuosa*, *Thaumatoporella* sp. and *Valvulina* sp. recovered from the limestone implies an Upper Triassic-Lower Jurassic age (Demirkol 1981, 1984). Using modern melange terminology the thrust sheet would be classified as 'broken formation' (e.g. Raymond *et al*, 1984), as the unit forms disrupted thrust sheets of blocks, upto 5km long, floating within the Ophiolitic Melange. Consequently, a detailed log of the entire succession is not possible because no meaningful correlation between the variably oriented blocks exists.

3.3 Tectonostratigraphy of the western Pisidian Taurides: the Dinar area (Fig.3.15)

After passing to the north of Lake Hoyran the strike of the B-H Nappes swings to the west and forms a bow-shaped outcrop 70km long and 10km wide (Fig.3.1). The nappes were subsequently covered by Neogene volcanics and Quaternary sediments, hence the outcrop appears fragmentary. The absolute western limit of the B-H Nappes occurs close to the town of Dinar, where Quaternary sediments, influenced by Neotectonic faulting, overlie and obscure the relationship with the Lycian Nappes to the west. The final study area of the B-H Nappes in the Pisidian Taurus Mountains was chosen in this area because of excellent exposure, ease of access and an important change in tectonostratigraphy. The Dinar area differs from the other Pisidian Tauride locations as the B-H Nappes in this area consist of three separate tectonostratigraphic units (Fig.3.15). Previously published maps and logs by Gutnic (1977) were field checked and remeasured; in particular, the role of recent extensional faulting was reassessed. Palaeotectonic and neotectonic features were not previously distinguished, e.g. tectonic breccias in the footwall of faults were inferred to be sedimentary in origin. In addition, several tectonic units were found to be structural repeats, either due to thrust imbrication or extensional faulting. The new revised map is shown in Fig. 3.15.

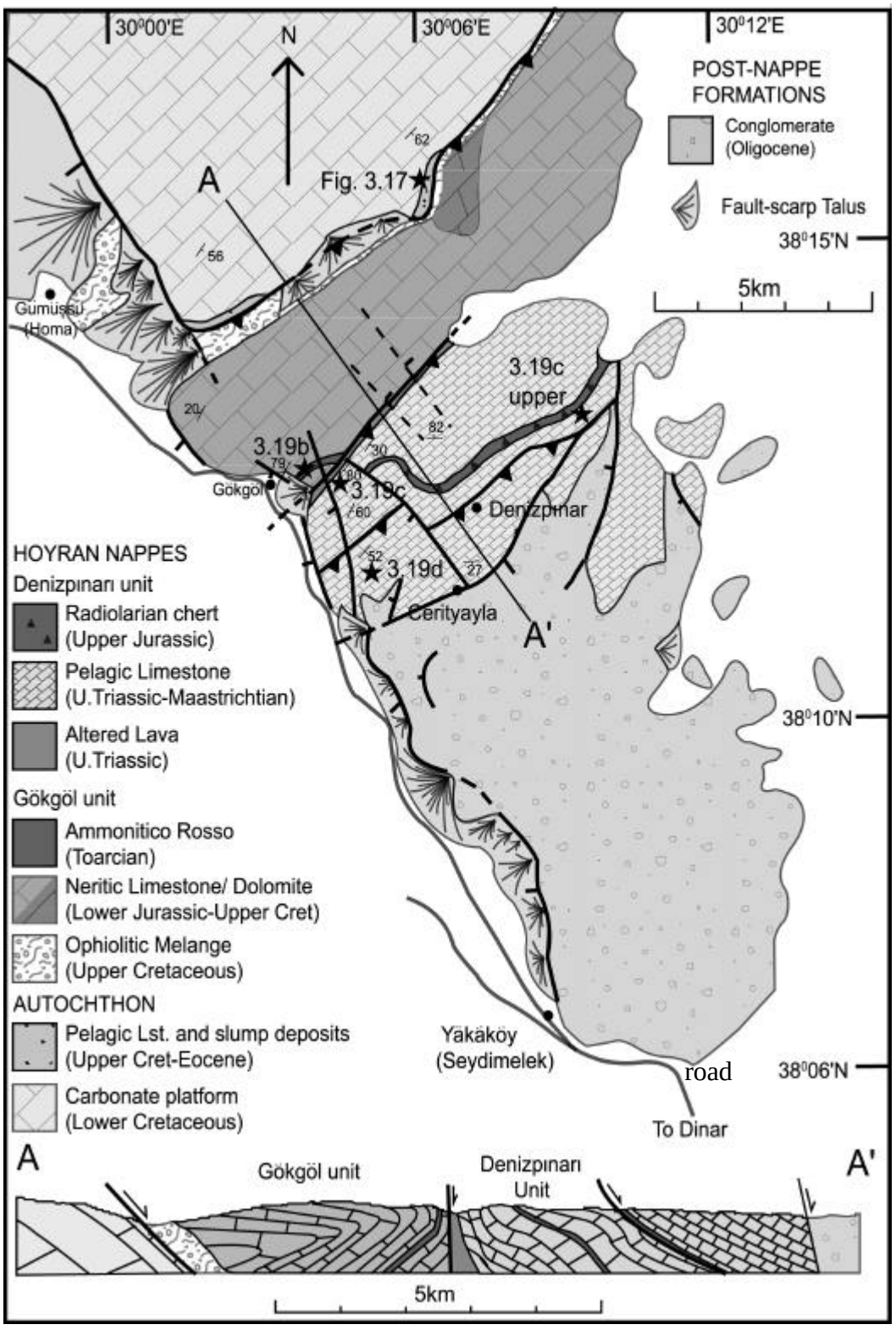

Fig.3.15 Geological map and cross section of the Dinar area (field checked and revised after Gutnic, 1977).

3.3.1 Regional Autochthon

The regional autochthon in the Dinar area is the extension of the Sultan Dag from the east. In this area, however, Precambrian basement, not seen in other areas, crops out (Gutnic, 1977; Gutnic *et al.*, 1979; Gürsu & Göncüoglu, 2001). Figure 3.16 shows the main subdivisions of the Precambrian to Early Palaeozoic autochthonous sequence in the Dinar area. The Palaeozoic-Mesozoic sequence was field checked, but no major work was necessary in redefining the tectonostratigraphy.

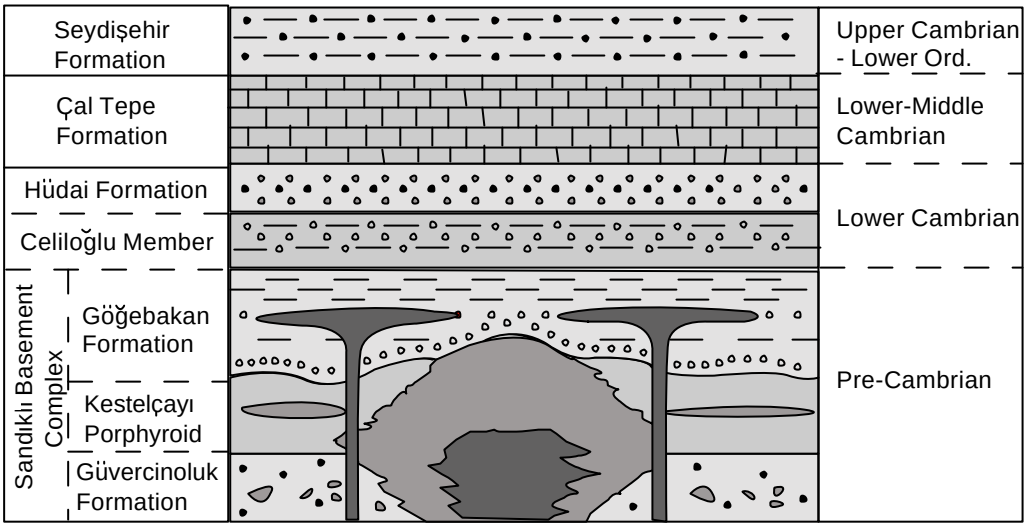

Fig.3.16 Generalised columnar section of the Lower Palaeozoic of the Sandikli (Dinar) area (from Gürsu & Göncüoglu, 2001).

3.3.1.2 The Precambrian Sandikli Basement Complex

The main outcrop of the Sandikli Basement Complex is found to the west of the town of Sandikli in western Central Anatolia. (Fig.3.1). The lowermost member (Güvercinoluk Formation) comprises a ca.800m sequence of low-grade metamorphosed and well-foliated, interbedded siltstone, sandstone and 'olistostromal' conglomerate, with rare dolomitic lenses. This is overlain and intruded by the Kestelçayi Porphyroid Suite, which is characterized by a deformed and highly sheared dome-shaped rhyolitic-dacitic body with a granitic core. This suite commonly has a mylonitic fabric overprinting the original igneous texture. The top of the Sandikli Basement Complex is represented by the Gögebakan Formation, which unconformably overlies the underlying formations. The lower part of the Gögebakan Formation is represented by basal conglomerates composed predominantly of rhyolite, lydite and recrystallised

limestone clasts, which pass vertically into intensly folded mudstone with intercalations of arkosic sandstone. This is interstratified with andesitic lava and pyroclastic flow deposits. A suite of doleritic dykes cuts all lithologies. The Gögebakan Formation passes transitionally into the Celiloglu member of the Early Palaeozoic Hüdai Formation (Göncüoglu and Kozlu, 2000; Gürsu & Göncüoglu, 2001).

3.3.1.3 Early Palaeozoic autochthonous succession: the Hüdai, Çaltepe and Seydisehir Formations.

The lowermost subdivision of the Hüdai Formation is locally known as the Celiloglu member, which consists of siliceous mudstones and quartzites, before passing into the Hüdai Quartzite Formation proper (Gürsu & Göncüoglu, 2001). Abundant trace fossils are preserved in the lower parts of the formation, which include *Cruziana* spp., *Rusophycos* spp., *Phycodes* spp., *Planolites* spp., *Diplichnites* spp., *Arenicolites* spp. and *Skolithus* spp. This ichnofossil assemblage indicates an Early Cambrian (Tommotian) age (Erdogan *et al*., 2001). The succession above passes into the Çaltepe and Seydisehir Formations, previously discussed in Chapters 2.3.1.1 and 2.3.1.2.

3.3.1.4 Mesozoic carbonate platform

The lower Palaeozoic sequence in this area is unconformably overlain by a Jurassic-Upper Cretaceous carbonate succession (Gutnic, 1977), similar to the Hacialabaz Formation, seen to the NW of Hoyran Lake (Demirkol, 1984). This succession was described in section 3.2.1.3. The thick (>500m) carbonate sequence forms some of the highest peaks in the Pisidian Taurus Mountains (e.g. Homa Ak Dag).

3.3.1.5 Early Tertiary

Upper Cretaceous well-bedded *Globotruncana*-bearing micritic limestone, situated towards the top of the Mesozoic sequence, passes conformably into disrupted Early Tertiary pelagic limestones and clastic sediments (Gutnic, 1977; Gutnic *et al*., 1979). No detailed data previously existed for the Early Tertiary succession; however, during this study detailed mapping and sedimentary logging show that rapid lateral and vertical facies changes exist (Figs.3.17 and 3.18). This is well illustrated in a locality approximately 8km to the ENE of Gumussu (formerly Homa) village (Figs. 3.15 and 3.17).

At this locality well-bedded cherty micritic limestones become increasing interbedded upsection with granular packstone, which constitutes 5-20% of the bedded lithologies. Where interbeds of packstone become more prominent, the sequence is slightly disrupted with discontinuous zones of soft-sediment slumping. Commonly, the disrupted beds form gently inclined to recumbent sub-horizontal asymmetrical folds verging to the west (Fig.3.5). In total, the thickness of this disrupted zone is ca. 50m. The sequence

passes back into less disrupted cherty micrites; however, zones of slumping are generally discontinuous and cannot be correlated laterally. Associated with the disrupted sequence are channelised pebbly limestone conglomerates (Fig. 3.18). This sequence remains undated, although if lithologically correlated with similar successions further east (i.e.Yukaritirtar Formation; chapter 3.2.1.2) a Palaeocene age is probable.

Locally above (but generally absent) is an 8m-thick sequence of pink pelagic biomicrite and silty limestone, similar to that of the Yukaritirtar Formation (chapter 3.2.1.2). Commonly, the lithology is cut by a spaced pressure solution cleavage giving it a distinctive wavy appearance.

The top of the section is represented by sandy turbidites and debris flows, of which only the lowermost ca. 10m is well exposed. Lower Eocene fauna have been recovered from the matrix, which includes the foraminifera *Nummulites* sp. and *Discocyclina* sp. (Gutnic, 1977). Cherty pelagic limestone, similar to that seen lower in the sequence, forms large blocks, up to 100m thick and 500m long, set in the sandy matrix of the debris flow deposit.

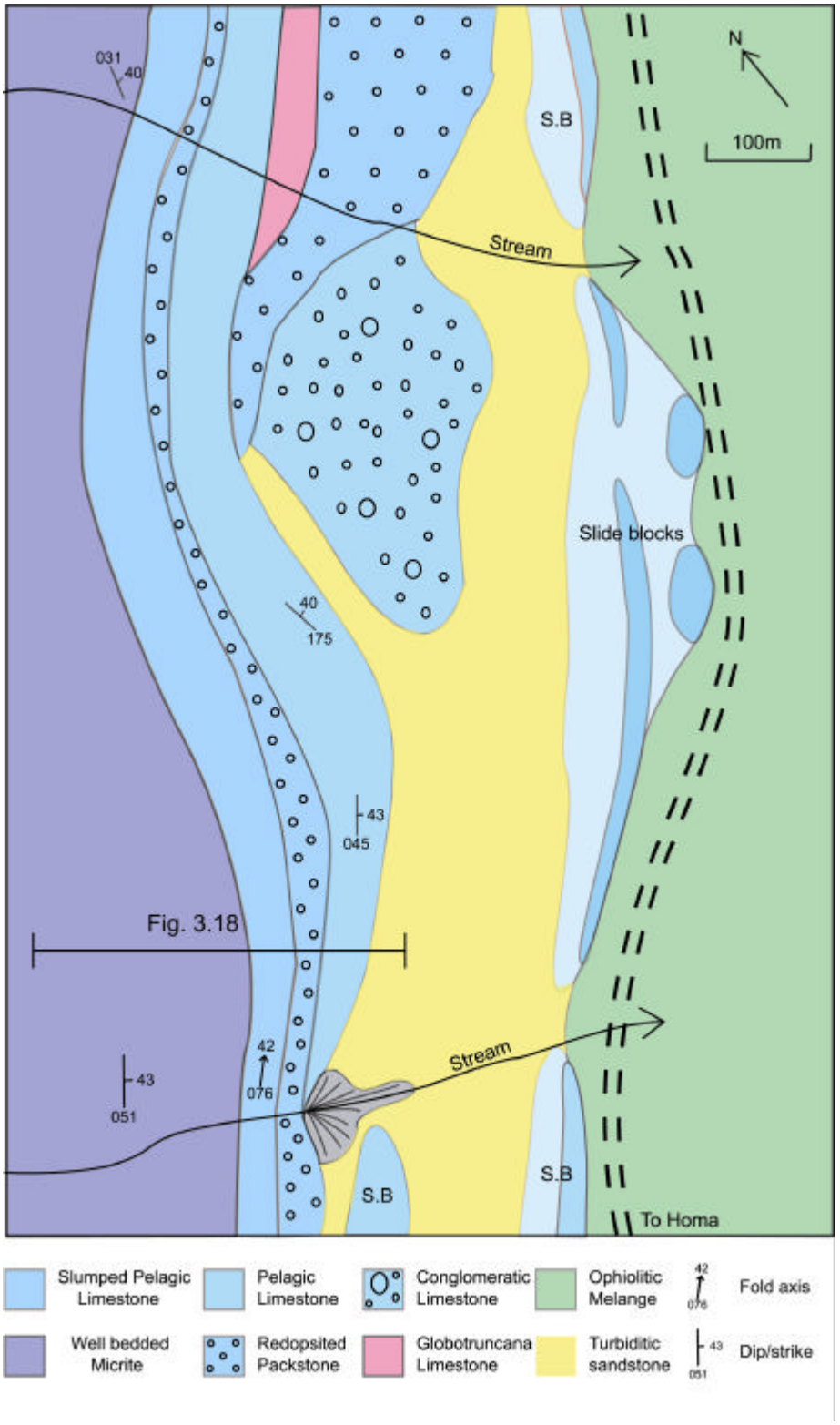

Fig.3.17 Detailed geological map of the top of the autochthonous succession exposed 8km ENE of Homa, showing lateral facies changes from channelised limestone conglomerate to sandstone (See Fig.3.15 for location).

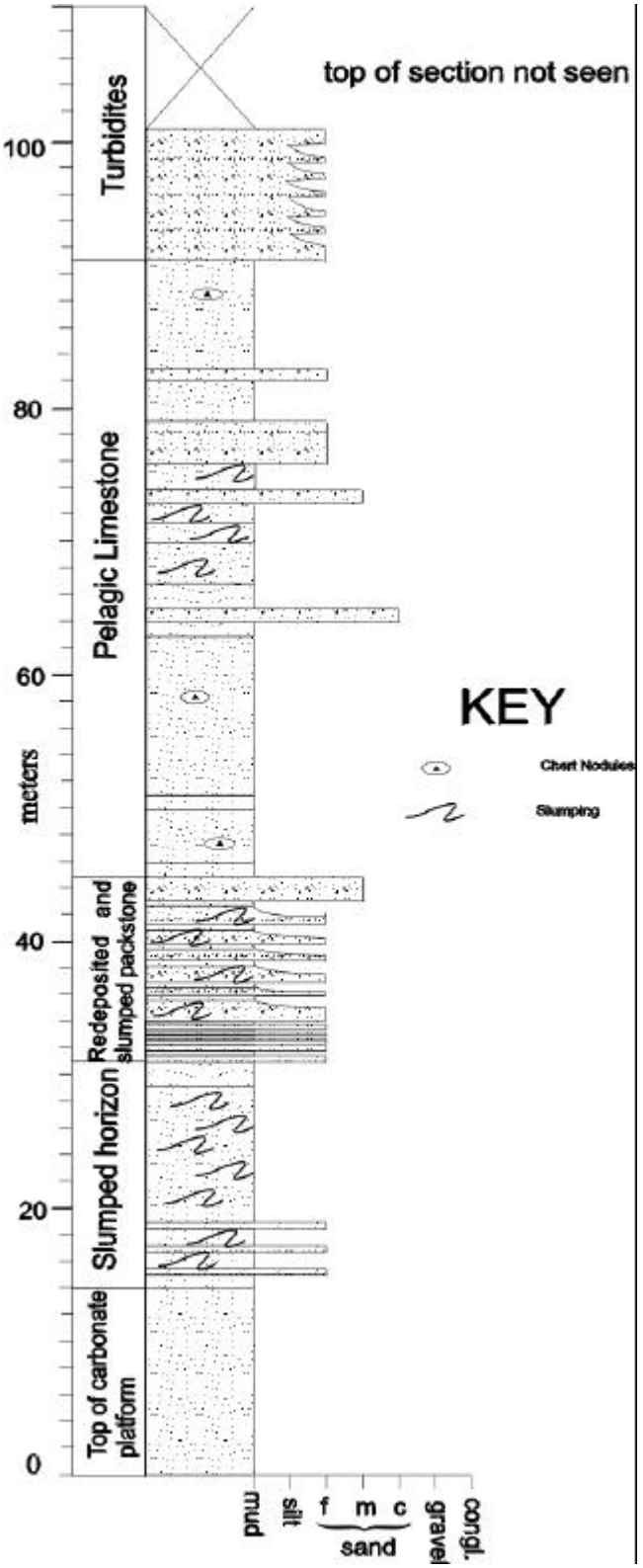

Fig.3.18 Measured log through the top of the autochthonous sequence in the Dinar area (Log 173 on Fig.3.17).

3.3.2 Allochthonous B-H Nappes in the Dinar area.

The B-H Nappes in this area form a small inlier covered at its margins by Quaternary sediments. Unlike elsewhere in the Pisidian Taurides, in the Dinar area the B-H Nappes are more complex and are composed of three tectonostratigraphical units, i.e. 1) Ophiolitic Melange, 2) Triassic-Upper Cretaceous Gökgöl Unit and 3) Mid-Triassic to Upper Cretaceous Denizpinari Unit. The south-eastern limits of the nappes are covered by Oligocene conglomerates (Gutnic, 1977). The allochthonous B-H Nappes were investigated during the course of this study, with new logs and data measured and presented below:

3.3.2.1 Ophiolitic Melange

The Hoyran Nappes begin with Ophiolitic Melange resting directly upon the autochthon. The melange consists predominantly of highly sheared volcaniclastic sandstone and mudstone, with metre-scale blocks of pelagic limestone, basalt, serpentinite and ribbon radiolarian chert floating in the matrix. The blocks of pink micritic limestone in the melange contain a fauna of pelagic foraminifera, including *Globotruncana* sp., which indicate an Upper Cretaceous age. The pelagic limestone is depositionally associated with pillow lava blocks in the melange. Approximately 5km east of Gumussu (formerly Homa), along the track to Düzbel (Fig.3.15) this relationship can be observed clearly. Blocks of highly sheared pillow lavas, with interstitial chert sediment, are spatially associated with pelagic limestone blocks and locally can be seen to be intergradational. Interstitial chert from the pillow lavas was collected with a view to date the timing of extrusion; however, when the chert was processed (methodology shown in Appendix A) the radiolarian fauna was found to be too sparse and recrystallised to be determinable. However, an Upper Cretaceous age can be inferred with some confidence from the relationship with the pelagic limestone blocks. Samples of basalt were collected from this locality for geochemical analysis, the results of which are presented in Section 6.2.

3.3.2.2 Gökgöl Unit

The lowest thrust sheet, the Gökgöl Unit (<500m, Fig.3.19b), comprises Triassic-Upper Lias neritic dolomite and limestone, depositionally overlain by a Toarcian to Upper Cretaceous pelagic succession (Gutnic, 1977). The unit is asymmetrically folded and stratigraphically inverted, with the NW limb gently dipping to the SE, but in the vicinity of Gökgöl village the SE limb is vertical to steeply dipping to the NW (Fig.3.15).

The major part of this unit comprises 300-400m of thick-bedded Upper Triassic neritic limestone, locally dolomitised at the base (Fig. 3.21). Common carbonate lithologies within the unit include grainstone and packstone, frequently with disarticulated bivalves, oncoids and other algal remains.

To the east of Gökgöl village, well-bedded pink nodular limestone (Ammonitico Rosso) is seen overlying the lower neritic limestone. This lithology contains an abundant fauna of ammonites. Previous studies have determined the following species, including *Phymatoceras elegans, Coeloceras (Telodactyhites)* cf. *remzi, Mercaticeras* cf. *mercati, Phymatoceras* sp., *Lytoceras* sp. and *Phyloceras* sp., which indicate a Toarcian age (Gutnic, 1977).

The Ammonitico Rosso is, in turn, overlain by approximately 60m of interbedded pelagic limestone and chert which marks the top of the Gökgöl Unit. The pelagic foraminifer *Globotruncana* is present, indicating an Upper Cretaceous age. The precise thickness is hard to obtain due to stratigraphic repetition and deformation caused by abundant small neotectonic extensional faults. Outcrops are obscured by a thick (upto 0.5m) fault breccia in the hanging wall of these faults, previously interpreted as sedimentary in origin (e.g. Gutnic, 1977).

3.3.2.3. Denizpinari Unit

The Denizpinari Unit lies tectonically above the Gökgöl Unit. The basal thrust which marks the boundary between the two units runs approximately along the NE-SW-trending gorge behind Gökgöl village. The eroded thrust plane provides good access to both the upper and lower units. Fig.3.19 shows a composite log through the predominantly pelagic succession measured at two localities, shown on Fig 3.15.

The lower section (Fig. 3.19c lower) begins with approximately 20m of highly sheared, but coherent, basalt. Discontinuous lenses of pink pelagic limestone (upto 0.5m thick) become more abundant, eventually forming coherent beds (1-2m thick) in normal contact with the lavas. The amount of pelagic limestone increases upsection until the sequence is entirely carbonate. The lowermost limestone consists of extremely well-bedded biomicrite, with abundant bivalve filaments (possibly *Halobia* sp.) and replacement chert nodules which occasionally coalesce into thin beds. At a specific horizon, 38m up the measured section, the pelagic carbonate is capped by a 1m thick limestone conglomerate. From this horizon upwards, redeposited limestone facies are present as fine-grained, extremely well-bedded, laminated calciturbidites, in places intercalated with radiolarian-rich pelagic limestones. Above this, between localities 3.19c and 3.19d, the succession resumes as a monotonous sequence of moderately bedded (dm) dark grey biomicrite, with thin beds of dark chert, for approximately 500m.

The top of the thick sequence of pelagic limestone is marked by redeposited limestone facies, best seen at locality 3.19c, approximately 5km SW of the village of Karti (Fig.3.15). There the sequence passes into 3m of matrix-supported limestone conglomerate, composed entirely of randomly oriented clasts of chert

and granular packstone set in a finer matrix of the same composition. The maximum clast size observed was 10cm, although the mean size was 2cm based on count size of 30 clasts spaced throughout the bed. Above, the section passes into 15m of poorly exposed, grey dm-bedded granular limestone, intercalated with thicker beds (0.5m) of coarse granular packstone.

This in turn is then overlain by a distinctive horizon, 20m thick, of ribbon radiolarian chert, interbedded with subordinate thinly bedded (5-10cm) micritic limestone and calcarenite. The calcarenite contains clasts of micritic limestone with ammonite remains. Locally the radiolarian chert is banded.

The top of the Denizpinari Unit is best observed along the track leading from Denizpinari to Karti (Fig.3.15). There, the lithology consists of well-bedded cherty pink micritic limestone with an abundant fauna of radiolaria and pelagic foraminifera, previously determined as *Globotruncana arca, G. contusa* and *G. flexuosa*, which indicate an Upper Campanian-Maestrichtian age (Gutnic, 1977; Gutnic *et al.*, 1979). The thickness of this unit is ca. 80m; however, due to the flat topography the outcrop is poorly exposed.

3.3.2.4 Cerityayla Unit

The uppermost thrust sheet of the Beysehir-Hoyran Allochthon in this area was locally known as the Cerityayla Unit. It crops out SE of the underlying Denizpinari Unit and NW of the unconformable Oligocene conglomerates (Fig.3.15). The contact with the conglomerates is normally faulted, with the Cerityayla Unit forming the hanging wall. A tectonic breccia and sub-parallel shear fabric commonly occurs in the hanging wall.

The upper nappe is predominantly composed of monotonous Triassic well-bedded micritic limestone interbedded with subordinate thick-massive granular limestone with abundant disarticulated shelly debris (Fig.3.19). Fauna recovered from the lower part of this unit include *Involutina sinuosa-pragsoides, I. sinuosa-sinuosa* and *Duostomina* sp., which indicate a Late Triassic age (Gutnic, 1977; Gutnic *et al*., 1979). The uppermost part of the thrust sheet is composed of Upper Cretaceous pink pelagic limestone (Gutnic, 1977). The lithologies are identical to the underlying Denizpinari Unit and are most likely to represent a structural repeat, rather than a separate tectonostratigraphical unit.

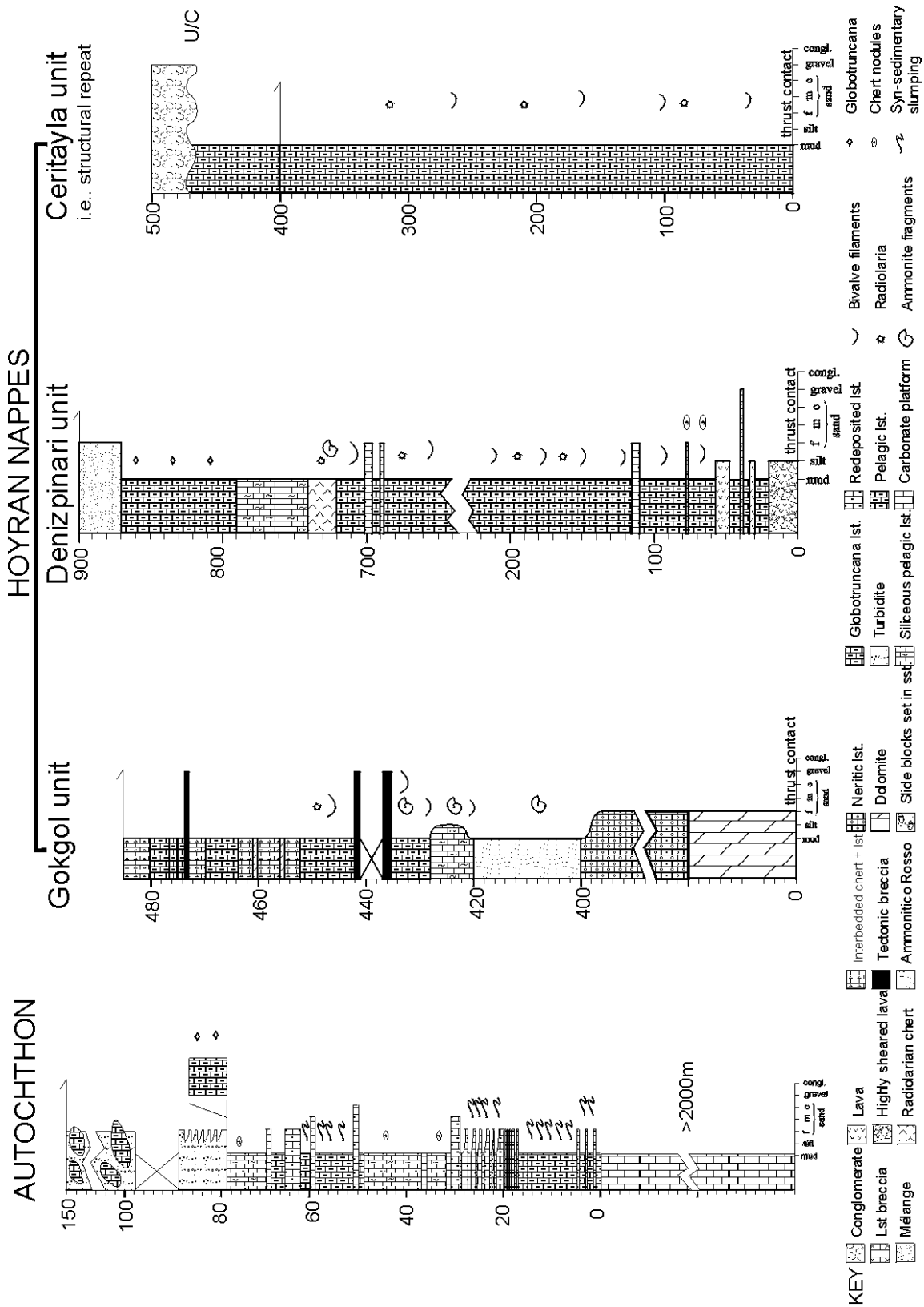

Fig.3.19 Measured logs of the Hoyran Nappes in the Dinar area.

3.4 Summary

For reference, the main lithostratigraphic data from the Sarkikaraagaç and Dinar areas are summarised in Figure 3.20. Thus, in conclusion, the following specific and general points can be made regarding the B-H Nappes and autochthonous units in the Pisidian Taurides:

1. The Palaeozoic Sandikli basement complex in the western region correlates with the Palaeozoic Sultan Dag autochthon in the east. Each of these autochthonous units share a similar Mesozoic and Early Tertiary stratigraphy.
2. The Early Tertiary top of autochthon is characterized by pelagic limestones, before passing into turbidites, debris flows and slide blocks of Mid-Eocene age. Evidence for slope instability is widespread during this time period.
3. Coherent ophiolite is only present in the Sarkikaraagaç area as thick slices of serpentinised harzburgite, locally with an amphibolite-grade metamorphic sole, all set in Ophiolitic Melange. The melange also includes blocks of sheeted dykes, gabbro, pillow lavas and radiolarian chert. Elsewhere in the Pisidian Taurides, ultramafic lithologies are restricted to blocks of serpentinite within melange.
4. Commonly, across most of the Pisidian Taurides, upper thrust sheet lithologies of the B-H Nappes are restricted to km-scale disrupted blocks of Triassic neritic limestone within the melange. Other units are present, but only as scattered blocks. Ammonitico Rosso is present as small thrust slices in the Sarkikaraagaç area, and is reworked as blocks of limestone breccia in the Kumdanli are, north of Lake Hoyran.
5. In the Dinar area, the B-H-Nappes begin with Ophiolitic Melange at the base, with no coherent ophiolite sequences present. Blocks of pelagic limestone bearing the pelagic foraminifera *Globotruncana* indicate an Upper Cretaceous age for the melange.
6. Above the melange is the Gökgöl Unit, consisting of stratigraphically inverted Triassic neritic limestones, overlain by Early Jurassic Ammonitico Rosso pink nodular limestone and finally Late Cretaceous cherty pelagic limestone.
7. The Denizpinari Unit starts with thin sheared lavas, overlain by a thick sequence of well-bedded pelagic limestone, Upper Jurassic radiolarian chert and Upper Cretaceous pink pelagic limestone.
8. The uppermost thrust sheet in the Dinar area,previously known as the Cerityayla Unit, comprises well-bedded Triassic pelagic limestones and Upper Cretaceous pink, pelagic limestone. This unit is similar to Denizpinari unit, although more imbricated; thus, is likely to represent a structural repeat.

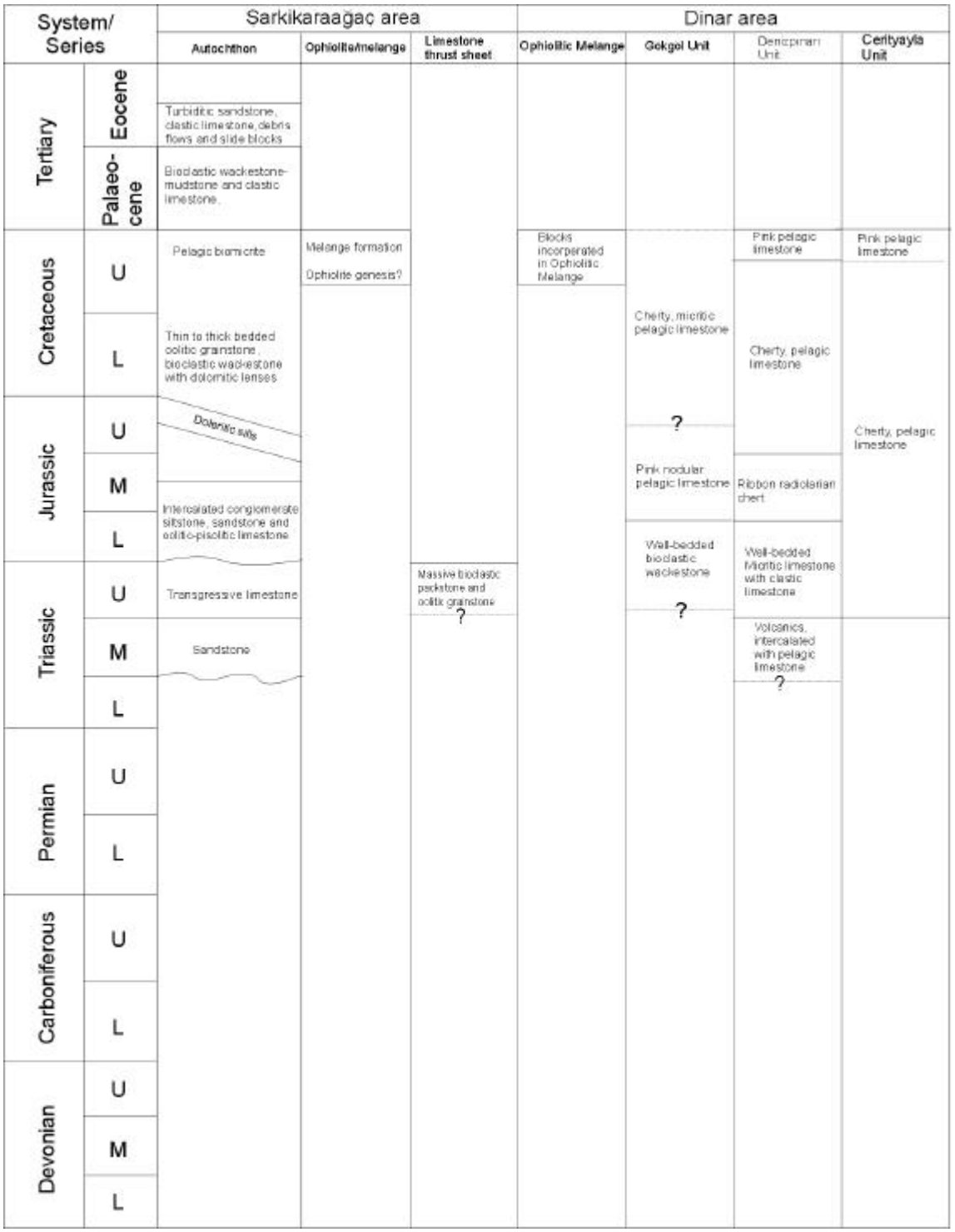

Fig. 3.20 Lithostratigraphic summary of the B-H Nappes in the Pisidian Taurides.

Chapter 4

4.TECTONOSTRATIGRAPHY OF THE B-H NAPPES IN THE BOZKIR-HADIM (CENTRAL) AREA

The Beysehir-Hoyran Nappes can be traced along strike from the preceding areas into the central Taurus Mountains. This chapter will discuss the extension of these units into this intermediate area. The focus is to detail the tectonostratigraphy of the allochthonous thrust sheets emplaced onto the underlying regional autochthon in order to facilitate regional correlations (Section 7.1). Autochthonous units previously referred to in earlier chapters are mentioned in context, but will not be dwelt upon unless significantly different from previous areas.

This area is critical for a number of reasons; 1) this central area is a link between the western and eastern areas, 2) the B-H Nappes are emplaced onto a different 'para-autochthonous' sequence not seen further west, 3) different relationships between thrust sheet stacking orders are observed and 4) an important new unit, not present elsewhere, has been identified.

4.1 Previous work

Much of the original mapping and recognition of units in the central Taurides was carried out by Blumenthal (1947, 1951, 1956, and 1960/63). However, the most comprehensive work on the classification of, and relationships between the tectonostratigraphical units was carried out by Özgül (l976, 1984, l997). This scheme is the most widely recognised in the literature, consequently the stratigraphic names introduced by Özgül (1976, 1997) are mostly retained to avoid confusion in nomenclature. In addition to his tectono-stratigraphic work, Özgül (1984) proposed a simple regional synthesis on the tectonic evolution of the Central Taurides, which is discussed in Section 7.2.4. The latest work on the B-H Nappes relevant to this study in the Bozkir area of the Central Taurides (e.g. Tekin, 1999) was a study of the biostratigraphy and systematics of radiolarian fauna from within the Dedemli Formation of the Huglu Unit.

The fieldwork focus was primarily on the Beysehir-Hoyran allochthonous units; thus, following sections discussing the tectonostratigraphy of the autochthonous units and lower thrust sheets (Sections 4.3, 4.4 and 4.5) are mostly derived from the literature. Data presented in these sections have been field checked for accuracy and original work is indicated in the text (e.g. Section 4.4.2). The majority of data presented on the Beysehir Nappes (Section 4.6) are new. Any additional relevant data from the literature are referenced accordingly. The only geological maps of the Central Taurus mountains were too large scale (i.e. 1:500,000) to permit detailed investigation of the B-H Nappes and related units. After reconnaissance, the map shown in Fig. 4.6 was drafted between the towns of Bozkir and Hadim.

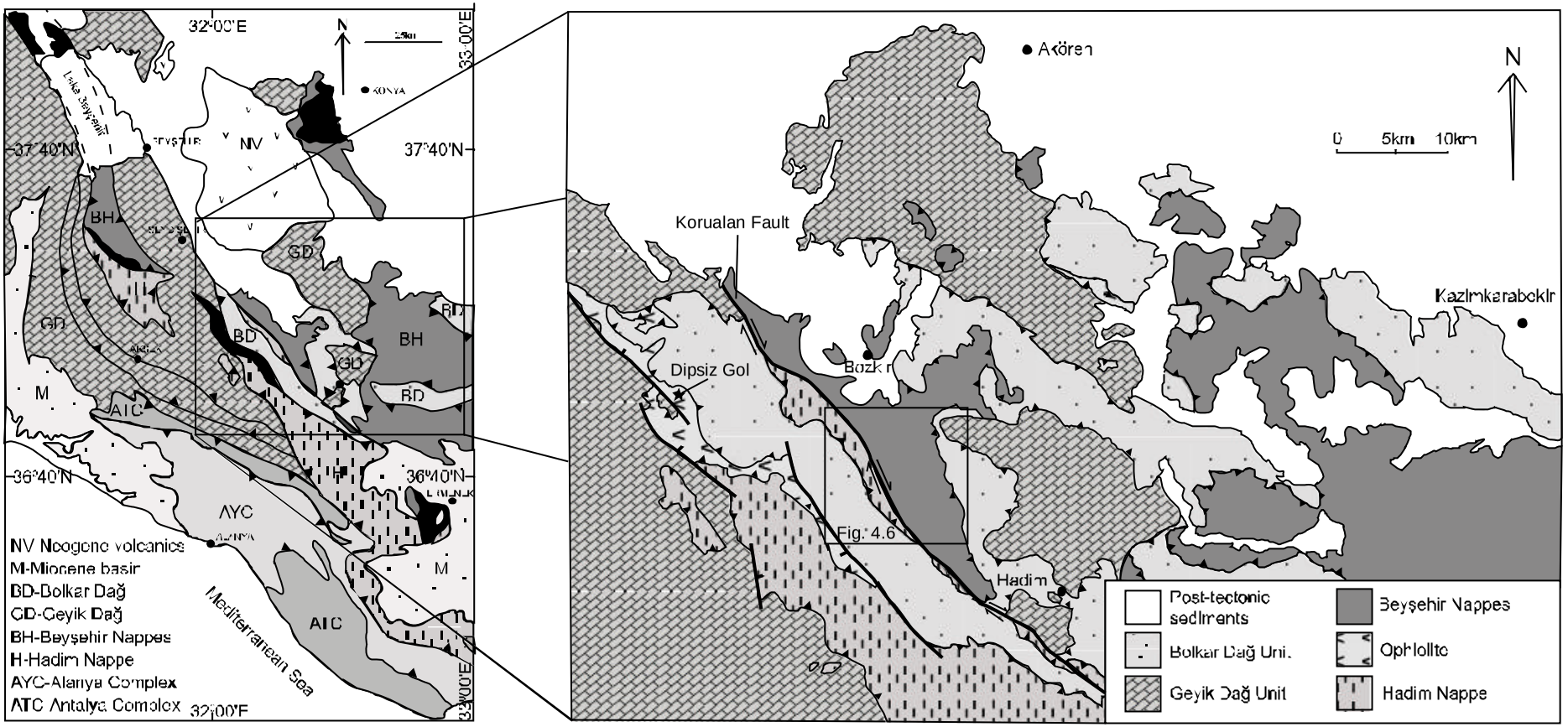

Fig.4.1 Geological maps showing the main subdivisions of the Central Taurides (after Özgül, 1984, 1997). Enlargement shows position of field area mapped during this study (Fig.4.6).

4.2 Summary of tectono-stratigraphy

The area chosen for this study to illustrate the B-H Nappes in the central part of the Taurus Mountains lies between the towns of Bozkir and Hadim (Fig.4.1). The regional autochthon of the central Taurides (Geyik Dag Unit) is overthrust by six thrust sheets in upward order, as follows: Bolkar Dag Unit, Hadim Nappe (also know as the Aladag Unit), Ophiolitic Melange (and ophiolite), Korualan Group, Huglu Unit and the Boyali-Tepe Unit, as summarised in Table 4.1 below. Previous workers (Özgül, l976, 1984, l997) recognized a continuity of the higher thrust sheets and by means of correlation have adopted the tectono-stratigraphic names introduced by Monod (1977) for the Beysehir area.

Autochthon	Allochthonous thrust sheets (in ascending order)		
			Beysehir Nappes
Geyik Dag Unit	**BolkarDag Unit**	**Aladag Unit (Hadim Nappe)**	Boyali-Tepe Unit *Late Triassic to Late Cretaceous*
			Huglu Unit *M.Triassic-Late Cretaceous*
Cambrian to Early Tertiary	*Devonian to Late. Cretaceous*	*Upper Devonian to Late Cretaceous*	Korualan Gp. *Late Triassic*
			Ophiolitic Melange *Maastrichtian*

Table 4.1 Main tectono-stratigraphical units and ages of the Central Taurides (after Özgül, 1976, 1984, 1997).

During the course of this study, each of the tectonostratigraphical units were field checked, but no additional work was added to the authochthon or the lowermost thrust sheets (Bolkar Dag Unit and Hadim Nappe); thus, these sections should be treated as literature reviews. The B-H Nappes were investigated more fully with new measured sections and collection of structural/sedimentological data presented in the relevant sections.

4.3 Regional Autochthon: Geyik Dag Unit

In the Bozkir-Hadim area of the Central Taurides, the Geyik Dag Unit once again forms the autochthon upon which the thrust sheets of the higher units have been emplaced. Like the Beysehir area (Chapter 2), the lowest exposed units in the autochthon comprise a Lower Palaeozoic basement of Cambrian-Ordovician rocks transgressively overlain by Mesozoic to Lower Tertiary platform-type sediments (Özgül, l976, 1984, l997). Figure 4.2 shows a stratigraphic section of the Geyik Dag Unit from the Hadim area.

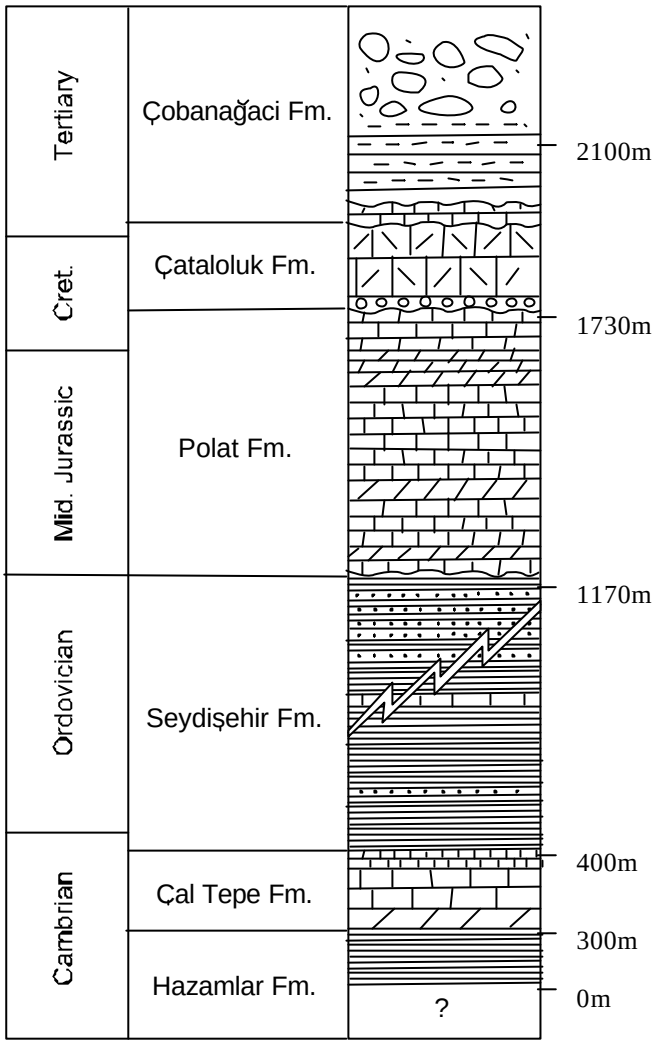

Fig. 4.2 Stratigraphic section of the Geyik Dag Unit in the Hadim area (field checked from Özgül, l997).

4.3.1 Lower Palaeozoic succession of the Geyik Dag Unit (Bagbasi Group)

The lowest exposed sequence of the autochthon in the Hadim area is the Lower Cambrian Hamzalar Formation, which comprises 300m of interbedded shales and siltstones (Özgül, l997). This is overlain by 100m of dolomitic limestones of the Çal Tepe Formation, which frequently has oolitic and stromatolitic horizons without. The uppermost 30m of the Çal Tepe Formation in this area consists of fossiliferous nodular limestone with abundant conodont fragments, disarticulated bivalves and trilobite remains, including *Agraulos* sp., *Corynexochus* sp. and *Paradoxides (s.l)* sp. The fossil assemblage in this upper part of the Çal Tepe Formation indicates an age range spanning Mid-Late Cambrian (Özgül, l997). The Çal Tepe Formation exhibits a gradual transition into shales and siltstones of the Seydisehir Formation, which is ca. 730m thick in this area.

4.3.2 Mid-Jurassic to Lower Tertiary succession (Kaplanli Group)

Overlying an angular unconformity at the top of the Lower Palaeozoic succession is a Mid-Jurassic to Lower Cretaceous carbonate sequence ca.560m thick, known locally as the Polat Limestone Formation (Özgül, 1997). Bajocian micritic limestone at the base of the formation passes into a dominantly dolomitic sequence lasting into the Late Kimmeridgian-Tithonian. A number of stromatolitic horizons are present in this Upper Jurassic sequence (Özgül, 1997). The top ca.120m of the Polat Formation is represented by Apsian-Cenomanian limestones with the benthic foraminifera *Dicyclina schulumbergeri* and *Nummoloculuna heimi* present (Özgül, 1997).

The Maastrichtian-Palaeocene Çataloluk Formation is present above a planar unconformity at the summit of the Polat Formation. Above ca. 20m of basal limestone conglomerates at the base of formation, lies a thick sequence (ca.100m) of shallow-water limestone containing abundant rudist corals, gastropods and benthic foraminifera, including *Orbitoides media*, *Lepidorbitoides minor* and *Siderolites calcitrapoides*. Towards the summit of the shallow-water limestones, this facies passes laterally into well-bedded micritic limestones containing *Rapydionina liburnica* (Özgül, 1997). The summit of the Çataloluk Formation is represented by ca.30m of Palaeocene algal limestones.

Unconformably overlying the Çataloluk Formation at the top of the autochthon is a 'flysch' sequence, reaching upto 400m thick at the type section north of Geyik Dag (ca.20km west of Taskent). The base of this sequence is represented by a 30m-thick Nummulitic limestone dated as Palaeocene (Özgül, 1997). This is, in turn, unconformably overlain by a clastic sedimentary succession upto 200m thick composed of lithicwackes and debris flows with limestone and shale interbeds. Clast compositions include lithologies incorporated from the underlying successions and exotic lithologies, such as radiolarian chert, volcanic extrusives and Permian limestone from the Bolkar Dag Unit (Özgül, 1997). This is overlain by a thick debris flow deposit up to 200m thick. Lithologies found as blocks within the shaley matrix include once again limestone from the Geyik Dag Unit below and other exotic lithologies such as radiolarian chert, volcanics, phyllite and serpentinite (Özgül, 1997).

4.4 Bolkar Dag Unit

The Bolkar Dag Unit of the Central Taurus Mountains crops out in its western extent south of Sugla Gölü and extends eastwards to the Eçemis Fault where it terminates. It forms part of the northern Tauride belt to the south of the Central Anatolian Crystalline Complexes, as shown in Fig.1.2 (Dermitasli *et al*., 1984). It is from the Bolkar Daglari (mountain range) to the east of this study area where the unit derives its name. In this type section area, the Bolkar Dag is the lowest exposed Tauride unit; hence, it was considered to be autochthonous. The situation is more complex, however,

as the unit forms a rootless thrust sheet over the Geyik Dag Unit in the west between Konya and Hadim, i.e. this study area (Özgül, l984).

Clear structural relationships show that in the east, the Bolkar Dag Unit is backthrust by Late Eocene compressional deformation over the Lower Tertiary Ulukisla basin (Dermitasli *et al*., 1984; Jaffey & Robertson, 2001; Clark, 2002). It appears that similar rethrusting has occurred, at least in part of the Hadim region of the Central Taurides. At Dipsiz Göl (Fig. 4.1), the Bolkar Dag Unit is demonstratably in a structurally elevated position above the Ophiolitic Melange, which occurs at the base of the higher Beysehir-Hoyran Nappes. This relationship is not seen elsewhere and the considerable difference in stacking order of the thrust sheets can only be satisfactorily explained by later rethrusting of the Bolkar Unit.

Unlike most other tectonostratigraphic units in the Central Taurides, the Bolkar Dag Unit has been affected by regional greenschist-facies metamorphism, increasing in grade to the north (towards the Central Anatolian Crystalline Complexes) and at deeper stratigraphic level, implying deeper burial. In the Hadim area only the Lower Devonian sequence has been affected by low-grade greenschist metamorphism (Özgül, l984).

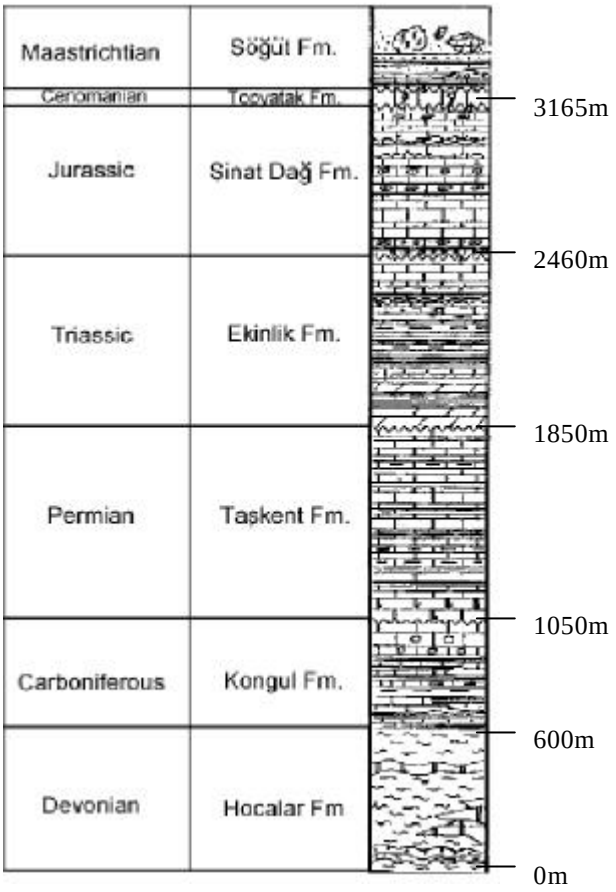

Fig. 4.3 Stratigraphic section of the Bolkar Dag Unit in the Hadim area (field checked from Özgül, l997).

4.4.1 Upper Palaeozoic succession of the Bolkar Dag Unit.

The lowermost part of the Bolkar Dag consists of a ca.500m succession of schists and marbles, of inferred Mid-Upper Devonian age from a fauna of corals and brachiopods (including *Favosites* sp., *Thanopora* sp., *Alveolites* sp., *Spirifer* sp. and *Productella* sp.), overlain by ca.300m of Lower Carboniferous shales, limestone and quartzites. This is overlain by ca.150m of Mid-Carboniferous limestone and dolomite. The sequence is especially oolitic towards the top. Fossils recovered from this sequence include benthic foraminifera, such as *Archaediscus* sp., *Tetretaxis* sp., *Millerella* sp., *Pseudovalvulina* sp. and *Fusiella* sp. (Özgül, l984, 1997). The succession then passes into ca. 800m of Upper Permian carbonates above an angular unconformity. Quartzite intercalations are common in the uppermost parts of the Permian sequence (Özgül, l984).

4.4.2 Mesozoic sucession of the Bolkar Dag Unit

Another low-angle unconformity separates the Upper Palaeozoic and Mesozoic of the Bolkar Dag Unit in the Hadim area. Above this discontinuity the sequence resumes with Triassic dolomitic limestones passing into ca. 350m of shale and quartzite. Reefal limestones above this sequence have been dated as Carnian-Norian (Özgül, l984). The Triassic sequence is then transgressively overlain by Lower Jurassic siliciclastic sediments (Fig. 4.3), which can be correlated with the Çayir Formation of the Geyik Dag in the Western Taurides.

During this study, it was found that this lithology extensively crops out on the northeast side of Dipsiz Göl valley (Fig. 4.1). There the Bolkar Dag Unit is rethrust to the southwest on top of the Ophiolitic Melange (Fig. 4.4c). The tectonic contact with the Ophiolitic Melange is not exposed, but directly above are poorly exposed relatively undeformed sandstones and mudstones. These are overlain by ca.10m of very dark laminated algal micritic limestone, which passes into channelised conglomerate. Well-bedded, medium to coarse-grained sandstone passes laterally into lensoidal shaped outcrops (up to 10m in length and 2m wide) of coarse cobble-sized, extremely well rounded conglomerate. The red coloured conglomerate is composed predominantly of reefal bioclastic limestone, quartzite, lithic fragments (predominantly sandstone and conglomerate), minor red and black chert and extremely rare volcanic clasts (>0.5%) set in a coarse to medium sandy matrix (Fig. 4.4a). The conglomerate is dominantly matrix supported, but locally, where the clast density is high it is clast supported (Fig. 4.4c). In total, this horizon is 10-15m thick at Dipsiz Göl, which is comparable to elsewhere in the Hadim area (Özgül, l984).

Fig. 4.4 (a) Pie chart showing clast composition of conglomerate, (b) Field photograph of conglomerates; (c) Schematic interpreted field sketch of Lower Jurassic clastic horizon at Dipsiz Göl.

Above the siliciclastic horizon the sequence changes to shallow-water platform carbonates which reach up to 800m thick. This carbonate succession becomes more oolitic and has frequent stromatolitic horizons in the Mid Jurassic portion (Özgül, l997). A small discordance is found at the top of the Mid Jurassic sequence, which separates the 90m-thick Kimmeridgian-Tithonian interval of shallow- water carbonate. Another discordance is found above this before the sequence passes into a Cenomanian-Turonian succession. This horizon typically comprises additional shallow-water carbonate with abundant rudists and both benthic and planktonic foraminifera, including *Hedbergella* sp., *Ovalveolina* sp., *Lenticulina* sp. and *Orbitolinidae* (Özgül, l997). Towards the top of the sucession interbeds of calciturbidites become more common. The top of the Bolkar Dag Unit is represented by a 'flysch' succession upto 200m thick. This begins with interbedded limestone and shale before passing into a polygenetic debris flow deposit. Fauna recovered from the matrix include *Globotruncana linneinana*, *G. bulloides*, *G. ventricosa* and *G. arca* which indicate a Maastrichtian age (Özgül, l997).

4.5 Hadim Nappe (Aladag Unit)

The Hadim Nappe in this central area is refered to as the Aladag Unit in the literature; however, it is widely accepted that they are equivalent (Özgül l976, 1984, l997; Dermitasli, 1984; Dermitasli *et al*., 1984). For the purpose of this study, the term Hadim Nappe will be used exclusively because it reduces unnecessary nomenclature. In addition, the Aladag is a separate mountain range in the Taurus Mountains, located to the east of the Eçemis Fault Zone (Fig. 1.2), unrelated to the Hadim Nappe but sharing the same name.

The Hadim Nappe has a limited exposure in the chosen study area, but always crops out to the south/southwest of the higher Beysehir Nappes, never to the north. The main outcrop of the Hadim Nappe outwith the study area forms a narrow NW-SE strip, ca.20km to the south of Sugla Gölü, which extends to the Mediterranean coast between the towns of Anamur and Silifke, a distance of ca.125km. The outcrop width of the Nappe broadens; as it does so, however, the Miocene shallow-marine Ermenek and Mut basins transgressively overlie the Hadim Nappe in the east of the area limiting the available exposure.

The outcrop of the Hadim Nappe in the study area forms a thin strip between the Bolkar Dag Unit and the Korualan Fault (Fig. 4.1), a 'young' right-lateral oblique fault downthrown to the northeast. The Korualan Fault runs from south of Sugla Gölü towards the town of Ermenek, for ca.100km, where it meets with the Miocene shallow-marine Ermenek basin (Özgül, l997) and probably joins up with the Neotectonic Göksu Valley extensional graben system. In general, where the tectonostratigraphy is unaffected by Neotectonic deformation, the Hadim Nappe occupies a structural position above the Geyik Dag autochthon and Bolkar Dag Unit, but beneath the Beysehir Nappes. To the south, the Hadim Nappe overlies both the Antalya Complex and the Alanya Complex (Özgül l976; Dermitasli, 1984; Dermitasli *et al*., 1984).

Fig. 4.5 Stratigraphic section of the Hadim Nappe from the Hadim area (after Özgül, l997). Scale is 1:3000.

4.5.1 Upper Palaeozoic stratigraphy of the Hadim Nappe

The lowest exposed sequence of the Hadim Nappe begins with Upper Devonian reefal limestones with dolomite intercalations, passing upwards into shale, sandstone and quartzite. In total, this sequence, locally known as the Gölbogazi Formation, reaches ca.1500m (Özgül, l997). Above, the sequence passes into ca.110m of Carboniferous shales, overlain by ca.750m of shallow-water limestones and quartzite of the Yaricak Formation. The Carboniferous succession ends in a small discordance, overlain by ca.180m of Lower Permian shallow-water carbonate encompassing the *Girvanella* and *Pseudoschwagerina* foraminifera biozones of the Lower Permian (Özgül, 1984, l997). Approximately 50m of quartzite separate the Upper and Lower Permian of the Çekiç Dagi Formation. The Upper Permian comprises a ca. 1500m-thick sequence of shallow-marine algal limestone, locally stromatolitic at the top (Özgül, l997).

4.5.2 Mesozoic stratigraphy of the Hadim Nappe

The Lower Triassic of the Gevne Formation is characterized by oolitic calcarenite, commonly with low-angle cross stratification, interbedded with micritic limestone, sandstone and conglomerate. This sequence grades into a 400m-thick sequence of Mid-Triassic micritic limestones, interbedded with sandstone and shale. The Upper Triassic sequence comprises ca.400m of red coloured siliciclastic sediments, including siltstone with channelised conglomerate and sandstone (Önder, 1984; Özgül, l984). In terms of lithology, this horizon can be correlated with similar deposits in the Geyik Dag and Bolkar Dag Units, which are Lower Jurassic in age (Özgül, l984).

The Lower Jurassic to Lower Cretaceous succession of the Hadim Nappe is dominated by a ca.600m thick sequence of dolomitic limestone, all overlain by Lower Cretaceous to Albian/Cenomanian neritic limestone. A discontinuity at the top of this 200m thick sequence is followed by thin Cenomanian shallow-water limestone, with abundant rudists and *Miliollidae* sp. (Özgül, l997). The Lower Jurassic-Upper Cretaceous Çambasi Formation can be directly correlated with the Çamlik Unit of the Beysehir area (Monod, 1977; Özgül, l997; Chapter 2). Above the Çambasi Formation lie polymict debris flows belonging to the Upper Cretaceous Zekeriya Formation. Lithologies incorporated include Carboniferous and Permian foraminiferal limestones and exotic lithologies derived from the Beysehir Nappes above, including pelagic limestone, volcanic clasts and ophiolite-derived material (Özgül, l997).

4.6 Beysehir Nappes

In this central area, the Beysehir Nappes are referred to in the available literature as the Bozkir Unit (Özgül, 1976, 1984, l997). The Bozkir Unit is essentially a generic name for allochthonous Mesozoic units in the Taurides derived from the Northerly Neotethyan realm; hence, the term includes units such as the Lycian Nappes and the Pozanti-Karsanti Ophiolite (Özgül & Arpat, 1973; Özgül, l976). Although broadly related, the Beysehir Nappes have demonstratably experienced a different tectonic history to these units; therefore separate tectonostratigraphic nomenclature should be used to reflect this. Although the names ultimately refer to related regional phenomena, this study uses the term 'Beysehir Nappes' in preference to the Bozkir Unit.

The Beysehir Nappes form the structurally highest unit emplaced over the Geyik Dag autochthon, the Bolkar Dag Unit and the Hadim Nappe. It was considered as melange due to the high level of tectonic disruption (Özgül, 1976); however, this study shows that locally the nappes consist of four coherent thrust sheets described in sequence, from lowest to highest, below. Figure 4.6 shows the field area between the towns of Hadim and Bozkir chosen to illustrate the tectonostratigraphy of the B-H Nappes in this study.

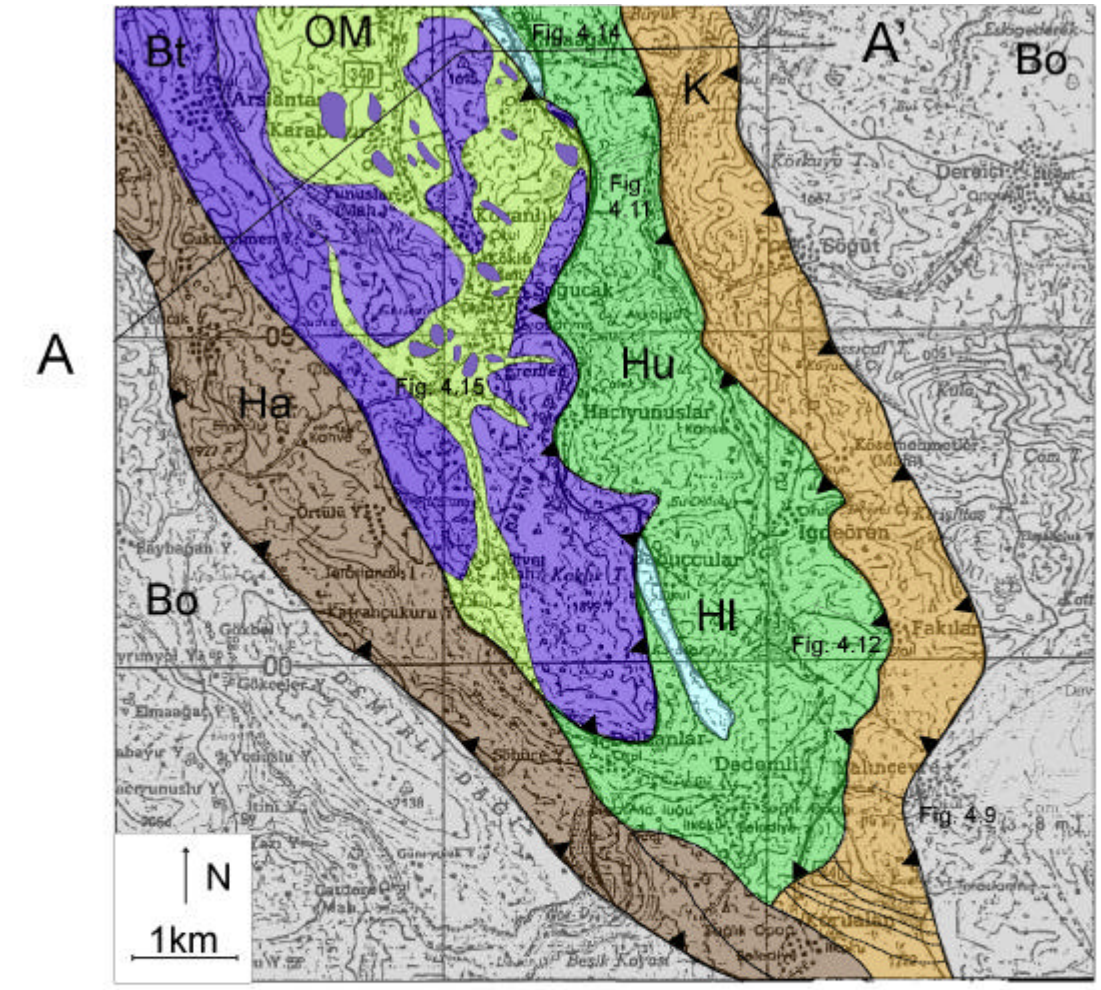

Fig.4.6 Geological map and cross section of the area between Bozkir and Hadim in the Central Taurides mapped during this study (for location see Fig. 4.1). **Bo**-Bolkar Dag Unit, **Ha**-Hadim Nappe, **K**, Korualan Gp., **Hu**-Huglu volcanics, **Hl**-Huglu limestone, **Bt**-Boyali Tepe Unit and **OM**-Ophiolitic Melange.

4.6.1 Late Cretaceous Ophiolitic Melange at Dipsiz Gol

Primarily due to (Eocene?) rethrusting and later neotectonic extensional faulting, the lowest thrust sheet, comprising Ophiolitic Melange with coherent slices of ophiolitic lithologies, is found outwith the mapped study area at Dipsiz Göl. At this location (Fig. 4.1) a thin (ca. 2km thick), but laterally continuous, sliver of Ophiolitic Melange is found sandwiched between the Geyik Dag Unit to the southwest and the Bolkar Dag Unit to the northeast. The original relationships between these two units and the Dipsiz Göl Ophiolite are unclear. However, the present-day boundary to the south is marked by a large fault scarp, ca. 10-20m high, indicating the presence of a major normal fault running NW-SE, downthrown to the northeast. The amount of displacement on this fault is hard to quantify and was outwith the scope of this project. The boundary to the north with the Bolkar Unit is marked by a low-angle thrust (mentioned in Chapter 4.4.2), inferred from the attitude of dip of Lower Jurassic sediments above. This difference in stacking order can only be satisfactorily explained if the Bolkar Dag Unit has been rethrust to a new position (Chapter 4.4).

The lowermost slices of the Dipsiz Göl Ophiolitic Melange consist of imbricated thrust slices of Palaeocene-Lower Eocene pelagic limestone associated with 100m-thick thrust slices of spilitic lava all set in a sheared serpentinte-rich matrix. The pelagic limestone imbricates are identical to the succession at the summit of the Geyik Dag autochthonous sequence (Özgül, 1984). As these lithologies are only found adjacent to the Geyik Dag Unit and nowhere else in the melange, and assuming ophiolite emplacement was in the Maastrichtian, as all the other evidence suggests, the logical interpretation is that the thrust slices of Palaeocene to Eocene pelagic limestone were incorporated into the melange during footwall collapse as the higher B-H Nappes were rethrust in Late Eocene time. The sequence then passes into km-sized blocks of ultrabasic lithologies aligned in the tectonic fabric (Fig. 4.7). These ultrabasic lithologies consist of fresh-highly altered harzburgite, with pods of sub-ordinate chromite and dunite found locally. A number of samples were collected for geochemical analysis from this location. The reader is referred to Section 6.3 for a more in depth study of the petrology and geochemistry of these lithologies.

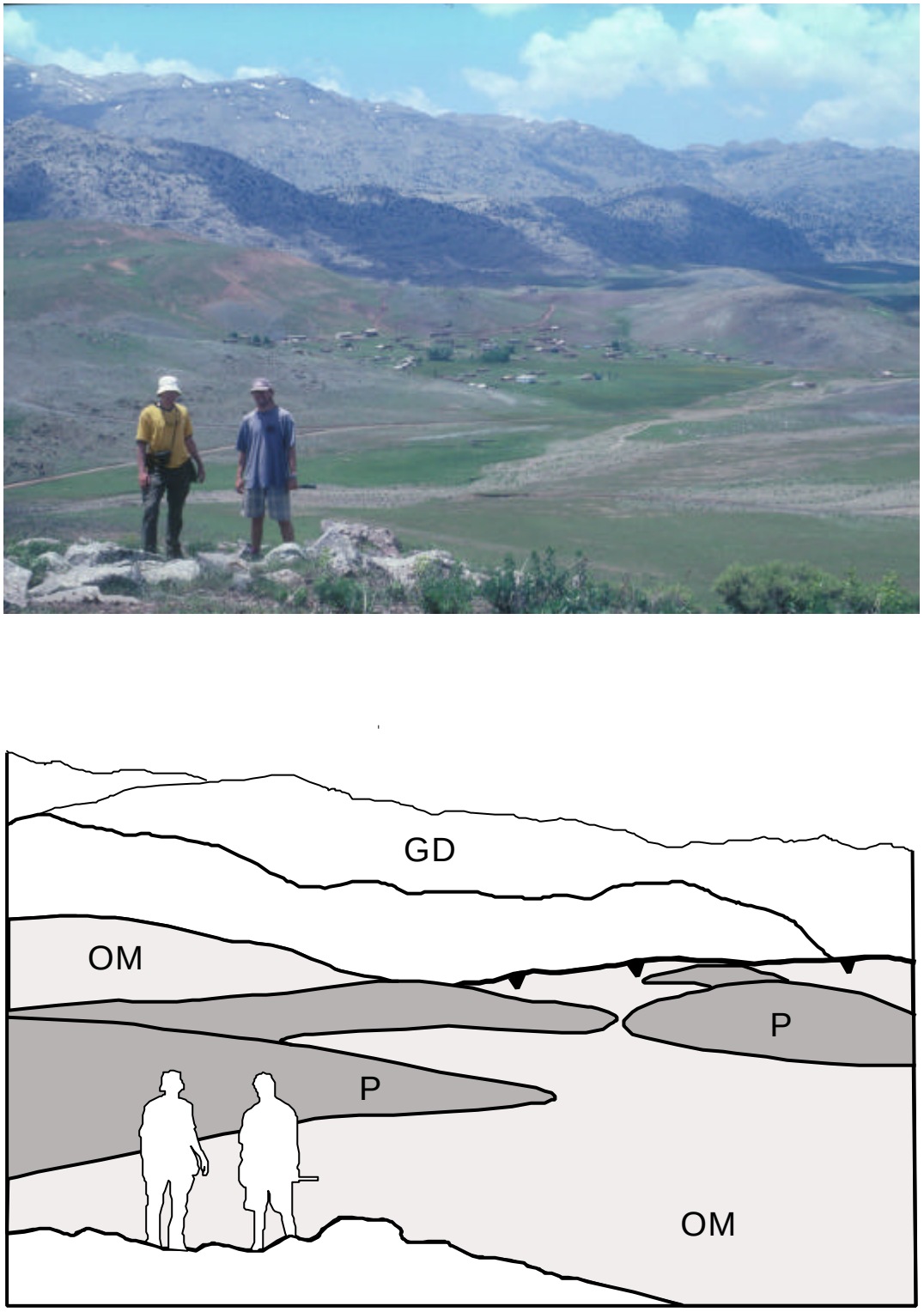

Fig.4.7 Field photograph and interpreted sketch looking southwards over the ephemeral Dipsiz Göl towards the Geyik Daglari (GD) in the background. The middle ground comprises thrust slices of peridotite (P) set in highly sheared Ophiolitic Melange (OM).

The top section comprises a volcano-sedimentary melange including blocks of pelagic limestone, basalt, spilite, serpentinite and gabbro. Fig.4.8 shows a schematic cross section through the uppermost ca.50m of the Ophiolitic Melange at Dipsiz Göl.

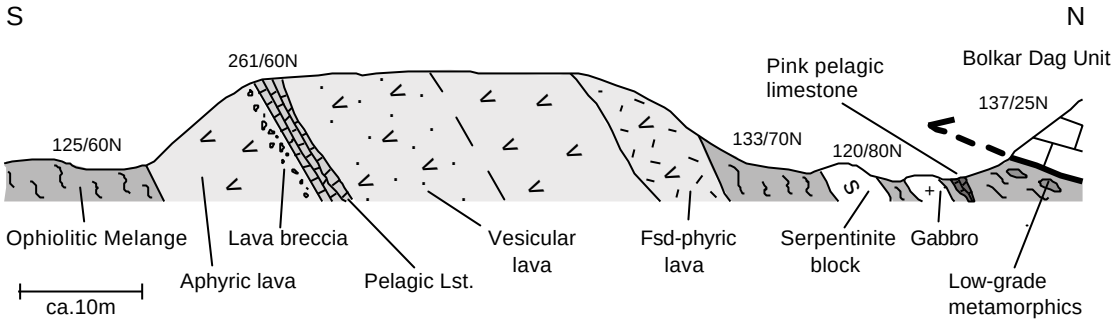

Fig.4.8 Schematic cross section of the upper contact of the Ophiolitic Melange at Dipsiz Göl.

The section begins with fine-grained serpentinite melange, with a moderate to steep shear fabric, in which is set a coherent block ca.40m thick of volcanic lithologies. The base of this inclusion is characterized by 10m of massive, aphyric and non-vesicular lava. The top metre is highly brecciated and overlain by steeply dipping, cm-bedded, grey micritic, cherty limestone. Clasts of medium-coarse grained, volcanic material are found in the lowermost beds, which are draped by subsequent pelagic micrite laminae. Rip-up clasts of the same grey pelagic limestone are also found in the top of the lava flow deposit in the zone of autobrecciation, suggesting the sediment deposition was coeval with extrusion of the volcanic material. The limestone then becomes finely laminated with pink and grey alternations of colouration, before passing back into more massive bedded, grey micrite. This is overlain by 15m of massive vesicular aphyric basalt, which becomes less vesicular towards the top of the unit. No structure is visible due to the degree of alteration, notably well developed epidosite veins. Above is a 5m-thick flow deposit, consisting of fine-grained, feldspar-phyric basalt. The section passes back into serpentinite melange, with a well developed, steeply dipping shear fabric. In this section of the melange, pods of serpentinite are often associated with red carbonate mud infilling fractures and veins. Also common are large blocks, up to 20m long, of highly altered gabbro pegmatite. This sequence is overlain by a thin 2m-thick layer of pink, unfossiliferous pelagic limestone. Towards the upper contact of the melange the shear fabric shallows slightly and small boulder-sized blocks of low-grade metamorphic lithologies (e.g. mica schist and phyllite) are incorporated.

4.6.2 Upper Triassic Korualan Group

In the mapped study area, the Korualan Group crops out as a thin N-S trending thrust slice, 200-300m wide, directly above the Bolkar Dag Unit in the trailing (eastern) edge of the nappe pile (Fig. 4.6). To the north of Korualan village the thrust sheet is intensely imbricated every ca.100m. Additional

structural complexity is encountered closer to the Korualan Fault, where the main fault splits into smaller splays and utilizes this pre-existing heterogeneity to create further offset. This structural repetition and deformation makes it hard to measure a type section in this area. Instead, a road section 2km to the north of Korualan leading to Yalinçevre village provides an ideal section through this lower thrust sheet (Fig. 4.6). Figure 4.9 show a measured log taken at this locality.

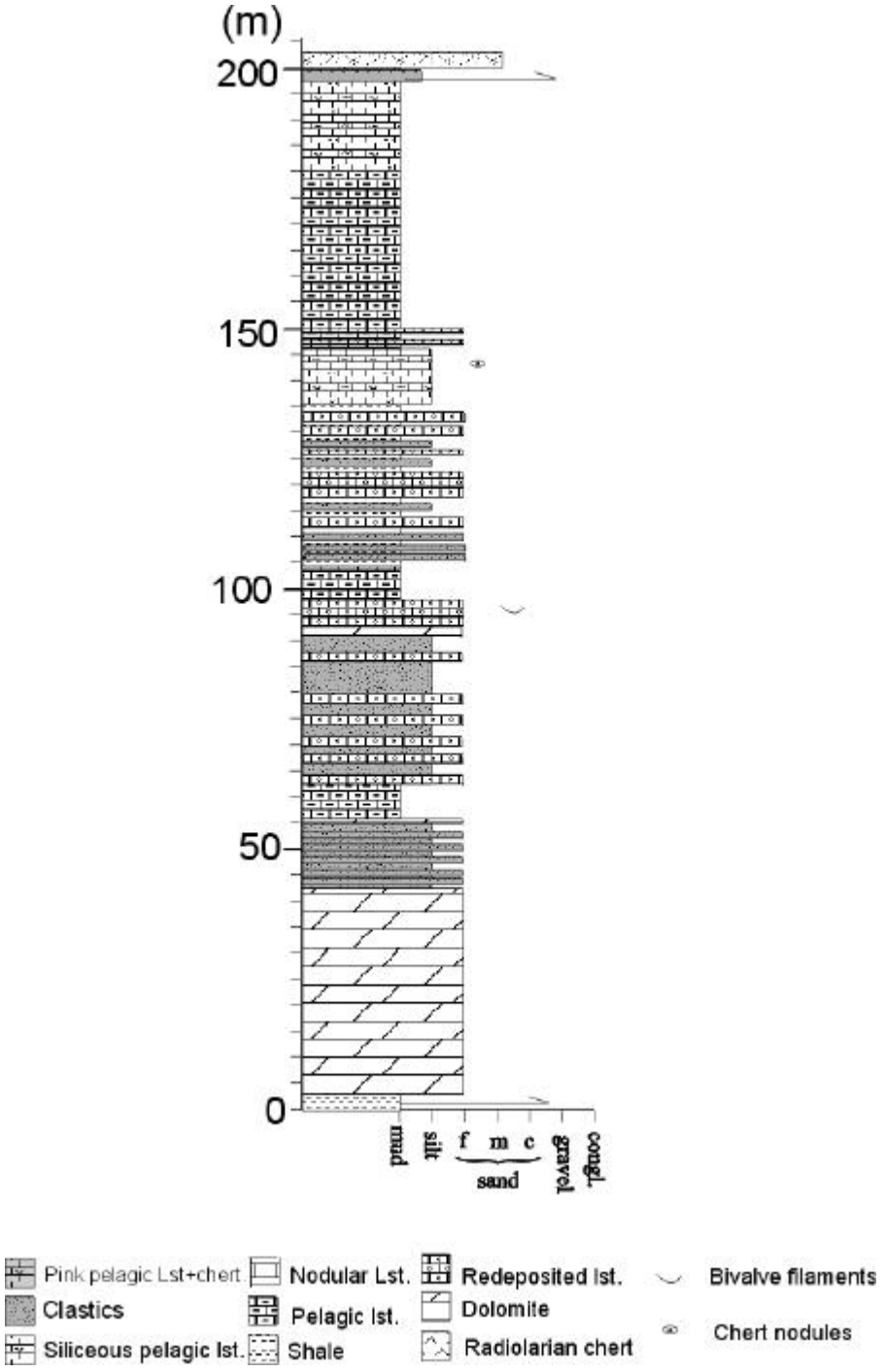

Fig. 4.9 Measured log of the Korualan Group from this study (see Fig. 4.6 for location).

Fig. 4.10 Highly sheared and boudinaged, yet coherent sequence of pelagic limestone and sandstone from the Korualan Gp. Photo taken 55m upsection on Fig. 4.9.

The section begins directly at the western limits of Yalinçevre village, where 40m of light grey, medium bedded, recrystallised dolomite tectonically overlies highly sheared shales of the Bolkar Dag Unit. The dolomitic sequence passes into a highly sheared, yet coherent, sequence of interbedded mudstone, siltstone, fine sandstone, calcarenites and micritic limestones (Fig. 4.10). 135m upsection this sequence of dominantly clastic sedimentation changes to hemi-pelagic, fine-grained carbonate deposition. A transition zone exists between the two consisting of dark grey, fine-grained, cherty carbonate packstone. Above lies a sequence ca.30m thick of medium-well bedded light grey pelagic limestone, commonly with curved bivalve filaments. The remainder of the overlying Korualan Group consists of a less coherent sequence with a melange-type character. In the type section this sequence is >100m thick. The melange consists of a variably buff-green coloured, scaley-clay matrix with blocks of exotic lithologies, up to 25m in long section, floating with random orientations in the matrix. Lithologies include ribbon radiolarites, massive chert, coarse volcaniclastic sediments, aphyric lava, fine metalliferous sediments with interfingering spilitic lava, pelagic limestone, coarse debris flows, limestone breccia and quartzite.

The age of the Korualan Group has been previously determined from a fauna of Upper Triassic bivalves (*Halobia* sp.) and Mid-Upper Triassic foraminifera including *Glomospira* sp. and *Involutina* sp. (Özgül, 1997). It has been reported that blocks within the upper melange include Senonian lithologies (Özgül, 1997), possibly related to initial Upper Cretaceous accretion/emplacement.

4.6.3 Late Triassic to Upper Cretaceous Huglu Group

In the literature the correlation of units from the Bozkir-Hadim area to the Beysehir area is well established, such that the uppermost thrust sheets share the same names (Özgül, 1976, 1984, 1997; Tekin, 1999). The Huglu Group in this central area is almost identical to the Beysehir area in all but one aspect: this thrust sheet is not found at the structurally highest level. The lower volcanic succession is locally known as the Dedemli Formation and is overlain by pelagic limestones of the Mahmut Tepe Formation (Özgül, 1997).

The main section measured during this study starts approximately 200m south of the road junction to Elmaagaç (Fig. 4.6) and heads west following a small incised stream valley providing good outcrop. The base of the section is covered by a thin veneer of recent alluvium, which subsequently passes into a thick volcanogenic sequence of massive to well-bedded, fine-grained, green tuff, interbedded with aphyric green (evolved?) lava, spilitic basalt and rare feldspar-phyric volcanic rocks (Fig.4.11). At certain horizons thin-bedded pelagic limestone, with abundant *Halobia*-type filaments, are interbedded with extrusive rocks. Locally, these horizons are negative weathering and provide no outcrop but abundant loose scree, hence are marked on the logs as such (Fig. 4.11). Towards the top of the section coarse-grained volcaniclastic sediments interfinger with thick-bedded lava flows and tuff before passing conformably into a 40m-thick sequence of well bedded pelagic limestone. The

thickness of this upper limestone unit is variable, primarily due to a major thrust cutting through the sequence. Another two sections were measured through the lower parts of the volcanogenic sequence to show facies variablity. The first of these short sections was measured along the road to the west of Fakilar village (Figs. 4.12 & 4.14).

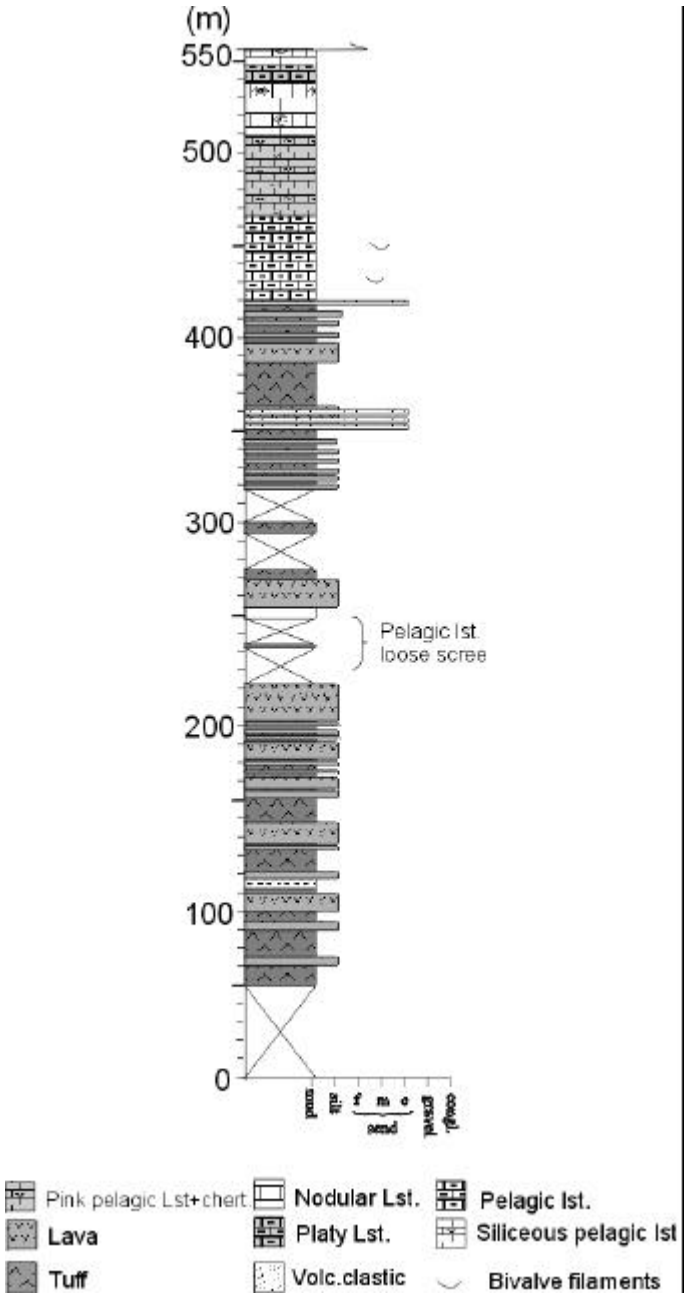

Fig.4.11 Main measured section from this study through the Huglu Group (for location see Fig. 4.6).

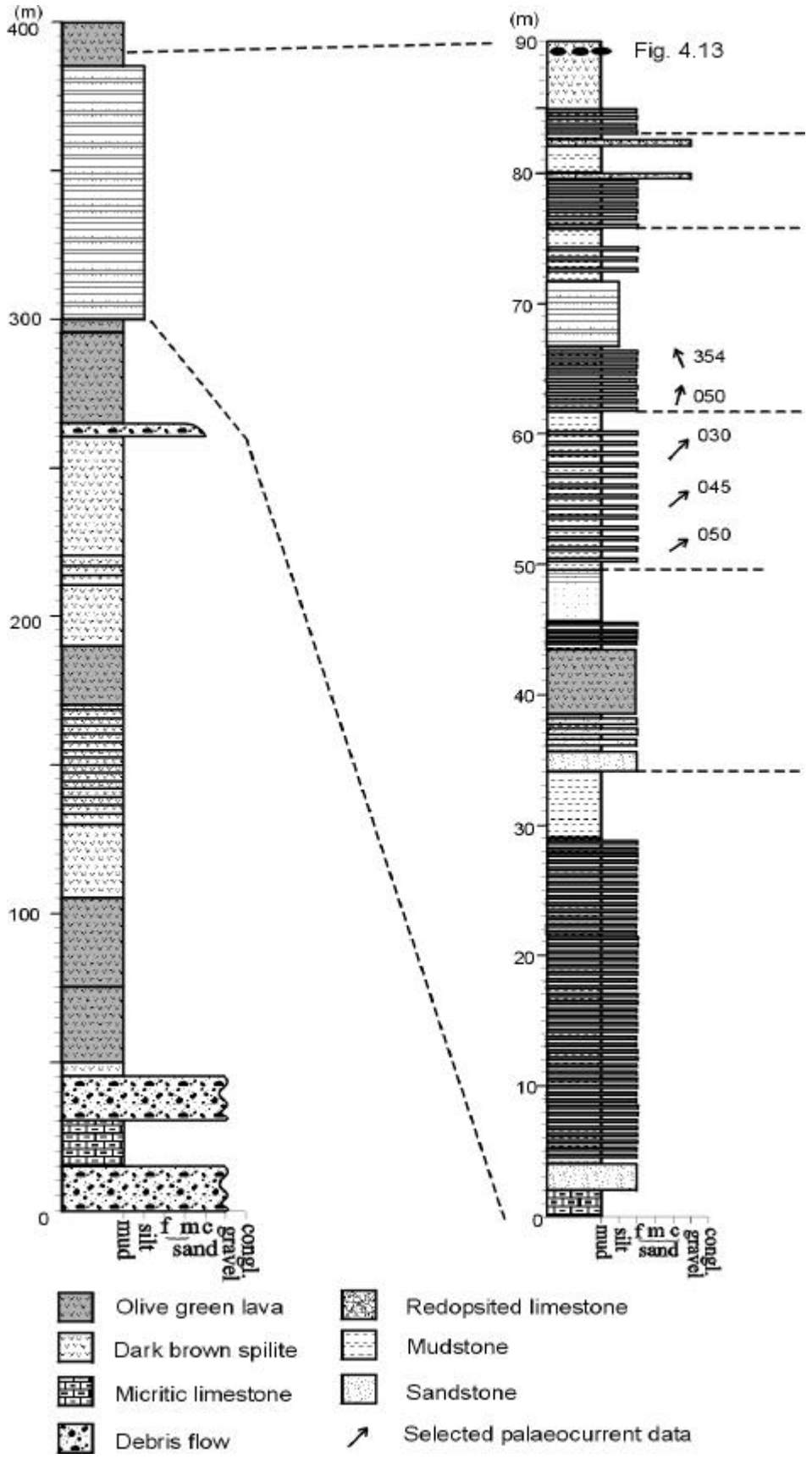

Fig. 4.12 Measured section at the base of the Dedemli Formation measured at Fakilar (Fig. 4.6).

The section at Fakiliar (Fig. 4.12) begins with a coarse, poorly sorted, but well-rounded, gravel-sized debris flow deposit, comprising clasts of fine quartzoze sandstone, pink pelagic limestone, grey micritic limestone, basalt and volcaniclastic sediments. This is overlain by grey, highly sheared and recrystallised micritic limestone with abundant bivalve fragments, which passes back into another coarse debris flow deposit. This comprises blocks (up to 30cm) of thick-bedded recrystallised limestone, fine sandstone and green fine-grained tuff. The sequence then passes in to ca. 250m of well-bedded to massive interbedded fine-grained tuff, brown spilitic lavas and fresh green volcanic extrusives. Towards the top of this sequence a coarse poorly sorted debris flow, consisting entirely of well-rounded, brown spilitic clasts, generally coarse gravel sized but reaching upto 0.5m in size, signals a change to clastic deposition above. This clastic regime consists of five turbidite sequences ranging in thickness from approximately 6m to 30m thick. Most of the sequences have a lower sandstone unit; however, some start directly with a sequence of finely interbedded, fine-grained, graded sandstone and mudstone turbidites, before passing into either a complete shale sequence, or mud-dominated turbidites. In each case the amount of sand in each sequence decreases upsection. Sedimentary structures such as grading, cross bedding and low-angle cross lamination are found in the more sandy horizons. Vary rarely the style of sedimentation departs from the classic turbidite sequence, as seen near the base where aphyric volcanic rocks interfinger, and towards the top where 0.5 to 1m thick beds of graded limestone gravel-sized conglomerate cut erosively into the sucession. The top of the ca. 80m thick clastic sequence is capped by a 5m-thick lava flow, consisting of well-jointed, fine-grained aphyric grey basalt. The top metre of the flow contains angular clasts of cherty grey micritic limestone ranging in size from <5mm to >30cm (Fig. 4.13).

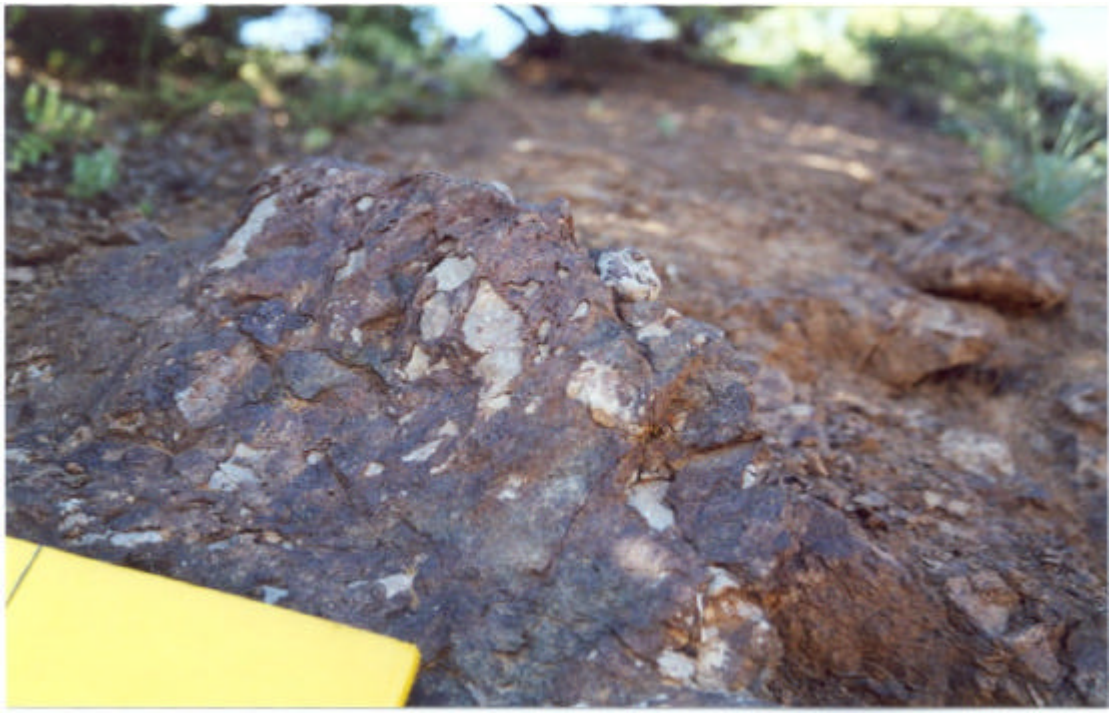

Fig. 4.13 Micritic limestone clasts set in lava flow (See Log 4.12 for location).

The second section through the base of the volcanic Dedemli Formation, measured 1.5km to the NNW (Fig.4.14) reveals a different situation to that seen at Fakilar. The bottom contact with the Korualan Group thrust sheet is not exposed once again due to recent alluvium from the Göksu River. Where the Dedemli Formation crops out it consists of interbedded brown spilite, green coloured volcanic extrusives, green tuffites with rare beds of coarse volcaniclastic sediments. Approximately 100m upsection the volcanic sequence is conformably overlain by 7m of thinly bedded, white micritic limestone with remains of bivalve filaments, similar in appearance to *Halobia* sp. This passes into 25m of massive to thick-bedded, pink micritic nodular limestone with muddy partings. This facies is similar in appearance to the Ammonitico Rosso facies but is apparently unfossiliferous. Abundant replacement chert nodules have formed parallel to bedding. This is overlain by 12m of white micritic limestone followed by 13m of pink pelagic limestone identical to the sequence described below. The limestones form a lenticular shaped outcrop and appear to be laterally continuous for ca. 500m. Above the limestone facies the sequence passes back into a volcanic succession typical of the Dedemli Formation as a whole.

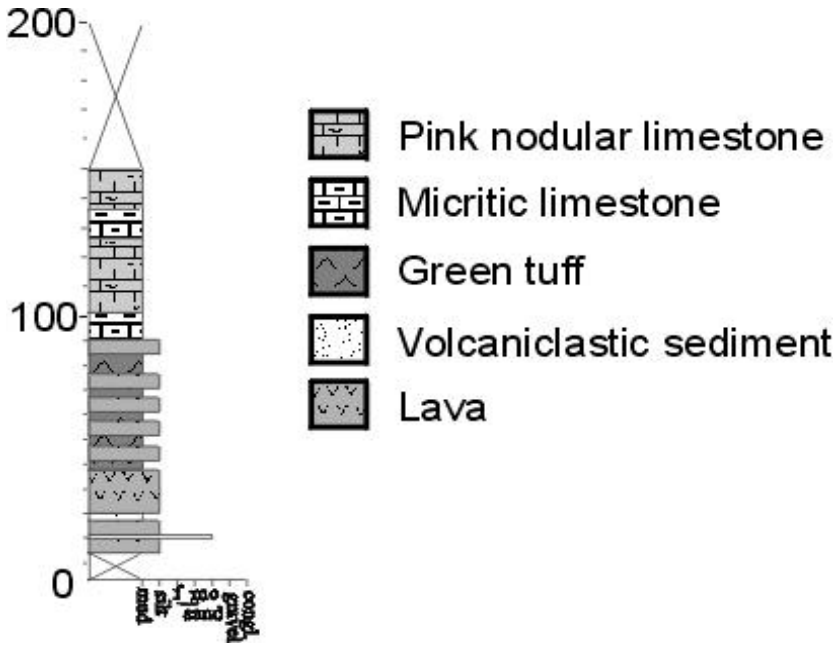

Fig.4.14 Log through the lower part of the Dedemli Formation. See Fig. 4.6 for location.

The volcanic nature of the Dedemli Formation makes it hard to determine a precise age, but a study of radiolarian fauna by Tekeli (1999), recovered from limestone intercalations at the base of the formation reveal a Middle Carnian age (*Tetraporobrachia haekeli* Zone). In addition conodonts, including *Paragondolella polygnatiformis noah* (MOSHER) and *Gladigondolella* sp., recovered from limestone near the top of the volcanic sequence also indicate a middle Carnian age (Tekeli, 1999). The pelagic limestone sequence at the top of the Huglu Group (Mahmut Tepe Formation) has been shown to continue through to the Maastrichtian from the presence of *Globotruncana* cf. *Concovata primiliva* and *G. tricarinata* (Özgül, 1997).

4.6.4 Upper Triassic to Upper Cretaceous Boyali-Tepe Group

The uppermost thrust sheet in the Bozkir-Hadim area is the Boyali Tepe Group, so called because of its almost identical stratigraphy to the Beysehir area (Özgül, 1976, 1984, 1997). Previous studies (Özgül, 1997) have separated this thrust sheet into three individual formations; 1) Upper Triassic-Lower Jurassic neritic limestone (Kuztepe Formation), 2) Jurassic to Upper Cretaceous pelagic limestone and radiolarian chert (Asar Tepe Formation) and 3) Upper Triassic neritic limestone (Sogucak Formation). Identification of the two neritic limestone units in the field proved to be difficult, consequently this study has amalgamated the two formations (of identical ages and lithologies) into a single unit. This thrust sheet comprises disrupted kilometre-decimetre sized blocks set in ophiolitic melange. Collectively these blocks show a coherent stratigraphy even though the thrust sheet is highly deformed; hence, a composite log has had to be constructed in order to illustrate the statigraphy of this unit. Fig. 4.15. shows one measured section from a block in the melange.

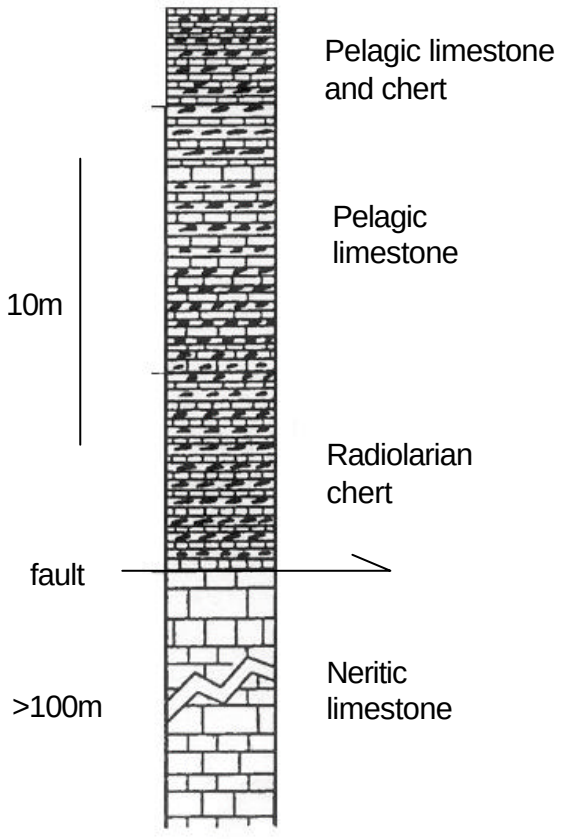

Fig. 4.15 Stratigraphy of the Boyali Tepe Group (Sogucak section from Özgül, 1997).

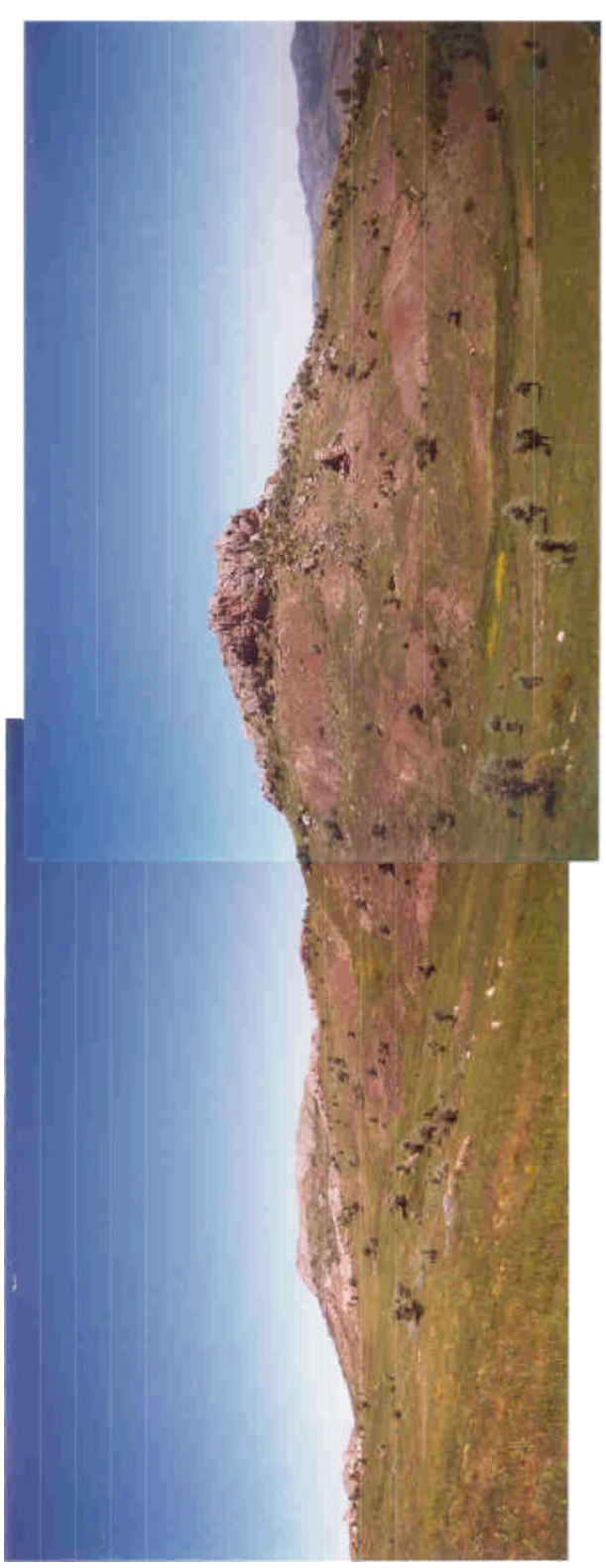

Fig.4.15 Block of the Boyali Tepe Group set in ophiolitic melange near Sogucak Village. Inset is the location of Fig. 4.16.

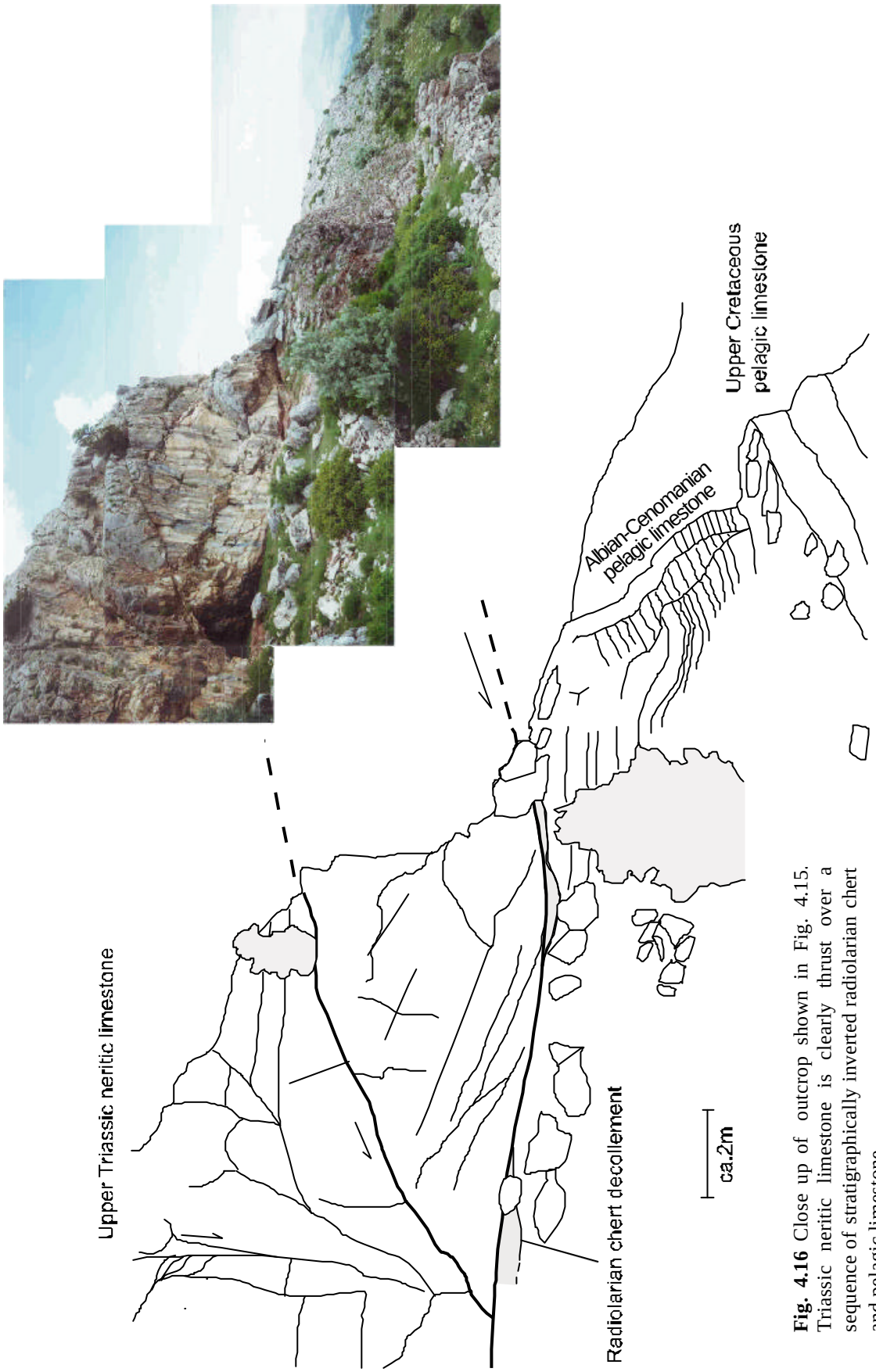

Fig. 4.16 Close up of outcrop shown in Fig. 4.15. Triassic neritic limestone is clearly thrust over a sequence of stratigraphically inverted radiolarian chert and pelagic limestone.

As can be seen from the field photographs and the interpreted sketches (Figs. 4.15 & 4.16), the thrust sheet is stratigraphically inverted and 'floats' in the melange. Close-up inspection of the block itself shows that it is highly deformed with many internal imbrications within the massive neritic limestone structurally at the top. Below, a major decollement has formed in the radiolarian chert subjecting it to extreme layer-parallel extension and shear deformation. Much of the deformation seems constrained to this rheologically 'weak' layer, as the underlying sequence in the footwall is intact and experiences only minor folding.

The lowermost exposed lithology of the Boyali-Tepe thrust sheet, consists of up to 400m of white highly recrystallised neritic limestone. Thickness varies and seems to depend on the size of the block the section is measured from. Stratigraphically above is a thin sequence of chert rarely more tham 1m thick. Original thickness is impossible to determine due to the deformation described above. The succession then passes into approximately 5m of well-bedded, grey micritic limestone, with abundant cherty interbeds, all overlain by well-bedded pelagic limestone with radiolarian chert interbeds. The sequence of overlying pelagic limestone has previously been dated as Albo-Cenomanian at the base to Lower Maastrichtian at the top (Özgül, 1997).

4.7 Summary

The B-H-H Nappes can be correlated from the Beysehir type area into the Bozkir-Hadim area, with only minor differences in stacking order and subtle differences in tectonostratigraphy. The major difference is the presence of a new unit at the base of the nappe stack. The following important points sum up the Bozkir-Hadim area:

1. The Palaeozoic to Early Tertiary autochthon (Geyik Dag Unit) is almost identical to the preceeding areas.

2. The Late Palaeozoic to Mesozoic Bolkar Dag Unit forms a rootless thrust sheet over the Geyik Dag Unit, and has a similar, but more condensed, stratigraphy to the Late Palaeozoic to Mesozoic Hadim Nappe. Other differences include regional greenschist metamorphism in the Bolkar Dag Unit, which is not seen in the Hadim Nappe.

3. The Hadim Nappe structurally overlies the Bolkar Dag Unit, but is beneath the B-H Nappes. Its stratigraphy is extremely similar to the Beysehir type area.

4. The uppermost levels of both the Bolkar Dag Unit and the Hadim Nappe consist of Maastrichtian clastic sediments and debris-flow deposits, whereas the Geyik Dag autochthonous sequence continues through to the Mid-Eocene, before similar lithologies are seen.

5. The serpentinized harzbugitic ophiolite and melange at Dipsiz Göl is emplaced directly onto the Hadim Nappe. The present-day juxtaposition of the ophiolite and the Geyik Dag autochthon is primarily the result of relatively recent extensional faulting. Minor back-thrusts are seen at Dipsiz Göl placing the Hadim Nappe onto the ophiolite. This relationship has not been observed elsewhere.

6. The Korualan Unit is the lowermost exposed thrust sheet of the B-H Nappes, and comprises ca. 400m of mainly redeposited carbonates, quartzose sandstones and mudstones, of Mid-Late Triassic age. The unit is internally imbricated creating structural repeats, yet despite this deformation a coherent sequence is present.

7. The overlying Dademli Formation comprises Mid-Late Triassic intermediate-acidic extrusives, volcaniclastics, siliciclastic sediments and minor pelagic carbonates, all overlain by thin (<100m) Upper Triassic-Upper Cretaceous cherty pelagic carbonate of the Mahmut Tepe Formation.

8. The uppermost thrust sheet is the Boyali Tepe Group, which comprises a stratigraphically inverted, broken formation of Jurassic shallow-water carbonate, Ammonitico Rosso condensed limestone, radiolarian chert and Upper Cretaceous pelagic limestone, all set in Ophiolitic Melange.

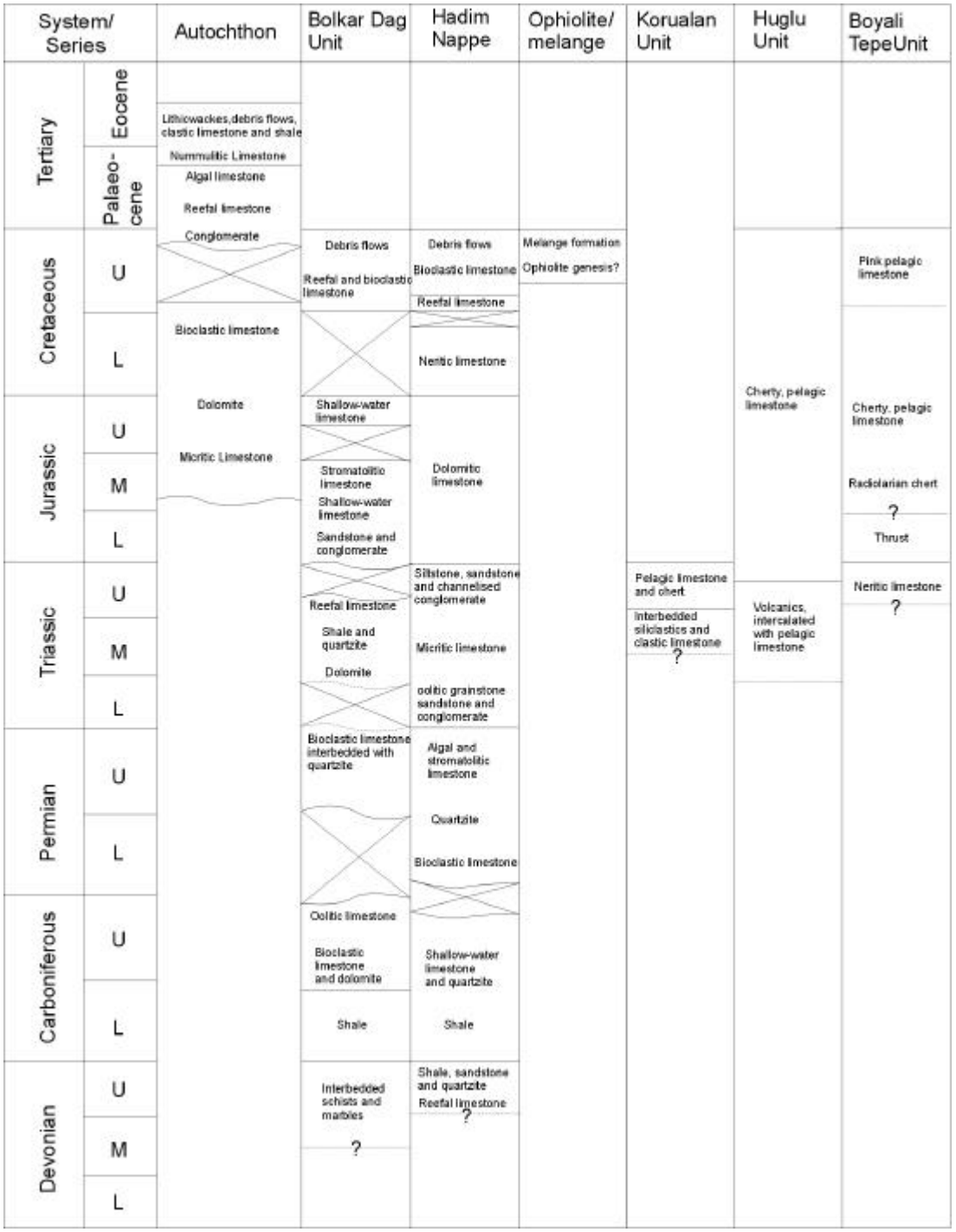

Fig.4.17 Lithostratigraphic summary of the main units in the Bozkir-Hadim area. Data from Özgül (l976, 1984, l997) and this study (B-H Nappes only).

Chapter 5

5.TECTONOSTRATIGRAPHY OF THE B-H NAPPES IN THE ERMENEK-KARAMAN (EASTERN) AREA

This final tectonostratigraphy chapter examines the geology of the far eastern outcrop of the B-H Nappes in the area between Ermenek and Karaman. This chapter focuses on the structure and stratigraphy of the B-H Nappes and the new work carried out during this study reflects this. Less attention is paid to the autochthonous units, which were discussed in previous chapters.

Two main fieldwork areas were chosen to examine this eastern area (Fig. 5.1). First, in the south the Ermenek area was chosen because (a) this study could utilise a previously determined tectonostratigraphic framework of Gökdeniz (1981); (b) varied topographic relief has resulted in excellent exposure which is easily accessible following construction of new roads, and (c) logistically, fieldwork in more remote areas would be impractical and unsafe. Due to the large outcrop area of the B-H Nappes a second fieldwork area in the north was necessary to cover the Ermenek area. The Karaman area (Fig. 5.1) was chosen for this purpose because of; (a) its proximity to the Ermenek area, (b) good access through road sections which additionally provide excellent exposure and (c) logistically, Karaman was an advantageous base to work from in terms of travel time and facilities.

5.1 Previous work

Once again, the earliest systematic geological study carried out on this part of the Central Tauride Mountains was by Blumenthal (1956) who used the term 'Schist-Radiolarite Formation' to describe the allochthonous units to the SW of Karaman which were then believed to be Cretaceous in age. Koçyigit (1976) followed on from this earlier work and described the allochthonous B-H Nappes in this area as Ophiolitic Melange containing blocks of Mesozoic limestone in an Upper Cretaceous matrix. A reasonably detailed 1:100000 scale map was produced from this study. A smaller scale investigation of the mineralogy and geochemistry of igneous rocks within the 'melange' SW of Karaman, near Bucakisla, was carried out by Tuzcu (1972), the main findings of which characterised the volcanism as intermediate in composition, essentially trachyte to rhyolite.

The most relevant previous work was carried out by Gökdeniz (1981), specifically on the Huglu-type lithologies found in the Ermenek area. The study also encompassed the regional geology and produced a detailed 1:25000 map and representative type successions of units found in the area.

Recently the focus of attention switched to the younger Miocene Ermemek and Mut basins which unconformably overlie the Mesozoic units, primarily as petroleum reservoir analogues (Umit & Nuran, 1990; Ozdogan & Sahbaz, 1999; X. Janson. pers. comm., 2000).

Less relevant geological work has also been carried out on the economic geology south of Ermenek, in particular important Pb-Zn mineralisation in ophiolite-related rocks near Goktepe (Kuscu, 2001).

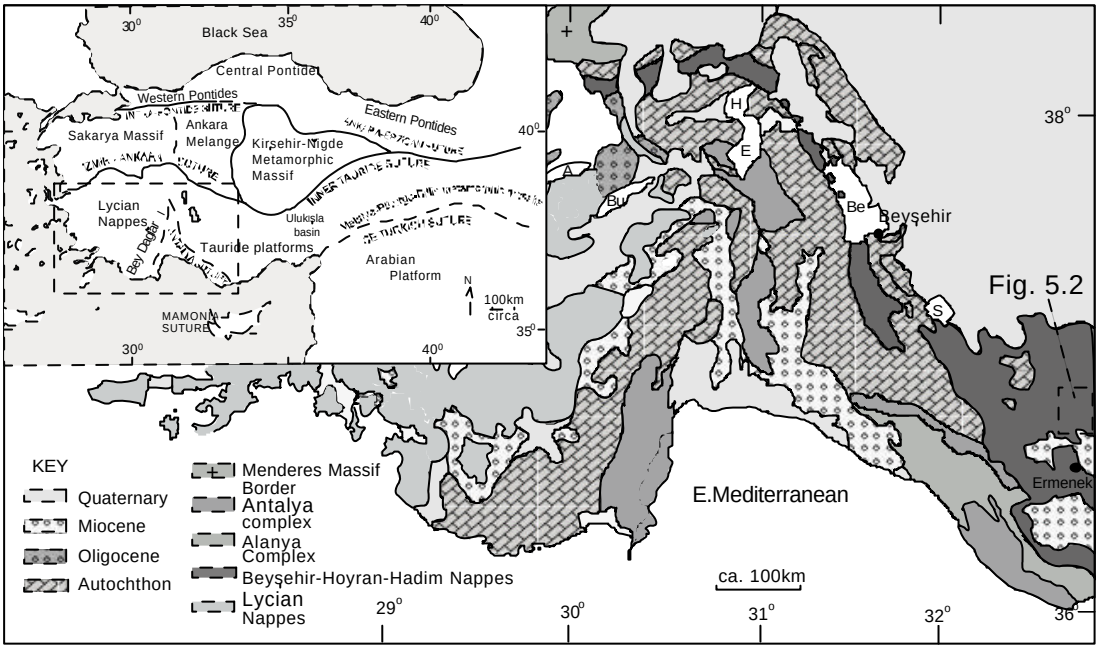

Fig.5.1 Regional geological map showing location of field study area. A- Lake Açi,, Be-Lake Beysehir, Bu- Lake Burdur, E- Lake Egirdir and H-Lake Hoyran.

After field checking, the tectonostratigraphy of Gökdeniz (1981) was found to be robust and is utilised in this study with minor revisions to the lower units (Bolkar Dag Unit). New sections were measured in the thrust sheets of the B-H Nappes to illustrate variability of the coherent sequences.

5.2 Tectonostratigraphy of the Ermenek area

In the Ermenek area, only the two highest thrust sheets of the B-H Nappes are exposed. In the south the highest 'Nappe' is unconformably overlain by a Miocene carbonate platform/basin system which obscures the underlying Hadim Nappe and the Mesozoic autochthon. Only glimpses of the underlying units are seen as inliers, for example ophiolitic rocks near Göktepe, which consist of serpentinised peridotite and melange (Erentöz *et al*., 1963). Tectonic relationships are hard to determine in this area because of the fragmentary exposure; hence, this study focused on the well-exposed higher nappes. To the south of Ermenek, where the Miocene basin is not present, the Hadim Nappe crops out all the way down to the Mediterranean coast near the towns of Silifke and Anamur where it tectonically overlies

the Alanya and Antalya complexes (Dermitasli, 1984). The Hadim Nappe is not found in the Ermenek area.

<table>
<tr><th>Autochthon</th><th>B-H Nappes</th><th>Post-Tectonic cover</th></tr>
<tr><td rowspan="2">Bolkar Dag Unit
(in the north)</td><td>Oyuklu Dag Unit
(U.Triassic-Cretaceous)</td><td rowspan="2">Ermenek basin
(Miocene)</td></tr>
<tr><td>Ihsaniye Unit
(Triassic-Upper Cretaceous)</td></tr>
</table>

Table 5.1 Summary of the tectonostratigraphy in the study area to the north of Ermenek (modified after Gökdeniz, 1981).

5.3.1 Bolkar Dag Unit

The lowest exposed sequence in the Ermenek area is the Bolkar Dag Unit. It only crops out in the north of the Ermenek study area (Fig. 5.2) where it consists of small tectonic windows near the villages of Adaköy, Kalaba and Akçaalan, and was formerly known as the Adaköy Unit (Gökdeniz, 1981). Lithologies consist predominantly of white, recrystallised neritic limestone with calcareneite and oolitic horizons. A Mid-Triassic age was previously determined from a fauna of foraminifera, bivalves and algae, including *Ammobaculites radstatensis* (Kristan-Tollman), *Lituolidae*, *Duostomina* sp., *Involutina sinuosa oberhauseri* (Salaj) and *Trocholina* sp. (Gökdeniz, 1981). The Bolkar Dag Unit also forms a thick (ca.400m) succession of well-bedded micritic limestone in the northern footwall of a large (as yet unnamed) graben which runs E-W near the town of Bucakkisla, previously termed the Nunu Unit (Gökdeniz, 1981) and the Jurassic-Cretaceous Bucakkisla limestone (Koçygit, 1976). During this study all these units are grouped together as the Bolkar Dag after Özgül (1984), to cut down on provincial terminology. As the regional Bolkar Dag succession has been previously described, the reader is referred to Chapters 4.4.1 and 4.4.2 for a summary of the stratigraphy. A more complete succession through the Bolkar Dag Unit is seen in the Karaman area and is described in Chapter 5.4.1.

5.3.2 Ihsaniye Unit (Huglu-type)

The lowermost exposed unit of the B-H Nappes crops out to the north of Okuylu Dag and is imbricated to form two main thrust sheets (Fig. 5.2). The internal sequence is locally imbricated and appears to be broken formation, e.g. Kale Tepe (Fig.5.3). The broken formation matrix does not include any exotic or redeposited lithologies and consists of highly sheared tuff and radiolarian chert derived from the sequence, which suggests that the deformation is related to the overriding thrust sheet. However, the thrust sheets do possess an overall coherency generally younging to the south. This Unit can be split into five mappable sub-units, as is summarised in Fig. 5.4. Investigation of the Ihsaniye Unit during this study is detailed in the following sections.

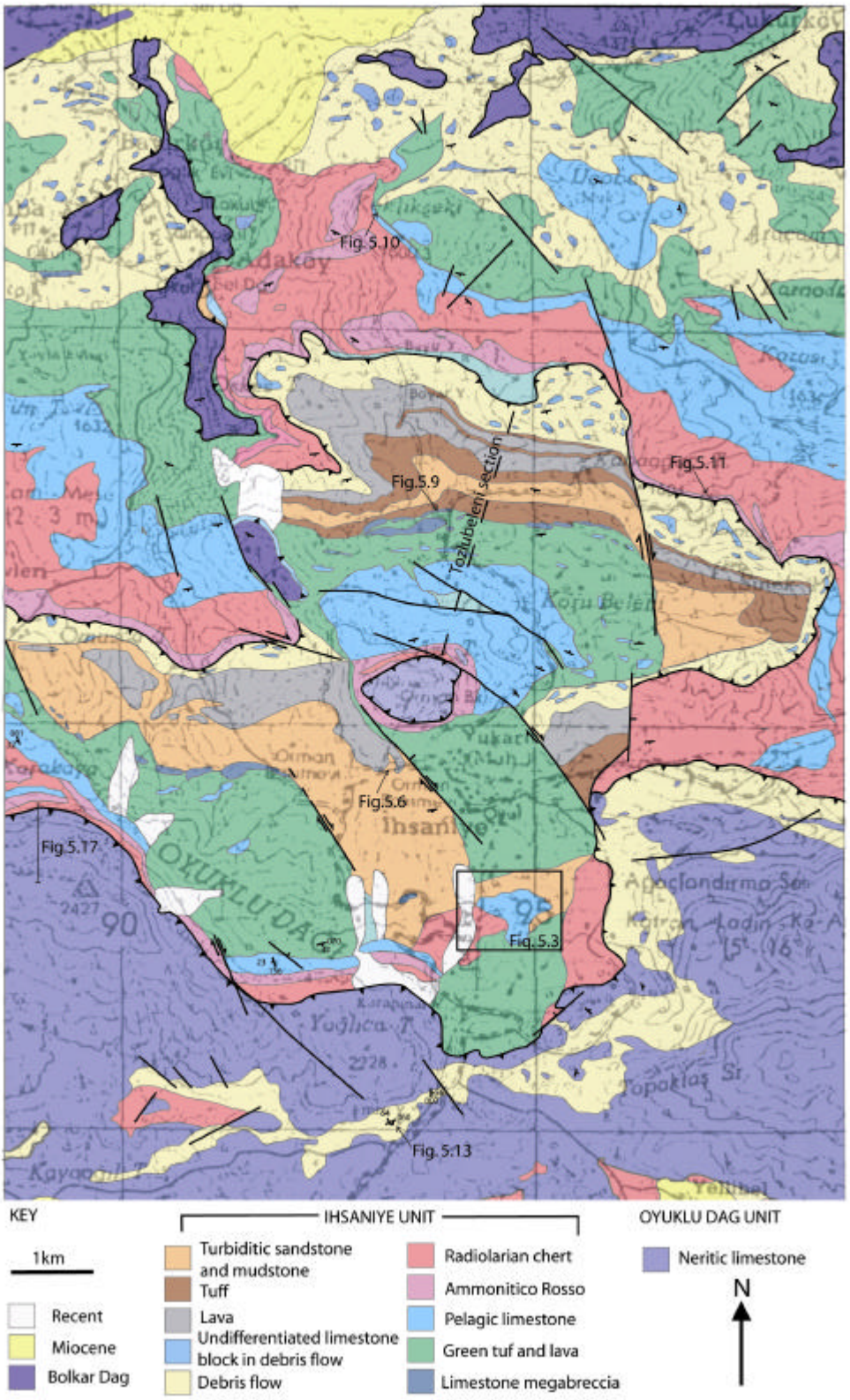
Fig.5.10
Fig.5.9
Tozlubeleni section
Fig.5.11
Fig.5.6
Fig.5.17
Fig.5.3
Fig. 5.13
OYUKLU DAG
KEY
1km
Recent
Miocene
Bolkar Dag
IHSANIYE UNIT
Turbiditic sandstone and mudstone
Tuff
Lava
Undifferentiated limestone block in debris flow
Debris flow
Radiolarian chert
Ammonitico Rosso
Pelagic limestone
Green tuf and lava
Limestone megabreccia
OYUKLU DAG UNIT
Neritic limestone
N

Fig.5.2 (previous page) Geological map north of Ermenek (field checked and redrafted from Gökdeniz, 1981). For location see Fig. 5.1.

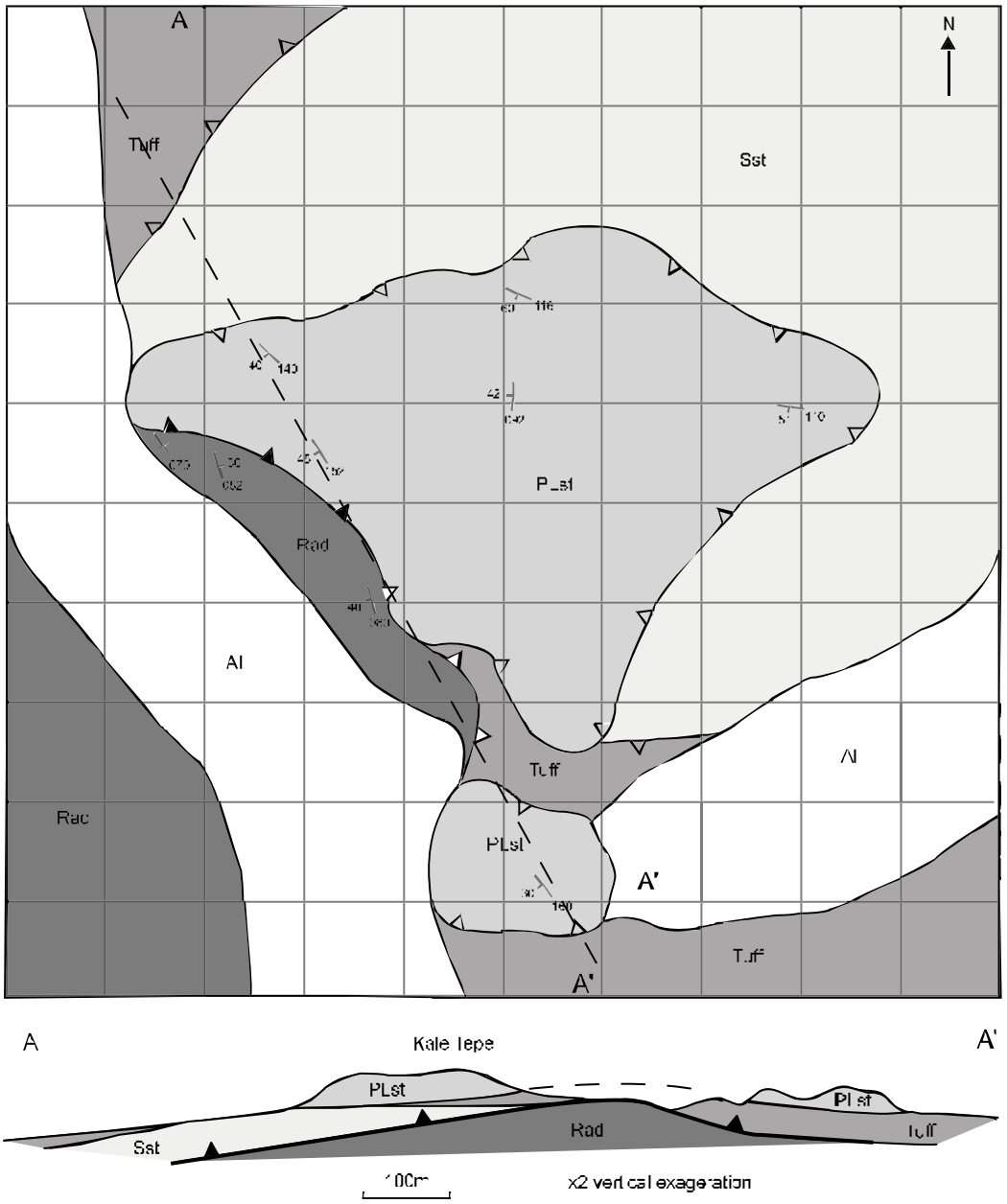

Fig.5.3 Detailed geological map and cross section of Kale Tepe locality showing structural repetition of the Ihsaniye Unit. Al, alluvium; SST, sandstone; PLst, pelagic limestone; Rad, radiolarian chert.

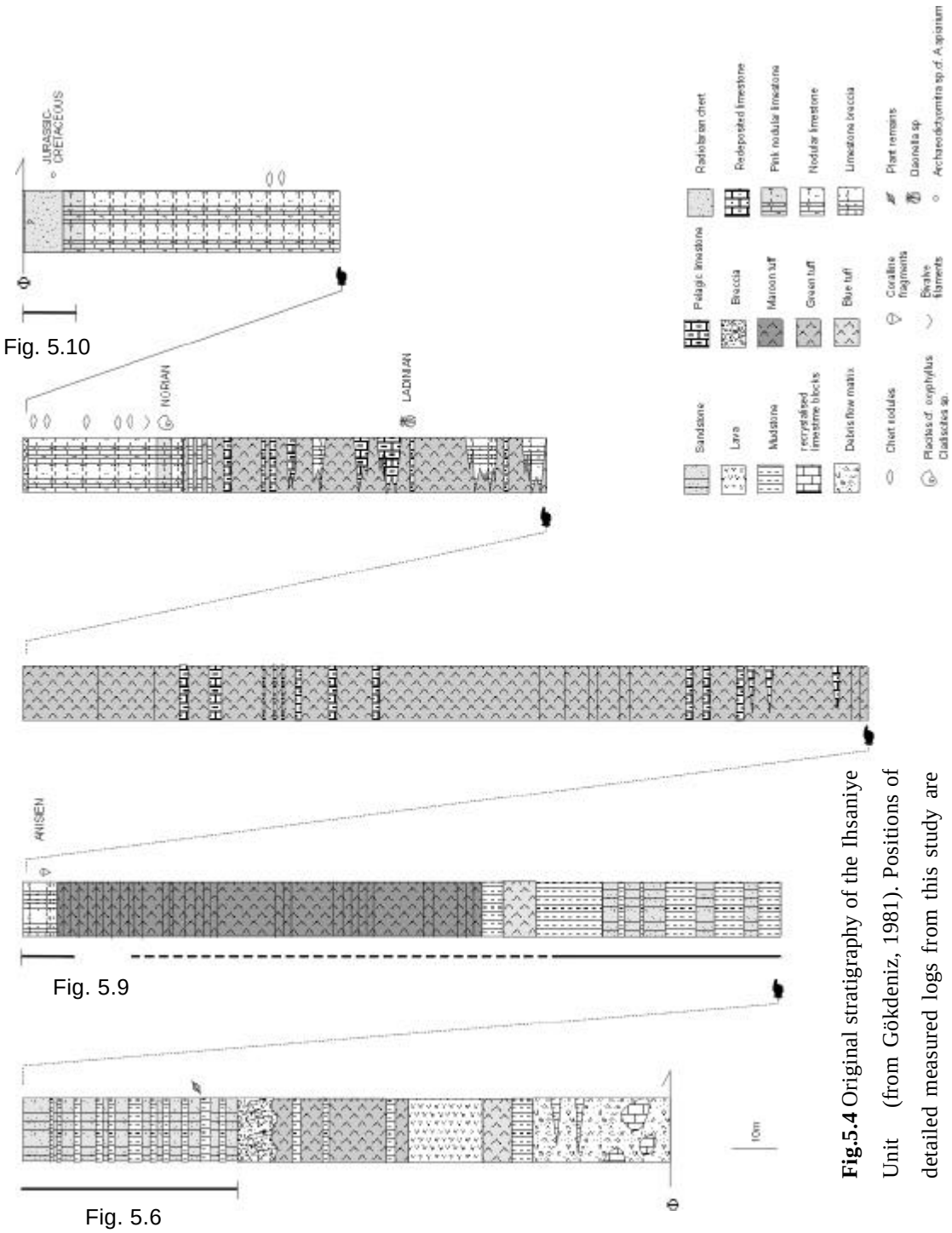

Fig.5.4 Original stratigraphy of the Ihsaniye Unit (from Gökdeniz, 1981). Positions of detailed measured logs from this study are shown above.

5.2.2.1 Basal debris flow member

The lowermost exposed part of the sequence consists of thick debris flow deposits (up to 50m thick). Lithologically, it comprises blocks of recrystallised limestone set in a coarse polygenetic sandstone matrix. The blocks range in size from <1m to > 20m and are randomly oriented in a matrix. However, local orientation of the blocks on a variety of scales is seen (Fig.5.2 and Section 5.4). The blocks consist predominantly of recrystallised neritic limestone. The matrix of this unit is generally not well exposed due to the fact that it usually crops out in topographic depressions and has a thick vegetation cover. Where it is accessible, the matrix consists of diverse elements such as quartz, calcite and lithic fragments of volcanic and metamorphic material. Previous studies have identified a varied fauna, including *Glomospirella* sp., *Glomospira* sp., *Permodiscus* sp., *Stafella* sp., *Globivalvulina* sp. and *Ammodicus* sp., within the blocks (Koçyigit, 1976).

5.2.2.2 Interbedded volcanic/clastic sub-unit

The basal debris flow member is overlain by a sequence of interbedded volcanic and clastic lithologies, ca.200m thick. The local sequence of this member is highly variable, also, it is not present in the northernmost thrust sheet. The only previously published section (Fig. 5.4) of this sub-unit located to the north of Azi Tepe, at Tozlubeleni Mevkif (Fig.5.2) details a sequence of interbedded lavas and tuffs at the base (ca. 50m), passing into a clastic horizon ca.100m thick, overlain by ca.90m of bedded tuffs (Gökdeniz, 1981). To illustrate the variability of this sub-unit the middle part of the sequence was logged in detail during this study on the road section to the south of Azi Tepe and to the west of Ihsaniye village (Figs. 5.2 and 5.5), as follows in Figure 5.6.

Ihsaniye village section (Fig. 5.6)

The lowermost part of the sequence is generally very disrupted and was not logged. The measured log begins where the succession becomes more coherent. Grey massive mudstone is overlain by altered, aphyric lava which, in turn, is interbedded with buff-coloured massive tuff. Depositionally above is a normally-graded sandstone, which is interbedded with finely bedded (<5cm) buff-coloured tuff. Upsection, the clastic influence disappears and the sequence passes into ca. 2-3m of thick bedded (<50cm) tuff overlain by ca. 1-2m of well-bedded (<5cm) brown tuff, which is repeated six times to make an overall volcanic succession ca. 25m thick. Siliciclastic material then returns and dominates the succession with a 20m-thick sequence of thinly-bedded, turbiditic mudstones, siltstones and fine-grained sandstones. Minor volcanic material is present as subordinate thin beds (<5cm) of brown fine-grained tuff. The top of the turbidite horizon is overlain by a shale-rich sequence with beds of massive aphyric basalt. Samples were collected from this horizon for geochemical analysis (Section 6.1). Some analyses of samples from this horizon are given in Section 6.1.2. This shale and lava-rich horizon is, in turn, overlain by a second siliciclastic turbidite package with intercalations of lava at 90m from the base of the logged succession. The general sediment grain-size becomes generally coarser up-section with silt/sand-dominated turbidites, culminating in a thick texturally immature, monomict conglomerate, the base of which is matrix-supported (70:30; matrix:clast). Clasts within the fine sand

matrix are entirely rip-up clasts of underlying sandstone and mudstone. The clast size increases upwards to a maximium of 2m by 1m and includes entire beds of redeposited turbidite. The uppermost 6m of the conglomerate are clast-supported in a ration of 30:70 (matrix:clast). The conglomerate facies is erosively overlain by another ca. 50m-thick package of mudstone/fine sandstone-dominated turbidites (Fig. 5.5) culminating in a normally graded sandstone package with m-to-dm thick beds. This horizon is rich in organic material, including debris <0.5cm in size of plant stems and leaf material (Fig.5.7). The succession passes into sheared mudstone/fine sandstone turbidites. The uppermost contact in this section is marked by a strike-slip fault (Fig. 5.8).

Fig. 5.5 Thinly-bedded, mud-dominated turbidites, from ca. 130m upsection on measured log shown in Fig. 5.6. Log measured south of Azi Tepe in Fig. 5.2. Hammer for scale.

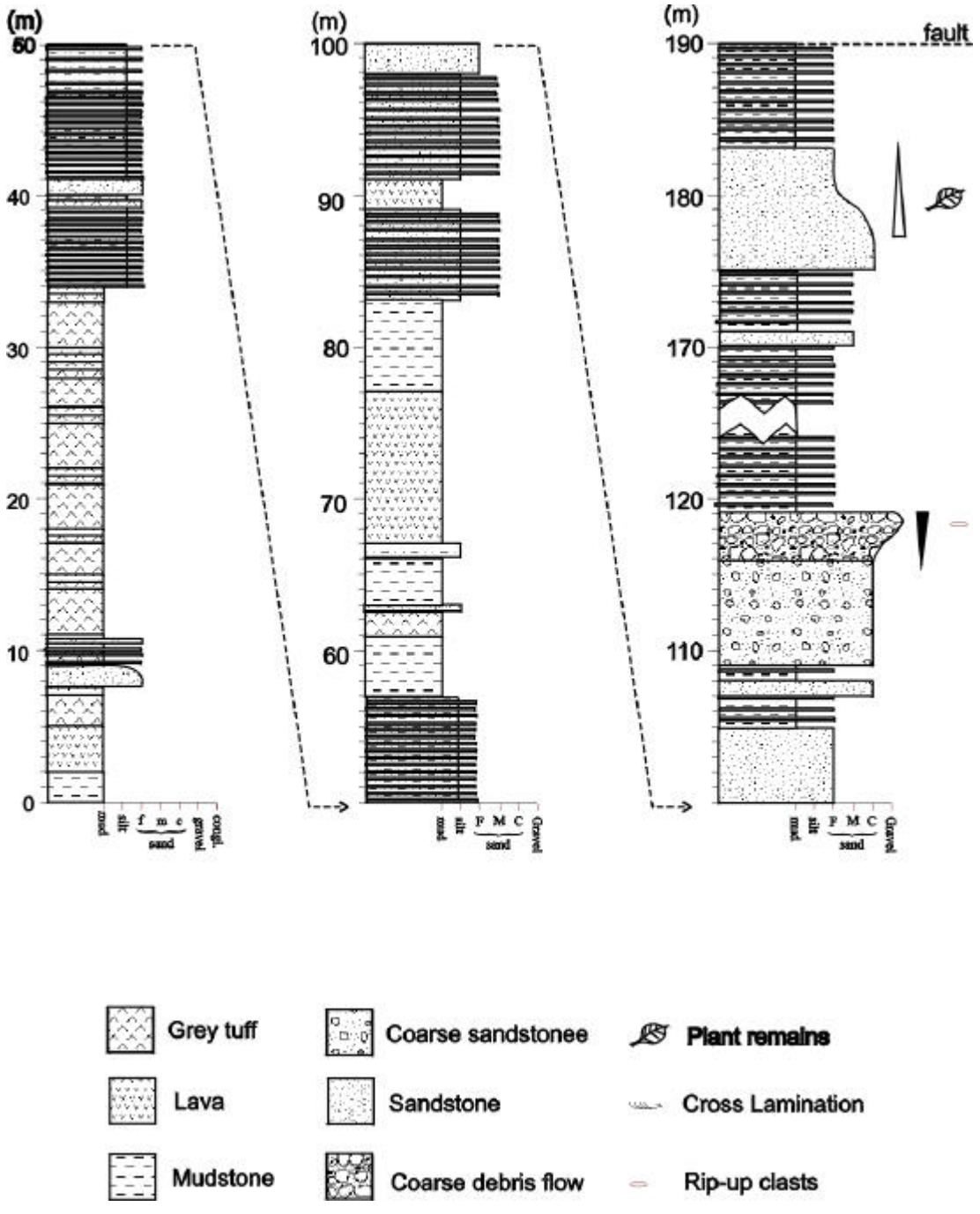

Fig. 5.6 Measured log through the volcanic/clastic sequence section to the south of Azi Tepe and west of Ihsaniye village (Fig. 5.2)

Fig. 5.7 Close up field photograph of organic material (black specks in broken block shown by arrow). Sample from ca. 180m upsection in log shown in Fig. 5.6.

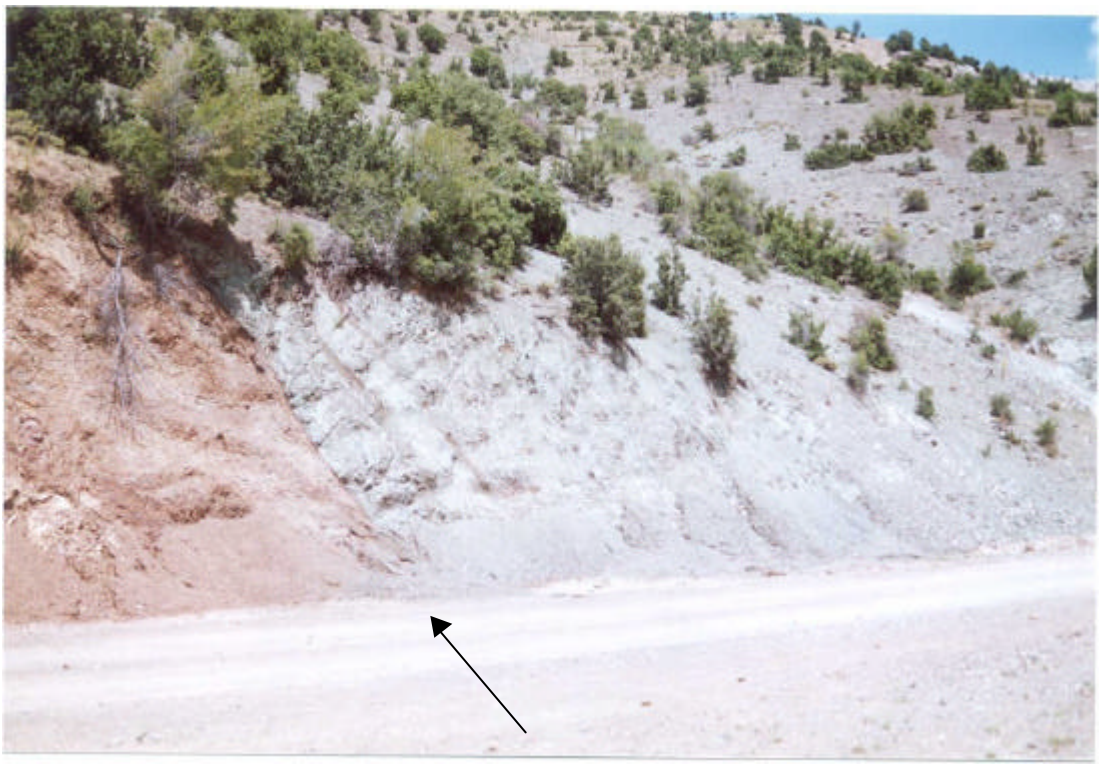

Fig. 5.8 Oblique fault (highlighted by arrow) marking the top of the measured section (Fig. 5.6). Sheared sandstone and mudstone lie to the left of the fault, with green tuff to the right.

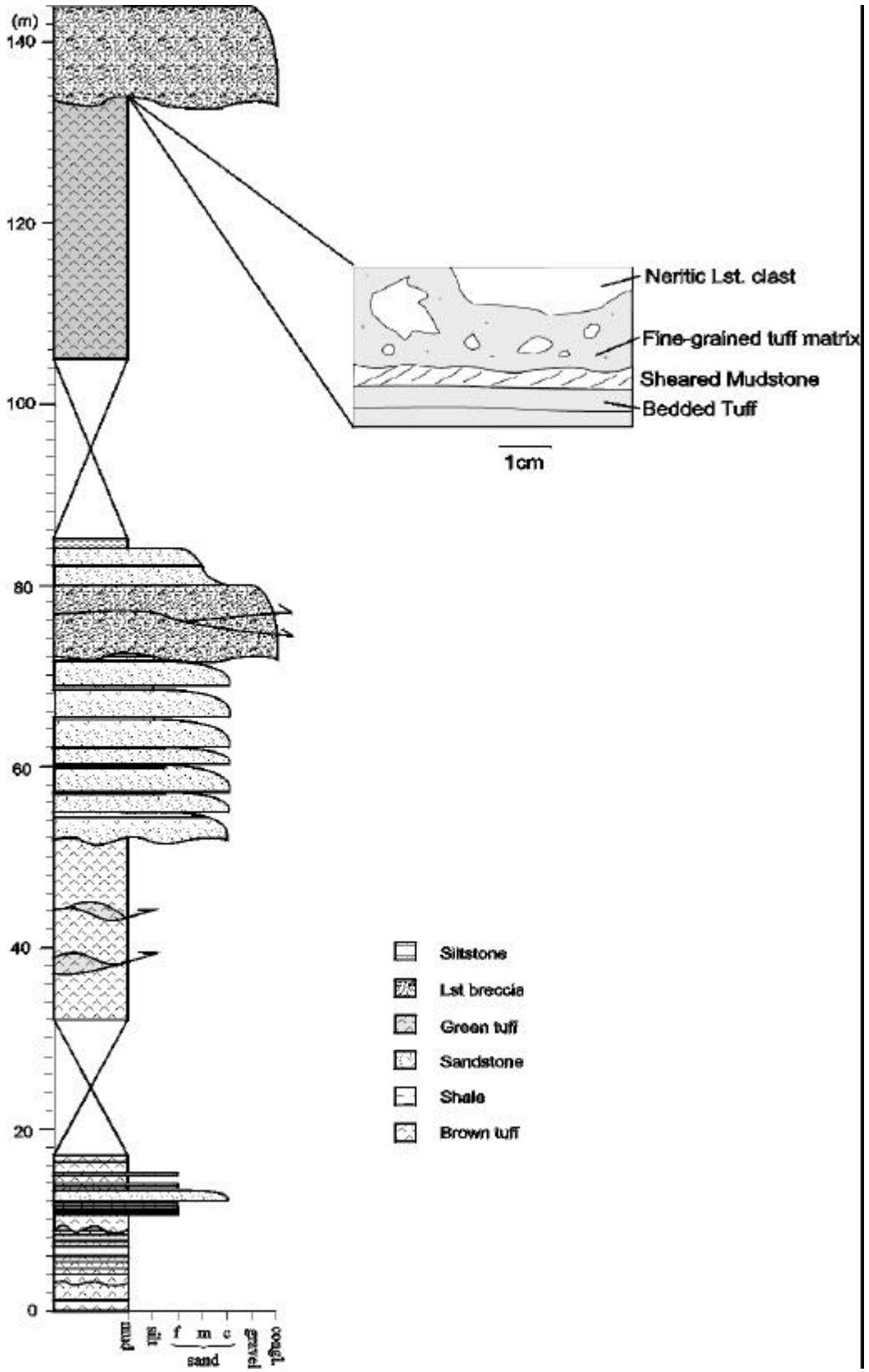

Fig.5.9 Measured log through limestone breccia found to the south of Tozlubeleni Mevkif (for location see Fig. 5.2). Inset shows field sketch close up of contact.

5.2.2.3 Volcanogenic member

In the absence of fault disruption the stratigraphical succession would be expected to pass into lensoidal limestone breccias, which commonly occur on or near the boundary with the overlying green tuff sub-unit, e.g. Çingen Tepe summit, to the south of Tozlubeleni Mevkif and to the east of Karakaya Mevkif (Fig.5.2). The previous interpretation is that these deposits resuled from volcanic activity violently destroying reefs capping submarine volcanoes (Gökdeniz, 1981). Detailed logging carried out during this study shows that this scenario is unlikely (Fig.5.9). Gökdeniz (1981) has determined the following fauna from the limestone breccia which indicates a Mid Triassic age; *Agathammina* iranica, *Endothyranella* cf. wirzi, *Galeanella* sp., *Variostoma* sp., *Trochammina* sp. and *Opthalmidium* sp.

As shown in Fig. 5.9, the lowermost ca. 20m section of the succession comprises fine-grained tuff becoming interbedded with coarse-fine grained sandstone upsection. A break of 15m is present where no definite exposure is present. However, abundant weathered sandstone scree suggests the siliciclastic sequence continues. At ca.30m the measured section continues with moderately sheared brown tuff with occasional boudins of green tuff, possibly reflecting an original interbedding between these two litholgies. This is followed by sheared, yet coherent sequences, up to 2-3m thick, of coarse calcareous sandstone, normally grading into siltstone repeated over 20m. An erosive contact at 72m in the log marks the transition to an 8m thick monomict limestone breccia. The presence of shear within the outcrop suggests this may not be the original thickness but the result of imbrication (thickening) or shear (thinning). The lithology comprises a poorly consolidated and sorted (mega)breccia with sub-rounded to sub-angular clasts ranging in size from >2m to <0.5cm. Approximately 95% of the clasts are neritic limestone with 5% chert. The dominant neritic limestone comprises fossiliferous wackestone with a varied fauna of disarticulated bivalves, high-spired gastropods, algae, coral and foraminifera. A smaller proportion of the neritic limestone clasts are boundstones, with abundant rudist coral and algal material present, also crystalline carbonate where the depositional texture is not apparent. The last 2m of the megabreccia is matrix supported. Here the matrix comprises fine-grained green tuff and mudstone. Up section the matrix is dominated by micrite, occasionally containing fine, straight bivalve shells, probably belonging to the genus *Halobia*. In places, where the clast density is highest, the matrix is clast supported. Throughout the outcrop, the clast size normally grades to the top surface, where the average clast size is 5cm and the maximum clast size is 0.5m. The sequence then grades into coarse calcareous sandstone composed of well-rounded grains of neritic limestone, which in turn fines upwards into well-bedded fine grained calcareous sandstone and finally mudstone. A break in exposure exists at the top of the sequence, which resumes with massive green tuff, and minor green bedded chert. Another erosive contact occurs at the base of the limestone (mega)breccia at the top of the section. The lithology seen is similar to that previously described above.

Depositionally above the interbedded turbidite/lava facies and the limestone breccia facies, is a sequence ca.250m thick consisting dominantly of green tuff with minor pelagic limestone and lava intercalations. This sub-unit is highly sheared in most localities making it hard to locate a reliable type section. Other than field checking the previously published log (i.e. Gökdeniz, 1981; Fig. 5.4) no new sections were measured in this study. However, a number of lava samples were collected from near Ihsaniye village for petrographic and geochemical analysis, as detailed in Section 6.1. The extrusive rocks formed intercalations and/or sheared bodies within the bedded green tuff, generally never more than 5m thick.

Up section through the volcanic sub-unit, the reoccurrence of pelagic limestone intercalations increases (Fig. 5.4). These intercalations consist of extremely well-bedded (5-15cm thick), grey to light green, mudstone with mud partings along bed boundaries. Locally, the succession is pseudo-nodular in appearance. Abundant *Halobia* sp. found during this study indicate a Mid-Late Triassic age.

5.2.2.4 Pelagic limestone member

Lying stratigraphically above the volcanogenic sub-unit is a thin sequence of pelagic limestone. Once again the succession is highly sheared and folded making a type section hard to define. The maximum thickness of the unit is 80m, measured in the Tozlubeleni section of Gökdeniz (1981), i.e. Figure 5.4. Above a transitional zone of interbedded pelagic limestone and green tuff the sucession begins with 3-4m of grey nodular mudstone, with green siltstone/mudstone partings. This passes into pink Ammonitico Rosso nodular limestone, up to 5m thick. Previous studies have identified a fauna of ammonites, including *Placites* cf. Oxyphyllus (MOJS) and *Cladiscites* sp., which indicates a Mid-Upper Norian age for this *Ammonitico Rosso*-type limestone (Gökdeniz, 1981). Above, the sequence continues with well-bedded monotonous grey coloured pelagic mudstone, with abundant replacement chert nodules. The top of the sequence is represented by 1-5m of platy, red coloured, laminated mudstone, rich in radiolaria.

This type section is characterised by all successions studied, however, the sequence is tightly folded and sheared which can lead to significant differences in the stratigraphy. To illustrate this variance in thickness and lithology the same sequence was measured at a different location to the north of the previous section during this study (Fig. 5.10).

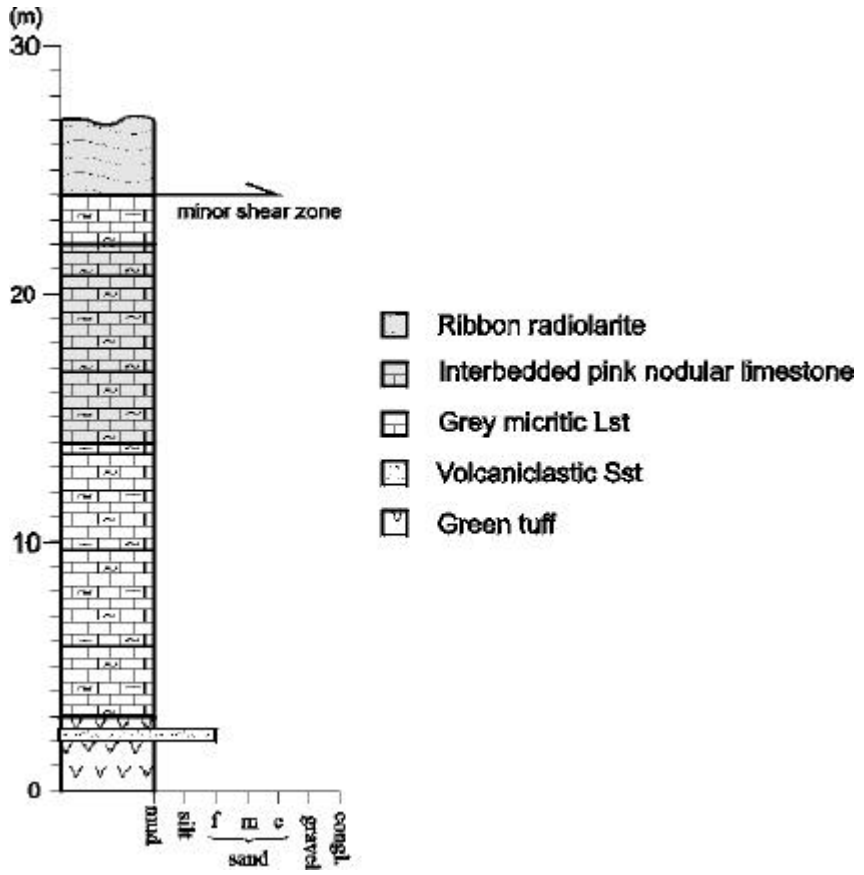

Fig.5.10 Log of pelagic limestone sub-unit measured near Keklikseki Tepe (for location see Fig. 5.2).

The measured section at Keklikseki Tepe (Fig. 5.10) begins within the uppermost units of the volcanogenic sub-unit. Medium-well bedded tuff with subordinate beds of fine volcaniclastic sandstone pass vertically into an 11m section of tightly folded cm-bedded grey pelagic limestone, which contain occasional bivalve filaments. This passes into 8m of cm-bedded pink nodular mudstone, interbedded with thin grey micritic limestone beds. The succession then grades back into the grey micritic limestone lithology. The top of the section is heavily deformed with the sequence tightly folded and verging generally to the south-east. The limestone sequence is overridden by sheared radiolarian chert above a low-angle shear zone, with a general top-to-the south sense of displacement (see Section 8.1.2 for more details of kinematics).

5.2.2.5 Radiolarian chert member

In the normal undisturbed stratigraphic sequence, a sequence of radiolarian chert exists at the top of the Ihsaniye Unit. The chert is highly sheared; hence, a precise thickness is hard to determine. One of the fieldwork aims was to study this radiolarian sequence in an attempt to provide a more detailed biostratigraphy. A relatively undeformed section through the sub-unit was logged to the east of Kabaagaç Tepe (Figs.5.2 and 5.11).

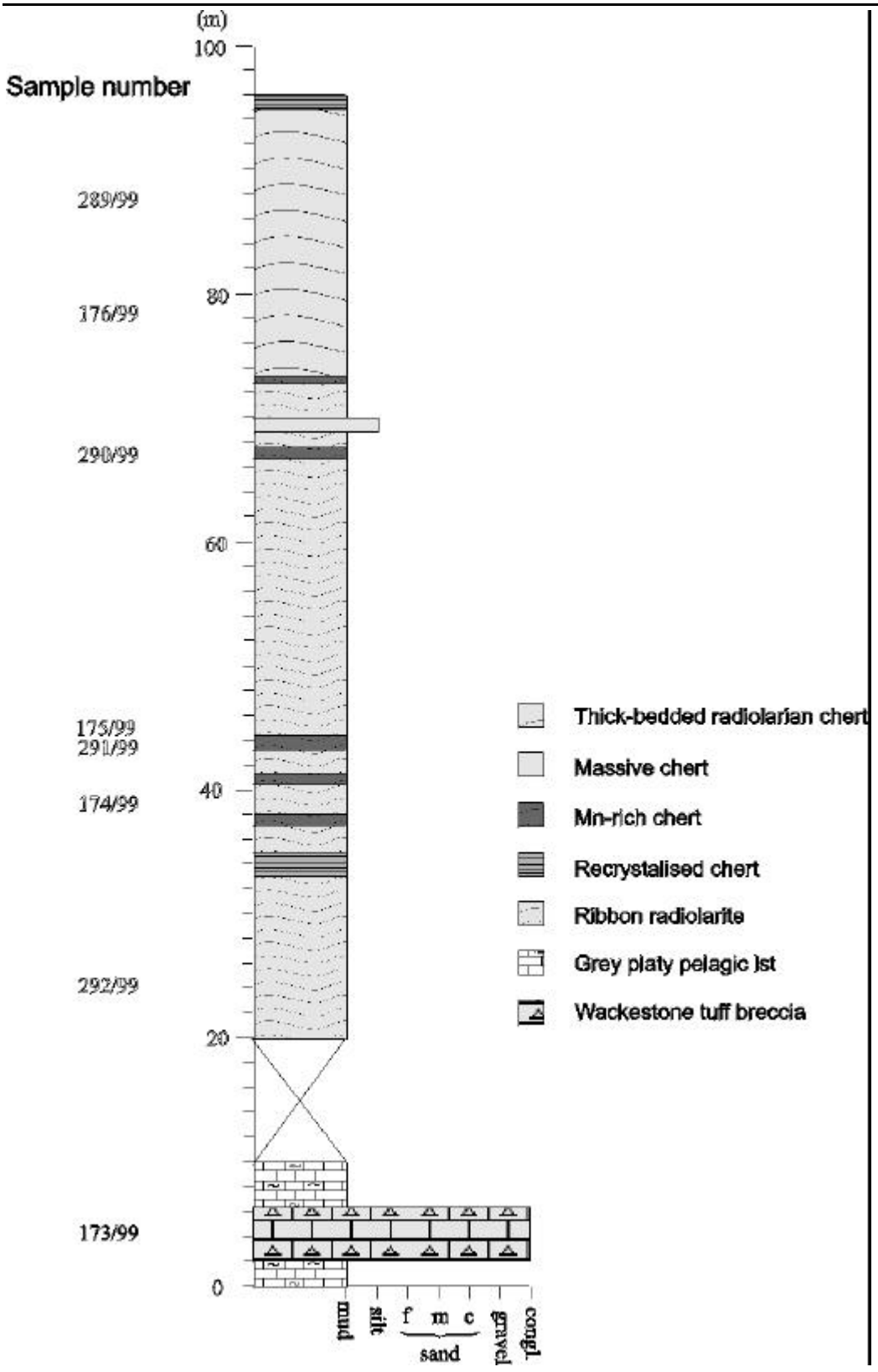

Fig.5.11 Log through the upper part of the radiolarian chert succession, measured to the east of Kabaagaç Tepe (Fig. 5.2 for location). Numbers of chert specimens collected for radiolarian extraction are shown in the column to the left of the log (Appendix 1).

A number of samples of chert were collected for extraction of radiolaria with a view to enable dating by Dr. Taniel Danelian (Université Pierre & Marie Curie, Paris VI). The main species identified from this work are shown in Table. 5.2. Unfortunately the material is badly preserved and a precise date other than post-Triassic was not possible. A full description of the work undertaken, supported by plates of the radiolarian fauna from the samples can be found in Appendix 1.

Sample number	Genus/species	Age data
E176/99	*Parvicingulidae sp.* *Triatrbs* sp. *Archaeodictyomitra* sp.cf. *A.*apiarium *Emiluvia* premyogii	Jurassic-Cretaceous
K292/99	*Archaeodictyomitridae sp.* *Hsuidae sp.*	Both post-Triassic forms

Table 5.2 A brief summary of the radiolarian fauna from the Kabaagaç Tepe section.

5.3 Oyuklu Dag Unit

The uppermost unit in the Ermenek area consists of a thick thrust sheet of predominantly neritic limestone, locally known as the Oyuklu Dag Unit, after the mountain of the same name (Fig. 5.2). This unit mainly crops out in the southern part of the study area where relief is higher, but it also forms a small 'klippe' at Azi Tepe. Figure 5.12 shows the view southwards from Azi Tepe towards Oyuklu Dag. This view nicely illustrates the thrust sheet stacking order and the sense of scale of the outcrop.

5.3.1 'Broken-formation' matrix

The Oyuklu Dag Unit is highly disrupted, especially towards the leading edge at the base, where it is extremely fragmented and forms kilometre-decimetre sized blocks set in a sandy matrix. Using the widely accepted melange terminology of Raymond et al (1984), it could be classified as 'broken-formation' (Section 1.6). The matrix consists of conglomerate to fine sand sized, generally rounded and well sorted, polygenetic clasts. Analysis of the clast composition indicates the material was most likely to have been sourced from the B-H Nappes themselves. Clasts are composed of green tuff, chert, micritic limestone, quartz, lithic fragments and volcanic-derived material, which are present in varying concentrations depending on location. Figure 5.13. shows a log through part of a matrix-rich sequence measured to the south of Yaglica Tepe.

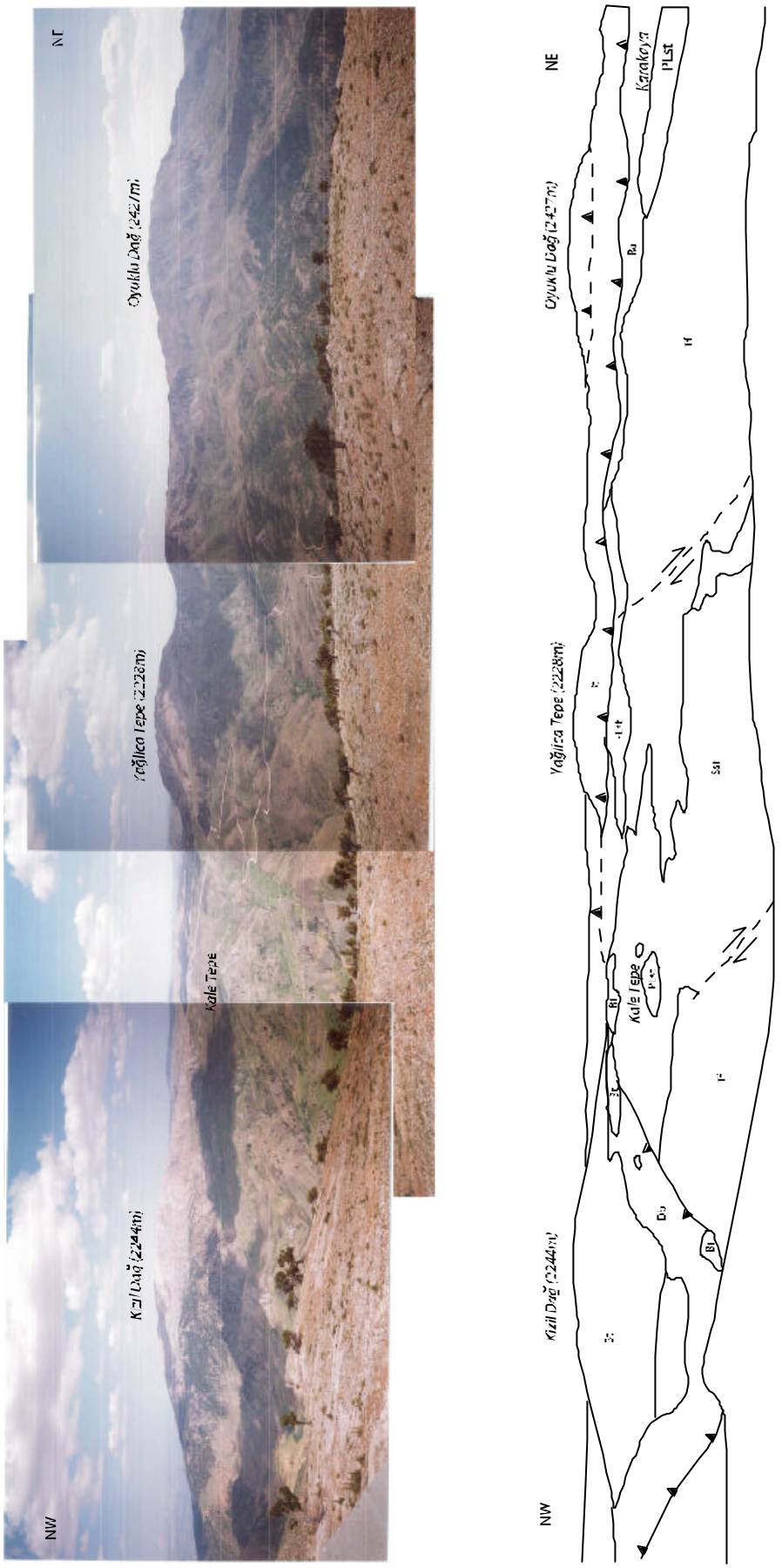

Fig. 5.12 Field photograph motage and interpreted sketch of the view southwards from Azi Tepe towards Oyuklu Dag showing thrust sheet stacking order.

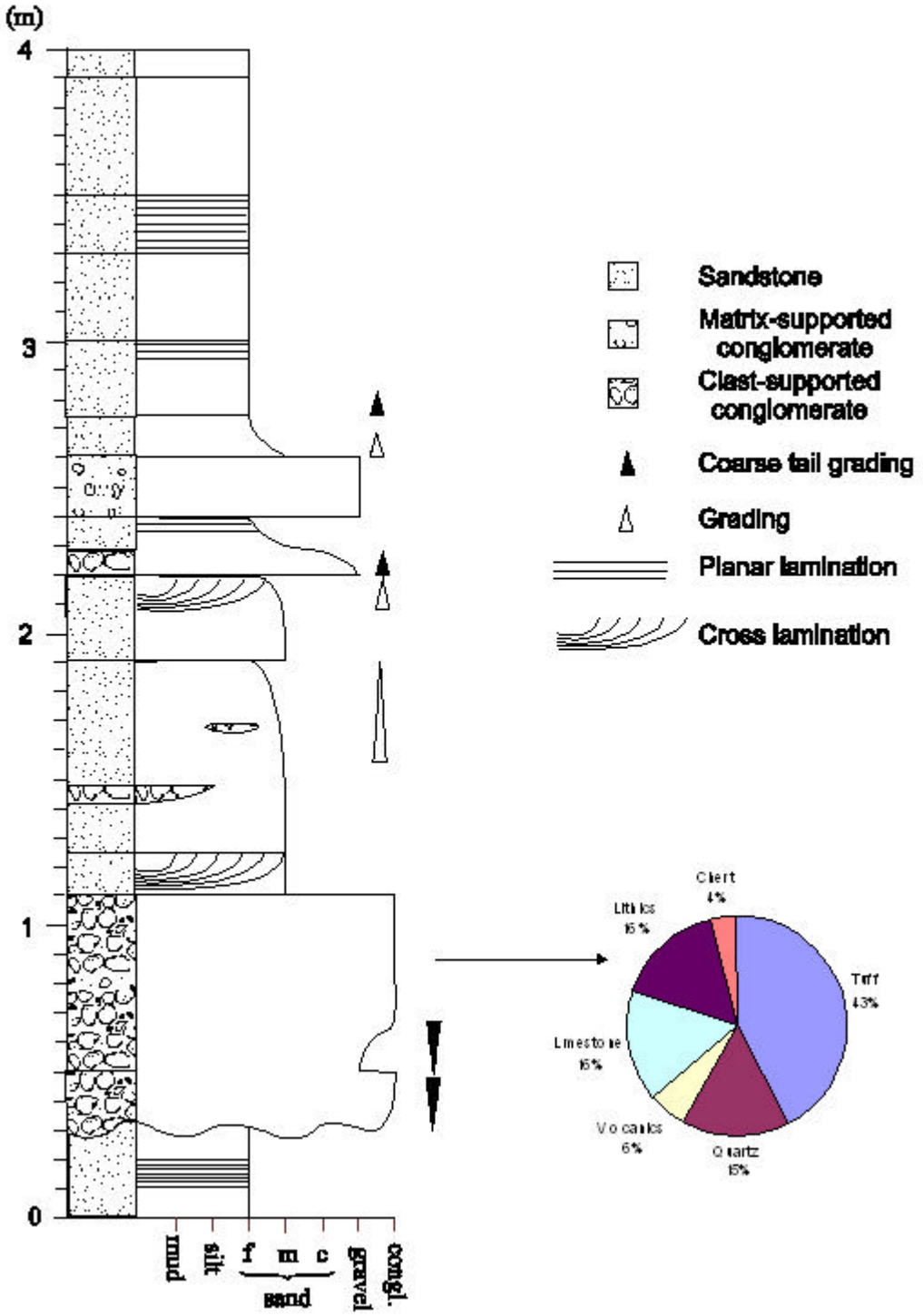

Fig. 5.13 Log through the matrix of the Oyulu Dag broken formation measured to the south of Yaglica Tepe (Fig. 5.2). Piechart shows frequency of clast lithologies in conglomerate from a sample population of 50.

Fig. 5.14 Close up of matrix from Fig. 5.15.

Fig. 5.15 Outcrop view of matrix-material. Note alignment of medium-sized blocks along bedding planes (as indicated by arrow). Photograph taken 7.5km east of Ihsaniye village, (Karaman sheet, 010825)

Fig. 5.16 Large scale blocks of recrystalised limestone set in matrix material. Photo taken 3.2km east of Ihsaniye village.

Blocks within the matrix are predominantly composed of limestone showing a wide range of sizes, from <10cm (Fig. 5.15) up to ca. 10 metres (Fig. 5.16). Lithological study of the blocks is limited because most are heavily recrystallised, but they are similar to the overlying limestone of the Oyuklu Dag Unit.

5.3.2. Triassic-Jurassic Oyuklu Dag 'broken formation'

Structurally above the basal siliciclastic sediments is a thick sequence (>500m) of massive grey recrystallised carbonate, the type section of which is seen on the north face of Oyuklu Dag. No complete measured section could be made through the entire unit due to the highly deformed nature of its structureless lithology. However, local sequences were measured to illustrate the nature of the unit (Fig. 5.17).

The lowermost exposed succession within the Oyuklu Dag sequence can be seen to the south of Karakaya Mevkif. It comprises a sequence of pink micritic nodular limestones and radiolarian chert, shown in Figure 5.18. An age of Upper Carnian was previously assigned for this facies by Gökdeniz, (1981), although no measured sections previously exist. The pink pelagic limestone facies then passes vertically into grey micritic carbonate.

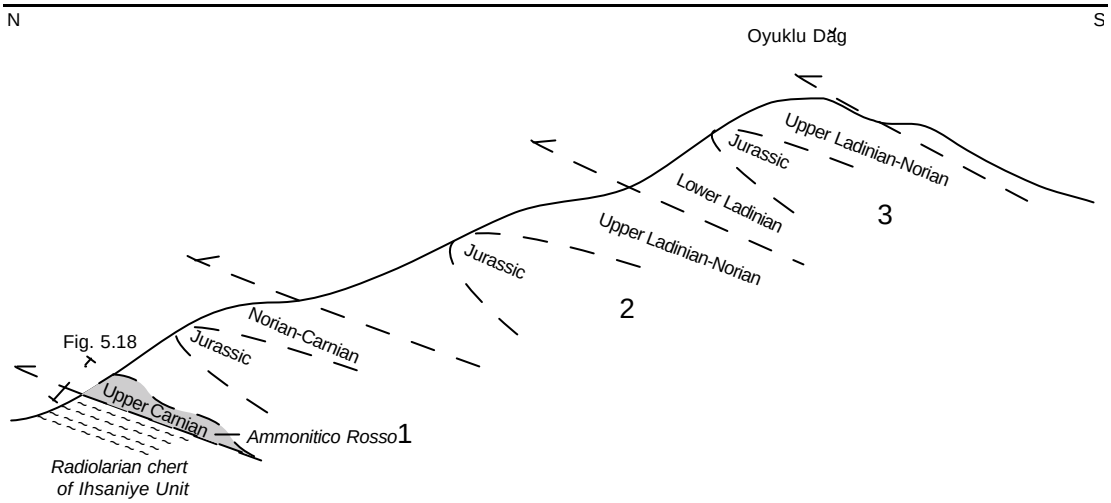

Fig. 5.17 Oyuklu Dag section after Gökdeniz (1981) showing position of Upper Triassic *Ammonitico Rosso* and new log measured during this study. Line of section shown on Fig. 5.2. Not to scale.

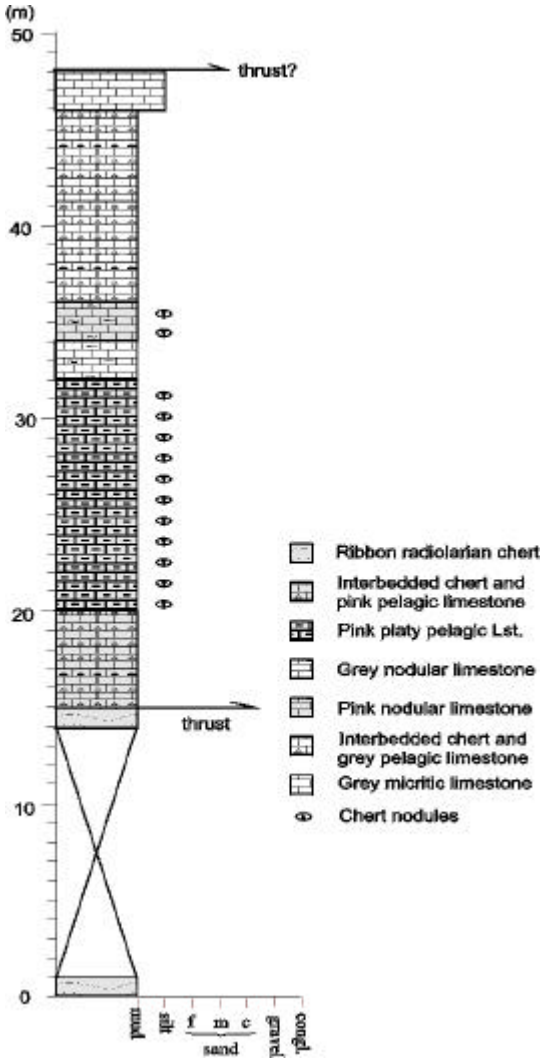

Fig.5.18 Log measured through Ammonitico Rosso facies at Oyuklu Dag.

The Ammonitico Rosso-type facies is structurally overlain by a number of thrust sheets, as depicted in Fig. 5.17. Each thrust sheet consists of massive grey micritic wackestones-packstones with an abundant fauna of foraminifera, algae, gastropods, echinoderms and bivalves.

5.4 Tectonostratigraphy of the Karaman area

The Karaman area lies to the NW of the previous field area and is essentially a continuation of the same units seen in Ermenek. The only detailed published map is by Koçyigit (1976) which was field checked and redrafted with minor additions to the Ak Tepe-Verme Tepe area, as shown Figure 5.19. No detailed formal stratigraphic nomenclature has been given for individual thrust sheets in this area so this study utilizes the terminology used by Gökdeniz (1981) in the Ermenek area. Table 5.3 summarises the tectonostratigraphy of the Karaman area.

<table>
<tr><th>Autochthon</th><th>B-H Nappes</th><th>Post-Tectonic cover</th></tr>
<tr><td rowspan="2">Bolkar Dag Unit
(Lower Jurassic?-
Upper Cretaceous?)</td><td>Oyuklu Dag Unit
(U.Triassic-Cretaceous)</td><td rowspan="2">Neogene</td></tr>
<tr><td>Ihsaniye Unit
(Triassic-Upper Cretaceous)</td></tr>
</table>

Table 5.3 Summary of the tectonostratigraphical units in the Karaman area.

In addition, as this area was believed to be melange (e.g. Koçygit, 1979) no detailed lithological or sedimentological data were available for the B-H Nappes in this area. After reconnaisance, type sections of allochthonous units were identified and measured. Also, the lower contact with the Bolkar Dag Unit was investigated to shed light on the emplacement history of the B-H Nappes. The findings are detailed in the following sections.

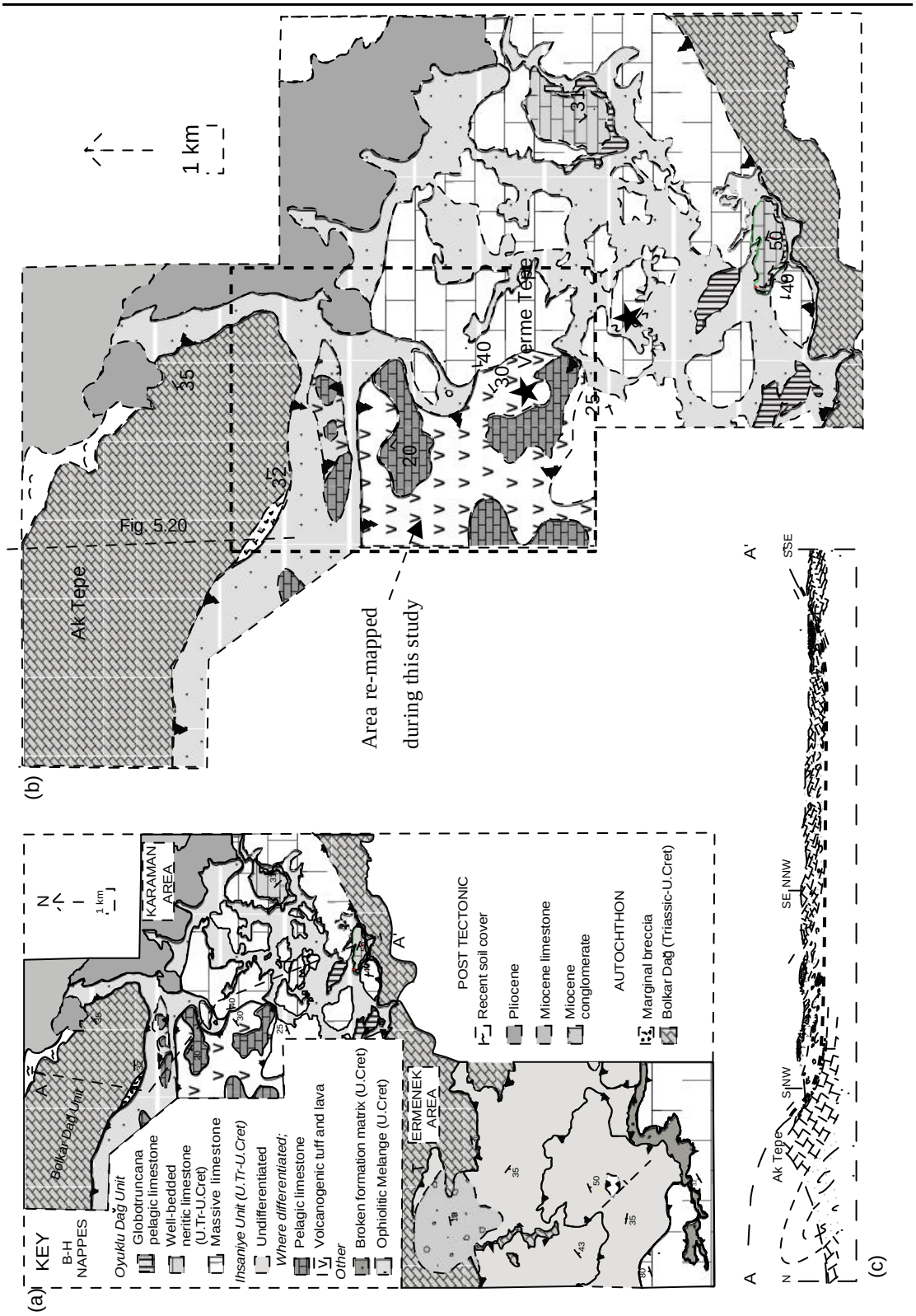

Fig.5.19 (a) Geological map of the eastern region, showing the Karaman area in relation to the Ermenek area (map adapted from Koçyigit, 1976 and Gökdeniz, 1981), **(b)** Close-up of the Karaman area showing position of logs, **(c)** cross section through the Karaman area.

5.4.1 Bolkar Dag Unit

As in the Ermenek area, the Bolkar Dag Unit is the lowest exposed sequence which crops out in the north of the study area (Figure 5.19). A section near Ak Tepe (hill) was chosen to illustrate the top of the sequence. As this unit was discussed previously, the reader is referred to Chapter 4.4.2 for a detailed outline of the statigraphy.

At Ak Tepe, the Bolkar Dag Unit forms a large recumbent anticline overturned to the north, as clearly seen in this section (Fig. 5.20). The core of the anticline (Fig.5.21) is made up of a distinct sequence of dominantly red-coloured siliciclastic sediments which can be correlated with the Lower Jurassic sediments seen in the Bolkar Dag elsewhere (Chapter 4.4.2), also with the Çayir Formation in the Geyik Dag autochthon (Monod & Akay, 1984) and the Derebucak conglomerate in the Hadim Nappe (Monod, 1977). The sequence comprises red arkosic sandstones interbedded with lensoidal pebble conglomerates. Clasts are dominantly composed of well-rounded, pebble sized limestone and red/black chert This siliciclastic sequence is normally overlain by well-bedded micritic limestone, with little or no distinguishing features. Locally the lithology is dominated by pisolitic and oolitic packstones-grainstones. Within the thick (ca.100m) limestone sequence, approximately E-W trending zones of tectonic breccia crop out, slightly discordant to bedding, which probably mark thrust planes within the limestone sequence. These zones are laterally continuous for hundreds of metres and reach up to 50m thick; however, outcrop is extremely poor and their presence is usually revealed from their morphological features (Fig. 5.22)

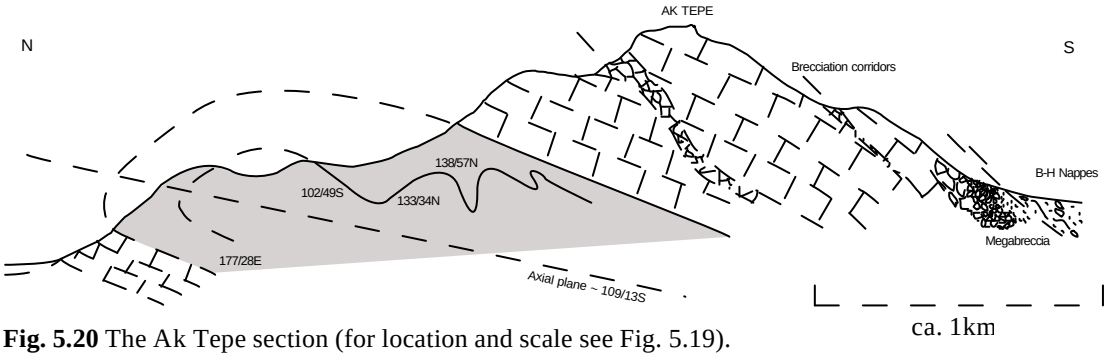

Fig. 5.20 The Ak Tepe section (for location and scale see Fig. 5.19).

The highest exposed part of the Bolkar Dag Unit is exposed in a quarry on the south side of Ak Tepe. There, the lithology consists of an extremely poorly-sorted megabreccia. Clasts are composed of highly angular micritic mudstone, wackestone/packstone and subordinate fine-grained sandstone. Clast size varies from >5m to <1cm. Diffuse bedding is defined by rafts of semi-coherent material floating in a matrix, which consists of variously coloured red-yellow micrite. Small planktonic

foraminifera (*Globotruncana?*) are present locally, which would indicate an Upper Cretaceous age for the matrix.

Fig. 5.21 Field photograph looking to the south-east at the core of the anticline at Ak Tepe.

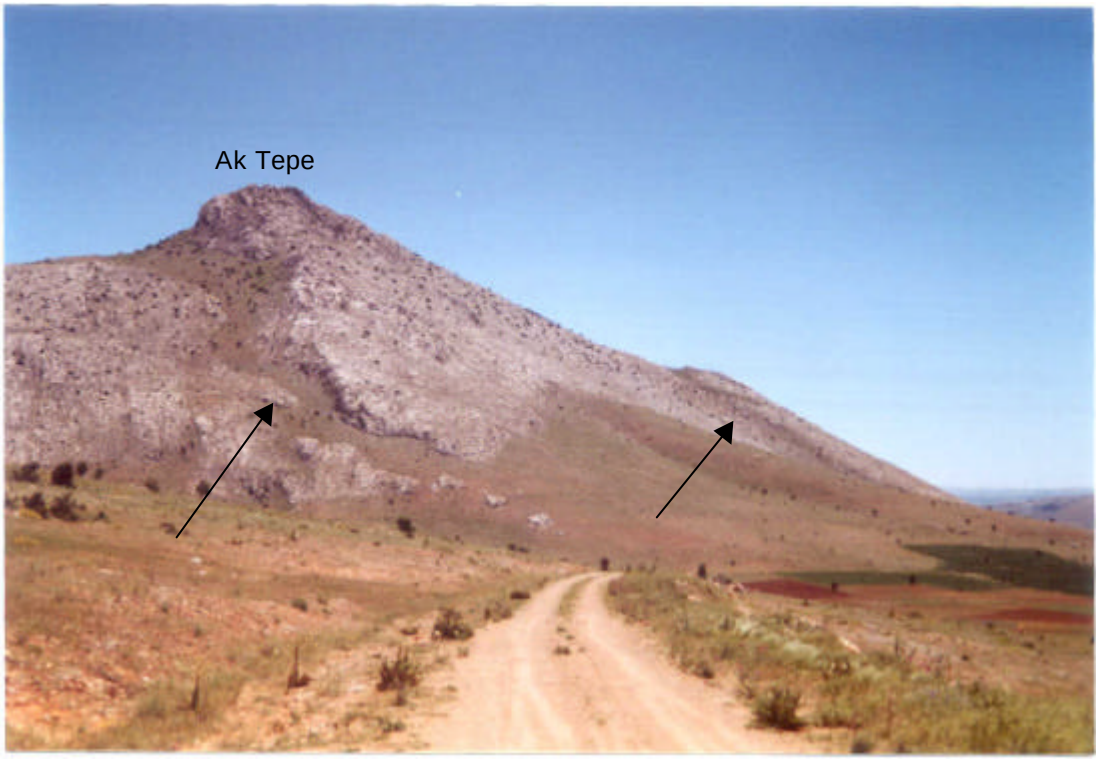

Fig.5.22 Field photograph looking due east at tectonic breccia corridors (marked by arrows) within the Bolkar Dag Unit at Ak Tepe.

This megabreccia passes vertically into poorly sorted and sheared conglomerate. Clast size varies within the debris flow from 3m to <1cm and is predominantly composed of redeposited limestone facies. A smaller proportion of the clasts (<10%) are composed of dark (volcanogenic?) chert, highly altered basalt and igneous clasts. Above this sequence lies Ophiolitic Melange belonging to the B-H Nappes, which clearly differs due to a drastically higher proportion of volcanic and ophiolite-derived material.

5.4.2 B-H-Nappes

In the Karaman area, the Bolkar Dag Unit is tectonically overlain by the B-H Nappes, which consist of three main units. The thrust sheets are in continuation with the Ermenek area, but are highly fragmented and set in Ophiolitic Melange. However, locally sequences exist that are coherent allowing sections to be measured and correlated.

5.4.2.1 Ophiolitic Melange

Ophiolitic Melange crops out extensively in the Karaman area (Fig. 5.19) and forms the matrix in which large kilometre-scale blocks of the Ihsaniye and Oyuklu Dag Units are set. The matrix of the melange generally comprises highly sheared green scaly clay enclosing boudinaged blocks on a variety of scales. A general bimodal clast population was discovered. Smaller phacoids (<1m to 100m) show a wide range of lithologies including calcarenite, radiolarian chert, basalt, recrystallised limestone, volcaniclastic sediment, pelagic limestone, quartzose sandstone, gabbro and locally serpentinite. A number of samples of fine-grained volcanic extrusive rocks were collected from the melange 2kmsouth of Verme Tepe for geochemical analysis (Section 6.2). Larger blocks (>1km) are almost invariably derived exclusively from the Ihsaniye and Oyuklu Dag lithologies.

5.4.2.2 Ihsaniye Unit within the Ophiolitic Melange

Although there is no strict boundary between the units in the melange, the Ihsaniye Unit tends to crop out towards the northwest in a low structural position within the melange. No type section existed for this unit in the Karaman area before this study. Reconnaissance fieldwork showed the Verme Tepe locality, approximately 4km west of Burhan village, exhibits the longest uninterrupted section through the unit, as shown in Figure 5.22.

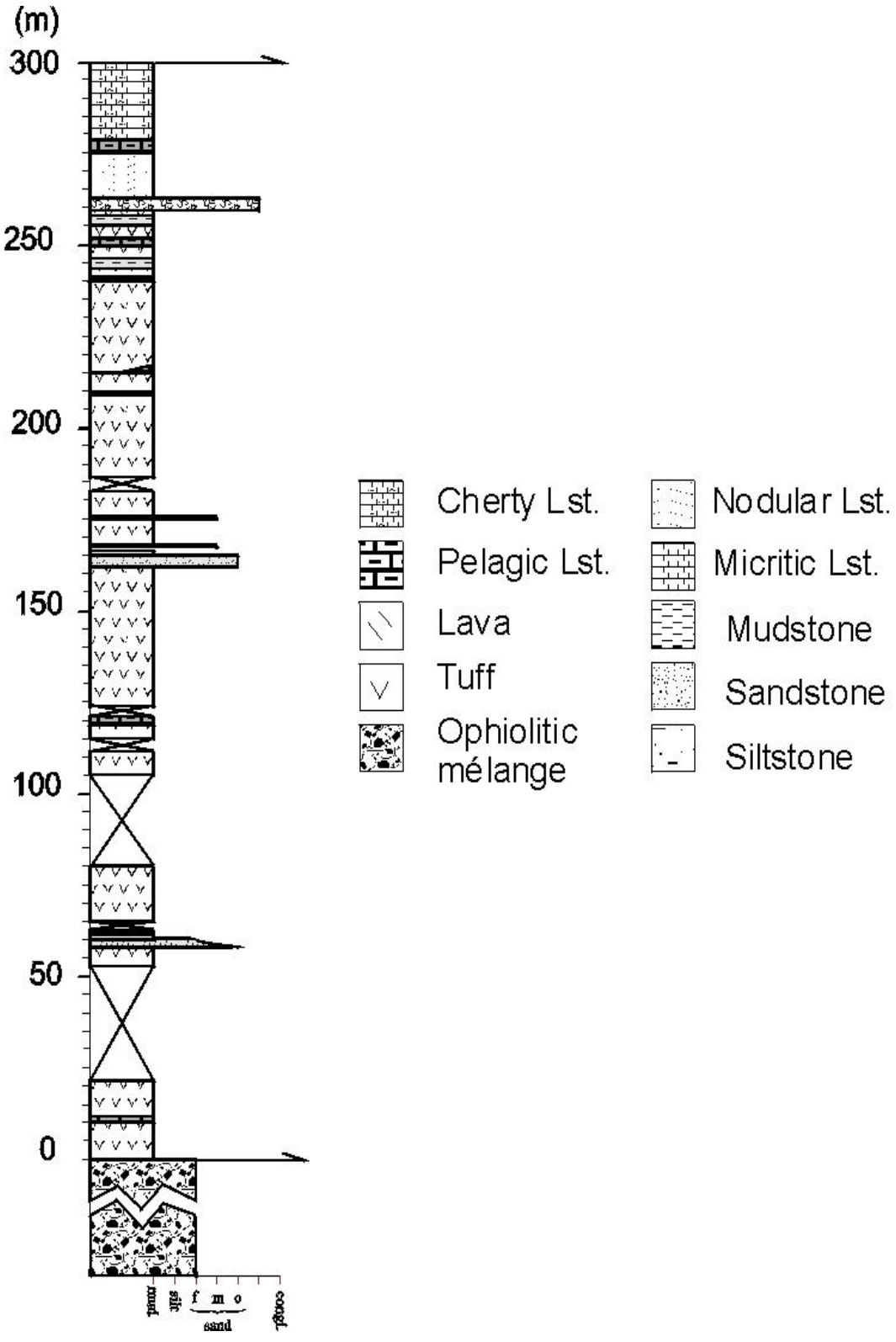

Fig.5.22 Log through the Ihsaniye Unit measured at the Verme Tepe type section (for location see Fig. 5.19)

The Verme Tepe section begins with thick-bedded, fine-grained, green tuff intercalated with well-bedded, *Halobia*-bearing pelagic limestone and fine granular calciturbidites. This succession continues for ca. 250m, above which it is normally overlain by a pelagic limestone sequence. A transition zone exists between the two facies. In the top 20m, the amount of interbedded calc-turbidites decreases and is replaced by green shale, before passing into a 2m thick limestone conglomerate horizon. Above, is a 12m-thick succession of pink nodular limestone interbedded with thin beds of dark grey micrite. Intraformational breccias are common within this horizon. The sequence then passes into massive mudstone, which in turn grades into thick-bedded cherty pelagic limestone (Fig. 5.22).

5.4.2.3 Oyuklu Dag Unit in the melange

The uppermost levels of the melange in the Karaman area are dominated by large kilometre-scale Oyuklu Dag Unit lithologies. Generally, most of the blocks consist of sheared white recrystallised massive limestone with little or no distinguishing features. A road cutting (location shown in Fig.5.19) provides a good section through the upper half of the unit (Fig. 5.23).

The log begins with a sequence of recrystallised neritic carbonate, occasionally with large bivalve remains resembling *Megalodons*, suggestive of a Late Triassic age. The thickness of this part of the succession is generally >100m depending on the size of the block in the melange. Above a local tectonic breccia, the sequence passes into well-bedded, siliceous white biomicrite, with abundant stylolites and replacement chert nodules. A small transition zone of interbedded chert and nodular limestone is present at the top of this sequence, which is overlain by ca. 20m of well-bedded, wavy, nodular, pink pelagic limestone. This is overlain by what appears to be a radiolarian chert sequence 12m thick. This is hard to quantify due to the lack of outcrop. Only the upper 2m is well exposed. This passes back into pink nodular limestone with chert interbeds.

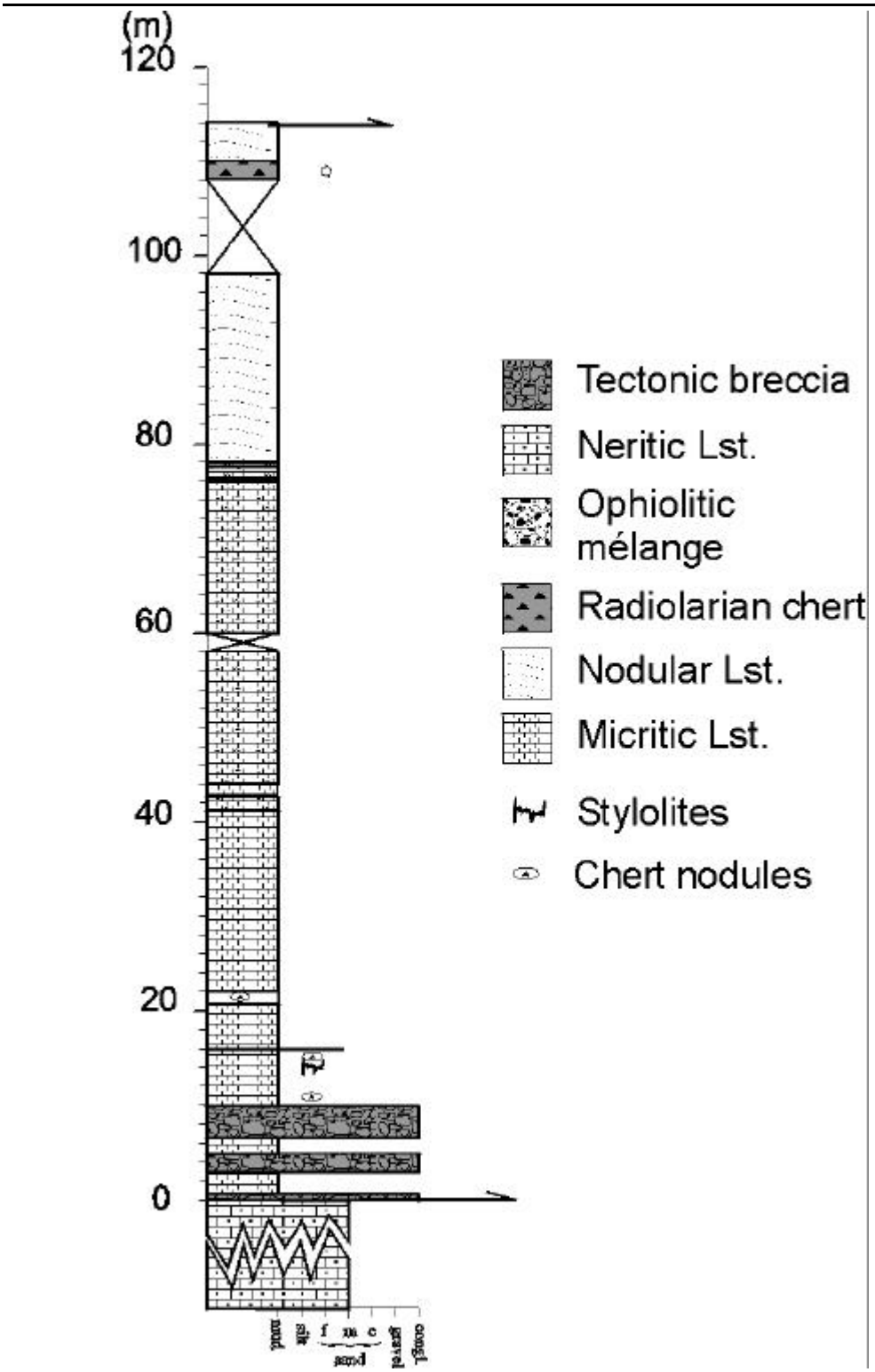

Fig.5.23 Log through the upper half of the Oyuklu Dag Unit in the Karaman area (for location see Fig. 5.19).

5.5 Summary

The area between Ermenek and Karaman forms the easternmost extent of the B-H Nappes. Investigation of the tectonostratigraphy has shown that it is comparable with the areas further west along strike. The following summary points are as follows:

1. The Hadim Nappe crops out far to the south of the study area, along with slices of serpentinized peridotite structurally on top.

2. The Bolkar Dag Unit forms the lowest exposed Tauride unit in this eastern area. The base is not exposed so it is not possible to tell if it is a rootless thrust sheet, as in the Hadim area, or whether it is relatively autochthonous as is the case further east in the Bolkar Daglari (Mountains). The uppermost levels of the Bolkar Dag Unit are disrupted and locally comprise massive megabreccias, probably of Late Cretaceous age.

3. The Ihsaniye Unit is the structurally lowest unit of the B-H Nappes, which is emplaced onto the Bolkar Dag Unit, as seen in several small tectonic windows in the Ermenek area and Ak Tepe (Hill) in the Karaman area. This unit begins with debris flows and siliciclastic sequences, before passing into a volcanic pile, ca. 1km thick. This is overlain by Upper Triassic to Jurassic pelagic limestones, radiolarian chert and Ammonitico Rosso pelagic limestone.

4. The Oyuklu Dag Unit is the highest exposed thrust sheet of the B-H Nappes in this area, consisting of Upper Triassic to Jurassic neritic limestone.

5. In the Karaman area (north) the B-H allochthonous units consist of broken formation with Ophiolitic Melange as matrix between the blocks. Further south, in the Ermenek area the thrust sheets are more coherent, yet internally imbricated.

6. The B-H Nappes form the ‘basement’ to a small Miocene carbonate platform in the Ermenek area, linked to the larger Mut Basin of southern Turkey, which obscures the relationship with lower Tauride units.

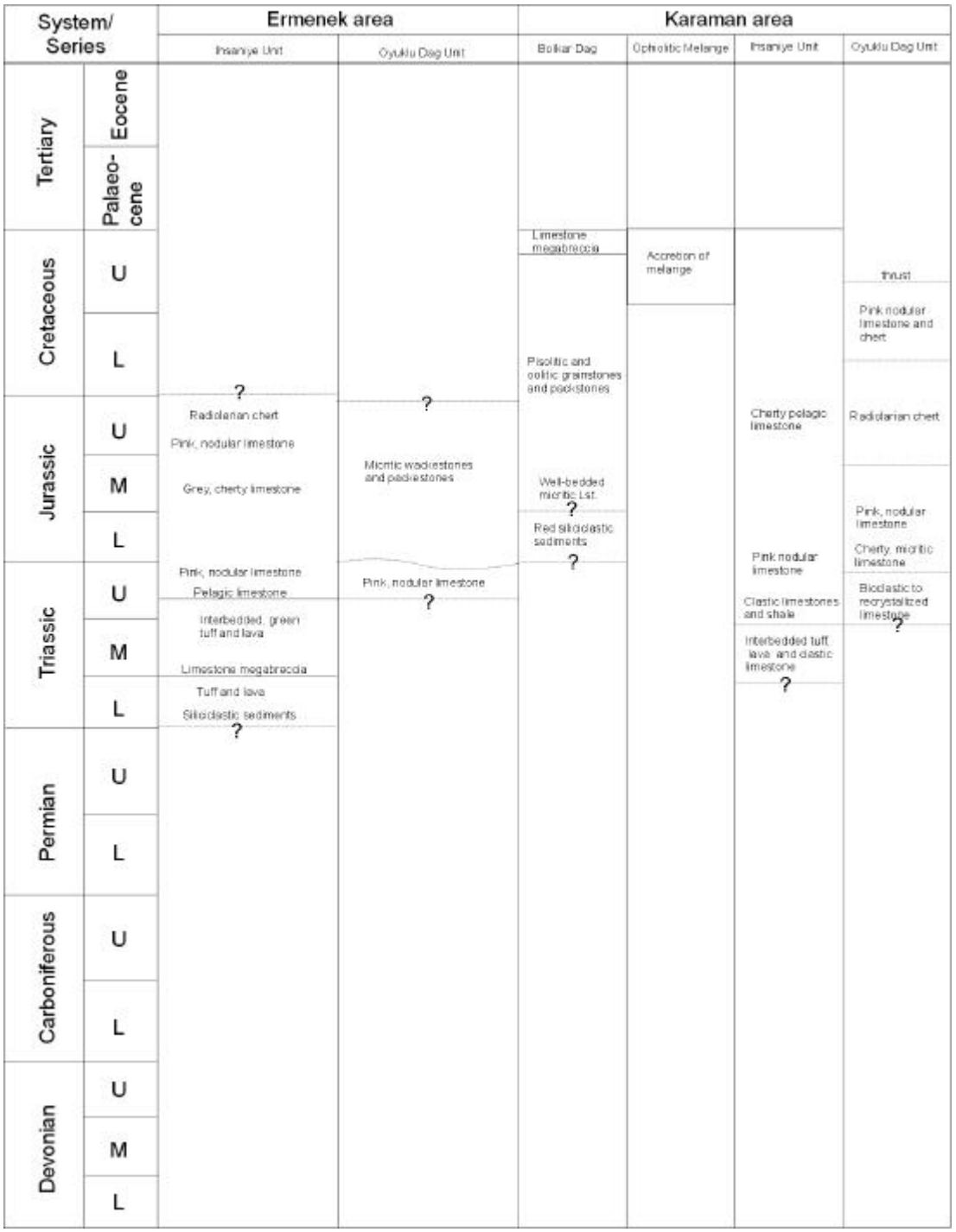

Fig. 5.24 Lithostratigraphic summary of the B-H Nappes in the Ermenek and Karaman areas.

Chapter 6

6. GEOCHEMISTRY OF THE OPHIOLITIC MELANGE AND OPHIOLITE

Geochemical studies of ophiolitic and volcanic rocks within the B-H Nappes have to date been limited in their extent. Of these, the studies by Monod (1977) and Gökdeniz (1981) used major element analysis only. Monod (1977) presents major element results from 28 samples collected from Ophiolitic Melange and two samples from the Triassic Huglu Unit in the Beysehir area. Lithologies analysed include ultrabasics, gabbros, dolerite dykes, pillow lavas, amphibolites and quartzites. In addition, Gökdeniz (1981) concluded that volcanics within the Triassic Ihsaniye Unit are of intermediate composition (dacite-trachyte) at the base and evolved to more acidic compositions towards the top.

The only modern studies of ophiolitic lithologies in the B-H Nappes are by Elitok (2000, 2002) and Ö. F. Çelik (pers.comm. 2001). Elitok (2000) focused on the Kizildag ophiolite and Ophiolitic Melange in the Sarkikaraagaç area north of Lake Beysehir (Chapter 3.2.2.1.2). These results will be compared with findings from this study. Çelik, as part of his PhD thesis, is studying metamorphic soles, from ophiolites across the Tauride mountain belt. During the second fieldseason in 2000, we collected a number of samples together from the Beysehir area. The results of Ar/Ar dating are to be included in his forthcoming thesis (Çelik, pers.comm. 2001), and preliminary data are briefly discussed here (Section 7.2.4).

Therefore, no comprehensive geochemical study of the volcanic and ophiolitic rocks of the B-H Nappes has been undertaken before and virtually no data exist in the literature on the geochemical character or likely tectonic setting of these igneous rocks. So, the principle aims of this chapter are;

- To examine the geochemical character of the Triassic volcanic Huglu/Ihsaniye Unit, and if possible, to infer the likely tectonic setting of formation.

- To document the geochemical character of the volcanic rocks within the Ophiolitic Melange across the entire extent of the B-H Nappes and to assess the likely tectonic settings in which these volcanics were extruded.

- To shed light on the geochemistry of the ophiolite and to determine the geotectonic environment in which it formed, if possible.

To achieve these goals, over 80 whole rock X-Ray Fluorescence (XRF) analyses were carried out on volcanic samples collected from the Triassic Huglu-Ihsaniye Unit, in the Beysehir and Ermenek areas and from a range of basaltic clasts and doleritic dykes in the Ophiolitic Melange. In addition, whole

rock XRF analysis and 75 electron microprobe analyses were carried out on peridotite samples collected from ophiolite in the Beysehir and Dipsiz Göl locations.

6.1 Triassic Huglu Unit

6.1.1 Petrography

A suite of 33 samples was collected for petrographical and geochemical analysis from the volcanogenic lower part of the Huglu Unit in the type area near Huglu village in the Beysehir area (see Chapter 2.6.3.1) and from the Ihsaniye Unit, the equivalent unit in the Ermenek area, (Chapter 5.3.2). The location of specimens collected is described in the relevant tectonostratigraphy sections. The reader is referred to Chapter 7 for an in-depth discussion of unit correlations across and within the B-H Nappes. All specimens are aphyric and olive green in hand specimen, apart from samples TA148, 166, 172, 178, 182 and 208, which are also aphyric but much darker in colour. In thin section, two distinct rock types were identified which all show variable alteration.

i) Acidic tuff

This suite of specimens is extremely fine-grained (0.1mm) and generally possesses a hypocrystalline to hypohyaline texture depending on the amount of glassy groundmass present. This patchy glass groundmass ranges from 10% - 100% in different specimens. In most, devitrification spots are present in the groundmass (Fig.6.1a). In unwelded specimens, which are microcrystalline, the groundmass consists of equigranular, hypidiomorphic crystals of quartz, lesser amounts of plagioclase feldspar, with subordinate opaque minerals. The extremely fine-grained nature of most of the specimens precludes any detailed thin section description and interpretation. Some of the samples are semi-welded and in addition show a range of curved crystal shard morphologies (e.g. TA120; Fig.6.1b). In all specimens the green colour is related to the high quantity of chlorite present in the groundmass (up to 50% in some specimens). Calcite is also present as a secondary mineral filling voids and veins within the samples.

ii) Trachytic-dacitic lava (Fig. 6.1c)

In thin section, these specimens possess a microcrystalline groundmass of interlocking acicular to tabular feldspar grains, with subordinate quartz and mafic minerals. Microphenocrysts occur in clumps and are generally sanidine and plagioclase feldspar. Augite rarely occurs as a phenocryst phase (e.g. specimen TA178). Chlorite forms up to 20% of the groundmass.

(a)

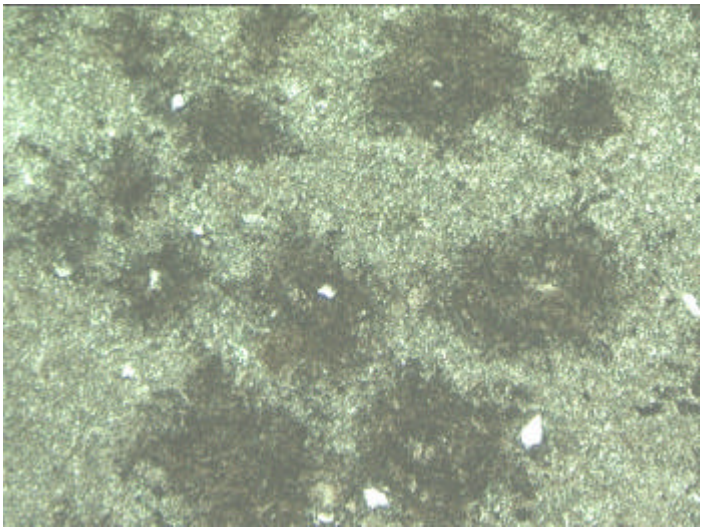

(b)

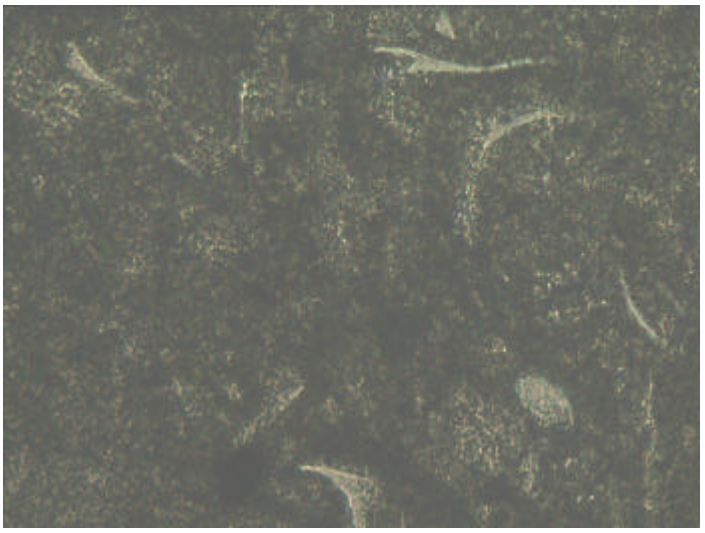

(c)

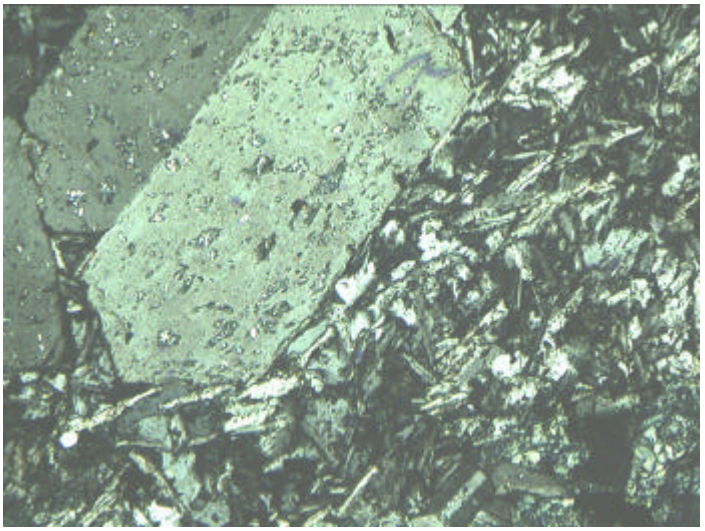

Fig.6.1 Photomicrographs of **(a)** devitrification spots within tuff, **(b)** curved shards within welded tuff and **(c)** sanidine phenocryst within trachytic lava. Note all photomicrographs were taken in XPL and fields of view are 2mm, except (b), which is 1mm.

6.1.2 Whole-rock x-ray fluorescence (XRF) analysis

Samples were trimmed to remove veins and weathered edges, then crushed, powdered and prepared for whole-rock XRF analysis, using the technique outlined in Appendix 2 (Fitton *et al.*, 1985, 1998). The resulting data gathered from the XRF analysis are presented in full in Appendix 2.

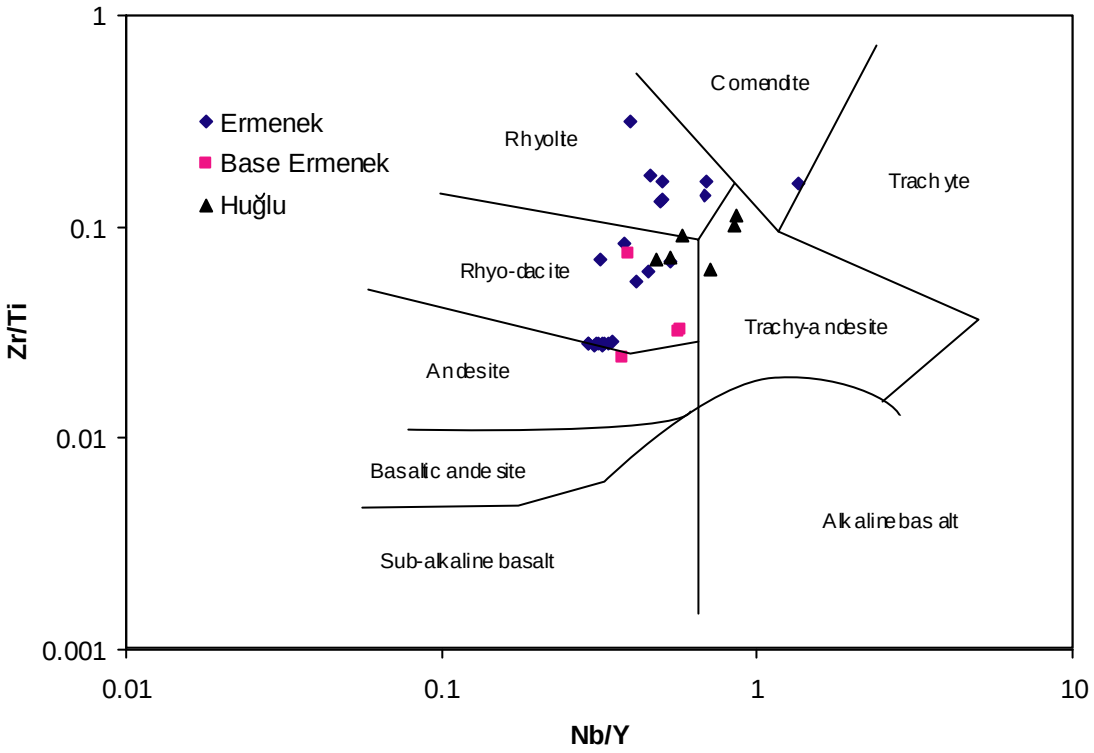

Fig. 6.2 Geochemical plot of Zr/Ti versus Nb/Y lava classification diagram (Winchester & Floyd, 1977). Data from Huglu and Ihsaniye Unit (Ermenek and Base Ermenek).

The data were initially plotted on a Zr/Ti – Nb/Y geochemical diagram (Fig. 6.2), which allows a classification of lava type (Winchester & Floyd, 1977). This plot is more reliable than the conventional total alkali elements versus silica plot (i.e. Si versus Na+K; Cox *et al.*, 1979), because each component of the plot used has been shown to be relatively immobile (Rollinson, 1993).

The data show the volcanogenic Huglu – Ihsaniye Unit to be highly evolved with an average rhyo-dacitic composition spreading into the rhyolitic, trachy-andesitic and andesitic fields. This highly evolved nature unfortunately precludes tectonic discrimination or basalt tissue typing that this study was initially hoping to achieve. However, the character and geochemical trends can be assessed from looking at variation diagrams (Figs. 6.3 to 6.5).

6.1.3. Variation diagrams

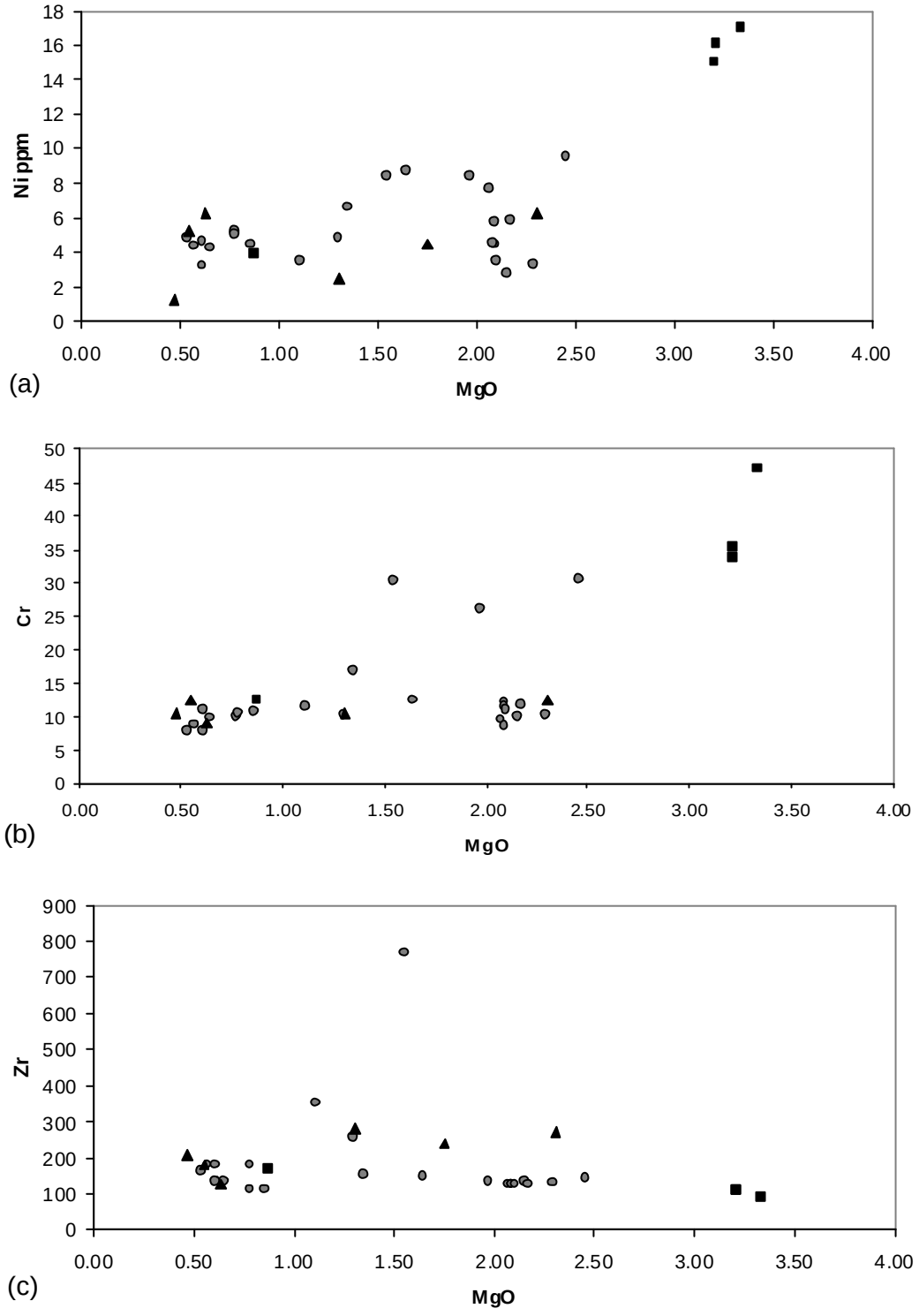

Fig.6.3 Data from the Ihsaniye Unit in the Ermenek area (circles-upper, squares-lower) and the Huglu Unit in the Beysehir area (triangles), plotted on Harker variation diagrams. **(a)** MgO (wt%) versus Ni (ppm), **(b)** MgO (wt%) versus Cr (ppm) and **(c)** MgO (wt%) versus Zr (ppm).

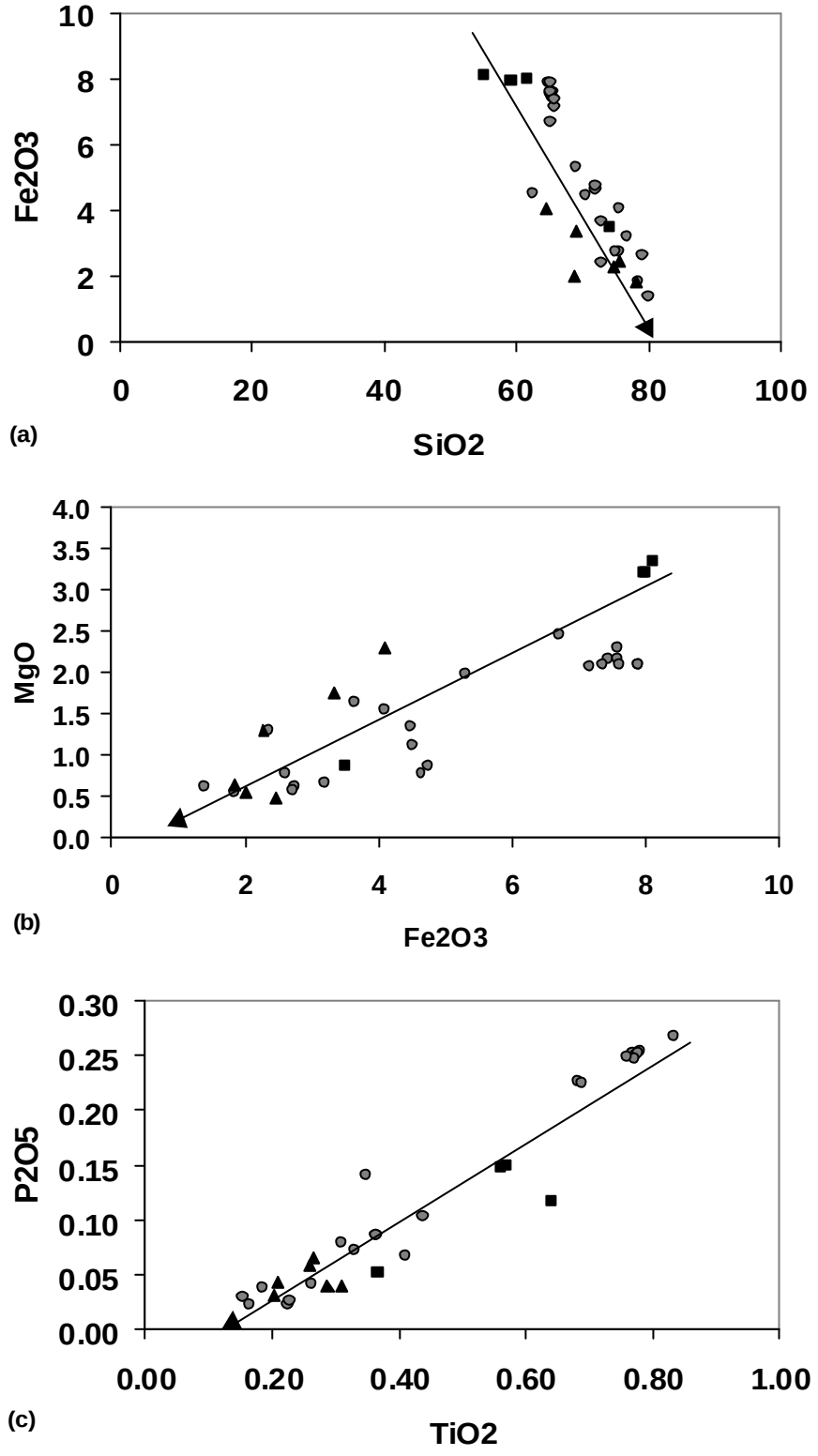

Fig. 6.4 Data from the Ihsaniye Unit in the Ermenek area (circles-upper, squares-lower) and the Huglu Unit in the Beysehir area (triangles), plotted on Harker variation diagrams. **(a)** SiO_2 (wt%) versus Fe_2O_3 (wt%), **(b)** Fe_2O_3 (wt%) versus MgO (wt%) and **(c)** TiO_2 (wt%) versus P_2O_5 (wt%).

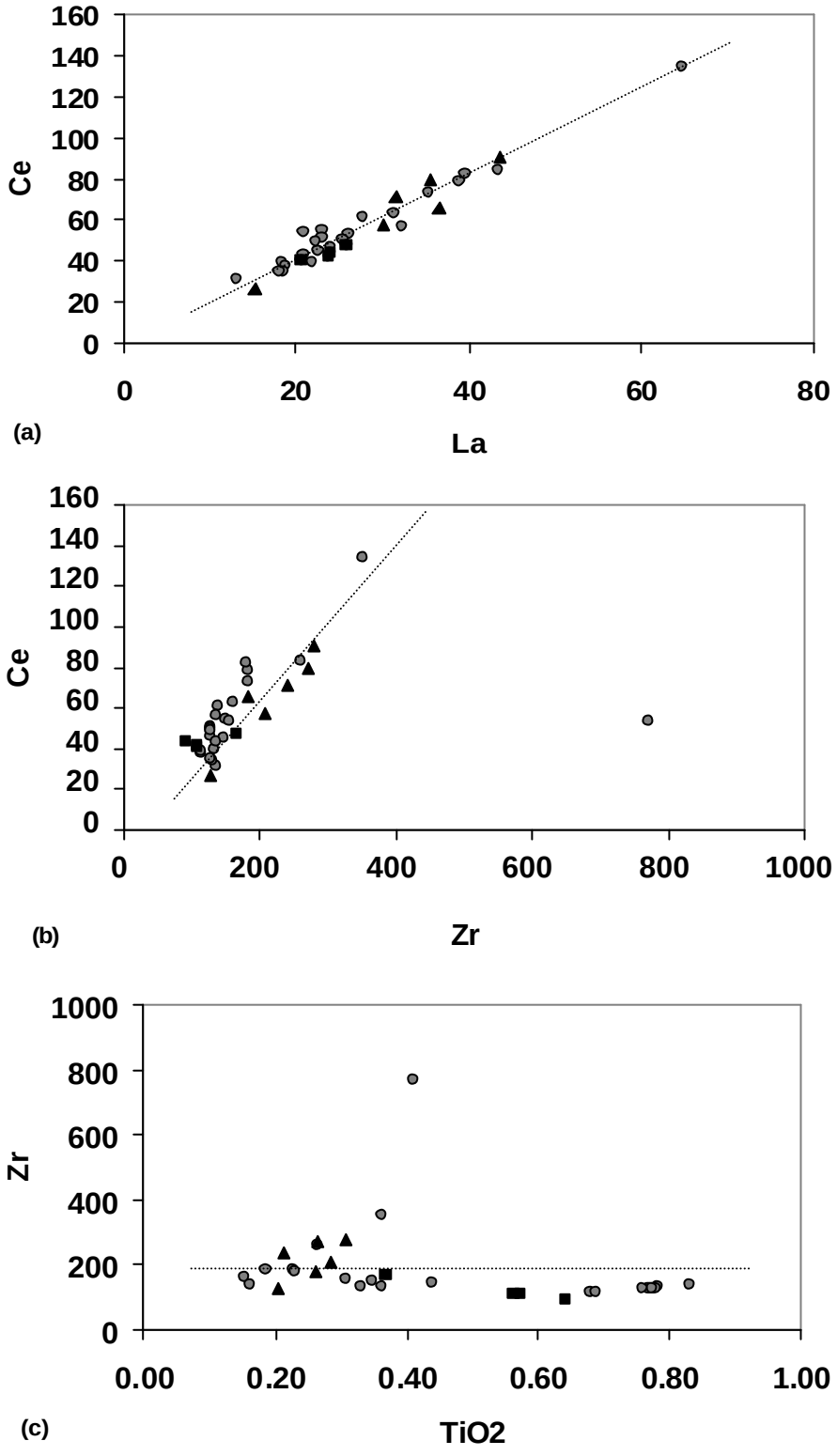

Fig. 6.5 Data from the Ihsaniye Unit in the Ermenek area (circles-upper, squares-lower) and the Huglu Unit in the Beysehir area (triangles), plotted on Harker variation diagrams. **(a)** La (ppm) versus Ce (ppm), **(b)** Zr (ppm) versus Ce (ppm) and **(c)** TiO_2 (wt%) versus Zr (ppm).

Figures 6.3 to 6.5 show a series of Harker-type plots, which illustrate element variability and trends within the volcanogenic Huglu - Ihsaniye units. Each of the diagrams show the entire data set, which is subdivided into three categories thus; 1) volcanic rocks from the Huglu area (triangles), 2) volcanics from the base of the Ihsaniye Unit (squares) and 3) volcanics from the main succession of the Ihsaniye Unit (circles). The aim of this subdivision is to interpret any trends related to geographical factors or magmatic evolution.

Figs. 6.3a and 6.3b show MgO plotted against the compatible trace elements Ni and Cr. In each case a positive correlation of decreasing compatible trace element content with falling MgO content is seen. This is probably a reflection of the extraction of Fe-Mg silicates and oxide phases in the late stages of magmatic evolution. Another interesting trend is observed in these diagrams. Data from the lower part of the sequence plot in the top right of the field, which suggests the magma evolved from a MgO content of 3 – 3.5%, towards depletion. Fig. 6.3c shows the Zr content (which is incompatible) remains approximately constant even with decreasing MgO content, i.e. there is no relationship between the two elements. The data are consistent with the low-pressure fractionation of Mg-bearing phases, but not zircon. However, one data point plots outwith this trend (sample TA166b) and is probably caused by the presence of zircon in the sample. It is worth noting that no variation can be observed between the geographic areas.

One of the diagnostic characteristics of the tholeiitic magma series evolution is the marked trend of iron enrichment during the early stages of fractionation, followed by Fe depletion in the later stages (e.g. Thingmuli volcano, Iceland; Carmichael, 1964). Fig.6.4a shows a linear correlation between Fe and Si in the Huglu-Ihsaniye volcanics. The lowermost samples collected in this study plot in the top left of the trend, which shows Fe decreasing with Si content during the later stages of fractionation. The data from the Huglu-Ihsaniye Unit does not record any early Fe enrichment, but it records the later Fe depletion stage extremely well. MgO is also strongly correlated with Fe and decreases with fractionation (Fig. 6.4b). This is also the case with TiO_2 (Appendix 2), which shows that FeTi oxides and biotite are probably crystallizing from the melt. Apatite is almost certainly crystallizing as TiO_2 and P_2O_5 are strongly correlated (Fig.6.4c). All these minerals are crystallizing leaving quartz and feldspar as the main phases remaining in the melt.

The strong Ce-La correlation (Fig.6.5a) suggests that the analytical data is reliable. There is a factor of three in the total variation in combined REE and Zr content across the suite (e.g. Zr – Ce in Fig. 6.5b), but it does not seem very closely related to the major element fractionation trend (e.g. TiO_2 – Zr in Fig. 6.5c). The simplest explanation is that REE's and Zr are both concentrated in evolved liquids and either are incorporated in one mineral phase or are scattered in pockets containing both zircon and a rare-earth mineral. Generally, powdered samples have randomly variable amounts of these high REE/Zr phases on their surfaces giving the observed correlations and range of absolute abundance (J. Dixon, pers.comm, 2002).

	SiO_2	Al_20_3	Na_20	K_20	S Fe/Mg
Tholeiitic association					
Basalt	51.57	15.91	2.41	0.44	1.45
Andesite	57.40	15.60	4.20	0.43	2.51
Dacite	79.2	11.10	3.40	1.58	3.94
Calc-alkaline association					
Basalt	50.59	16.29	2.89	1.07	0.98
Andesite	59.64	17.38	4.40	2.04	1.33
Dacite	66.80	18.24	4.97	1.92	1.51
Huglu-Ihsaniye Unit					
TA 161b	75.59	12.13	4.43	1.63	2.63
TA 178a	72.18	12.88	5.47	2.06	5.96
TA 201a	75.64	11.84	4.32	2.10	4.53

Table 6.1 Representative compositions of island arc and continental margin volcanic rocks (examples from Jakes & White, 1972). Analyses from rhyo-dacitic samples from Huglu-Ihsaniye Unit are included for comparison.

Table 6.1 shows a series of representative tholeiitic and calc-alkaline volcanics from the literature, with selected analyses from the Huglu-Ihsaniye Unit. It is widely recognised that the most important chemical differences between tholeiitic and calc-alkaline series is the alkali contents and iron/magnesium ratios. The calc-alkaline series is marked by high alkali content and a low iron/magnesium ratio (Wilson, 2001). When compared using the same criteria, little-altered rhyo-dacitic samples from the Huglu-Ihsaniye Unit show tholeiitic characterisitics (Table 6.1).

In summary, the available geochemical and petrographical data suggest the Huglu volcanics probably represent evolved members of a tholeiitic suite showing marked Fe and Ti depletion after an implied stage of Fe-Ti enrichment at the andesitic stage of fractionation.

6.2 Ophiolitic Melange

Volcanic inclusions from the Ophiolitic Melange were collected, with a preference for little-altered aphyric basic lava clasts where possible. The samples were then prepared for whole-rock XRF analysis of the usual major and trace elements using the methodology of Fitton *et al*. (1985, 1998). The data are presented by geographical area to show the range of rock types and tectonic settings present in the Ophiolitic Melange. Three main areas (with subsets) were chosen across the B-H Nappes as follows;

1) Pisidian Taurides (western)- Gümüssu and Kumdanli sub-areas
2) Beysehir (central)- Çamlik and Durak sub-areas
3) Karaman (eastern)-south of Verme Tepe

The reader is referred to the relevant chapters (Chapters 2, 3 and 5) for a more detailed location of these sub-areas and sample collection strategy.

6.2.1 Screening of samples

In multi-element discrimination studies (e.g. Pearce, 1982, 1983) fresh basalts are the ideal. Samples and the acquired data were therefore screened to remove as far as possible altered, evolved or otherwise dubious material.

After removing samples which were clearly sedimentary or volcaniclastic, the data was filtered to remove samples lying outside the limits 43-55% SiO_2, 5-15% CaO and MgO significantly greater than 4% (i.e.10%) This usually eliminates evolved rocks and strongly metasomatised or carbonated samples. Samples with high MgO but no associated enrichment in Ni and Cr are inferred to have been chloritised, rather than being originally olivine-rich. These were removed. As a further precaution, samples with loss on ignition (LOI) values greater than 10% were flagged as they may have been subject to greater than average element mobility. All remaining samples were then recalculated on a volatile-free basis before plotting (Appendix 2).

6.2.2 Geochemical plots

Previous work has shown that rock-type and tectonic environment can be determined from the abundance and ratio of stable trace and major elements (Pearce and Cann, 1973; Floyd & Winchester, 1975; Winchester & Floyd, 1977). This study uses two main lines of investigation to determine likely tectonic settings;

(a) MORB-normalised multi-element spider plots (Figs.6.6 to 6.9)
(b) Tectonic discrimination diagrams (Figs. 6.11 to 6.15)

(a) *The multi-element 'spider diagram'*

Assessment of the variations in trace element distribution can be graphically represented with a multi-element 'spider diagram' (Pearce, 1983). The convention is to plot mobile large ion lithophile elements (LILE) on the left with incompatibility increasing from left to right (Sr-Ba). Immobile elements are generally plotted on the right of the diagram with incompatibility increasing from right to left, which includes the high field strength elements (HFSE) Nb, Zr, Ti and also the rare earth elements (REE) La, Ce and Nd. By normalising values to MORB, patterns of relative element enrichment and depletion emerge, which are characteristics of distinct tectonic environments (Pearce, 1983).

(b) *Tectonic discrimination diagrams*

Another widely used method of distinguishing likely tectonic settings of magma genesis is to use published discrimination diagrams. A whole range of discrimination diagrams exist in the literature, each based on the correlation between concentrations of certain immobile trace elements (or ratios of trace elements) and tectonic environments. Rollinson (1993) gives a good discussion of the previous work in this field. Discrimination diagrams use differing trace elements and selected major element ratios, so the suitability of each method is dependent upon each situation. In this case, samples were collected from sheared Ophiolitic Melange, so it is very likely that some degree of alteration has occurred to the samples. Hence, only discrimination diagrams using relatively immobile major and trace elements are used in this study. HFS elements (Ti, Zr, Y and Nb) remain stable during post-eruption alteration and weathering (Pearce & Cann, 1971, 1973; Pearce 1975; Cann, 1970), whilst Cr has been shown to be stable under most conditions (Pearce & Cann, 1973). Accordingly, the following tectonic discrimination diagrams have been chosen for use in this study:

- Ti – Zr (Pearce, 1982)
- Ti/Y – Nb/Y (Pearce, 1982)
- Zr/Y – Zr (Pearce & Norry, 1979)
- Cr – Y (Pearce , 1982)
- Nb – Zr – Y (Meschede, 1986)

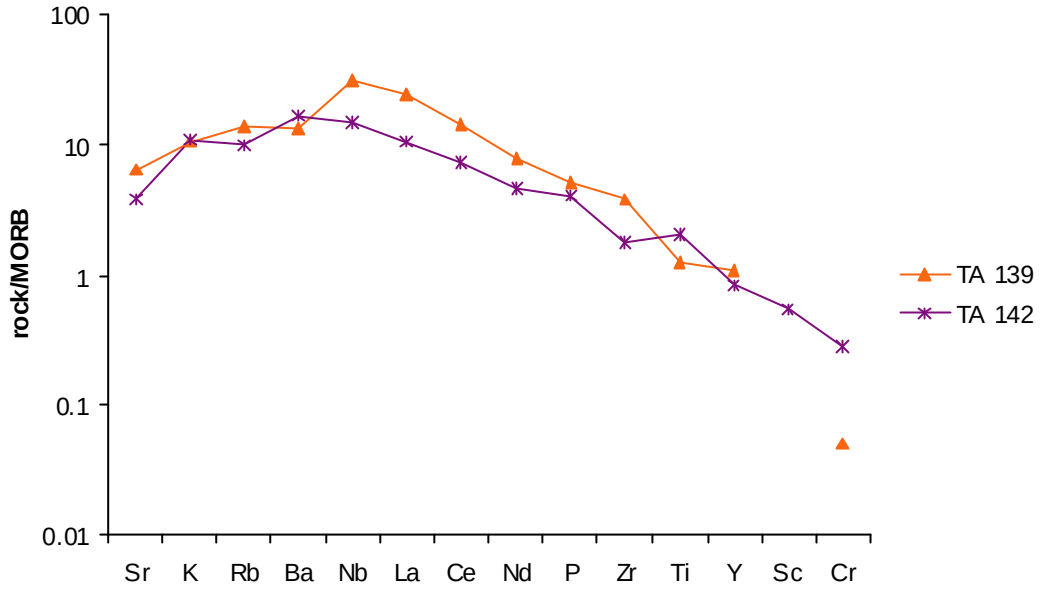

Fig.6.6 Selected MORB-normalised multi-element plots of basalt clasts from the Ophiolitic Melange in Durak sub-area of Beysehir. The humped pattern of trace element concentrations is indicative of WPB.

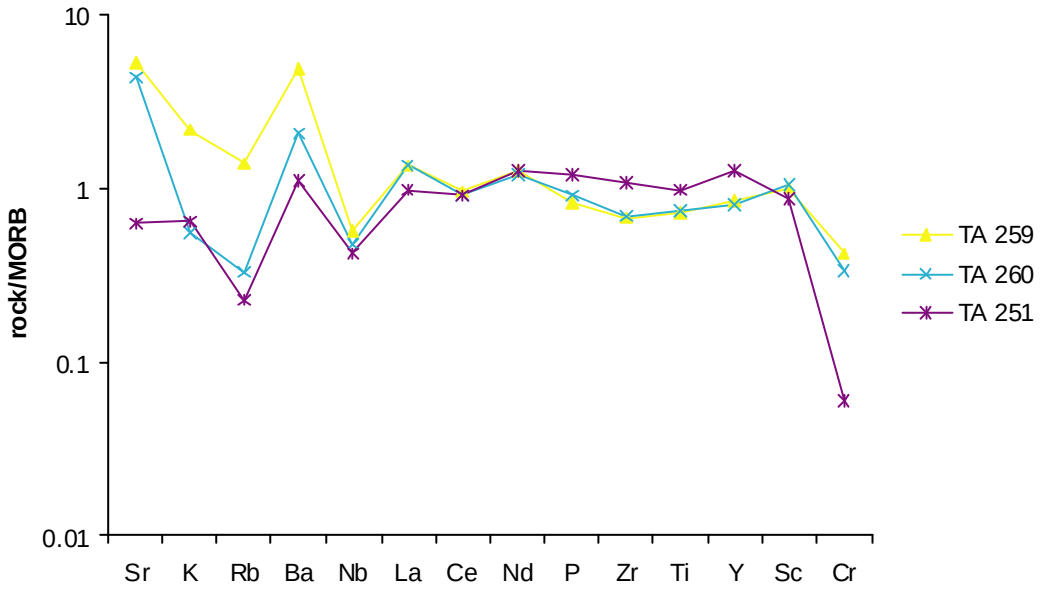

Fig.6.7 Selected MORB-normalised multi-element plots of basaltic clasts from the Ophiolitic Melange in the Pisidian Taurides.

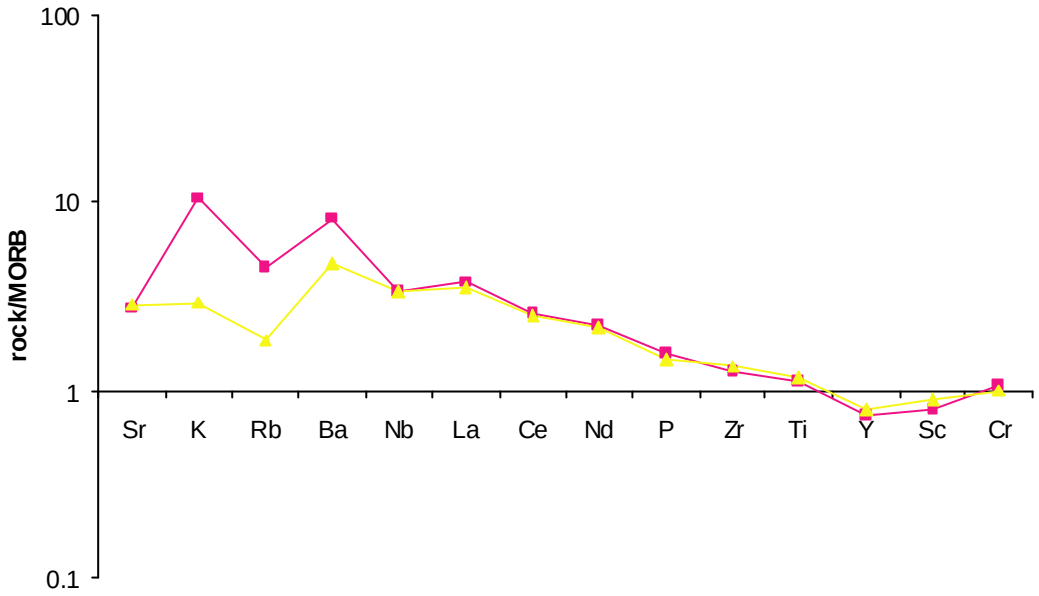

Fig.6.8 Selected MORB-normalised multi-element plots of basaltic clasts from the Ophiolitic Melange in the Karaman area.

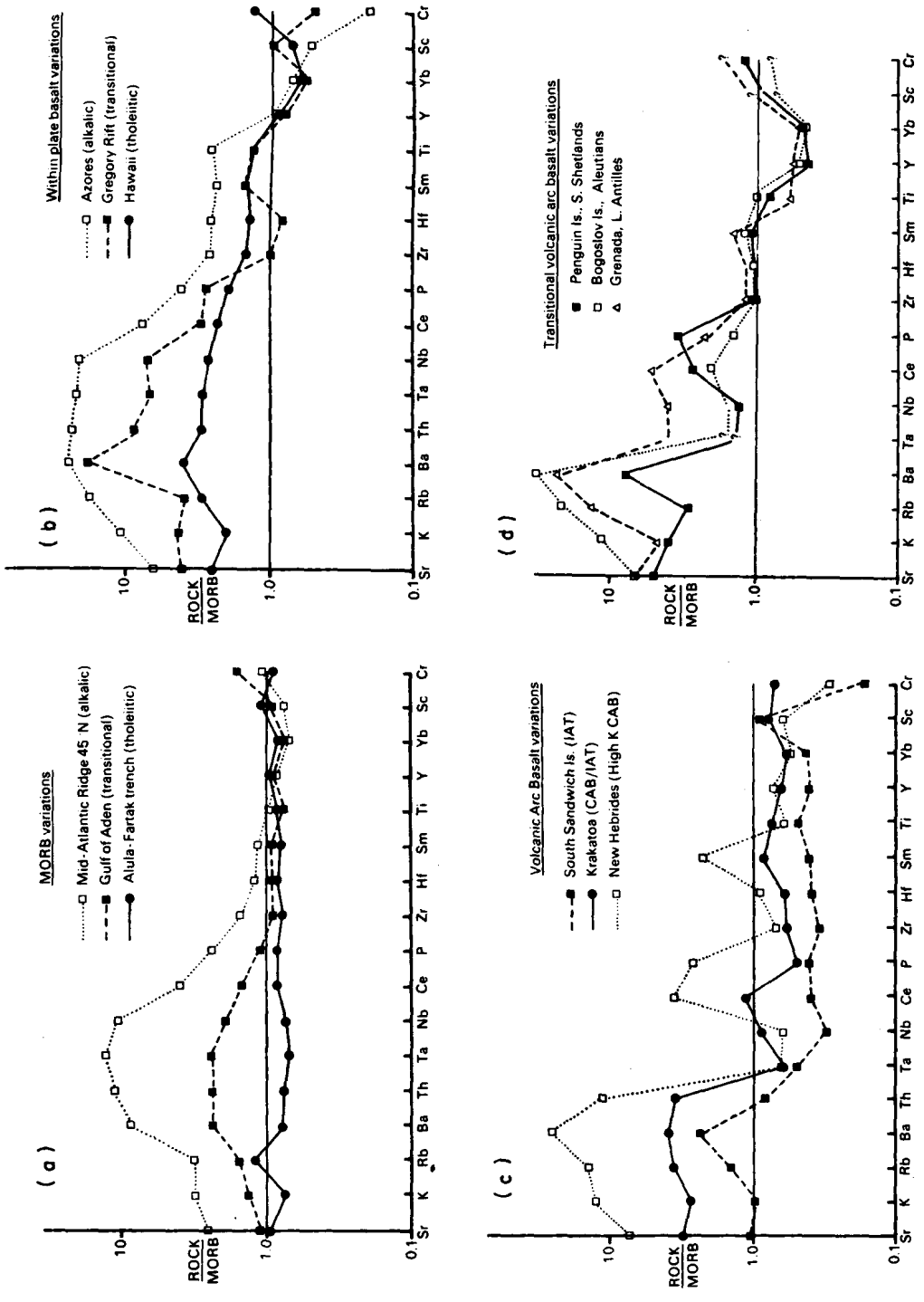

Fig. 6.9 Selected mid-ocean ridge basalt-normalised trace element patterns for **(a)** MORB and variations, **(b)** Within plate basalt and variations, **(c)** Volcanic arc basalt and variations and **(d)** Transitional volcanic arc basalt and variations. From Pearce (1982).

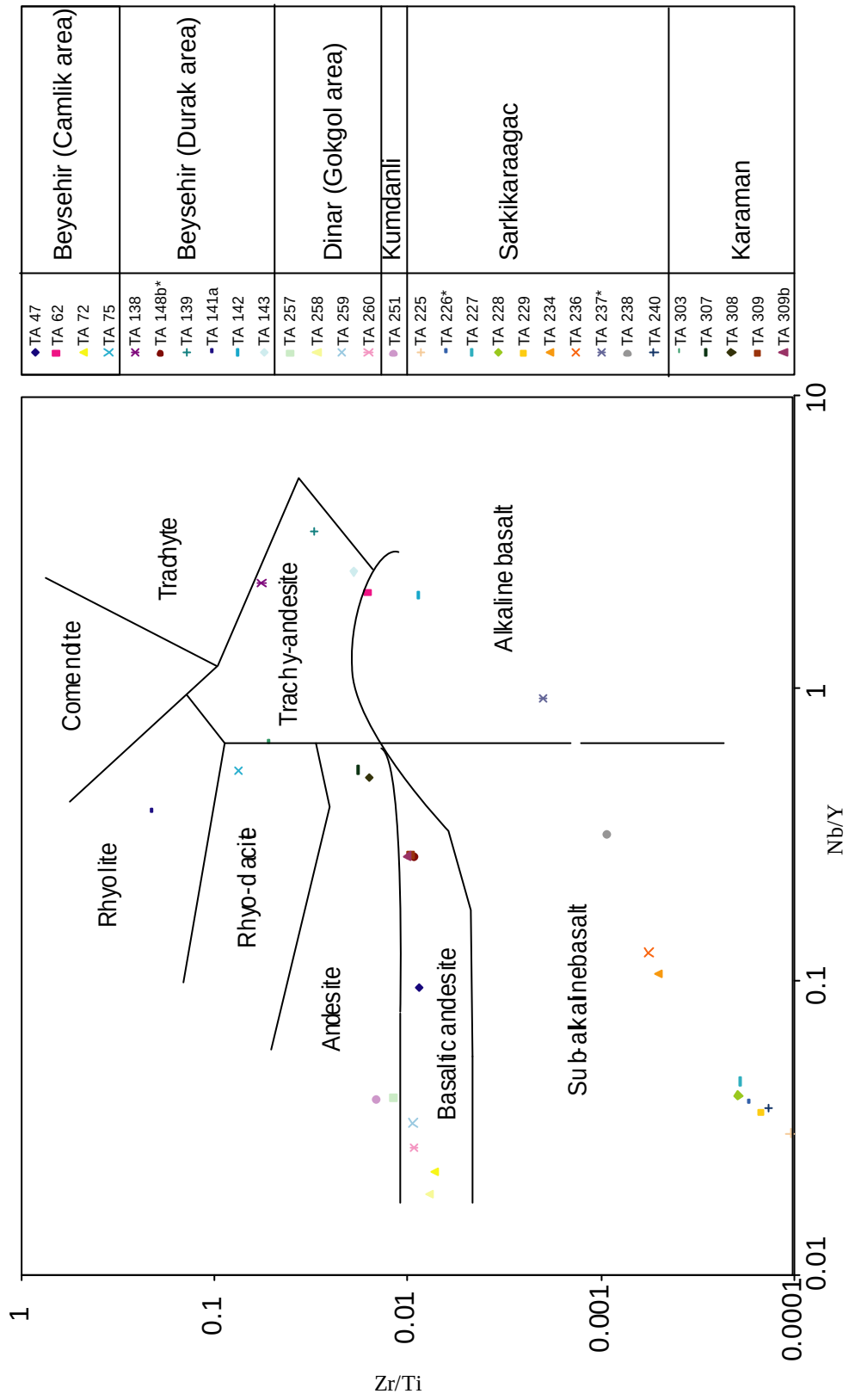

Fig. 6.10 Geochemical plots of Nb/Y v Zr/Ti showing lava classification (after Winchester & Floyd, 1977). Data set includes all samples analysed from the Ophiolitic Melange.

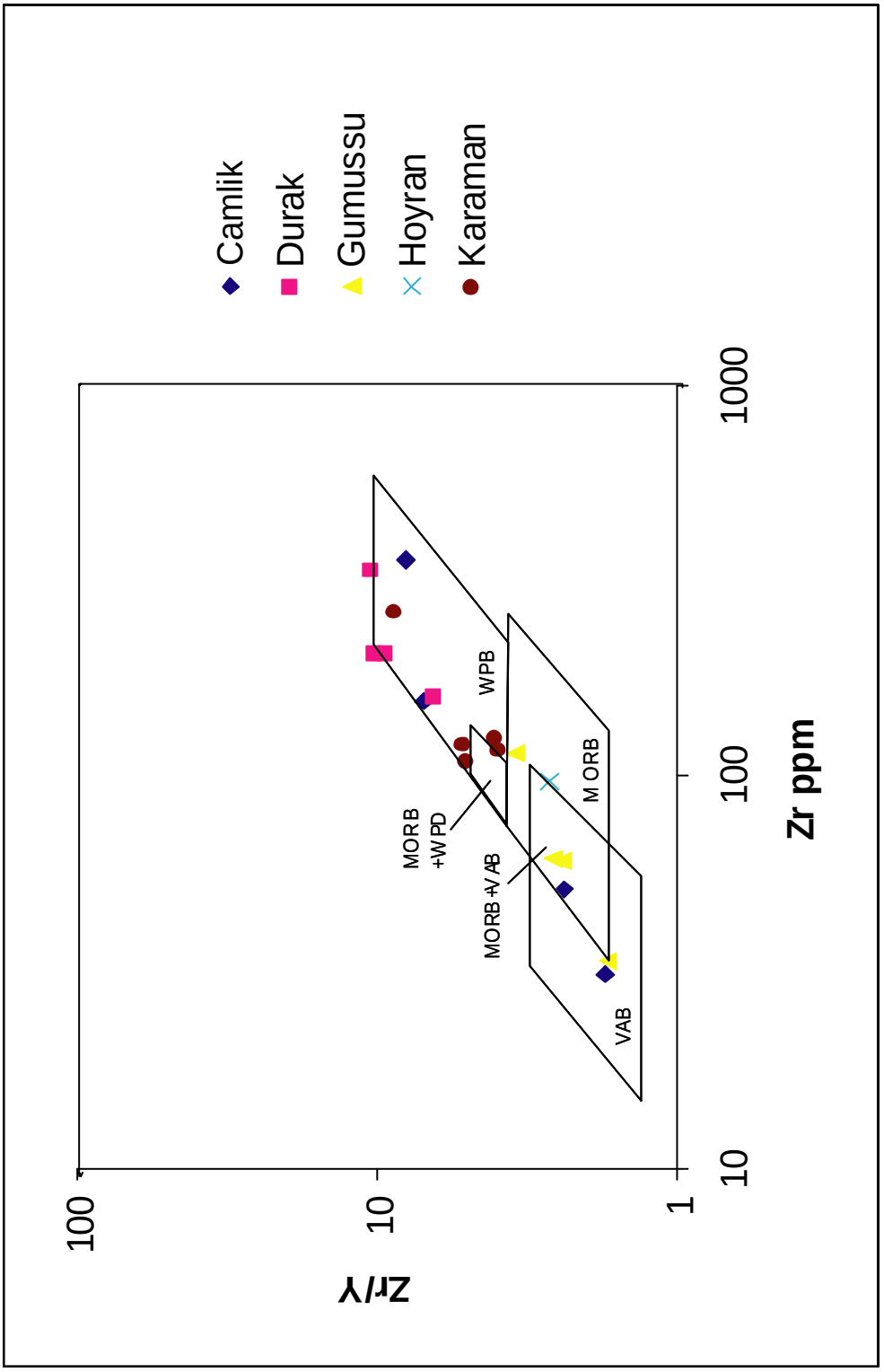

Fig. 6.11 Zr - Zr/Y tectonic discrimination diagram (after Pearce & Norry, 1979). Only data from basaltic inclusions within the Ophiolitic Melange are plotted.

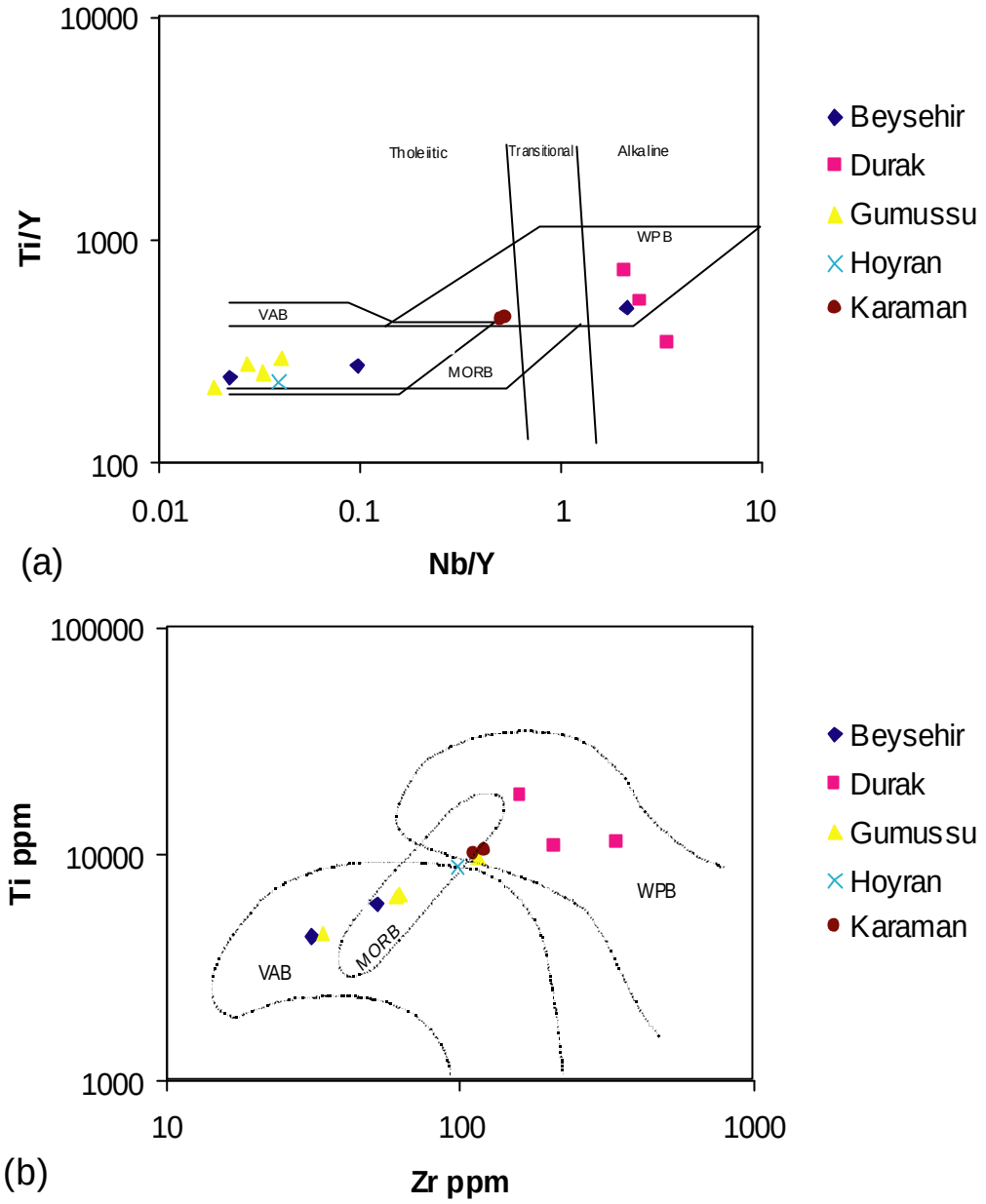

Fig. 6.12 Geochemical plots of: **(a)** Nb/Y v Ti/Y discrimination diagram (after Pearce, 1982). Data from basaltic inclusions within the Ophiolitic Melange are plotted, **(b)** Zr (ppm) v Ti (ppm) discrimination diagram (after Pearce, 1982). Data from basaltic inclusions within the Ophiolitic Melange are plotted.

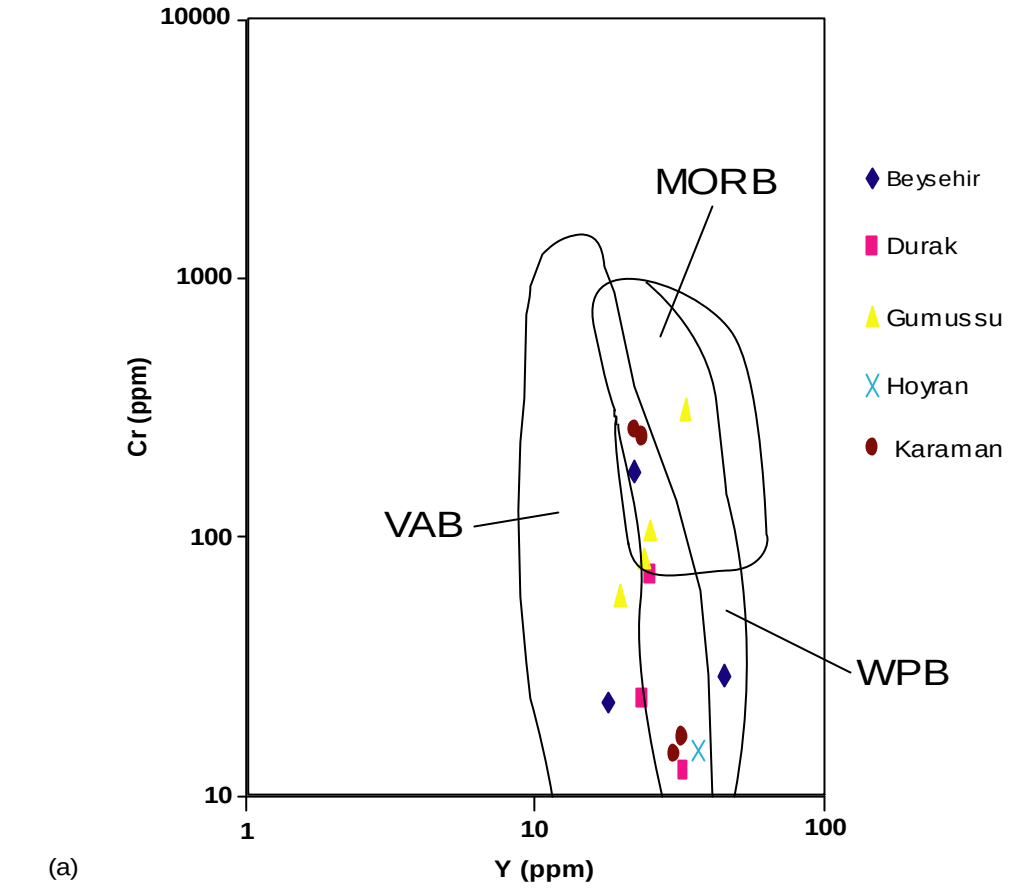

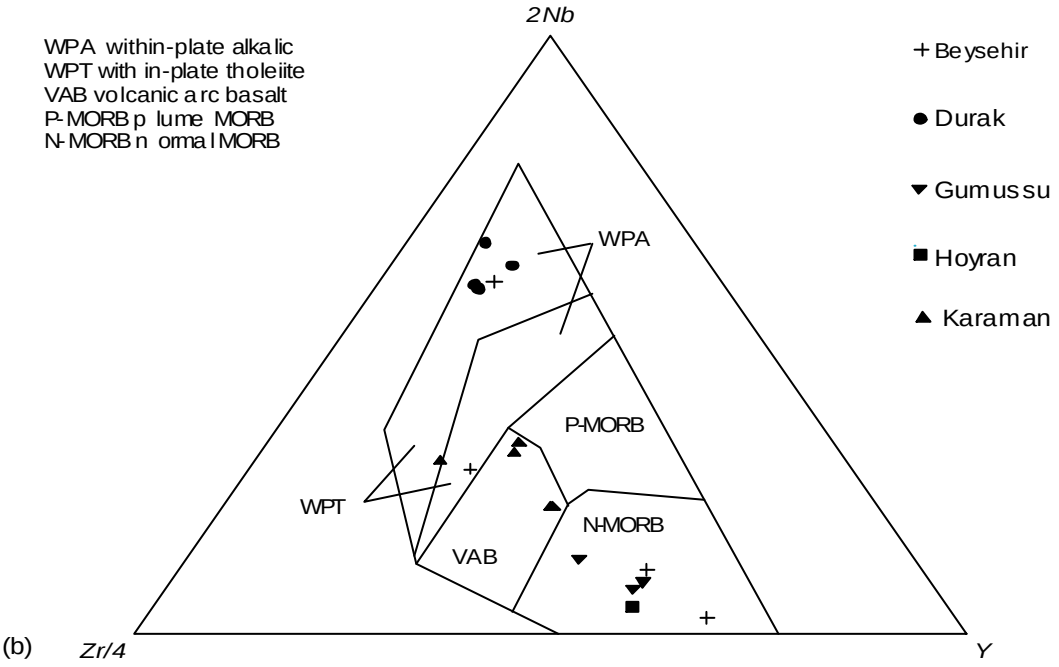

Fig.6.13 Geochemical plots of **(a)** Y (ppm) v Cr (ppm) discrimination diagram (after Pearce, 1982), **(b)** Nb-Zr-Y discrimination diagram (after Meschede, 1986). Data from basaltic inclusions within the Ophiolitic Melange are plotted.

6.2.3 Discussion of results

Figure 6.10 shows all the XRF data for the ophiolitic melange plotted and classified on a Ti/Zr versus Nb/Y diagram (after Winchester & Floyd, 1977). This diagram is useful for lava classification since all the discriminating elements are immobile. Samples collected from Çamlik (Beysehir area) show a wide range of compositions from basaltic andesite to alkaline basalt (TA62) and rhyo-dacite (TA75); however, lavas from Durak (Beysehir area) generally plot as alkaline basalts to trachy-andesites. One sample (TA 141a) plotted well within the rhyolite field. Lavas from the Pisidian Taurides (Dinar and Kumdanli areas) generally plot as basaltic andesite, with two falling within the andesite field (TA 257 and TA 251). The bulk of the Karaman samples plot as andesites with a small spread into the basaltic andesite field and trachy-andesite field (TA 303).

Selected MORB–normalised multi-element spider diagrams (Figs. 6.6-6.8) show that a range of patterns exist in the lava samples analysed. Figure 6.9 (a)-(d) shows a range of selected trace element patterns from the literature for comparison. Figure 6.6 shows a characteristic humped pattern (TA 142/139 from Durak), similar to present-day within-plate basalts (WPB) from the Azores (Pearce, 1982), which is caused by enrichment of the large ion lithophile elements (LILE- Sr, K, Rb, Ba) and the light rare earth elements (LREE- La, Ce, Nd). However, the LILE's show slight enrichment indicating a certain degree of element mobility. Other samples from the Pisidian Taurides are shown in Fig. 6.7 (TA 259/260). They show a flat high field strength elements (HFSE) content without significant depletion of Nb relative to Ce. The spider diagram is very similar to the present-day MORB patterns, albeit with variable mobility of the LILE's and minor Nb depletion. Samples 307 and 308 from Karaman (Fig. 6.8) are relatively enriched in LILE's and LREE's and show a plot that is similar to present-day tholeiites from Hawaii (Fig. 6.9; Pearce, 1982).

In the Zr versus Zr/Y discrimination diagram (Fig. 6.11; Pearce & Norry, 1979), lavas from Durak fall consistently within the WPB field, whilst samples from Karaman cluster in the WPB field near the MORB/WPB overlap. Samples from the other areas display a range of affinities. Figure 6.12a (Nb/Y versus Ti/Y after Pearce, 1982) shows a similar trend. The Durak lavas plot again in the WPB field and are alkalic. The Karaman lavas cluster in the WPB field close to the MORB and VAB boundaries. Lavas from other areas plot within the MORB/VAB overlap area. In the Ti (ppm) versus Zr (ppm) tectonic discrimination diagram (Fig. 6.12b) a similar relationship is observed. Once again the samples from Durak plot within the WPB field. The Karaman lavas fall in the WPB field close to the MORB boundary. Again lavas from the other areas plot in the MORB/VAB overlap. In the Y (ppm) vs. Cr (ppm) discrimination diagram (Fig. 6.13a; after Pearce, 1982) the Durak samples again plot in the WPB field, which overlaps with VAB, whilst the Karaman samples plot mainly in the WPB field which overlaps with the MORB and VAB fields. Again, the other samples plot across the range of fields. The final type of tectonic discrimination diagram used here (Fig. 6.13b; after Meschede, 1988)

is interesting. The Durak lavas generally plot as alkalic WPB. The Karaman lavas plot mainly in the VAB field, with a spread of data for the other areas.

6.2.4 Ophiolitic Melange conclusions

In summary (Fig 6.14), the available data from this study suggest that the volcanics in the Ophiolitic Melange record several different tectonic settings, thus;

1) All plots of the Durak (Beysehir) extrusives are consistently of WPB-type and possess a characteristic humped WPB pattern on the spider diagram. Likewise, the Karaman extrusives mostly plot in the WPB fields but show a less enriched WPB pattern in the spider diagrams. The geochemical evidence from these volcanics could reflect either rifting or record a seamount in the Neotethys ocean.

2) Samples from the Pisidian Taurides (Dinar and Kumdanli) show general MORB affinities in the tectonic discrimination diagrams and show MORB trace element affinities in the multi-element spider diagrams. However, they must have been derived from a slightly Nb-depleted source. The simple conclusion is that they are derived from a MORB-source overlying a subduction zone at the time, or the Nb slab-signature is inherited from some earlier subduction setting in the region. This subduction inheritance is believed to be a common feature of many Tethyan ophiolites (e.g. Greece; Pe-Piper 1998, Danelian & Robertson, 2001).

3) The remaining area (Çamlik) displays a range of tectonic associations from MORB to WPB-affinities, although this is likely to in part reflect the small sample population. More data are required before decisive conclusions can be drawn.

Area	Nb/Y - Zr/Ti classification (Winchester & Floyd, 1977)	Zr -Zr/Y	Ti/Y – Nb/Y	Ti-Zr	Cr-Y	Nb-Zr-Y	Multi-element spiders	Modern analogues
Çamlik	Basaltic andesite	WPB MORB VAB	MORB VAB WPB	VAB MORB	VAB WPB MORB	WPA WPT N-MORB	n/a	n/a
Durak	Alkaline basalt - rhyo-dacite	WPB	WPB	WPB	WPB VAB	WPA	Alkalic WPB pattern	Azores
Dinar	Basaltic andesite	MORB VAB	MORB VAB	MORB VAB	VAB WPB	N-MORB	MORB pattern	Alula-Fartak MORB
Kumdanli	Basaltic andesite	MORB	MORB VAB	MORB VAB	VAB WPB	N-MORB	n/a	n/a
Karaman	Andesite – basaltic andesite	WPB	WPB	WPB MORB	WPB MORB VAB	VAB	Tholeiitic WPB pattern	Hawaiian Tholeiites

Fig. 6.14 Summary result table of XRF analysis of basaltic clasts within the ophiolitic melange sorted by area. Tectonic discrimination fields ranked in order of probable affinity from top to bottom. Modern analogues from Fig. 6.10 (after Pearce, 1982).

6.3 Ophiolite

One of the principle aims of this chapter was to determine the likely geotectonic environment in which the ophiolite at the base of the B-H Nappes was formed. In order to achieve this a number of samples of peridotite from the Kizildag ophiolite (Beysehir area- Chapter 2.5.3.3) and the Dipsiz Göl ophiolite (Hadim area- Chapter 4.6.1) were analysed using whole-rock XRF and electron microprobe techniques. A number of doleritic dykes associated with the ophiolite in the Sarkikaraagaç area (north of Lake Beysehir) were also analysed for the usual major and trace elements using whole-rock XRF analysis in order to determine their tectonic setting.

6.3.1 Petrography of peridotite

Thin section analysis shows the peridotite consists of dominantly serpentinised harzburgite, ranging from fresh to 100% altered, as shown in Figs. 6.15 and 6.16, with minor pyroxenite, dunite and chromite pods occurring on outcrop scale.

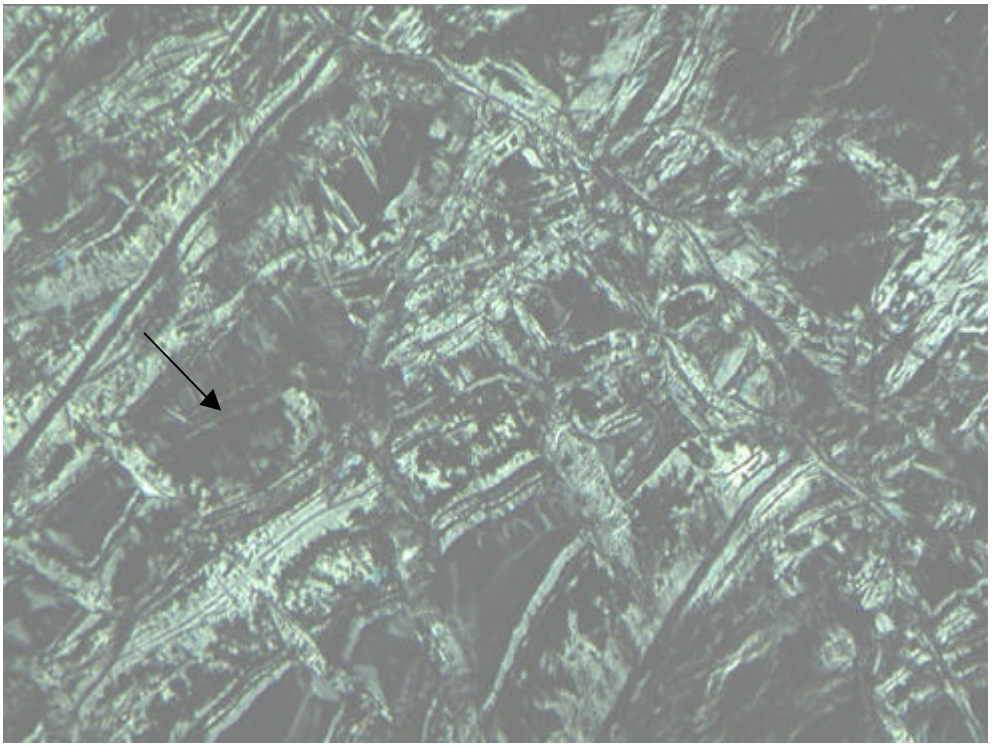

Fig.6.15 Photomicrograph taken under XPL of serpentinite. Note the pseudomorphs after olivine (probably lizardite) shown by arrow. Field of view is 2mm.

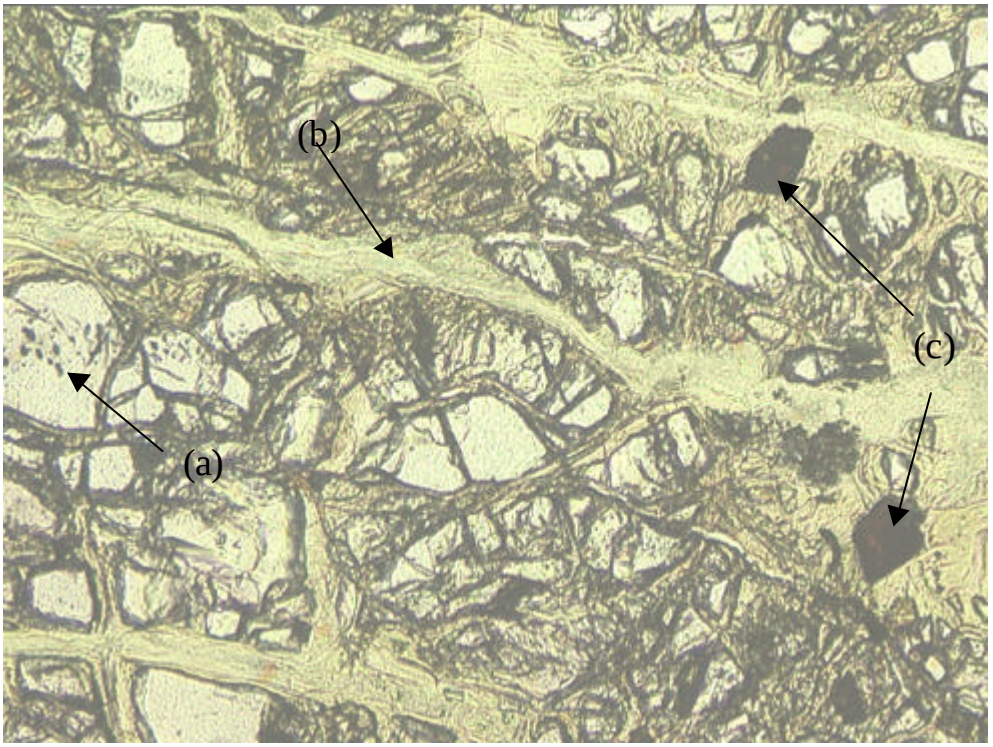

Fig.6.16 Photomicrograph in PPL of peridotite (sample 276) showing **(a)** fractured olivine, **(b)** fibrous serpentine vein fill (probably chrysotile) and **(c)** small euhedral chrome spinel grains. Field of view is 2mm.

In the more heavily serpentinised samples psuedomorphs after olivine and pyroxene are common (Fig. 6.15). This habit is most commonly shown by lizardite (Wicks & O'Hanley, 1988). Other forms of serpentine are also present in the peridotite as fibrous vein infill on a cm to mm scale (Fig. 6.16). This form is most commonly the chrysotile phase of serpentine (Wicks & O'Hanley, 1988). This mineral assemblage of pseudomorphic lizardite and fibrous chrysotile is predicted for low-temperature retrograde hydration of enstatite and olivine (Wicks & O'Hanley, 1988).

The next most common mineral present in the peridotite, apart from olivine (up to 90%), enstatite (generally <5%) and serpentine (% dependent upon alteration at the expense of olivine), is chrome spinel which constituted from 1% up to 10%. This mineral phase is present in a range of forms from small (>0.5mm) euhedral crystals (Fig. 6.16) to larger amoeboid shaped crystals (Fig. 6.17). Colour ranges from dark blood red to opaque depending on the thickness.

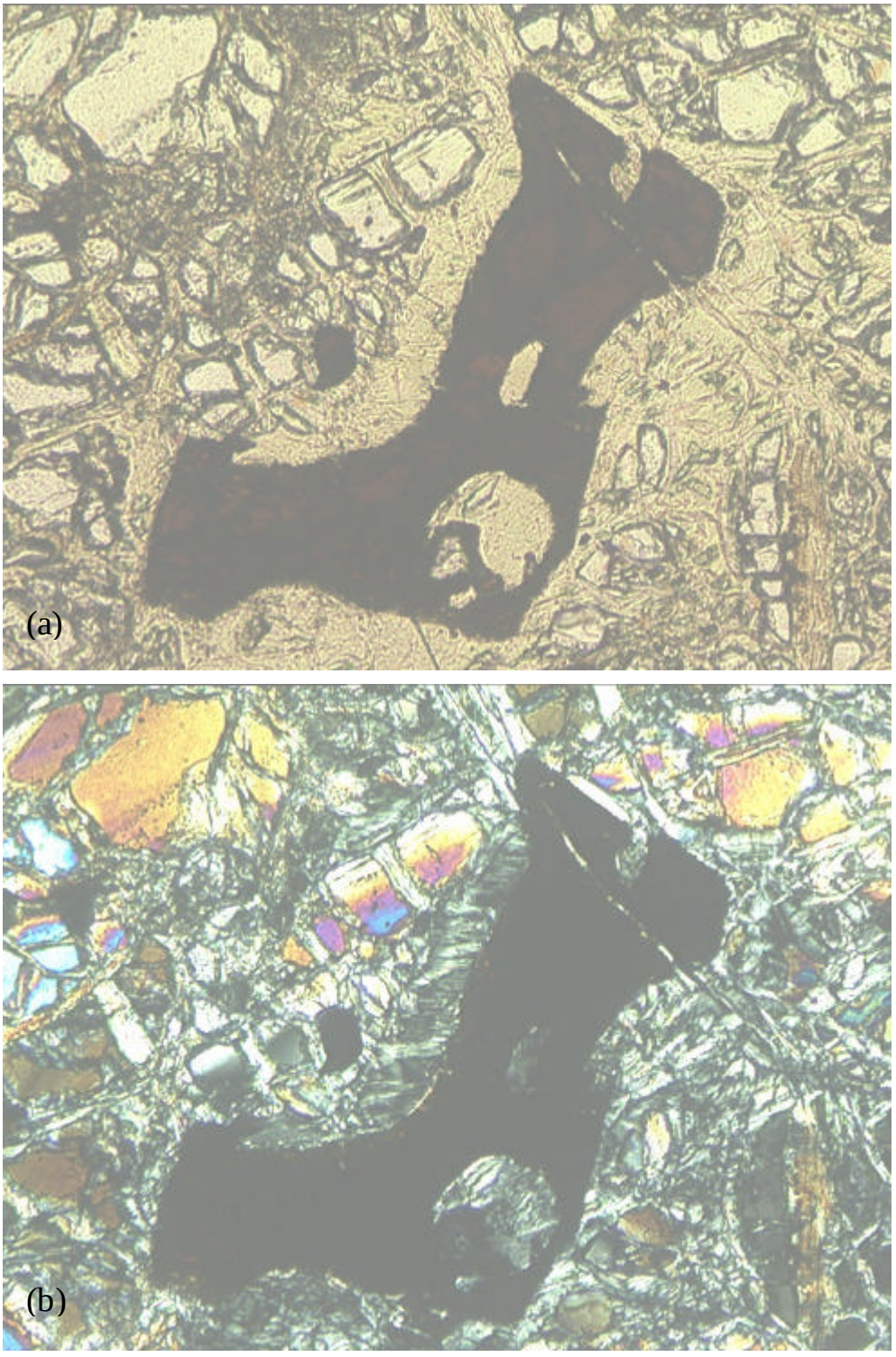

Fig. 6.17 Photomicrographs in **(a)** PPL and **(b)** XPL of anhedral chrome spinel from peridotite sample 276. Note surrounding rim of serpentine (low relief and yellow in PPL, fibrous black and white in XPL) and heavily fractured olivine with serpentine infill. Field of view is 2mm.

6.3.2 Whole-rock XRF analysis of peridotite

Once again samples were trimmed to remove weathered edges, then crushed/powdered and prepared for XRF analysis using the technique outlined in Appendix 2 (Fitton *et al.*, 1985, 1998). When plotted on a multi-elememt plot (after Roberts, 1988), normalised to a bulk mantle estimate (Sun and Nesbitt, 1977) a significant trend is observed (Fig. 6.18). The peridotites from the B-H Nappes are generally depleted in Al and Ca (compatible elements partitioned into liquid) and Ti (moderately refractory) and are slightly enriched in Ni (a refractory element), when compared to both mantle estimates and more fertile Western Mediterranean peridotites (Apennine and Ligurian). This trend is a feature of other eastern Mediterranean ophiolites, e.g. Orthis and Troodos (Menzies and Allen, 1974; Roberts, 1988) and the Lycian Peridotite thrust sheet (Collins, 1997). Petrographic analysis confirmed that the analysed samples were not significantly serpentinised which suggests that the Ca depletion is real and not due to metasomatic alteration.

Figure 6.19(a) shows a depleted element (Aluminium) plotted against an enriched element (Nickel) from the same data set. This geochemical plot discriminates further between depleted eastern Mediterranean peridotite and the more fertile western Mediterranean peridotites. The more depleted east Mediterranean discriminant field corresponds with the supra-subduction zone (SSZ) ophiolites of Pearce *et al*. (1984) and conversely the west Mediterranean field with MORB (Roberts, 1988). The peridotite samples from the B-H Nappes fall partly within the SSZ discriminant field and are generally more depleted than western Mediterranean peridotites.

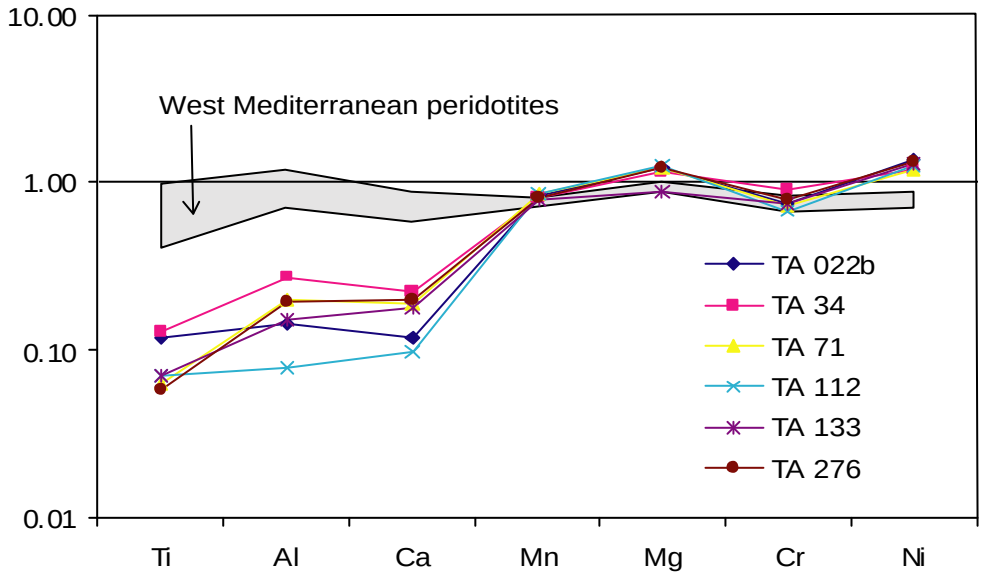

Fig. 6.18 Multi-element plot normalised to Sun and Nesbitt's (1977) bulk mantle estimate, showing the general depleted nature of the Beysehir (Kizildag) and Dipsiz Göl peridotite (after Roberts, 1988).

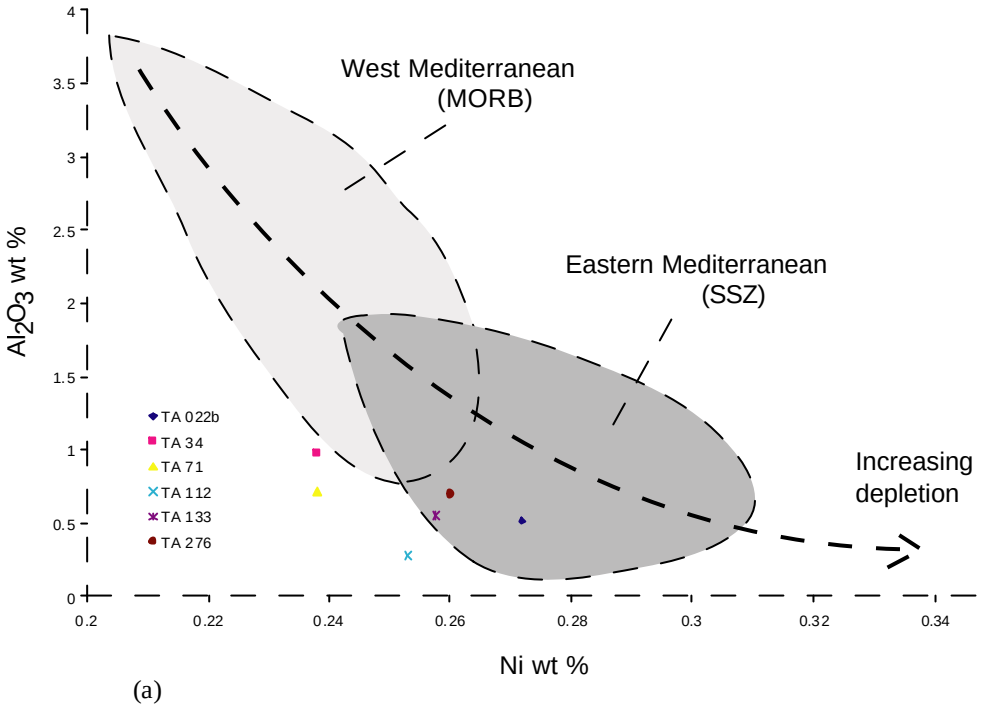

(a)

Fig. 6.19 (a) Whole rock Al_2O_3- Ni plot (after Roberts, 1988).

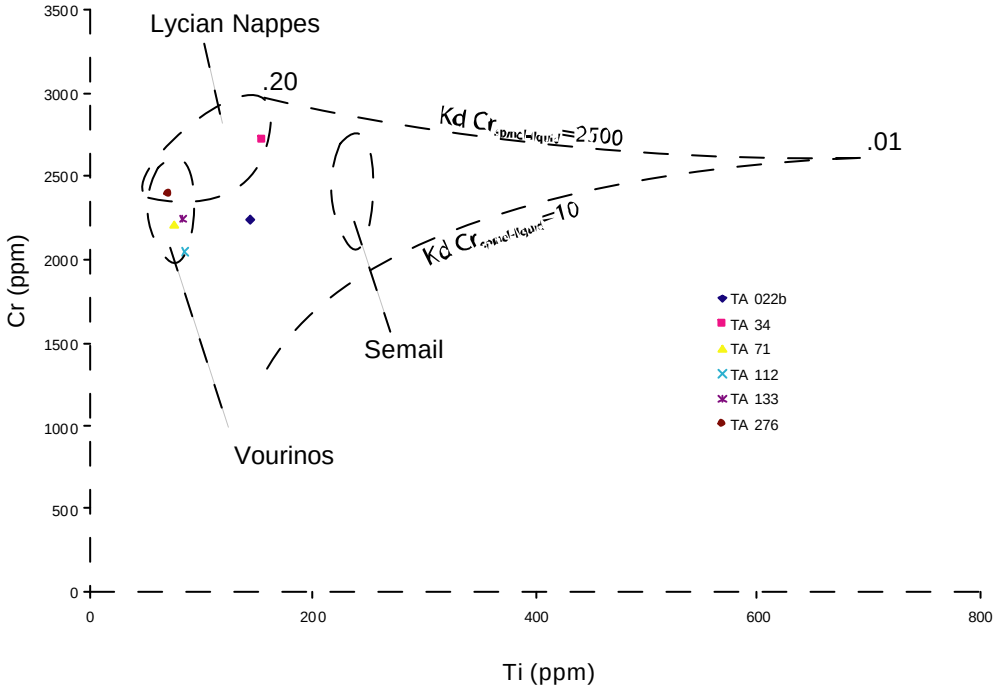

Fig. 6.19 (b) Geochemical plot of Cr (ppm) plotted against Ti (ppm). Partial melting pathways for depleted lherzolite are shown (after Roberts, 1992). Partial melt fractions are shown along the top of the upper pathway. Vourinos and Semail fields from Roberts (1992) and Lycian field from Collins (1997).

Figure 6.19(b) compares the degree of partial melting that the B-H peridotite has undergone compared with other Eastern Mediterranean ophiolites. Partial melting pathways follow simple batch melting for variable partition coefficients (Kd Cr in diagram) for chromium in a spinel-liquid system (Roberts, 1992). The data from this study plot close to the Vourinos and Lycian fields and suggest the B-H peridotite could have formed from a >20% partial melt. This is a large and rather unlikely figure for direct melting of the bulk mantle. It is more likely that the peridotite formed as a residue after extraction of a partial melt from a previously depleted abyssal peridotite (chemically similar to Apennine peridotite), as has been inferred for other eastern Mediterranean ophiolites (e.g. Lycian Nappes; Collins, 1997).

Figure 6.20(a) is a tectonic discrimination diagram, after Pearce *et al*. (1994) which separates SSZ peridotites from MOR-type peridotites. This diagram is similar to 6.19(a) in that one compatible element (in this case Ti) is plotted against a relatively incomptible element (Cr). A similar relationship is also seen, since the majority of the data plot in the SSZ-field.

6.3.3 Electron microprobe analysis of chrome spinel

Chrome-rich spinel has been shown to be an extremely sensitive petrogenic indicator without playing a significant geochemical role (Irvine, 1965; 1967; Thayer, 1970; Evans and Frost, 1975; Dick, 1977; Fisk and Bence, 1980); hence, previously used spinel compositions were used to infer the tectonic settings of magma genesis. The following technique is widely accepted to distinguish between abyssal peridotites (i.e. ocean lithosphere formed at mid-ocean ridges) and oceanic lithosphere with a sub-volcanic arc genesis, i.e. SSZ-type ophiolites (Dick and Bullen, 1984). The basic rationale is that a changing Cr and Al ratio reflects increasing degrees of partial melting in the mantle, which is ultimately related to the tectonic setting. Dick and Bullen (1984) analysed a wide range of chrome spinels from ophiolites and compared them with spinels recovered from the present day deep ocean and lava extruded in a number of settings. This empirical approach distinguished two distinct populations; firstly, Cr compositions similar to abyssal peridotite and MORB (Type I), and secondly those with spinel xenocrysts like arc basalts (Type III) and an overlapping field (Type II).

During this study ca. 75 chromian spinels from eight peridotite samples were analysed on a Cameca Camebax electron microprobe at the University of Edinburgh. Samples were collected from the main ophiolitic units of the B-H Nappes, i.e. the Kizildag ophiolite in the Beysehir area (Chapter 2.5.3.3) and the Dipsix Göl ophiolite in the central area (Chapter 4.6.1). Peridotite specimens from the third main ophiolite in the Pisidian Taurides (Sarkikaraagaç) were not analysed because they have been studied by Elitok (2000). The results and methodology of the electron microprobe analysis are given in Appendix 3. The data were plotted as a ratio of Cr/Mg (shown in Appendix 3). Figure 6.20(b) shows the resultant geochemical plot. The dominant trend is for the spinels to plot outwith the abyssal field and show a similarity with the Type III spinels (i.e. subduction-influenced) of Dick and Bullen (1984).

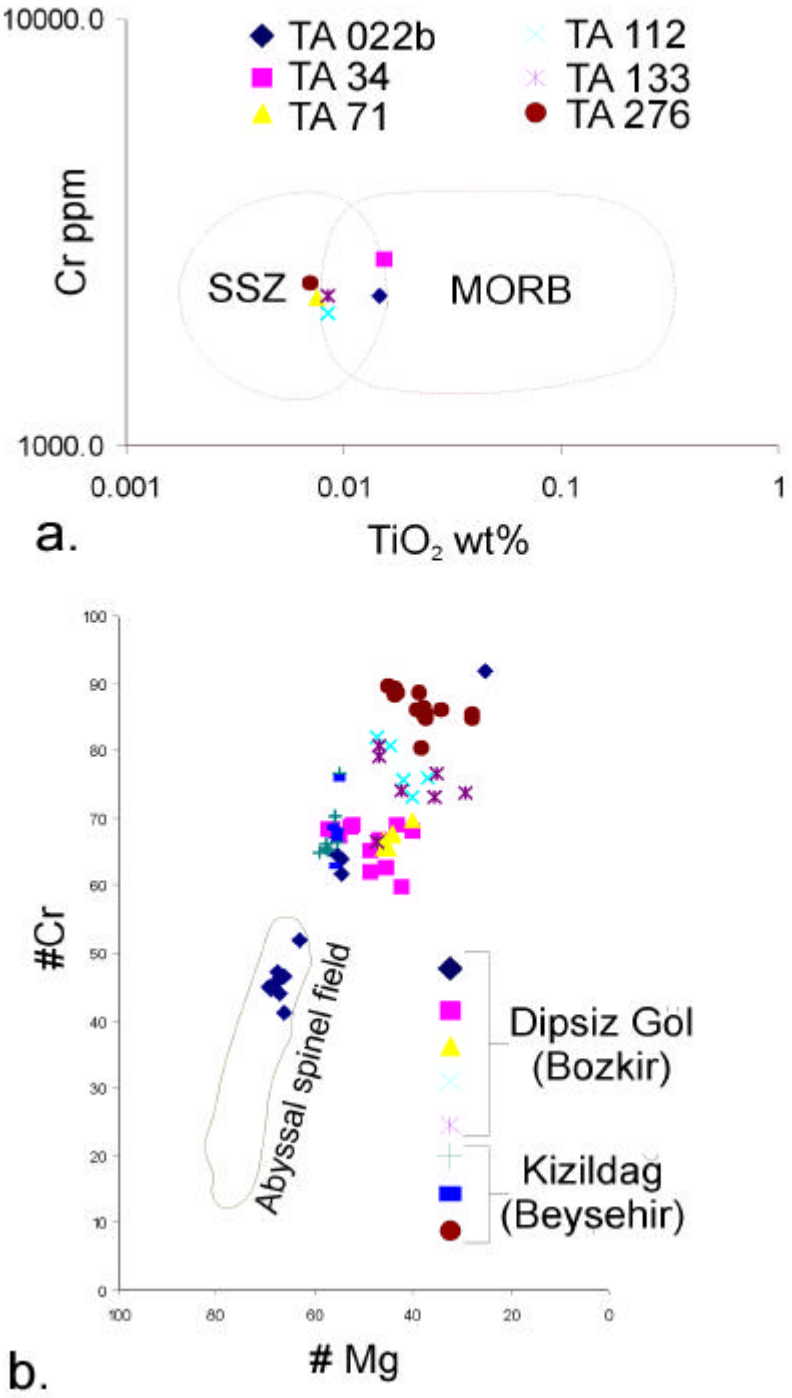

Fig. 6.20 (a) Geochemical plot of TiO_2 (wt %) versus Cr (ppm). Supra-subduction zone (SSZ) and mid-ocean ridge (MORB) tectonic discrimination fields from Pearce *et al*. (1984). The bulk of the data plot in the SSZ field. **(b)** Chrome spinel compositions plotted on Cr versus Mg diagram (after Dick and Bullen, 1984).

6.3.4 Doleritic dykes associated with the ophiolite

The dyke samples originate from the Ophiolitic Melange in the Sarkikaraagaç area north of Lake Beysehir and were collected from a block ca. 300m in size, which consisted entirely of sheeted dykes (Chapter 3.2.2.1.2; in particular Fig. 3.10). The sheeted dykes were closely associated with other ophiolitic lithologies (gabbros, pillow lavas and serpentinite) and were structurally located above, yet spatially close to, the main ophiolitic body of peridotite. It is for this reason that the dykes are believed to be part of the original ophiolite assemblage in this area.

6.3.5 Whole-rock XRF analysis of doleritic dykes

The samples were then prepared for whole-rock XRF analysis of the usual major and trace elements using the methodology of Fitton *et al.* (1985, 1998), the results of which are shown in Appendix 2. The samples were screened using the methods described in Chapter 6.2.1. When the remaining data was plotted on Nb/Y v Zr/Ti lava classification diagram (after Winchester & Floyd, 1977) the doleritic dyke samples from Sarkikaragaç group together with the main abundance falling in the sub-alkaline basalt field. Only one sample (TA 237) plotted outwith this group with an alkaline basalt composition (Fig. 6.11).

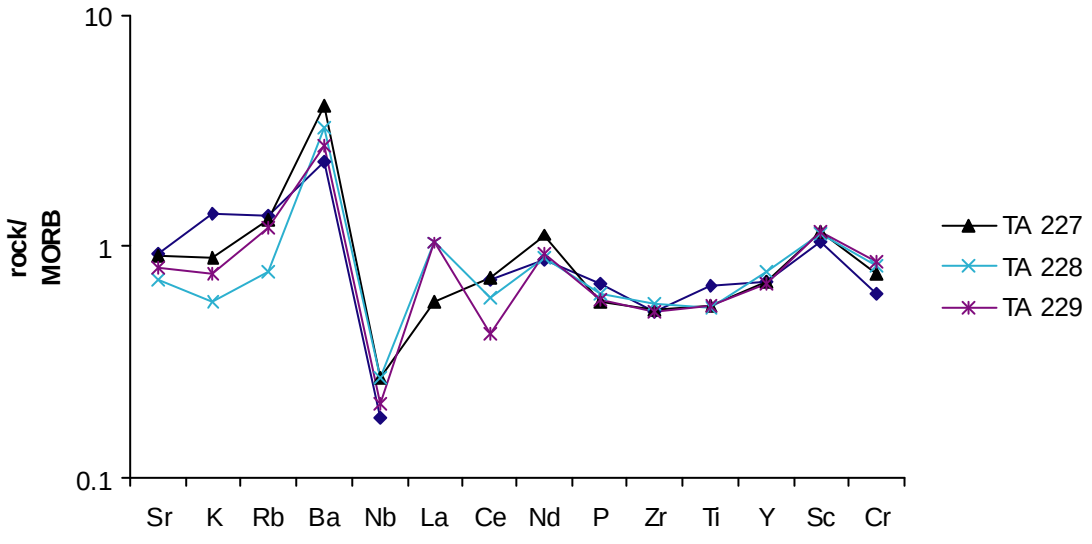

Fig.6.21 Selected MORB-normalised multi-element plots of sheeted doleritic dykes from the Ophiolitic Melange in the Sarkikaraagaç area.

Fig. 6.21 shows a suite of samples, from the sheeted dyke block in Sarkikaragaç, showing consistent depletion in the HFSE's (Nb, Zr, Ti), markedly so for Nb. This pattern is a characteristic of volcanic arc lavas and is comparable to modern south Sandwich island arc tholeiites (Fig.6.10c; Pearce, 1982). This negative Nb spike can be indicative of a subduction-influenced setting (Pearce *et al.*, 1990). This geochemical characteristic is thought to occur because the LILE have a low ionic potential and are easily mobilised by aqueous fluids (Pearce, 1982). Nb has a high ionic potential and is immobile in aqueous fluids and thus enrichment does not occur above a subduction zone setting. However, the presence of a Nb anomaly is not absolute proof of a subduction influence as assimilation of crustal rocks in continental rift settings can also prevent enrichment of Nb (Pearce & Cann, 1973; Keskin, *et al*., 1998). The lithology of the sheeted dykes, however, makes this setting unlikely.

On the Nb/Y v Ti/Y discrimination diagram, the sheeted dyke suite from Sarkikaragaç clusters in a group within the MORB/VAB overlap (Figure 6.22a), although a couple of samples have a low Ti/Y ratio and plot just in the VAB field. In a Zr v Ti discrimination plot (Fig. 6.22b) the dyke samples from Sarkikaragaç plot mainly within the MORB/VAB overlap. The third discrimination diagram (Zr - Zr/Y)shows the dykes to cluster together in the MORB/VAB overlap. One sample plots just in the VAB field (Fig. 6.23a). Finally, in the Y-Cr discrimination diagram the Sarkikaragaç dykes mainly plot in the VAB field, which overlaps into both the MORB and WPB fields (Fig. 6.23b)

In summary. the Sarkikaragaç dykes exclusively plot in the VAB field; none are found outwith this association. The MORB-normalised 'spider diagrams' for the same samples show *severe* Nb depletion, indicative of a subduction-related environment (Pearce, *et al.*, 1984). As the specimens were collected from a sheeted dyke complex as a detached block in the melange it is likely that they possess a different origin to the extrusives previously discussed in Chapter 6.2, furthermore they are probably part of the ophiolite itself.

6.3.5 Main ophiolite conclusions

In summary, the whole rock XRF data confirms that the B-H peridotite is more depleted than the bulk mantle and is also more depleted than western Mediterranean/Apennine peridotites (Figs. 6.18 and 6.19a). If the B-H peridotite was assumed to have formed directly from the bulk mantle then fairly large degrees of partial melting must have occurred (Fig. 6.19b). However, it is more likely that the peridotite formed in two stages; as a residue after extraction of a 20% partial melt from a previously depleted abyssal peridotite (chemically similar to Apennine peridotite), which is consistent with the data presented here. Pearce *et al.* (1984) suggest that remelting of depleted peridotite is most likely to occur through solidus depression due to a hydrous influx from an underlying subducting slab of oceanic crust. Tectonic discrimination diagrams infer genesis in this kind of SSZ-type setting (Figs. 6.19b and 6.20a). Furthermore, whole-rock XRF analysis of doleritic dykes associated with the ophiolite suggest formation in this kind of subduction-related setting.

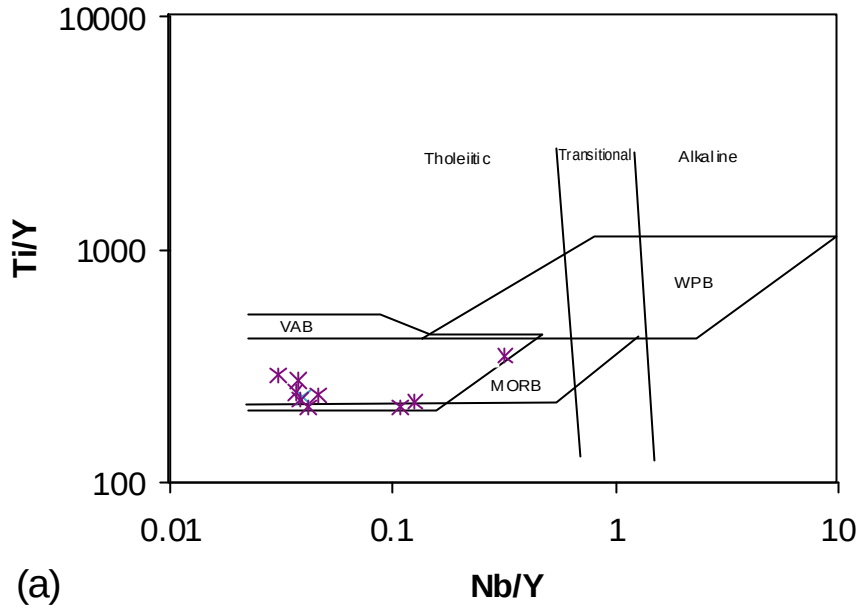

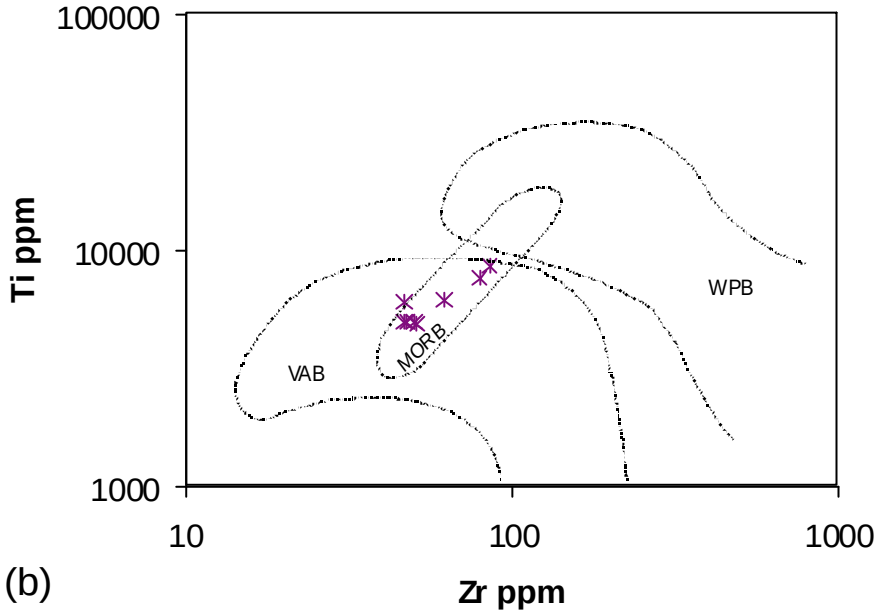

Fig.6.22 Geochemical plots of: **(a)** Nb/Y v Ti/Y discrimination diagram (after Pearce, 1982). Data from sheeted dykes within the Ophiolitic Melange at Sarkikaraagaç **(b)** Zr (ppm) v Ti (ppm) discrimination diagram (after Pearce, 1982). Data from sheeted dykes within the Ophiolitic Melange at Sarkikaraagaç.

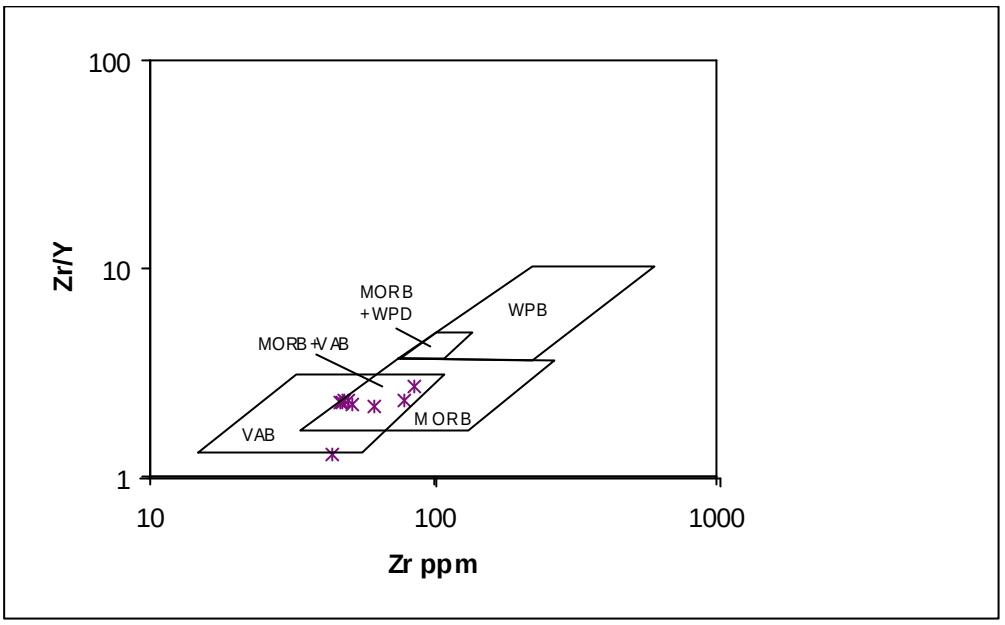

Fig.6.23a. Zr v Zr/Y tectonic discrimination diagram (after Pearce & Norry, 1979). Data from sheeted dykes within the Ophiolitic Melange at Sarkikaraagaç.

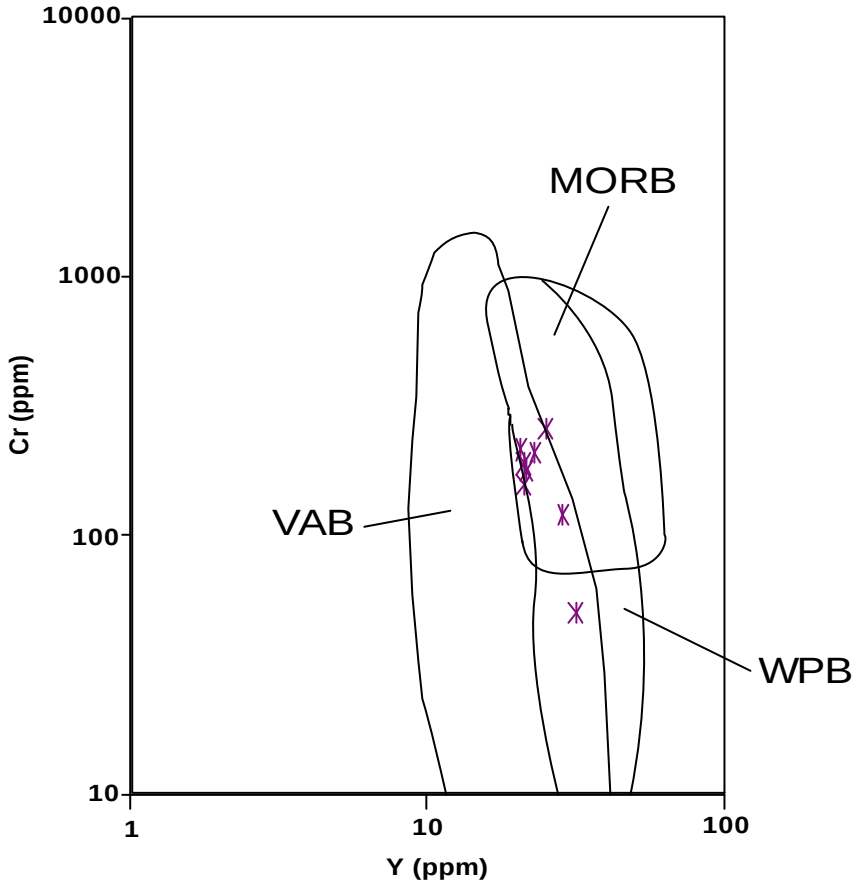

Fig. 6.23b Geochemical plot Y (ppm) v Cr (ppm) tectonic discrimination diagram (after Pearce, 1982). Data from sheeted dykes within the Ophiolitic Melange at Sarkikaraagaç.

6.4 Main geochemical conclusions

The main geochemical findings from this study are summarised below;

1) Triassic Huglu – Ihsaniye volcanics

33 samples were analysed using whole-rock XRF and petrographic techniques, which concluded;

- two main volcanic lithologies are present ; i) Acidic Tuff
  ii) Rhyo-dacitic lava
- the volcanics probably record Fe depletion during the end stages of tholeiitic fractionation.

2) Ophiolitic Melange

Over 30 volcanic clasts within the Ophiolitic Melange from across the B-H Nappes were analysed. The results show at least two main tectonic settings are recorded in the melange;

- Enriched WPB-type, indicative of a seamount or rifted setting
- MORB-type, with a probably inherited subduction signature

3) Ophiolite

Six harzburgitic peridotite samples from two areas (the Kizildag ophiolite-Beysehir area and Dipsiz Göl ophiolite-Hadim area) were analysed using whole-rock XRF techniques. In addition 75 electron microprobe analyses were carried out on chromian spinel grains. The main conclusions are;

- Peridotites are more depleted than MORB and western Mediterranean peridotites
- They are most likely of SSZ-type origin

Ten associated doleritic dykes were analysed using whole-rock XRF techniques, which showed;

- HFSE depletion and severe negative Nb spike in spider diagrams
- VAB affinities in tectonic discrimination diagrams

Chapter 7

7. TECTONIC CORRELATION AND REGIONAL INTERPRETATION

The Beysehir-Hoyran-Hadim Nappes are a major geological unit of the Taurus mountain belt and crop out over 700km across southwestern Anatolia to the Mediterranean coast. Chapters 2 to 5 of this thesis have discussed the tectonostratigraphy of selected areas across the B-H Nappes, to provide representative coverage of this large area. On this basis it is now clear that major similarities exist between each of the areas. Previous workers briefly compared units of the B-H Nappes between local areas, as summarised in Table 7.1 (Özgül, 1976; Monod, 1977; Gutnic, 1977; Gökdeniz, 1981). Comparisons were on the whole conjectural, based on oral communications between authors and lacked conclusive evidence. To address this problem, new logs were measured of critical units, in addition to revisiting, field checking and re-measuring pre-existing logs, detailed mapping of selected areas and collection of structural data. The results of this correlation work are summarised in Figure 7.1. An additional complication was the lack of coherent tectono-stratigraphic nomenclature between the Turkish, French and English literature. This study utilises descriptive terms for the main thrust sheets of the B-H Nappes, the lower allochthonous units (i.e. the Hadim Nappe) and the autochthon (Table 7.1). These terms are primarily based on the well-established nomenclature of Monod (1977) and Özgül (1976), which are widely accepted in the literature. To avoid confusion with specific areas and sections, the suffix *–type* has been added where local terms are used, e.g. the Ihsaniye Unit of the Ermenek area is referred to as the Huglu-type unit.

7.1 Regional Correlations

7.1.1 Late Cretaceous-Early Tertiary top of autochthon

The structurally upper part of the autochthon in the Pisidian Taurides through to the Beysehir area of the Central Taurides is extremely consistent considering the large distance, ca. 100 km (Logs 11-15; Fig. 7.1). In each case Upper Cretaceous neritic facies pass into Palaeocene pelagic carbonate (ca. 10-80m). This unit shows various signs of slope instability including redeposited facies, soft- sediment slumping and slide blocks. Consistently above is ca. 20-30m of Eocene siliciclastic turbidites, also showing evidence of slope instability, then Mid-Eocene (Lutetian) slide blocks and debris flows. The similarities of lithology, facies and age suggest that the autochthon formed a persistent unit across these areas. Assuming the above facies at the top of the autochthon record a single episode of nappe emplacement, it is unclear why the thrust sheets in the Dinar area (e.g. the Dinar Nappes of Gutnic, 1977; Gutnic *et al*., 1979) should be considered as a separate tectono-stratigraphic unit from the B-H Nappes.

	Area	**Autochthon**	**Allochthonous lower units**		**Allochthonous Beysehir – Hoyran Nappes**	
This study	*Entire B-H Nappes*	*Geyik Dag autochthon*	*Bolkar Dag Unit*	*Hadim Nappe*	*Huglu-type unit*	*Boyali Tepe-type unit*
Gutnic (1977): noted similarities to Beysehir area but considered to have a different origin.	Dinar	Sandikli Series	not present	not present	Dinar Nappes	
					Denizpinari Unit	Gökgöl Unit
Monod (1977): Defined Beysehir-Hoyran Nappes	Beysehir	Beysehir– Seydisehir Series	not present	Bademli – Çamlik Units of the Hadim Nappe	Huglu Unit	Boyali Tepe Unit
Özgül (1979): directly compared area to Beysehir	Hadim	Geyik Dag Unit	Bolkar Dag Unit	Aladag Unit	Bozkir Nappes	
					Huglu Unit	Boyali Tepe Unit
Gökdeniz (1981): directly compared area to Beysehir	Ermenek	_	_	Adaköy-Nunu Unit	Ihsaniye – Bayiköy Unit	Oyuklu Dag Unit

Table 7.1 Tectono-stratigraphic nomenclature of the Beysehir-Hoyran-Hadim Nappes according to previous work and this study.

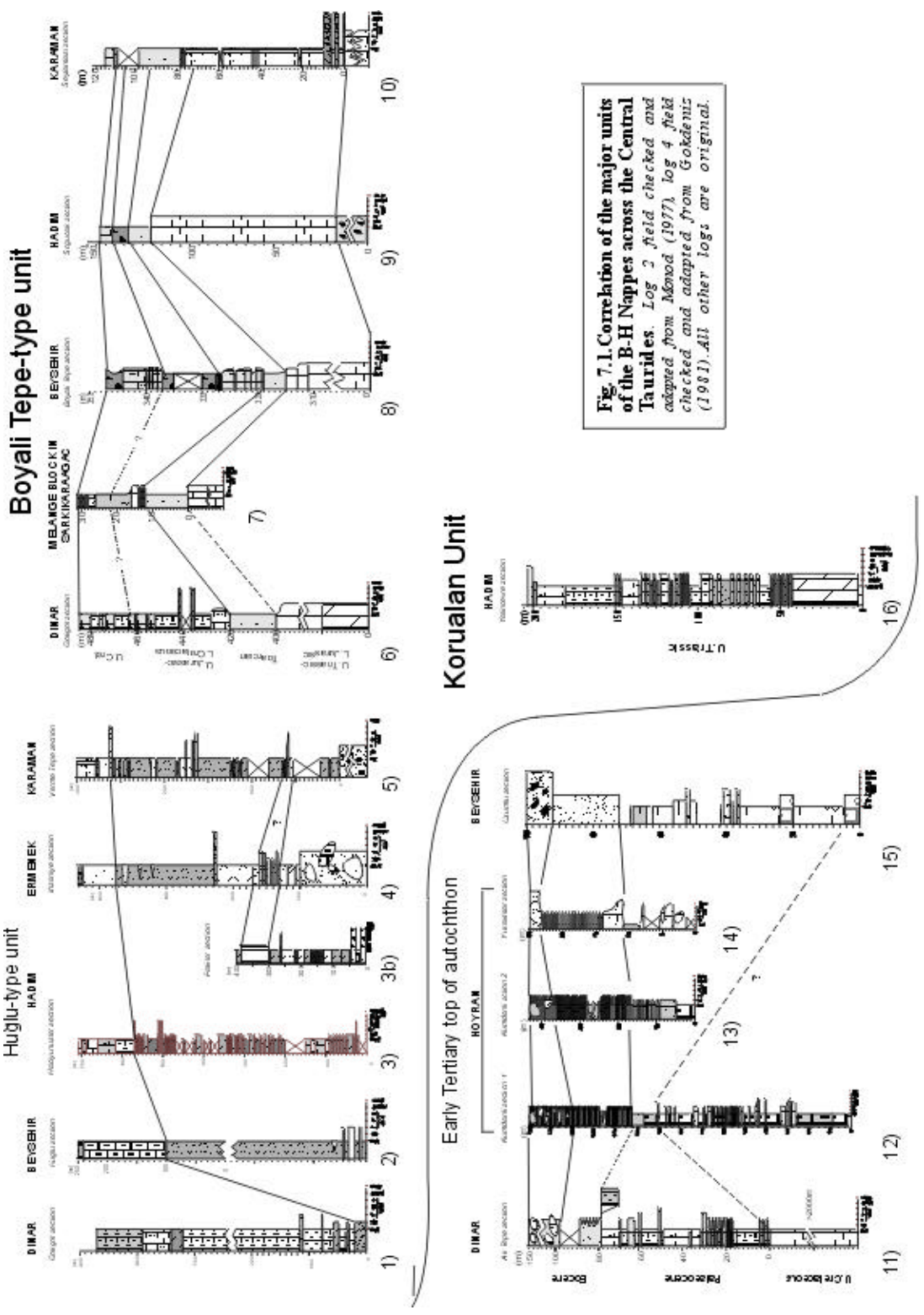

Fig. 7.1.Correlation of the major units of the B-H Nappes across the Central Taurides. *Log 2 field checked and adapted from Monod (1977), log 4 field checked and adapted from Gokdemir (1981).All other logs are original.*

7.1.2 Huglu-type Unit

Definition: The Mid-Triassic to Upper Cretaceous Huglu-type unit is characterised by a bipartite stratigraphy (Fig.7.1); the lowermost part is dominantly volcanogenic, commonly composed of green tuff interbedded with intermediate to acidic volcanic rocks (Section 6.1). The uppermost part of the unit is primarily a thin pelagic limestone sequence, with or without radiolarian chert.

The Huglu-type unit is present across all of the Central Taurides from the Beysehir area to the Karaman area. It is absent from the Pisidian Taurides north of Lake Beysehir to Sandikli, but is present once again in the far western Dinar area (Logs 1-5; Fig. 7.1). Its structural position is summarised in Fig. 7.2; generally, it is found at or near the bottom of the nappe stack in the eastern regions, but is towards the top of the pile where present in the west. The unit is remarkably coherent and similar to the Huglu-type section (Beysehir) in most areas. Divergence from this norm is discussed below.

The basal half of the volcanogenic sequence in the Ermenek area is characterised by debris flows, which pass into intermediate-composition volcanics, interbedded with siliciclastic turbidites (Section 5.3.2.2). This clastic-dominated sequence can be traced into the Hadim area (Fakilar section; Section 4.6.3), where it is present as a thick turbidite sequence, and possibly into the Karaman area (Verme Tepe section; Section 5.4.2.2) as minor redeposited clastic horizons. The transition from this mixed volcanic-clastic sequence to a purely volcanogenic origin is marked in the Ermenek area by a limestone megabreccia not present in the other studied areas (e.g. Çingen Tepe megabreccia; Section 5.3.2.3).

In the Dinar area, the lowermost volcanics form an unusually thin sequence of predominantly sheared lavas, without the distinctive green tuffs which are characteristic of the Huglu-type unit elsewhere. The overlying pelagic sequence is extremely well developed though, reaching a thickness of ca. 700m, compared with <100m to ca. 150m in other areas. The inferred Upper Jurassic section is dominated by radiolarian chert. Chert within the Huglu-type unit of this thickness is only found in the Ermenek area (Section 5.3.2.5), and as discrete blocks within melange on the south shore of Lake Beysehir (Section 2.6.3.2). The Cerityayla Unit is inferred to be a structural repeat of the Denizpinari Unit due to similarities in lithology and age (Section 3.3.2.4).

7.1.3 Boyali Tepe-type Unit

Definition: The Triassic to Upper Cretaceous Boyali Tepe-type unit is defined by thick Triassic neritic limestone, commonly overlain by Ammonitico Rosso pelagic limestone and radiolarian chert. Figure 7.2 summarises the structural position of the Boyali Tepe-type unit within the nappe stack. In the east the unit is found in the structurally highest position; however, elsewhere it is found towards the base of the pile. The Gencek Unit is incorporated into this classification because of its tectonostratigraphic similarities.

The Boyali Tepe-type unit is characterised by a thick Mid-Upper Triassic neritic carbonate in all areas (Fig. 7.1). This is overlain by Toarcian Ammonitco Rosso pelagic limestone, except in the Pisidian Taurides east of the Dinar area. However, this type of pelagic limestone is present in these areas as discrete blocks in melange; e.g. Ammonitico Rosso block in the Sarkikaraagaç melange (Section 3.2.2.1.2) and Ammonitico Rosso limestone breccia blocks in the Kumdanli area (Section 3.2.2.2.1). The normal stratigraphic succession of this unit then passes into radiolarian chert of Oxfordian – Early Hauterivian age in the Beysehir type section (T. Danelian, pers.comm, 2001). A similar, but undated, succession is seen east of Beysehir. This radiolarian chert interval is not present in the Dinar section (Fig. 7.1).

7.1.4 Other units

As seen in Fig.7.2, there are some units specific to local areas, namely the Triassic Korualan Unit of the Hadim area. The Korualan Unit is characterised by interbedded siliciclastic sediments and pelagic limestone and chert (Section 4.6.2). This unit is extremely important as it represents a type of tectonic facies (defined in Section 7.2.1) not seen elsewhere in the B-H Nappes.

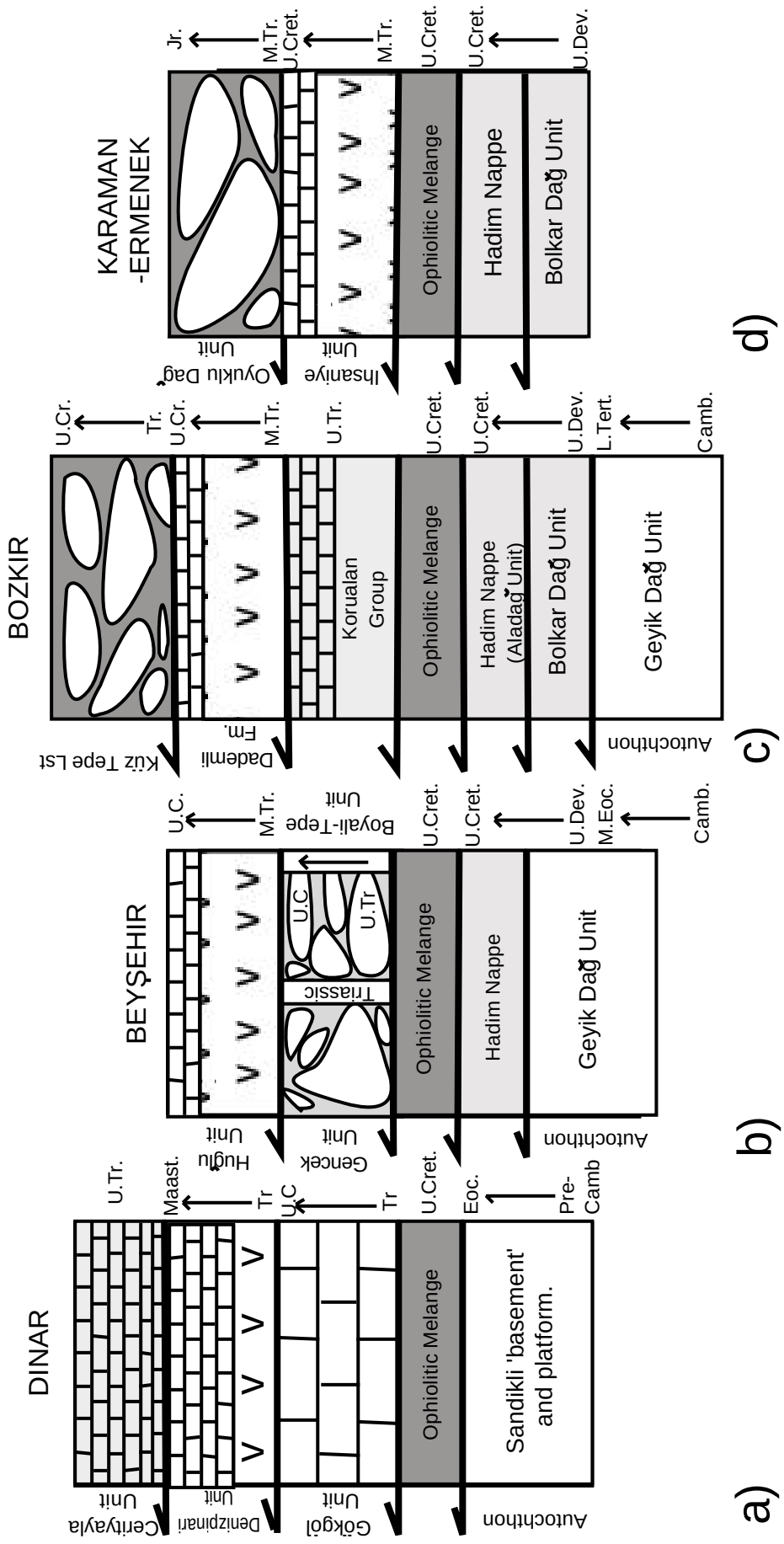

Fig. 7.2 Summary cartoon diagram showing tectonostratigraphic correlation and structural position of thrust sheets within the B-H Nappes, from west to east. Not to scale.

Autochthon	1. The similarity of the top of the autochthon across ca. 100km suggests the Dinar area is linked through to the Beysehir area.
Ophiolite	2. Ophiolitic Melange is always present at the base of the B-H Nappes. 3. Ophiolite occurs as slices of serpentinised peridotite in four main areas only; north (Sarkikaraagaç) and south (Kizildag) of Lake Beysehir, Dipsiz Göl and south of Ermenek. 4. Ophiolitic Melange is found at higher structural levels in the eastern areas.
Huglu-type Unit	5. Not present in the Pisidian Taurides east of Dinar through to north of Lake Beysehir. 6. Volcanogenic sequence not well developed in Dinar area, which could reflect an original deposition feature or later tectonic removal. 7. Dinar area has thick accumulation of pelagic sediments from Upper Triassic onwards, suggests more basinal setting. 8. Radiolarian chert in sequence only in the extreme southeast and northwest.areas. 9. Thick accumulations of terrigenous sediments towards base of succession in southeasterly areas.
Boyali Tepe-type unit	10. Characterised by Triassic neritic carbonate at the base of the sequence 11. Includes the Gencek Unit from the Beysehir area, as essentially it is dominantly Triassic neritic carbonate 12. Toarcian Ammonitico Rosso not incorperated in the coherent thrust sheets in the Pisidian Taurides east of Dinar through to north of Lake Beysehir. This facies is found as blocks in melange suggesting this facies was originally there but has not been preserved. 13. Radiolarian chert not present in the Boyali Tepe-type sequence in the Dinar area
Pisidian Taurides	14. The allochthonous units in the Dinar area were previously thought to be separate from the B-H Nappes (Gutnic, 1977; Gutnic et al., 1979). A more likely scenario that this study favours is that the Dinar allochthonous units are part of the B-H Nappes because they share the same emplacement history, have a similar tectononstratigraphy and are geographically the along strike continuation of the B-H Nappes.

Table 7.2 Specific and general points regarding the ccrrelation of the Beysehir–Hoyran Nappes through the Pisidian Taurides and the Central Taurides

7.2 Tectonic setting interpretation

This section draws together all the available lithostratigraphic, palaeontological, sedimentary and geochemical data from the previous five chapters to present a tectonic facies oriented interpretation of the setting of the B-H Nappes. These settings are subsequently incorporated into a number of alternative tectonic models in Chapter 8. In this thesis, emphasis is placed on the B-H Nappes and the uppermost levels of the autochthon. Deeper levels of the autochthon and other allochthonous units are discussed only briefly to help place the B-H Nappes in a regional context. Due to the complexities of the regional tectonics of the Eastern Mediterranean, this thesis discusses phases of tectonic development that occurred to the Beysehir-Hoyran Nappes before attempting to integrate these findings into the wider context of the Tethyan system.

7.2.1 The tectonic facies concept

In this particular scenario, conventional sedimentary facies analysis of individual litho-stratigraphic units can provide a wealth of detailed data, which could prove to be a hindrance in the recognition of large-scale tectonic settings. Instead, to help conceptually link the outcrop geology presented in this thesis to possible plate-scale processes the tectonic facies concept (analogous to sedimentary facies) is preferred. Based on comparison with modern oceans and margins and well-constrained land settings, the tectonic facies concept allows the recognition of discrete tectonic settings preserved within orogenic belts. The definition of a tectonic facies from Robertson (1994) is as follows;

" A tectonic facies constitutes the combined lithological and structural features that allow systematic recognition of past tectonic settings within an orogenic belt (e.g. an oceanic seamount)."

Difficulties may exist in poorly exposed or highly deformed areas where available data could be consistent with more than one tectonic facies (e.g. metamorphic terranes). The concept works best in cases where modern settings are well documented and where facies models for individual tectonic settings are unique (Robertson, 1994). Even though the tectonic facies model was originally developed in the Eastern Mediterranean region, the concept recognises global geological features that arise from discrete tectonic settings, consequently, the technique in theory can be applied to any orogenic belt. Based on data presented in this thesis, the following sections illustrate tectonic facies this study recognises in the B-H Nappes, which allow the regional tectonic evolution to be discussed. A number of distinct phases are recorded in the B-H Nappes, thus;

1) Rifting.
2) Passive margin subsidence.
3) Oceanic spreading.
4) Intra-oceanic convergence.
5) Subduction and accretion.
6) Initial collision.
7) Suture zone tightening and final nappe emplacement.

7.2.2. Initial rifting and passive margin subsidence of the Tauride units

The Precambrian to Lower Palaeozoic sequence of the Tauride autochthon, i.e. the Sandikli Basement Complex and the overlying Seydisehir Formation, are widely interpreted to represent Pan-African continental basement and cover, overlain by Upper Triassic shales and siliciclastic sediments deposited on the rifted fragment of the north-Gondwana shelf (Dean & Özgül 1994, Göncüoglu & Kozlu, 2000).

Overlying Mid-Late Triassic shallow-water carbonates record a subsiding Bahama-type carbonate platform, whilst latest Triassic fluvial to shallow-marine clastic sediments (Çayir Formation) are believed to record fault-related uplift and erosion of the underlying basement (Monod & Akay 1984), possibly a compressional effect related to the final emplacement of the Karakaya Complex in the Pontides further north (Robertson & Pickett 2000). The regional Tauride autochthon was dominated for the remainder of Mesozoic time by neritic carbonate deposition, indicative of carbonate platform conditions (Sengör & Yilmaz, 1981; Dercourt *et al.*, 1986; Robertson, 1994).

Where present, the Hadim Nappe exhibits a similar Paleozoic-Cretaceous succession to the Autochthon. The Upper Devonian-Upper Cretaceous succession records a shallow-marine carbonate platform setting, punctuated by emergence and erosion in latest Triassic time, coinciding with the deposition of shallow-marine to fluvial clastic sediments (Çayir Formation; Monod & Akay 1984). However, the Geyik Dag Autochthon and the Hadim Nappe differ in the Late Cretaceous interval as Ophiolitic Melange is present on the latter, showing that the Hadim Nappe was overthrust by oceanic crust that did not reach the Geyik Dag further south. Only in the Hadim/ Bozkir area are the Hadim Nappe and Bolkar Dag Unit seen together. They share a similar stratigraphy; thus, consequently are seen as facies variants within the original Tauride carbonate platform (Geyik Dag), with the Bolkar Dag Unit, in particular, showing a relatively thin and variable succession.

The rifting and passive margin subsidence phases, as recorded in the main thrust sheets of the B-H Nappes are now discussed in the following sections. For simplicity, each tectonostratigraphic unit is discussed separately.

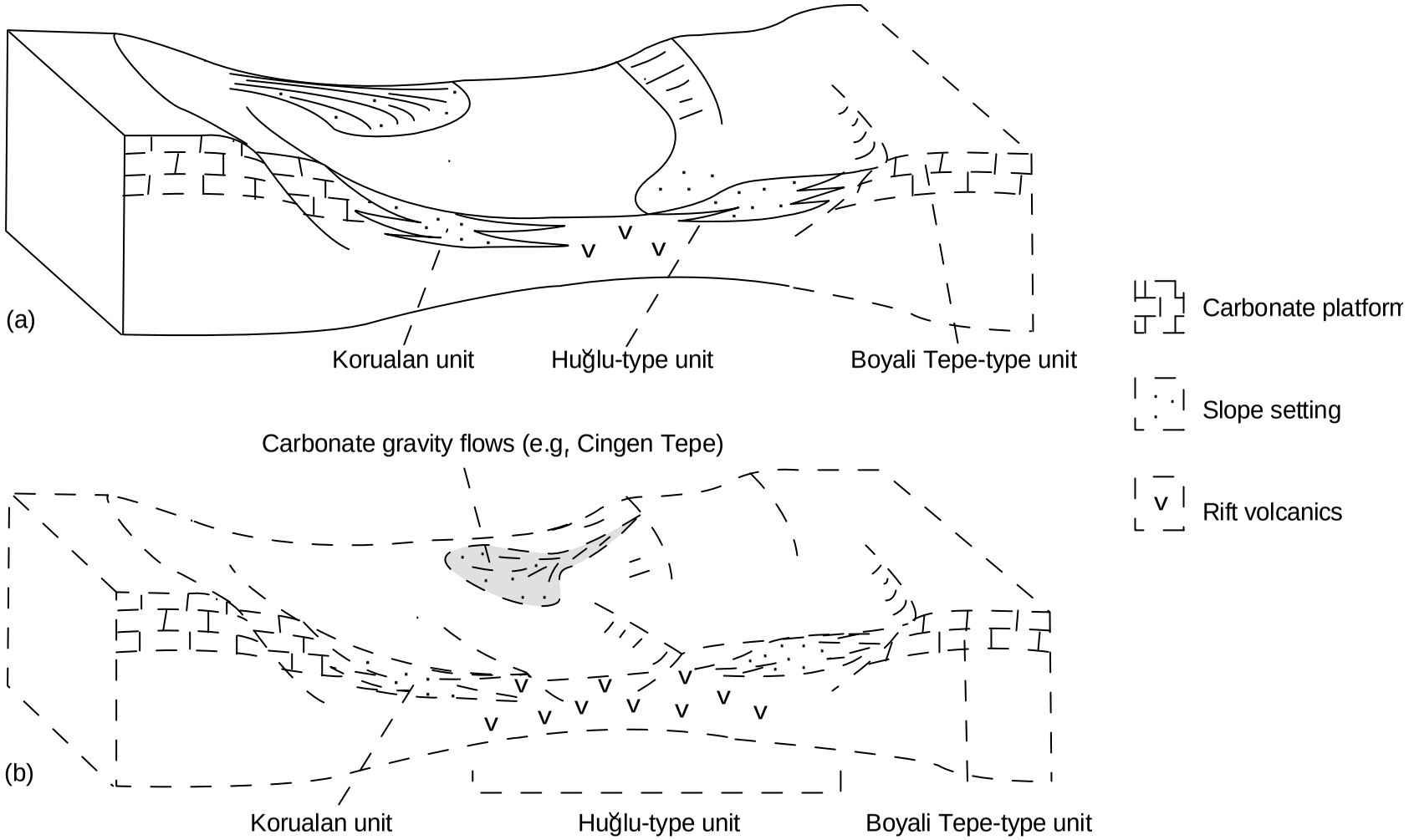

Fig. 7.3 Cartoon diagrams of the tectonic settings recognised in the B-H Nappes,. **(a)** Initial rifting, **(b)** Continued rifting and maximum volcanic activity in the Mid-Triassic.

7.2.3. Mid-Triassic volcanogenic rift unit and Late Triassic-Late Cretaceous pelagic cover: the Huglu-type units

The lowermost part of the Mid-Triassic succession can be best interpreted by combining evidence from the more southerly regions (i.e. the Hadim area; Section 4.6.3 and the Ermenek area; Section 5.3.2). The sequence comprises intermediate-composition volcanics and tuffaceous material interbedded with thick (ca. 100m) siliciclastic sequences of sandstone and mudstone. Extrusion of the volcanics occurred at, or near, the sea floor, as clasts of micritic limestone that are locally incorporated into lava flow units (Fig. 4.13). Generally the turbidite sequences are mud-dominated and suggest a relatively basinal facies or flow bypass; however, locally where the grain size is coarser (e.g. Tozlubeleni section, Ermenek area; Section 5.2.2.2), thicker arkosic sand packets contain plant remains, which indicate a continental provenance for the turbidites, locally deposited by northward-directed currents (e.g. Fakilar section, Hadim area; Fig. 4.12).

Later, in Mid-Triassic time, the basinal sequence was inundated by acidic volcanics (Fig. 7.3). During the Carnian of the Hadim area, a volcanic build-up was extruded, ca.1km thick. The transition from a mixed clastic-intermediate volcanic basinal sequence to a thick acidic volcanic pile is locally marked, in the Ermenek area, by ca.20m-thick channelised lenses of matrix-supported, limestone megabreccia, containing Anisian-aged reefal material (Section 5.2.2.3). This facies probably resulted from mass wasting of the platform margin as debris flows which bypassed the upper slope and were deposited in lower slope or basinal settings. Similar carbonate gravity flow deposits are, for example, present in Upper Cretaceous sequences in the Sopeira region of the south-central Pyrenees (Drzewiecki & Simo, 2002). Trigger mechanisms for this intense reworking remain unknown in this case, although factors such as seismic activity, margin oversteepening and erosion during sea level low-stands have been previously suggested for similar rudaceous flows (e.g. Franklinian Shelf; N. Greenland, Surlyk & Hurst, 1984; Cow Head Group; Newfoundland, Hubert *et al*, 1977).

This Mid-Triassic mostly volcanic sequence is punctuated by pelagic carbonate lenses, local volcaniclastic sediments, chert and calcturbidites, which accumulated during periods of relative volcanic quiescence (e.g. Hadim area, Fig. 4.14; Huglu section-Beysehir area, Fig. 2.21; Verme Tepe section-Karaman area, Fig. 5.22).

In Late Triassic time the volcanic activity generally waned and pelagic limestone deposition predominated; this was probably related to post-rift subsidence (Fig. 7.4a). The onset of this subsidence was possibly slightly diachronous across the Taurides, as illustrated by the age of the onset of main pelagic limestone deposition; i.e. Anisian-Ladinian time in the Beysehir area (Section 2.6.3.2), Mid-Late Carnian in the Hadim area (Section 4.6.3) and Mid-Late Norian in the Ermenek

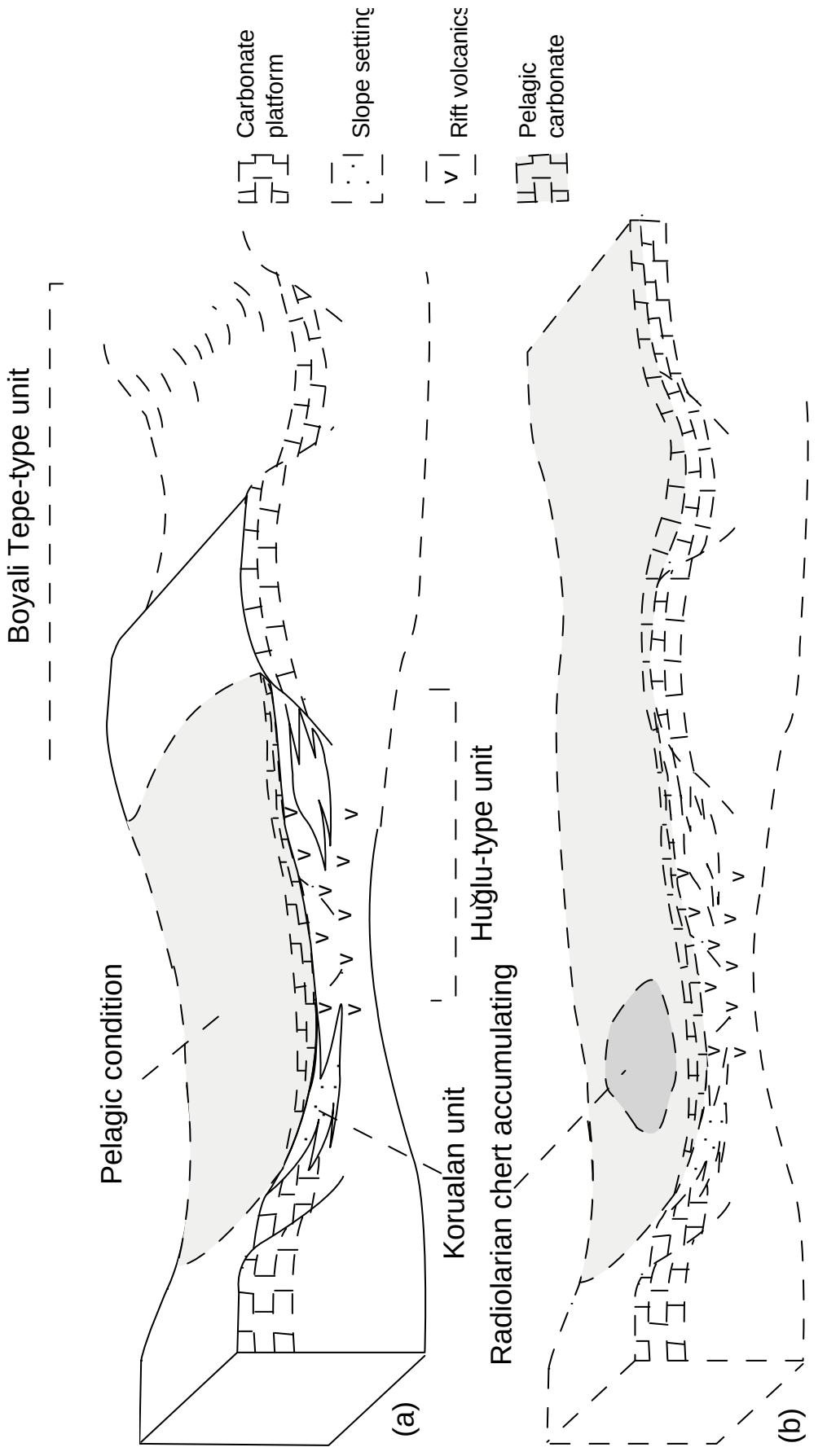

Fig. 7.4 Cartoon diagrams of the recognised tectonic settings present in the B-H Nappes. **(a)** Initial Late Triassic post-rift subsidence, **(b)** Continued subsidence in early Jurassic time.

area (Section 5.3.2.4). Precise age data do not exist for the Dinar area or the Karaman area and the palaeontological dating needed to test for diachronicity was outside the scope of this work. However, if the age data provided by previous work are reliable, then the onset of post-rift subsidence might have occurred ca. 5 Ma earlier in the western regions than the east. Pelagic conditions prevailed up to and including Late Cretaceous time with deposition of a thin succession (ca. >150m) of pelagic limestones. In the more outboard areas (i.e. Dinar in the northwestern and Ermenek in the southeastern regions) radiolarian chert was deposited. Unfortunately, precise ages for this period of chert deposition do not yet exist because of difficulties in dating the poorly preserved radiolarians accurately. An Upper Jurassic age is likely for the Dinar area and possible for the Ermenek area (see Appendix A).

In summary, the Huglu-type Unit, especially the lower siliciclastic turbidites (e.g. Ermenek area) are indicative of a basinal setting within a continental rift that was inundated by volcanics after Mid-Triassic time (Fig. 7.3). The intermediate-acidic nature of the volcanics may reflect the late stages of tholeiitic evolution, i.e. melting of underlying continental crust undergoing low extension. The rifting was followed by Late Triassic post-rift subsidence and pelagic carbonate deposition at, or near, the Carbonate Compensation Depth (CCD) until Late Cretaceous time (Fig. 7.4). Radiolarian chert accumulated in the more basinal areas (e.g. Dinar and Ermenek).

7.2.4. Mid-Upper Triassic slope facies: the Korualan Group

The lowest level of this thrust sheet is exposed in the Yalinçevre section (Section 4.6.2). Sediments there record neritic carbonate deposition of inferred Mid-Triassic age, which pass into fine-grained lithic sandstone turbidites and mudstone. This facies was punctuated by brief periods of pelagic carbonate deposition, possibly reflecting background sedimentation and/or the onset of deepening conditions. Interbedded redeposited limestone facies throughout this sequence indicate a continuing slope influence adjacent to an eroding neritic carbonate platform source area. The likely candidate is the regional Tauride carbonate platform. A fundamental change occured in Late Triassic time with fine-grained hemi-pelagic carbonate deposition recording a switch from clastic sedimentation to deeper water carbonate and siliceous hemipelagic facies. Radiolarian chert, with interbedded calcturbidites, are associated with this facies in the Korualan section, indicating that the background pelagic sedimentation was interupted by influxes of redeposited carbonate. Similar facies are seen in other allochthonous Tauride units (e.g. the Yilanli Unit of the NE Antalya Complex; Waldron, 1984).
The uppermost levels of the Korualan Group are characterised by melange, which consists of inclusions of radiolarian chert, aphyric volcanics, volcaniclastic sediment, metalliferous sediment interfingering with spilitic lava, pelagic limestone, limestone breccia and quartzite. Although undated, these units are interpreted as having been accreted, possibly during the Late Cretaceous accretion/emplacement of this unit (Section 7.2.8).

The Korualan Unit, known only in the Bozkir/Hadim area at the base of the Beysehir Nappes, is interpreted as a Triassic slope, to base-of-slope unit, adjacent to a carbonate platform. Pelagic conditions were established by end-Triassic time. The Korualan Group was possibly tectonically cut out in other areas during emplacement.

7.2.5. Triassic neritic carbonate and Jurassic-Cretaceous condensed pelagic cover: Boyali Tepe-type units

This subsiding carbonate platform tectonic facies begins in Mid-Late Triassic time with a thick sequence of neritic carbonate deposited in all areas, except in Ermenek. Pelagic conditions dominated there with nodular limestone being the main facies present (Section 5.3.2). Elsewhere, shallow-water limestone, representing carbonate platform conditions, continued to be deposited until Early Jurassic (Toarcian) time. Pink, nodular limestone (Ammonitico Rosso) of this age probably reflects the onset of deepening conditions beginning in the Toarcian (Fig. 7.4b). This deepening was a regional event across most of the oceanic setting that the B-H Nappes represent. This event does not correlate with the Ermenek area in the southeast, which possibly represents a more distal facies-equivalent at the edge of the basin. Elsewhere, subsidence of the Boyali Tepe platform persisted and radiolarian chert was the dominant sediment, probably reflecting deposition below the carbonate compensation depth (CCD). The timing of this event is poorly constrained, although the oldest radiolarian fauna recovered in this study (Appendix A) from the chert sequence in the Beysehir Boyali Tepe sequence is of Late Jurassic age (Oxfordian). Chert from the Hadim sequence is unsuitable for this kind of study as it is highly sheared and forms no coherent sequences, whilst radiolarians recovered from the Karaman section are poorly preserved such that only a post-Triassic age could be assigned with confidence (Appendix A). Chert is also absent from the Dinar succession, indicating the conditions were different in Late Jurassic time in the far western area. Pelagic limestone there was deposited right through to Late Cretaceous time. Siliceous pelagic sedimentation probably ended in Early Cretaceous time (Early Hauterivian), as inferred from the youngest radiolarian fauna to be recovered from the chert sequence in the Beysehir area (Appendix A). Deep-marine conditions prevailed until Late Cretaceous time, with pelagic limestone deposition in most areas. The central Beysehir area returned to siliceous sedimentation in Late Cretaceous time indicating fluctuating conditions, before an abrupt facies change. The uppermost preserved sequence of this unit is a polymict breccia, derived from a seamount or ophiolitic source as indicated from exotic volcanic clasts (Section 2.6.2). Reworking of the underlying sequence is apparent. This abrupt change of facies suggests extreme erosion and reworking in the proximity of a volcanic source, probably in latest Cretaceous time.

The Boyali Tepe-type successions are interpreted as a more distal, Triassic carbonate platform removed from a continental source, as shown by the absence of siliciclastic sediment. In the Toarcian the carbonate platform subsided and was later overlain by deeper-water Ammonitico Rosso condensed pelagic carbonates. Ribbon radiolarites then accumulated in Late Jurassic to Early Cretaceous followed by Late Cretaceous pelagic carbonates.

7.2.6 Oceanic spreading

Basaltic blocks in the Ophiolitic Melange are interpreted as remnants of oceanic crust and accreted seamounts (Section 6.1.7 and 7.2.8). Other evidence for oceanic crust having developed to the north of the Tauride platform (Section 8.) are the Beysehir-Hoyran ophiolites, interpreted as forming in a SSZ-type setting (Section 6.3.5 and 7.2.8). The true age of the oceanic substratum in the Beysehir-Hoyran area is unknown, but must post-date initial Permo-Triassic rifting. Limited biostratigraphical data from radiolarian chert in oceanic accretionary complexes within the Izmir-Ankara suture zone imply this ocean had an age span of at least late Norian to Albian (Bragin & Tekin, 1996; Beccaletto & Stampfli, 2000; Göncüoglu *et al.*, 2000; Okay *et al.*, 2001). This oceanic crust is inferred to have subducted almost without trace during Late Cretaceous convergence.

7.2.7 Late Cretaceous intra-oceanic convergence

An amphibolite facies metamorphic sole locally occurs beneath the peridotite and is well exposed in the Sarkikaraagaç area, north of Lake Beysehir (Section 3.2.2.1.1; Elitok 2000, 2002). Greenschist and amphibolite facies rocks unusually occur as detached blocks within the Ophiolitic Melange, above the main body of the ophiolite in the Beysehir area (Section 2.5.3.2; Monod 1977). Although no specific evidence exists in the Beysehir area, given their lithology and association with the ophiolite, they probably represent fragments of metamorphic sole as inferred by other workers (Thuizat *et al*., 1981; Dilek *et al*., 1999; Çelik, 2001)

These amphibolite blocks commonly have an alkaline to sub-alkaline character, with an incompatible trace element composition typical of ocean island basalt (OIB); thus, a within-plate tectonic setting is inferred (Çelik *et al.*, 2001, Elitok, 2002). Preliminary K/Ar age determinations from their study, based on hornblende minerals indicate a crystallization age of ~88 Ma for the metamorphic sole in the Beysehir area. The metamorphic sole is generally inferred to represent oceanic crust and sediments that were underplated to the still hot ophiolite while in an oceanic setting near to its spreading axis, prior to emplacement over a continental margin (Woodcock & Robertson, 1977; Spray *et al.*, 1984). Assuming sole formation does not significantly post-date ophiolite genesis, this would imply intra-oceanic underplating of WPB-protoliths to the hanging wall began in Late Cretaceous time (Fig. 7.5a). The timing of this process is coeval with related Tauride ophiolites, e.g. Lycian Nappes, Collins, 1997; Collins & Robertson, 1998; Posanti-Karsanti ophiolite, Parlak *et al.*, 2000; thus, it is extremely likely that a similar mechanism inferred to create these metamorphic soles occurred in the Beysehir area. Furthermore, it is widely interpreted that the Late Cretaceous Tauride ophiolites are remnants of a single vast ophiolite thrust sheet generated within the Northern Neotethyan ocean (Özgül, 1976, 1984; Monod, 1977; Sengör & Yilmaz, 1981; Robertson & Dixon, 1984; Lytwyn & Casey, 1995; Dilek *et al*, 1997, 1999; Robertson in press). Although it is not the intention of this thesis to comprehensively discuss alternative mechanisms proposed for ophiolite metamorphic sole generation, it is worth noting that ophiolitic 'sole' rocks can form in a range of other tectonic settings where hot crust is faulted against cooler mafic crust, as shown in Figure 7.5 (b)-(f) (Bébien *et al.*, 1980; Hall, 1982; Robertson & Woodcock, 1982; Whitechurch *et al*.,1984; Spray, 1984)

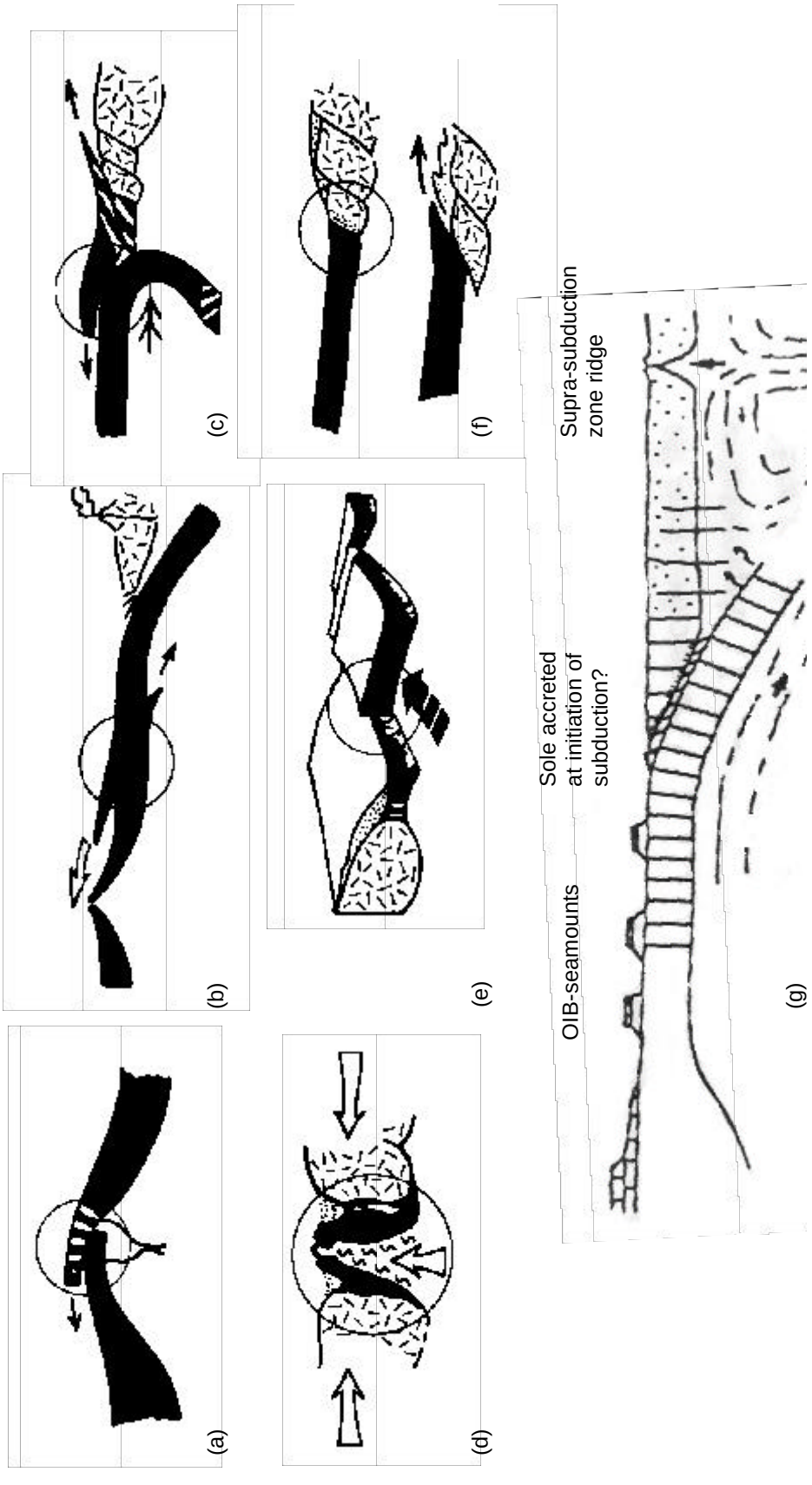

Fig. 7.5 Alternative mechanisms proposed for ophiolite amphibolitic sole generation. Site of sole formation is ringed **(a)** At an overlapped ridge crest during asymmetrical ridge collapse (Robertson & Dixon, 1984), **(b)** low angle shearing, parallel to an adjacent subduction zone (Whitechurch *et al.*,1984), **(c)** During 'roll to' following 'roll-back' (Spray, 1984), **(d)** Diapiric up-welling of upper mantle and basaltic crust in a pull-apart rift zone (Bébien *et al.*, 1980), **(e)** Transform activated juxtaposition of an active ridge segment against cold, marginal oceanic crust (Robertson & Woodcock, 1982), **(f)** Emplacement-related shearing superimposed on an earlier thermal aureole generated at the continent ocean boundary (Hall, 1982) and **(g)** formation of supra-subduction zone crust and mantle. Diagrams originally from Robertson & Dixon (1984).

An important point concerning the metamorphic sole in the Beysehir area is that it is not found in the normal sub-ophiolite position as for other Tauride ophiolites (e.g. Sarkikaraagaç area, Elitok, 2000; Lycian peridotite, Collins, 1997; Posanti-Karsanti ophiolite, Parlak *et al.*, 2000). Instead, the metamorphic sole is present as detatched blocks above the ophiolite. In known cases where a similar situation occurs, it appears that the units have undergone significant rethrusting (e.g. the Loumnitsa Unit of the Pindos, Jones, 1990; Baer-Bassit ophiolite, Al-Riyami, 2000). It is likely that a similar rethrusting event has occurred in the Beysehir area (Section 8.2.2).

7.2.8 Ophiolite genesis

Large coherent slices of serpentinised peridotite occur within the Ophiolitic Melange in several areas, e.g. to the north and south of Lake Beysehir, Bozkir (Dipsiz Göl) and to the south of the Ermenek area. Presently, these are dated only as pre-Maastrichtian by the age of the melange matrix (Section 7.2.3) and the metamorphic sole (ca. 88 Ma; Ö.F. Çelik, pers.comm. 2001).

The peridotite is dominantly serpentinised harzburgite, ranging from fresh to 70% altered, with minor pyroxenite, dunite and chromite pods (Monod, 1977; Elitok 2000, 2002). Dolerite dykes that cut the peridotite exhibit chilled margins and local metasomatic calcic alteration. Whole-rock XRF analysis of relatively unaltered peridotite (Section 6.3.2) reveals Cr and Ti contents comparable with inferred supra-subduction zone-type (SSZ) ophiolites (Pearce *et al.* 1984). Analysis of chrome spinel grains, using an electron microprobe, confirms enrichment in Cr relative to Mg (Section 6.3.3), as in present-day island-arc rocks and inferred SSZ-type ophiolites (e.g. Oman ophiolite; Dick & Bullen 1984). Peridotite from north of Lake Beysehir, when normalised to N-type MORB, shows enrichment in large ion lithophile elements (LILE) relative to HFS elements. Such enrichment is attributed to mantle wedge metasomatism by LILE-enriched hydrous fluids derived from subducted oceanic crust in a SSZ setting. Finally, whole-rock analysis of sheeted dolerite dykes from Sarkikaraagaç associated with the ophiolite (Section 3.2.2.1.2, Figure 3.10) reveal an immobile trace-element composition similar to SSZ-type basalt (Section 6.3.5).

Özgül (1984) envisaged that the Dipsiz Göl ophiolite was formed by rifting of the Tauride carbonate platform in Late Cretaceous time, for which supporting evidence was not found during this study. Instead, the available geochemical data from the peridotite thrust sheets is consistent with genesis in an intra-oceanic SSZ setting, shown in Fig. 7.5(g), as for other "depleted" Neotethyan peridotites (e.g. Oman, Troodos, Pearce *et al.* 1984; Lycian Peridotite thrust sheet, Collins & Robertson 1998). Alternative models for SSZ-ophiolites include spreading during collapse of spreading ridges, incipient subduction zones and fore-arc/back-arc settings (Dilek *et al.* 1999, Robertson in press). Thus, the chemical data must be treated with caution in tectonic synthesis. Further discussion is given in Chapter 8.

7.2.9 Late Cretaceous subduction/accretion: Ophiolitic Melange

Ophiolitic Melange is always at the same relative structural position, i.e. above the Hadim Nappe (where present), but below the Upper Nappes (Fig. 7.2). Ophiolitic Melange is also found at structurally higher levels in both the Bozkir and northern Ermenek-Karaman areas, usually as the matrix of dismembered units ("broken formation").

The melange is dominated by a chaotic admixture of neritic and pelagic limestone, radiolarian chert, basic volcanic rocks, serpentinite, volcaniclastic sediments (including debris flow deposits), gabbro and amphibolite, set in a sheared, incompetent matrix of ophiolite-derived sandstone and mudstone. The melange matrix is dated as Late Cretaceous (Maastrichtian) based on planktonic foraminifera, including *Globotruncana arca*, from blocks of pink pelagic limestone in the Bozkir area (Özgül 1997). The dominantly deep-sea nature of the melange matrix and the similarity of deformation fabrics with modern oceanic fore-arc complexes (e.g. the Barbados arc; Mascle & Moore 1990) suggests the melange is a subduction/accretion complex, as has been inferred for numerous similar Tethyan melanges throughout the Palaeozoic and Mesozoic, e.g. the Upper Palaeozoic Karaburun-Chios Melange, Turkey-Greece (Robertson & Pickett, 2000); the Jurassic Avdella Melange, Pindos, Greece (Jones, 1990); the Jurassic Pagondas Melange of Evia, Greece (Danelian & Robertson, 2001); the Upper Cretaceous Lycian Melange, Turkey (Collins & Robertson, 1997); the Upper Cretaceous-Early Tertiary Indus Suture Zone melanges (Robertson, 2000).

Whole-rock X-ray fluorescence (XRF) analysis of the basaltic clasts from the Ophiolitic Melange in the Pisidian Tauride, Beysehir and Karaman areas, reveal the presence of two main compositional groups (Section 6.1.7). One is relatively enriched in the high-field-strength (HFS) elements compared to normal mid-ocean ridge basalt (N-MORB) and shows within-plate affinities on tectonic discrimination diagrams (Section 6.1.6). This group of clasts could record either Neotethyan rifting, or the presence of a seamount in the Neotethyan ocean. Coupled with sedimentary evidence (volcano-chert breccias; Section 2.5.3.2), the likely setting of eruption is on a topographic slope, possibly on a rift-block or on the flanks of a seamount. However, the lack of terrigenous sediment in the melange associated with these blocks suggests a more outboard setting, i.e. a seamount. Present-day examples of seamount/trench collision can be found in the Eastern Mediterranean (e.g. Eratosthenes seamount; Robertson, *et al*., 1995) and the Japan Trench (Daiichi- Kashima Unit; Taira *et al*., 1989).
The other compositional group of volcanics from the Pisidian Taurides have MORB-like geochemical characteristics commonly with a negative Nb anomaly, which is generally suggestive of a subduction-influenced melt (Pearce *et al*.,1990). If this Nb signature was due to a local volcanic arc or rifted back-arc basin setting related to contemporaneous subduction, then it would be likely that this type of related unit would be present in the melange. Silicic tuffaceous material, extrusive andesite and related intrusive rocks are notably absent from the melange in the Pisidian Taurides; therefore, neither of these settings seems likely. An alternative is that the subduction influence was inherited from a pre-

existing subduction event, as suggested for other Triassic Tethyan rift-related volcanics (Robertson & Dixon, 1984).

The inclusions within the melange are likely to be the remnants of oceanic basement, seamounts and cover sediments scraped from the downgoing slab during subduction. However, neritic units, e.g. the kilometre-sized blocks of *Fusulinid*-bearing Permian limestone beneath the ophiolite in the Beysehir region (Section 2.5.3.4 in this study; Monod, 1977) are unlikely to have formed in such a setting and are likely to represent near-margin units. Volcaniclastic and rudaceous debris flow sediments in the Ophiolitic Melange indicate that sedimentation processes were important in its formation. These types of sediments may have developed as trench turbidites and slump deposits from the accretionary prism. Structurally, however, the melange fits into the d-type of unit (Raymond, 1984) or the Type III melange designation ('block in matrix chaos'; Cowan, 1984). A number of mechanisms have been suggested to be active in formation of this type of melange, some of which are summarised in Table 7.3 below. Apart from local sedimentary origins for the melange, evidence for different processes, other than tectonic interleaving, is obscured by a pervasive tectonic overprint.

Mechanism	Reference
Imbricate thrusting within accretionary complex	Hsü (1973)
Subduction-driven flow of unlithified sediments beneath accretionary complex	Cloos (1982)
Mud diapirism/fluid expulsion	Rau (1973), Pudsey & Reading (1982), Robertson *et al*. (1995)

Table 7.3 Some mechanisms for melange formation in the literature

In summary, the Ophiolitic Melange is inferred to have developed mainly by accretionary proccesses at a destructive plate margin, similar to modern-day settings such as the Nankai Trough (Fig. 7.6). The accretionary prism included relatively near-margin units that were incorporated during initial Maastrichtian tectonic emplacement over the continental margin (i.e. Triassic rift-related neritic limeston and pre-rift Permian *Fusulinid* limestone in the Beysehir area); also, accreted Neotethyan oceanic crust (MORB and seamounts) and oceanic sediments. No melange lithologies younger than Late Cretaceous (Maastrichtian) are known in the melange in the central and eastern areas (Bozkir-Ermenek), suggesting the accretion had ended by this time.

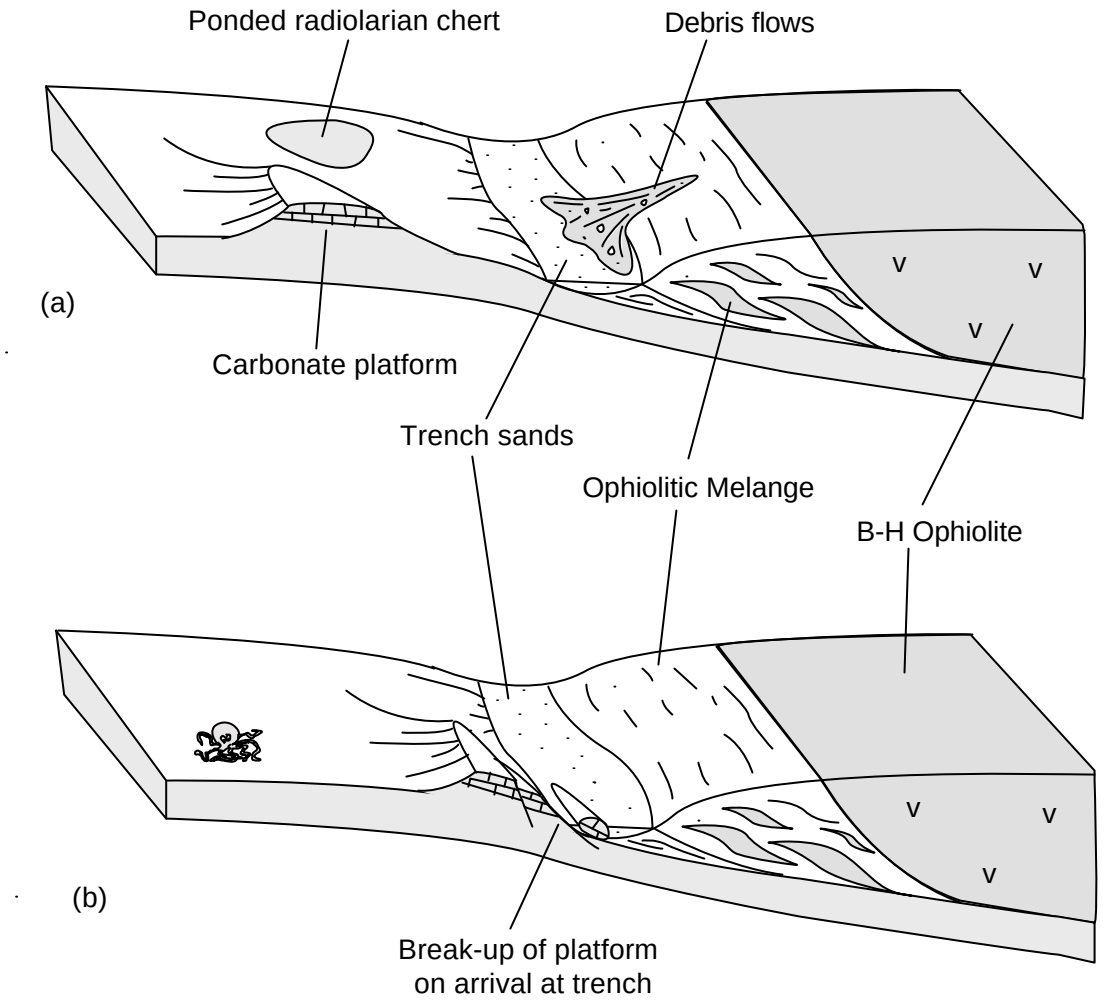

Fig. 7.6 Cartoon interpretation of the ophiolitic melange, broken formation and matrix forming in a subduction/accretion system. Diagram not to scale.

7.2.10 Late Cretaceous accretion: broken formation

Each of the allochthonous units of the B-H Nappes form coherent sequences within thrust sheets. Individual thrust sheets are commonly dismembered to form broken formation, with ophiolitic melange and/or sandy turbidites present as matrix material. Frequently, this matrix material separates individual thrust sheets. A number of questions need to be addressed concerning the timing of disruption, the significance of the different matrix material and formation processes. Firstly, a minimum age for the timing of dismemberment is given by the ages of the units themselves. In the upper thrust sheets (Huglu-type and Boyali Tepe-type) sedimentation was terminated abruptly in Late Cretaceous (Maastrichtian) time. Furthermore, the style of sedimentation changed considerably in the Boyali Tepe-type unit, from pelagic conditions to clastic ophiolite-derived debris flows, in the latest Cretaceous. Where the units are dismembered and enclosed in Ophiolitic Melange, the matrix has been dated as Maastrichtian (Özgül, 1997). All this evidence strongly suggests that the units were

incorporated into an accretionary prism (represented by the Ophiolitic Melange) in late Cretaceous time. The lowermost thrust sheets above the melange in the Beysehir and Ermenek area are enclosed in sandy turbidites (wildflysch), limestone conglomerates and ophiolite-derived debris flow deposits (Section 2.5.2/ 2.6.1and Section 5.2.2.1/ 5.3.1). This matrix is entirely sedimentary in origin and it is inappropriate to conclude that it is the same as the Ophiolitic Melange, which has a predominantly tectonic origin. It is clear that this matrix was derived from an ophiolitic source and that it is spatially associated with the melange; therefore, the preferred interpretation is that these clastic sediments represent trench turbidites and debris flow deposits (as shown in Figure 7.2), that are locally sourced from the allochthonous units (Section 2.5.2 & 5.3.1). As the marginal Beysehir-Hoyran units collided with the trench they proceeded to break up and were incorporated wholesale into the accretionary complex. As no basement for the B-H Nappes are preserved it is inferred that only the uppermost levels of the marginal units were accreted. The arrival of an oceanic seamount at a trench has already been shown to involve break up; for example, the Daisha seamount in the Japan trench (Taira et al., 1989). At least one seamount in the Mariana and Izu-Bonin trench area exhibits fracture zones which trend parallel to the trench axis (Fryer & Smoot, 1985). This kind of process, relating to extreme layer-parallel extension during accretion and high pore pressures, commonly associated with accretionary complexes, can account for the fractured fabrics of the Boyali Tepe-type broken formation. As the units broke up it is probable that injection of trench sediment and fluids along these fracture planes could occur, allowing the blocks to 'float' in a matrix of trench-type material (Fig. 7.6b). The pervasive nature of the sandstones as a matrix between blocks and dismembered slices (broken formation) is good evidence for this kind of trench environment (e.g. Figs. 2.18, 4.15, 5.16). This initial accretion process can produce tectonic folding within the accretionary complex which can induce stratigraphic inversion and folding of the accreted slabs, which has been documented in the Diasha seamount in the Japan trench (Taira *et al*., 1985). A similar kind of process could be responsible for the widespread overturning of the Boyali Tepe-type unit seen in most areas.

7.2.11 Late Cretaceous (Maastrichtian) obduction

Accretion along the leading edge of the upper plate of the subduction zone terminated abruptly in Maastrichtian time as indicated by the age of incorporated lithologies and the matrix (Section 7.2.8; Özgül, 1997; Monod, 1977); this coincides with the timing of regional ophiolite obduction in the western and central Taurus Mountains (e.g. Pozanti-Karsanti ophiolite, Polat & Casey, 1995; Lycian Nappes, Collins, 1997). It is likely that ophiolite obduction in the Beysehir-Hoyran region occurred contemporaneously. Direct evidence for the timing of ophiolite emplacement is the Maastrichtian age of the Zekeriya Formation at the top of the Hadim Nappe in the Bozkir-Hadim area, upon which the ophiolite was originally obducted (Özgül, 1997; Section 4.5.2).

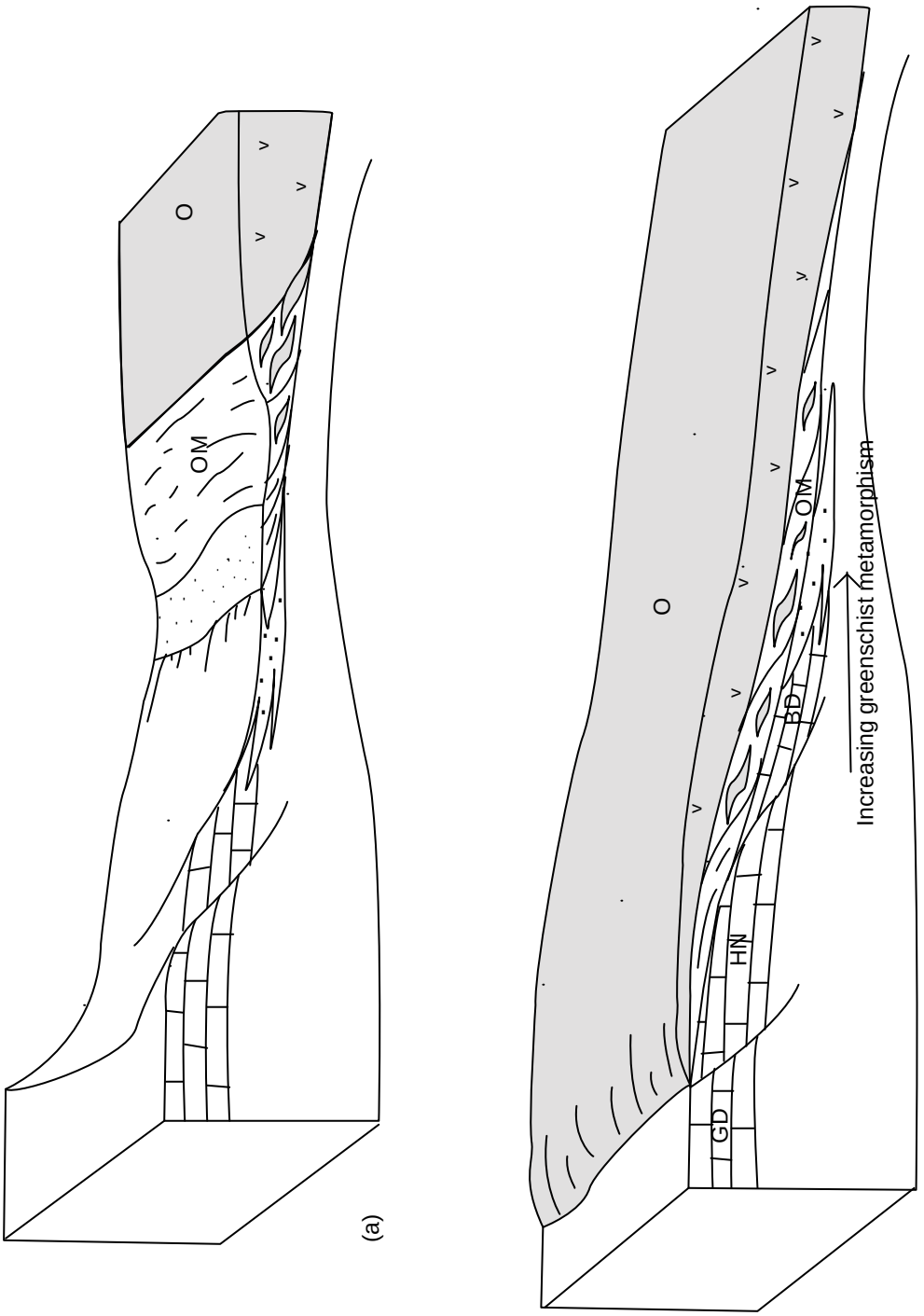

Fig. 7.7 Cartoon diagrams showing **(a)** initial trench-passive margin collision and **(b)** Latest Cretaceous ophiolite (O) obduction over an inferred accretionary complex and B-H units (OM) onto the Bolkar Dag (BD) and Hadim Nappe (HN). The Geyik Dag unit (GD) is inferred to have escaped initial Upper Cretaceous ophiolite obduction. It is worth noting that regional greenschist metamorphism could be related to burial during obduction. Not to scale.

Continued convergence probably led to collision of an intra-oceanic trench with the Tauride passive margin (Fig. 7.7a), ultimately resulting in ophiolite obduction as widely accepted for other Tethyan ophiolites, as shown in Fig. 7.7b (e.g. Oman, the Muti Formation, Robertson, 1997; Himalyas, Robertson & Degnan, 1993; Pozanti-Karsanti ophiolite, Polat & Casey, 1995; Lycian Nappes, Collins, 1997). As the ophiolite was obducted in latest Cretaceous time over the accretionary complex onto the margin, ophiolitic melange and broken formation was also emplaced, e.g. the Ak Tepe section in the Karaman area; Section 5.4.1). The highly disrupted Bolkar Dag sequence ends in the Upper Cretaceous, suggesting the B-H Nappes (as melange and broken formation) were emplaced during this time. If emplacement was later, then slices of younger lithologies would be expected to be present (e.g. Dipsiz Göl; section 4.6.1). This is not the case in most other areas.

7.2.12 Early Tertiary collision

The Late Cretaceous to Early Tertiary autochthonous sequence, particularly of the Pisidian Taurides, records the final emplacement of the B-H Nappes exceptionally well. The thick Jurassic–Cretaceous neritic succession is overlain in all areas by Late Cretaceous – Palaeocene pelagic sediments recording deepening conditions (e.g. Tasevi and Yukarititar Formations; Logs 11-15 in Fig.7.2). This switch to pelagic carbonate and deepening was tectonically controlled. Pelagic facies are interbedded with redeposited carbonate lithologies (granular sand-grade limestone, limestone conglomerates and debris flows; Dinar and Kumdanli areas), suggesting a slope setting. The clasts are exclusively composed of carbonate, implying a lack of siliciclastic material in the source area, which was most likely the Tauride carbonate platform itself. There is substantial evidence for slope instability during Palaeocene to Mid-Eocene time. Soft-sediment slumping is present in the Palaeocene of the Kumdanli and Dinar sections (Sections 3.2.1.2 and 3.3.1.5). When the poles to the hinge plane of these soft-sedimentary slumps were plotted on a stereographic projection (Fig. 3.5) a northeast – southeast trend is apparent, which is probably the consequence of original slope orientation. Regional palaeomagnetic data suggest the western area (at least) has undergone post-Eocene 40^{o} clockwise rotation as part of the eastern limb of the Isparta Angle (Kissel *et al.,* 1993; Tatar *et al.,* 2000). Taking this into account a more northerly slope direction is implied.

Further evidence of slope instability is present in the Yukarititar section near Lake Hoyran (Fig. 3.3; Log. 14 in Fig. 7.2). Upper Cretaceous pelagic limestone blocks, up to 10m in size, are present in Palaeocene redeposited carbonate facies. These blocks are interpreted as slide blocks and debris flows and not as tectonic melange because the block lithologies were probably sourced from the underlying Upper Cretaceous sequence rather than being exotic. Also, they are set in a redeposited sand-grade carbonate matrix and form part of a normal, undisturbed stratigraphic sequence.

The overlying Mid-Eocene siliciclastic sequence was deposited by turbidity currents, as shown by erosional bases, normal grading, planar lamination and sole marks. Petrographically, they consist

predominantly of carbonate, red chert and volcanic grains, which suggests they were not derived from the Tauride autochthon but have an exotic source. The most likely source area is from the B-H Nappes themselves. Where it is possible to obtain good palaeocurrent data, e.g. cross bedding from the Çeleptas Formation in the Hoyran area; Section 3.2.1.2, the data are consistent with a northeasterly source, after regional post-Eocene rotations have been considered (Fig. 3.6).

In the Kumdanli (Hoyran) sections (Logs 13-14 in Fig. 7.2; also Section 3.2.1.2) slumped horizons within the turbiditic sequence provide yet more evidence for slope instability. The uppermost part of the siliciclastic sequence contains large blocks of Late Cretaceous pelagic limestone and other blocks probably sourced from the autochthon, e.g. Dinar and Hoyran area; Section 3.2.1.2. As these blocks are not of exotic lithologies and are contained in a sandy matrix they are interpreted as debris flows and slide blocks (olistoliths) derived from the autochthon. In the Beysehir area (specifically near Üzümlü and Derebucak), this upper rudaceous member is highly sheared, yet consists of smaller dm to m-sized clasts. Lithologies consist of altered volcanics, radiolarian chert and limestone, and are thus likely to be sourced from the B-H Nappes and not the autochthon (Section 2.3.2.3). However, this is exceptional.

Previous studies have interpreted the clastic Palaeocene to Mid-Eocene sucession as a 'flysch' sequence developed in a foredeep ahead of an advancing nappe stack (Özgül, 1976; Monod, 1977; Gutnic, 1977; Gutnic *et al*., 1979). This assumption primarily dates the final emplacement of the B-H Nappes as Lutetian. This study concurs with the previous work about the timing of events, but provides more information of the depositional/tectonic processes involved.

In summary, during Palaeocene time the Tauride platform began to subside, probably related to the initial effects of collision, with maximum subsidence in Late Eocene time when the Tauride autochthonous platform collapsed as a flexural foredeep ahead of the emplacement of the Beysehir-Hoyran-Hadim Nappes. Material was shed northwards into this foredeep from the autochthon, as carbonate debris flows and block gravity slides, and generally southwards from the advancing nappes as rudaceous debris flows and turbidity currents.

<table>
<tr><th colspan="2">Age</th><th>Korualan</th><th>Huglu-type</th><th>Boyali Tepe-type</th></tr>
<tr><td rowspan="5">Cretaceous</td><td rowspan="2">Upper</td><td rowspan="9"></td><td rowspan="3">Pelagic marine conditions</td><td>Initial platform break up</td></tr>
<tr><td>Deep sea ooze</td></tr>
<tr><td rowspan="2">Lower</td><td rowspan="2">Pelagic marine conditions</td></tr>
<tr><td rowspan="4">Jurassic</td><td>Upper</td><td>Accumulation of deep-sea radiolarian ooze (below CCD?)</td><td rowspan="2">Accumulation of deep-sea radiolarian ooze (below CCD?)</td></tr>
<tr><td>Mid</td><td rowspan="3">Beginning of post-rift subsidence</td><td>Initial subsidence of carbonate platform</td></tr>
<tr><td>Lower</td><td rowspan="2">Carbonate platform conditions</td></tr>
<tr><td rowspan="4">Triassic</td><td rowspan="2">Upper</td><td>Deep-sea</td></tr>
<tr><td>Base of slope conditions</td><td rowspan="3">Initial rifting and volcanic build-up</td></tr>
<tr><td rowspan="2">Mid</td><td>Slope</td><td rowspan="3">Basement?</td></tr>
<tr><td>Platform conditions?</td></tr>
<tr><td>Lower</td><td>?</td><td></td></tr>
</table>

Table 7.4 Summary table of the main tectonic and sedimentary processes occurring in the Beysehir-Hoyran area of the Pisidian and central Taurides during the Mesozoic.

Chapter 8

8. PALAEOTECTONIC RECONSTRUCTIONS

The main aim of this thesis was to investigate the evolution of the Beysehir-Hoyran Nappes in a regional tectonic context. Using the revised tectonostratigraphic framework and tectonic facies interpretations detailed in the preceding chapters, four possible palinspastic and palaeotectonic reconstructions are presented and described here. The advantages and disadvantages of each scenario are considered and a favoured model is proposed. In order for any reconstructions to be accurate, an appreciation of the structural history is first required. Thus, an assessment of the main deformation phases and the tectonic displacement during the emplacement of the thrust sheets is presented below.

8.1 Deformation phases

Evidence for three main stages of deformation are recorded in the B-H Nappes, as follows;

1) **Late Cretaceous** initial compression was associated with ophiolite emplacement. The ophiolite was dismembered and emplaced above an inferred accretionary prism, represented by the Ophiolitic Melange, in Maastrichtian time. The structurally higher volcanogenic and neritic units were also initially detatched from the basement and accreted in latest Cretaceous time. The oceanic crust was probably emplaced directly onto the submerged Hadim, Bolkar and Sandikli platform units, whilst the Geyik Dag platform was still well to the south and escaped this emplacement.

2) **Early Tertiary** emplacement was marked by collapse, beginning in the Palaeocene, of the Taurus Autochthon (Geyik Dag) as a foredeep, later accumulating Lower-Middle Eocene siliciclastic turbidites and then debris flows, before finally being overthrust by the Hadim Nappe (where present) and higher units. The Geyik Dag autochthon is internally imbricated with 'corridors' of Middle Eocene siliciclastic turbidites underlying individual thrust imbricates (Özgül 1976, Monod 1977). The provenance of the siliciclastic sediment was probably from the basement of the overriding Hadim Nappe. Where the Hadim Nappe is absent in the west (Dinar area) the foredeep at the top of the Sandikli autochthonous carbonate platform succession contains large Eocene foraminifera (*Nummulites*), siliciclastic turbidites, debris flows and slumps.

3) **Neotectonic** deformation in the Taurides regionally began in the Miocene (e.g. the Aksehir-Afyon Graben, Koçyigit *et al.*, 2000; Büyük Menderes Graben, Yilmaz *et al.*,2000; Bozkurt, 2000). In most outcrop areas of the B-H Nappes, the late Mesozoic and Early Tertiary fabric is cut by localised extensional systems; as yet this period of neotectonic extensional faulting remains undated. Previous authors have not distinguished between neotectonic and palaeotectonic fabrics (e.g. an inferred sedimentary origin for tectonic breccias in the Dinar area; Gutnic, 1977). Although locally significant,

the neotectonic extensional faulting does not obscure the Early Tertiary emplacement fabric but actually helps to increase the exposure. In general, the neotectonic grain is parallel to the Early Tertiary compressional fabric and is partly responsible for large-scale geomorphological features, e.g. Lakes Hoyran and Beysehir (Sections 3.2.2.1, 3.3, 4.6.1). In the Dinar area, the outcrop of the B-H Nappes is terminated by an extensional fault array, which forms the eastern bounding fault of a NW-SE trending half-graben system along strike from the Büyük Menderes and Gediz Grabens further west. Displacement is inferred to be large and relatively young as individual exposed fault scarps are in the order of 100m and are associated with thick talus cones shed from the uplifted footwall. The area between Ermenek and Karaman is also cut by a large E-W trending graben with similar displacements on the bounding faults. The neotectonic extensional activity is outwith the scope of this thesis and merits a project in its own right.

8.1.1 Kinematic evidence for emplacement direction

An azimuth for the direction of emplacement can be obtained using kinematic indicators. Phases of deformation sequentially overprint previous fabrics, so great care needed to be taken during data collection in the field; areas clearly subjected to neotectonic activity were discounted. Extreme layer-parallel extension is inferred to have occurred, as the thrust sheets are commonly vertically stacked and sub- parallel to each other. This deformation has produced a shear fabric that is commonly also sub-horizontal, and thus hard to quantify an accurate azimuth. With this in mind, data were collected from several areas and are summarised in Fig. 8.1.

8.1.2 Discussion of kinematic shear sense

Kinematic data from shear zones developed at the base of the B-H Nappes and between the thrust sheets were measured to infer the direction of emplacement. The base of the thrust sheets is well exposed southwest of the Beysehir area. A roadside cutting north of Derebucak (Section 2.3.2.3) reveals a shear zone, ca. 30m thick, developed in Mid-Eocene coarse, heterogenous debris flow deposits derived from the overriding thrust sheets. Brittle-shear fabrics (e.g. thrust-horse geometry, slickenside fabrics) indicate a top-to-the-SW sense of movement. (Figs. 8.1i/j and 8.2). Poles to the shear fabrics and slickenline data, when plotted on stereographic projections, indicate vergence to the SW with some scatter (Fig. 8.2). In addition, C-S fabrics developed in similar Mid-Eocene debris flows near the village of Üzümlü (Section 2.3.2.3) indicate a dominant E-W component of shear (Fig. 8.1c). Metre-decimetre scale folds in this locality are commonly northwest facing and verging to the southeast (Fig. 8.1b), although owing to the small sample population the data must be treated with a degree of caution. Well-bedded lithologies within the thrust sheets are commonly tightly folded, as seen in pelagic limestone of the Huglu-type unit which crops out on the south shore of Lake Beysehir. Data collected here shows that fold axial surfaces predominantly verge to the west, with a small

scatter to the south (Fig. 8.1a). Similarly, tightly folded ribbon radiolarian chert in the Huglu-type unit 2km south of Ihsaniye village (Ermenek area) exhibit fold vergences predominantly to the southeast-southwest (Fig. 8.1d). Furthermore, slickenline lineations developed in subjacent interbedded tuff and lava indicate locally the transport direction was probably NE-SW (Fig. 8.1e). In the Hadim area, C-S shear fabrics (Fig. 8.1f), fold vergences (Fig. 8.1g) and slickenline lineations (Fig. 8.1h) collected from a sequence of moderately sheared, well-bedded tuffs in the Huglu-type unit (Section 4.6.3; Fig. 4.11) show the transport direction was south-southeasterly directed.

Collectively these data sets are consistent with an overall tectonic transport generally to the southwest, locally to the south. It is worth noting that in general, the shear fabric data set from each area is bimodal reflecting the regional sub-horizontal fabric. Regional palaeomagnetic data suggest the western area (at least) has undergone post-Eocene 40^{o} clockwise rotation as part of the eastern limb of the Isparta Angle (Kissel *et al.* 1993, Tatar *et al* 2000). Taking this into account an overall southerly transport direction for the Beysehir-Hoyran Nappes is implied.

An interesting question would be to address whether the emplacement direction during initial Upper Cretaceous deformation was the same as the final Mid-Eocene event; however, the data presented here cannot distinguish between these two events. The lack of a clear temporal or spatial limit between deformation associated with latest Maastrichtian-Palaeocene obduction and Palaeocene-Early Miocene continent-continent collision in western Anatolia has been commented on by previous workers (Okay, *et al.,* 2001), which makes it hard to provide a detailed kinematic history as has been carried out in other Tethyan areas (e.g. the Mamonia Complex Suture Zone; Bailey *et al.,* 2000).

8.1.3 Estimates of orogenic shortening/ displacement

A minumum displacement can be determined from knowledge of the regional stratigraphy. If the B-H-H Nappes were derived from the north, as inferred from available kinematic and stratigraphic data, then the minimum displacement can be calculated as the distance from the northern edge of the existing autochthonous Tauride platform to the present outcrop, ca. 100km in the Pisidian Taurides, to over 200km in the eastern areas (Fig. 1.2).

The most accurate method of obtaining an estimate of the degree of orogenic shortening is to use balanced cross sections that conserve the volume between deformed and undeformed states (Dahlstrom, 1969; Hossack. 1979; Elliott and Johnson, 1980). In compressional regimes, two principle types of palinspastic restorations are used; line balancing and area balancing. Line balancing involves the construction of deformed and undeformed sections with marker horizons (pins) common to the two sections. The separation between the pins approximates to the displacement along the thrust plane. In grossly allochthonous units, as is the case with the B-H Nappes, there are seldom suitable marker horizons available. The second technique, area balancing, requires the depth to detachment in the thrust stack to be known; thus, the area of an undeformed portion of the thrust sheet can be determined. In the case of the B-H Nappes, where the frontal and the back regions of the nappes are not preserved and layer-parallel extension is extreme, it is considered inappropriate that balanced sections should be attempted to quantify the amount of shortening involved.

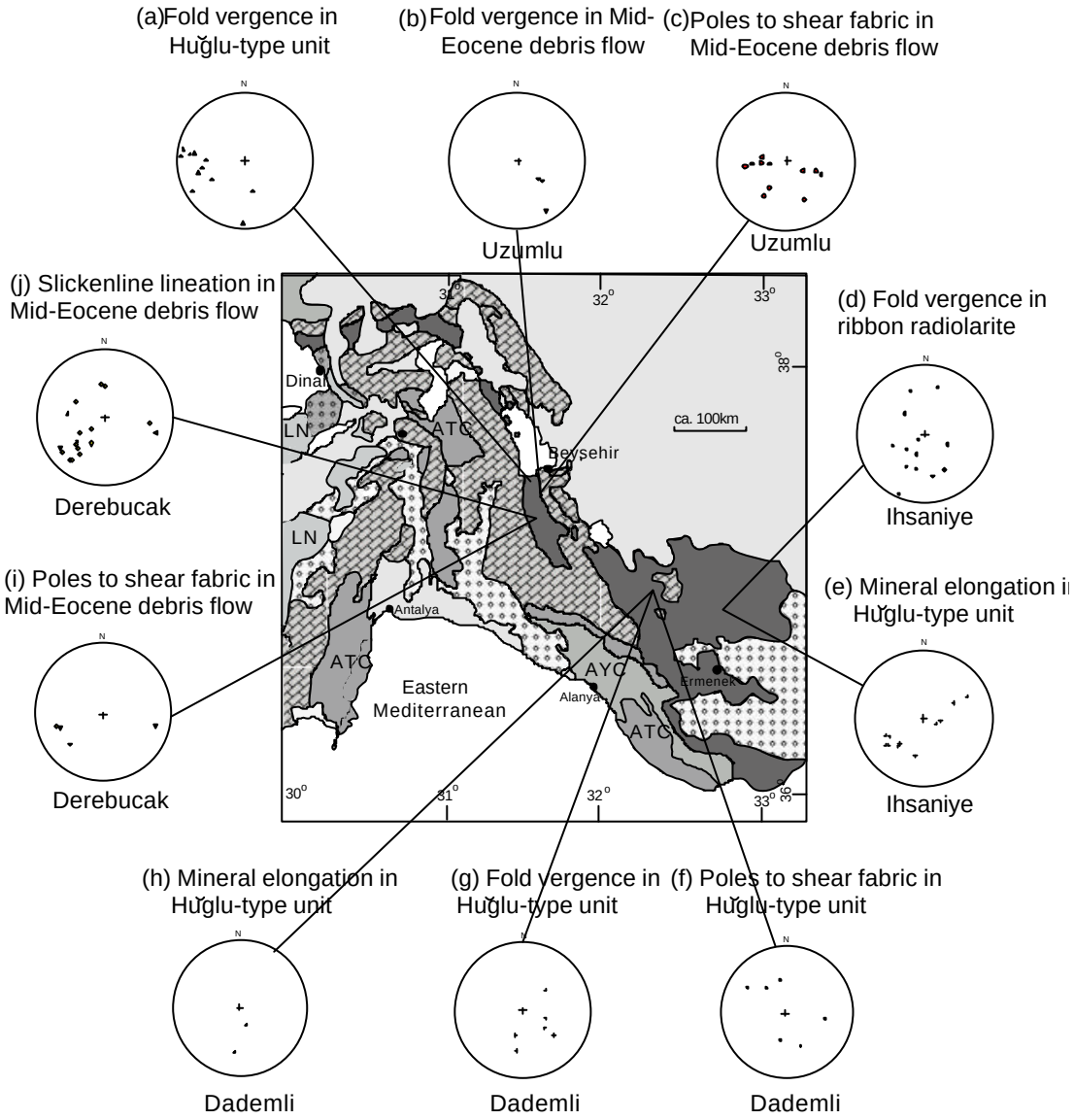

Fig. 8.1 Kinematic data plotted by area on equal area lower hemisphere stereographic projections. Data plotted are present day azimuth values, uncorrected for post-Eocene rotation. ATC, Antalya complex; AYC, Alanya complex; LN, Lycian Nappes.

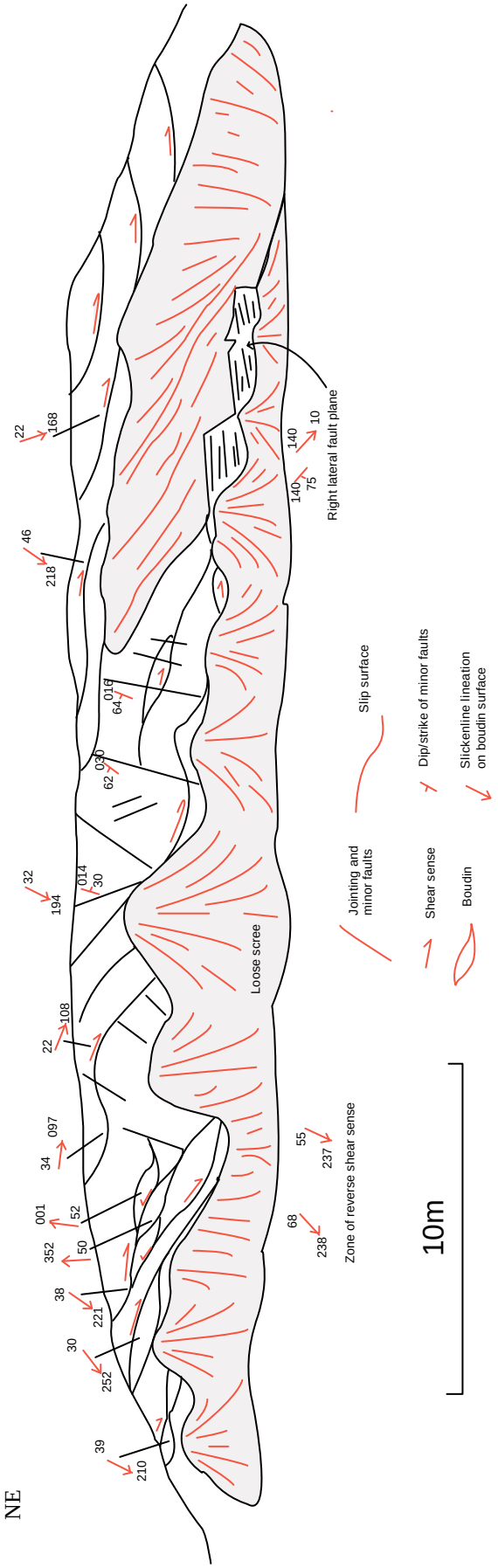

Fig. 8.2 An interpreted field sketch of roadside cutting, ca. 1km north of Derebucak. A shear zone, ca. 30m thick, has developed in Mid-Eocene coarse, heterogenous debris flow deposits derived from the overriding thrust sheets. Brittle-shear fabrics (e.g. thrust-horse geometry, slickenside fabrics) indicate a top-to-the-SW sense of movement.

8.2 Paleotectonic reconstructions

Several attempts have been made to provide an overall synthesis for the Eastern Mediterranean region, but there is no general consensus, as discussed in Chapter 1 (e.g. Sengör & Yilmaz, 1981; Sengör *et al.*, 1984; Robertson & Dixon, 1984; Stampfli *et al*., 1991; Dercourt *et al*., 1992; Ricou *et al*, 1984; Okay *et al*. 1984; Stampfli, 2000). This study bases the palaeogeographical reconstructions on widely accepted previous work, in particular the idea of a northerly/southerly Neotethys and northwards subduction (Robertson & Dixon, 1984; Sengör *et al.*, 1984; Dercourt et al. 1992; Stampfli, 2000; Robertson, 2000).

Conventionally, many emplaced margins in the Tethyan region, have been restored assuming downward foreland thrust propagation of allochthonous units (in-sequence thrusting), with higher thrust sheets restoring progressively towards the hinterland, e.g. Othris, Greece; Smith *et al*., l979, Pindos, Greece; Fleury, l980, Degnan & Robertson, l998, Antalya, SW Turkey; Robertson, l993. Previous work has rarely considered alternative thrust propagation scenarios. However, out-of-sequence thrusting (or re-thrusting) has been shown to play an important role in some emplaced continental margins (e.g. Oman, Searle *et al.*, 1990).

Taking into account the direction of thrust emplacement, the Beysehir-Hoyran-Hadim Nappes can potentially be restored to several alternative positions within a northerly Neotethyan ocean basin. Critically, how the nappe stack is restored depends upon whether either in-sequence (Fig.8.3), or out-of-sequence thrusting (Fig. 8.4) is assumed. The following section introduces the two end members and discusses the implications for the B-H Nappes before suggesting a preferred emplacement model.

Finally, the regional palaeogeography is discussed with respect to other Tauride units and alternative models are considered and tested in light of data presented in this thesis, e.g. the Beysehir-Hoyran allochthon as a strike-slip terrane and a southwards subduction polarity model.

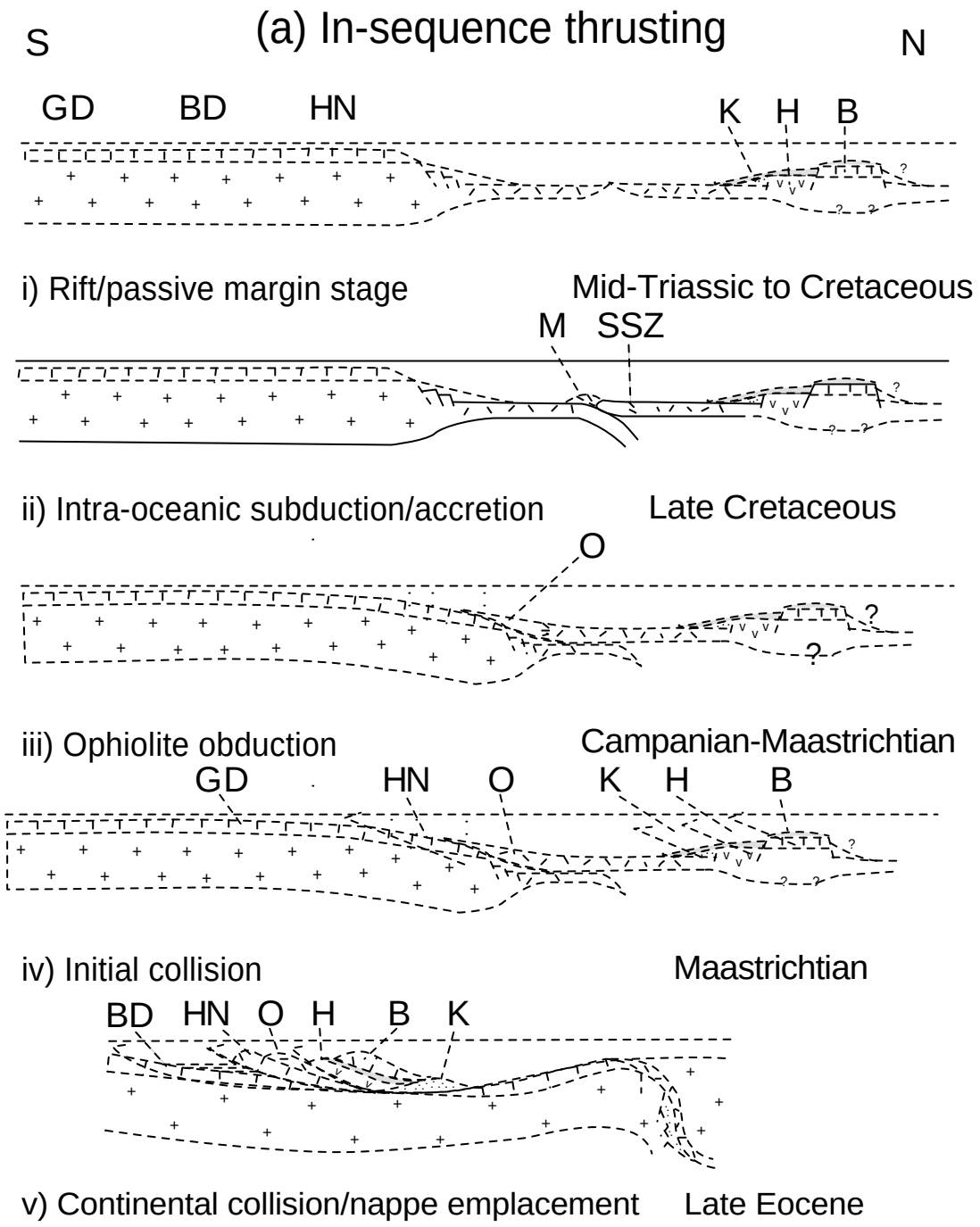

Fig. 8.3 Reconstructed tectonic setting assuming in-sequence thrusting. Rifts separated the southern Tauride carbonate platform and off-margin fragment. After SSZ ophiolite genesis, the ophiolite and off-margin units were emplaced onto the continental margin in Maastrichtian time. During Late Eocene suturing and tightening the former platform margin was detatched and thrust southwards, carrying the previously assembled thrust stack passively above. BD, Bolkar Dag Unit, GD; Geyik Dag Unit; HN, Hadim Nappe; O, Ophiolite; SSZ Supra-subduction zone spreading; M, Ophiolitic Melange; K, Korualan Unit; H, Huglu-type Unit; B, Boyali Tepe-type Unit.

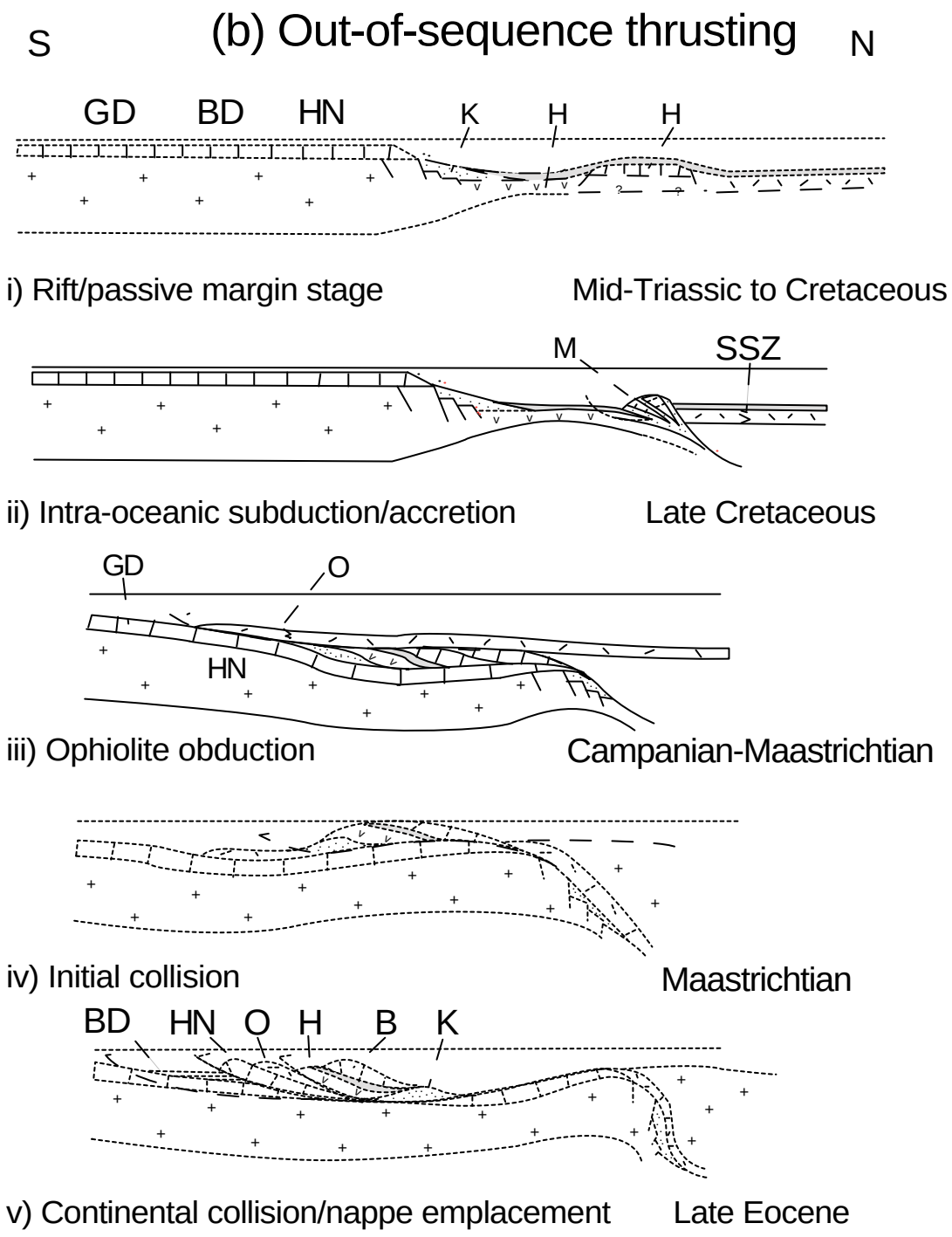

Fig. 8.4 Reconstructed tectonic setting assuming out-of-sequence thrusting. As Fig. 8.2, but the spreading centre developed northwards of the rifted carbonate platform. SSZ ophiolite genesis was followed by accretion of platformal-basinal units beneath the overiding ophiolite, which was later emplaced over the carbonate platform (Geyik Dag). During collision the accreted units were rethrust above the ophiolite. Rethrusting in Late Eocene time occurred as in Fig. 8.2. BD, Bolkar Dag Unit, GD; Geyik Dag Unit; HN, Hadim Nappe; O, Ophiolite; SSZ Supra-subduction zone spreading; M, Ophiolitic Melange; K, Korualan Unit; H, Huglu-type Unit; B, Boyali Tepe-type Unit.

8.2.1 Reconstructed tectonic setting assuming in-sequence thrusting (Fig. 8.3)

By restoring successive higher units in the nappe stack progressively further north in the Neotethyan ocean, the situation shown in Figure 8.3 can be envisaged. The upper B-H units restore as an off-margin continental fragment separated from the southern Tauride carbonate platform by an oceanic basin and spreading ridge. The off-margin fragment consisted of platform (Boyali Tepe-type), basin (Huglu-type) and slope (Korualan) units. The basement of this fragment is unknown. The Hadim Nappe and Bolkar Dag Unit would restore as the northerly extension of the Tauride carbonate platform (Geyik Dag Unit). Late Cretaceous intra-oceanic convergence gave rise to northwards subduction of the oceanic crust, consistent with regional evidence, followed by genesis of a SSZ-type ophiolite. Ophiolitic Melange formed in an accretionary complex developed along the leading edge of the upper plate of this subduction zone. Convergence continued until the trench collided with the passive margin, leading to ophiolite obduction onto the continental margin in Maastrichtian time. The former platform margin was detatched and thrust southwards as the Hadim Nappe during Late Eocene suturing and tightening carrying the previously assembled thrust stack passively above.

8.2.2 Reconstructed tectonic setting assuming out-of-sequence thrusting (Fig. 8.4)

An alternative to the in-sequence model would be for the B-H Nappes to restore as marginal units of the Tauride microcontinent, with the Neotethyan spreading axis located an unknown distance to the north. Initial rifting of the Tauride platform would give rise to the basinal and slope units of the Huglu-type and Korualan units in Mid-Triassic time, and also the more outboard carbonate platform Boyali Tepe-type Unit. Intra-oceanic convergence and SSZ ophiolite genesis in Late Cretaceous time was followed by accretion of platformal-basinal units beneath the overiding ophiolite, which was later emplaced over the carbonate platform (Geyik Dag) in Maastrichtian time as in the previous model. A period of erosion is inferred during the Palaeocene to remove the upper levels of the ophiolite, as little or no crustal rocks are associated with the ophiolite itself. No trace of a cover sequence is preserved as is the case in the Lycian Nappes further west (Collins, 1997).

During collision the accreted units were rethrust above the ophiolite; otherwise, rethrusting in Late Eocene time occurred as in the in-sequence thrusting scenario, with the Tauride margin being imbricated as the Hadim Nappe and being thrust to the south with the assembled Beysehir-Hoyran units carried passively above.

8.2.3 In-sequence versus out-of-sequence thrusting

The question of in-sequence versus out-of-sequence thrusting could also be considered in terms of whether the B-H Nappes restore north or south of the inferred Neotethyan spreading axis, e.g. as a separate micro-continent within the Northern Neotethyan ocean or as marginal units of the Tauride platform. The main advantage of the in-sequence model is that it is the most simple option. However, a number of problems exist which cannot easily be explained by this model:

1) No Tauride slope/margin units are preserved, as expected in this kind of in-sequence thrust system. The slope-like Korualan unit has to restore as a more distal off-margin unit.
2) This model also does not explain the presence of Ophiolitic Melange in the highest levels of the thrust sheets. To account for this using in-sequence thrusting terms a second subduction/accretion complex would be required to the north of the B-H units.
3) The in-sequence model would restore the B-H units far to the north of the Tauride margin. The conjugate of this margin is in the Pontides (Ustaömer & Robertson 1997, Yilmaz *et al.* 1997). The main problem is that the Pontide and Anatolide/Tauride margin evolution are dissimilar, e.g. with the major latest Triassic "Cimmerian" orogenic event being restricted to the Pontide margin, whereas Triassic rifting and Jurassic passive margin subsidence continued on the Anatolide/Tauride margin without a comparable major orogenic event (Robertson & Pickett 2000). The B-H Nappes show no evidence for a latest Cimmerian orogenic event, thus are unlikely to be derived from anywhere near the Pontide margin.

Despite the above problems, the in-sequence hypothesis cannot be completely dismissed as insufficient data exist to completely disprove this model. However, the out-of-sequence template fits all the available data and is the preferred model based on this study.

Additional complexities are introduced if the B-H Nappes are considered in a regional context. Figure 8.5 presents possible palaeogeographic variations for a single northerly Neotethys (Göncüoglu et al., l996-l997) and those for a separate Inner Tauride Ocean are shown in Figure 8.7 (Oktay, 1973; Görür *et al*., 1984).

8.2.4 Regional palaeogeographical models

When considering the regional palaeogeography of the northern Neotethys two main schools of thought exist. The palaeogeographical interpretations presented here include the position of the B-H Nappes within a single northerly Neotethys (Göncüoglu *et al*., l996-l997), and also considers the case of a separate Inner Tauride Ocean (Oktay, 1973; Görür *et al*., 1984). In each case the potential location of the nappes is presented for the in-sequence and out-of-sequence scenarios. Each of the palaeogeographic reconstructions are not to scale.

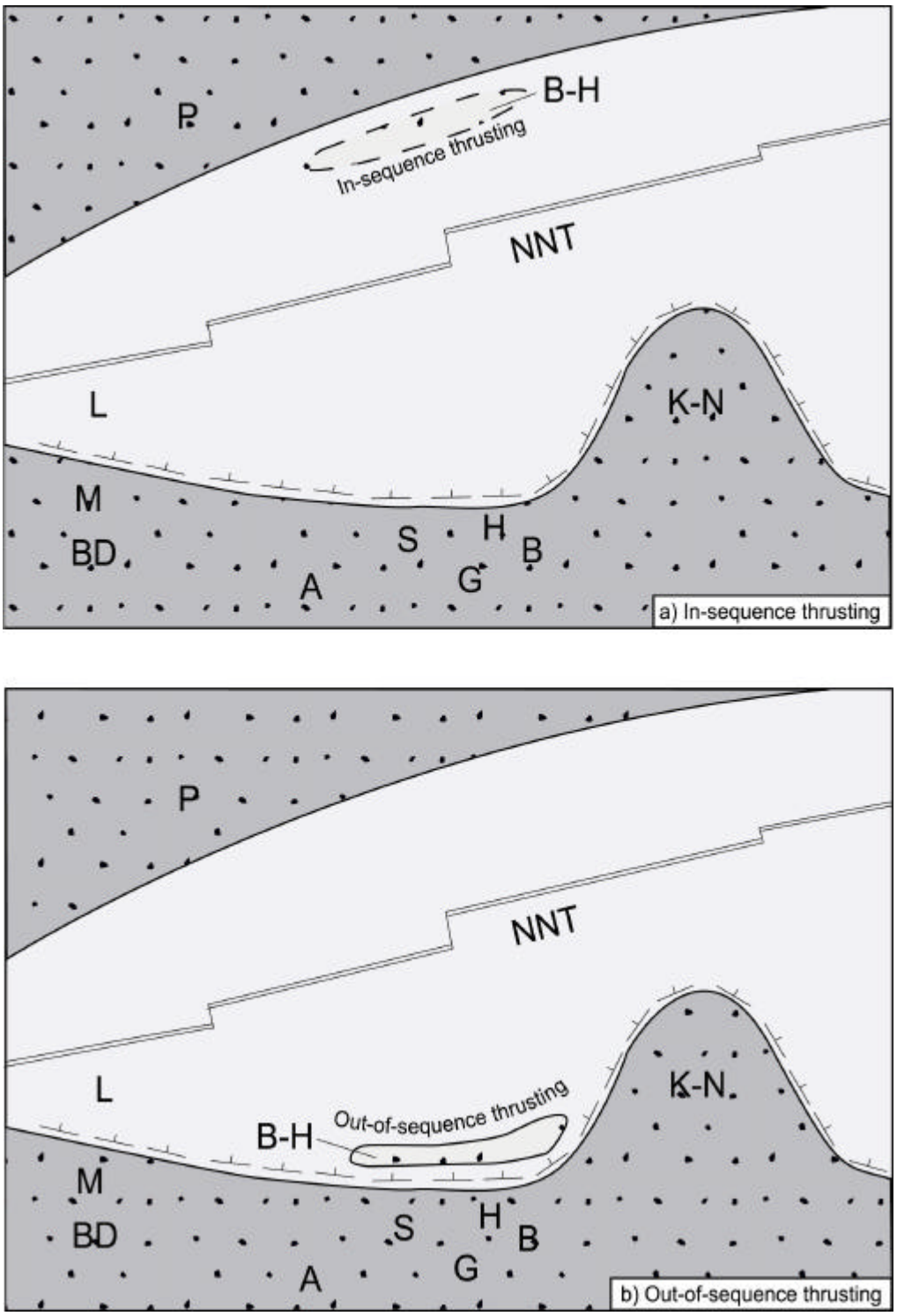

Fig. 8.5 Palaeogeographical sketch maps of the Northern Neotethys during Mid-Jurassic time. Single Northern Neotethys with promentories. **(a)** north and **(b)** south alternative settings of the B-H Nappes according to to in-sequence or out-of-sequence thrusting. A, Antalya Unit; B, Bolkar Dag; BD, Bey Daglari Unit; B-H, Beysehir-Hoyran Nappes; G, Geyik Dag Unit; H, Hadim Nappe; ITO, Inner Tauride Ocean; K-N, Kirsehir-Nigde Massif; L, Lycian Nappes; M, Menderes Massif; NNT, Northerly Neotethys spreading axis; P, Pontides; S, Sakarya Unit.

8.2.5 Single northern Neotethys

In Figure 8.5 (a) and (b) the Bey Daglari, Geyik Dag, Sandikli Unit, Bolkar Dag and Hadim Nappe formed an E-W trending southerly continental margin. The Kirsehir-Nigde massif formed a promontory of this continental margin (Göncüoglu et al., l996-l997), with the conjugate in the Pontides (Ustaömer & Robertson 1997, Yilmaz *et al.* 1997). Assuming, the out-of-sequence thrusting model the B-H Nappes would restore to a rifted continental fragment bordering the Anatolide-Tauride platform (Fig. 8.5b), or the Pontide margin if in-sequence thrusting is inferred (Fig. 8.5a).

8.2.6 The Inner Tauride Ocean (Fig. 8.6)

The previous model infers that the Kirsehir-Nigde massif (or Central Anatolian Crystalline Complex) was attatched to the Tauride margin throughout the Mesozoic. Evidence from the Tüzgölü area (Fig. 1.2) located presently between the Kirsehir-Nigde massif and the Tauride platform suggests a narrow oceanic basin once separated both continental blocks (Görür *et al.,* 1984). The proposal that Neotethys incorporated more than one ocean basin is not accepted by the entire geological community. Ricou *et al*. (1979; 1984) proposed a single ocean basin origin for all of the Neotethyan units in Turkey. However, over the last decade most workers have come to prefer a multiple ocean basin hypothesis (Dercourt *et al*. 2002; Stampfli 2000; Robertson 2000).

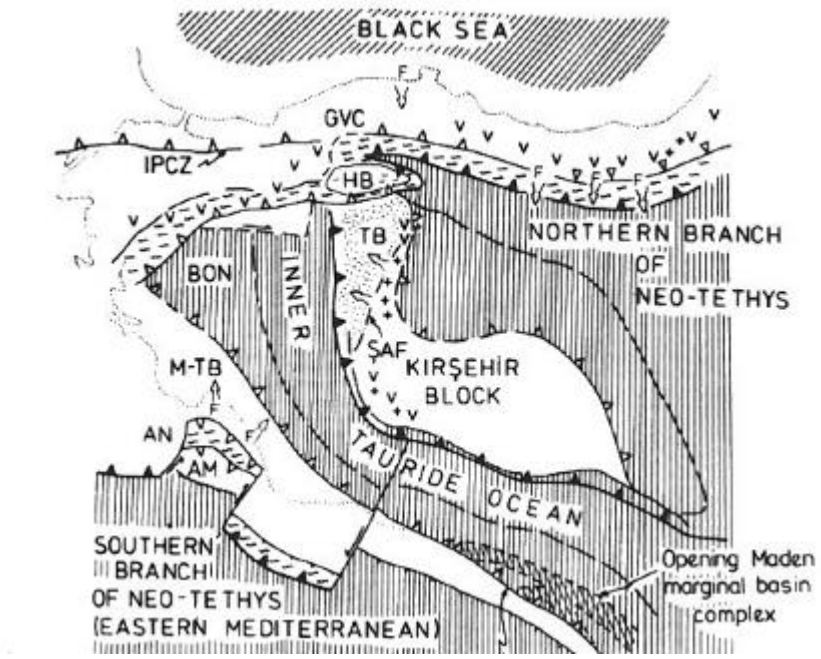

Fig. 8.6 Palaeotectonic map of the Eastern Mediterranean in the Palaeocene, from Görür *et al.* (1984). The Inner Tauride Ocean is depicted as a narrow seaway between the Kirsehir Block to the north and the Menederes-Tauride Block (MTB) to the south. GVC, Galata Volcanic Province; IPCZ, Intra Pontide Convergence Zone; HB, Haymana Basin; TB, Tuzgölü Basin; SAF, Sereflikoçhisar / Aksaray Fault; BON, Bozkir Ophiolite Nappe (i.e. Lycian Nappes and B-H Nappes); AN, Antalya Nappes; AM, Alanya Massif.

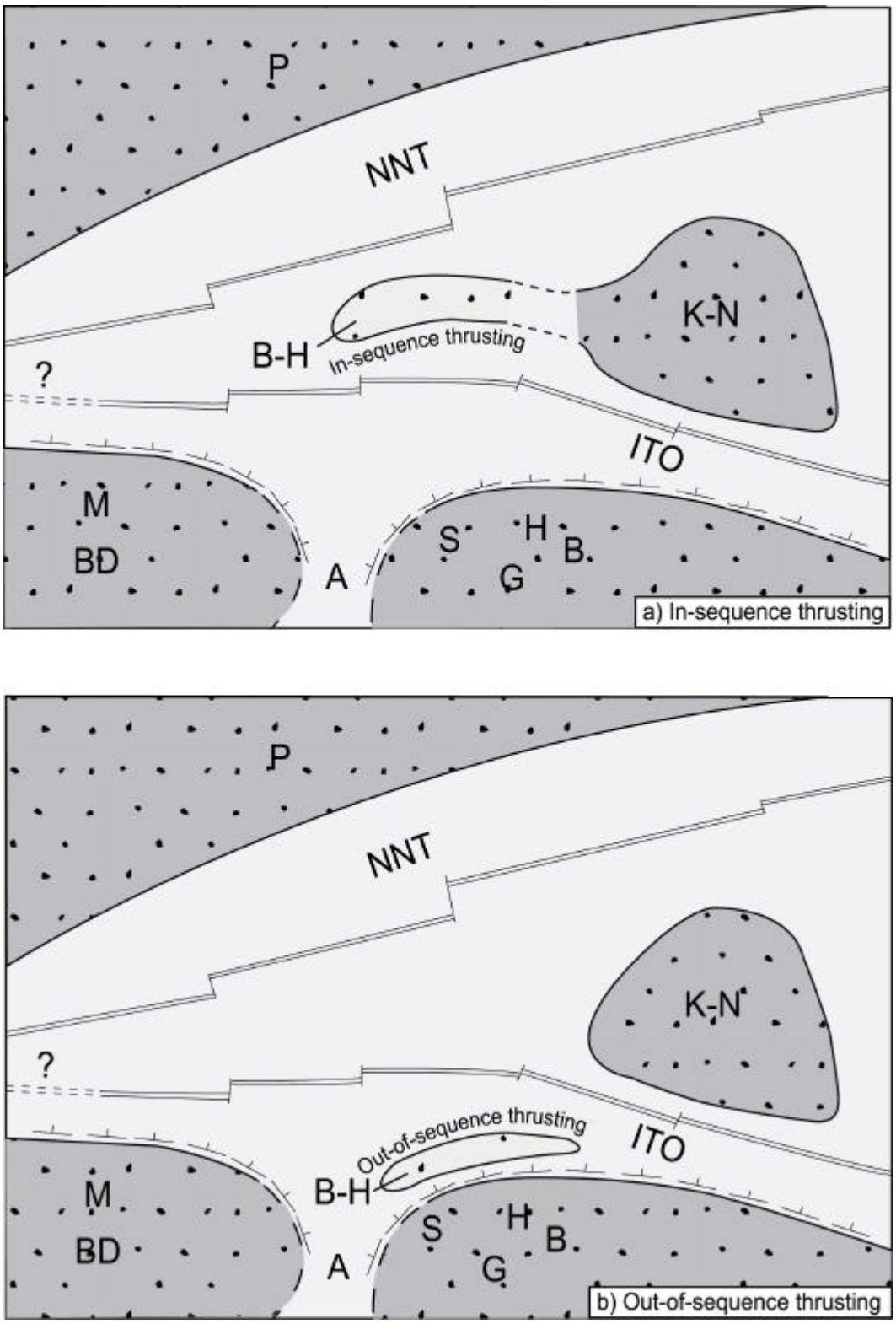

Fig. 8.7 Palaeogeographical sketch maps of the Northern Neotethys during Mid-Jurassic time, with Inner Tauride Ocean and an additional seaway connecting the southerly Neotethys **(a)** north and **(b)** south alternative settings of the B-H Nappes according to to in-sequence or out-of-sequence thrusting. A, Antalya Unit; B, Bolkar Dag; BD, Bey Daglari Unit; B-H, Beysehir-Hoyran Nappes; G, Geyik Dag Unit; H, Hadim Nappe; ITO, Inner Tauride Ocean; K-N, Kirsehir-Nigde Massif; L, Lycian Nappes; M, Menderes Massif; NNT, Northerly Neotethys spreading axis; P, Pontides; S, Sakarya Unit.

8.2.7 Northern Neotethys with Inner Tauride seaway

In Figure 8.7 (a) and (b) the Northern Neotethys was split into two branches, a main northerly oceanic strand and a southerly strand, termed the Inner Tauride Ocean, which split off a Kirsehir-Nigde microcontinent (Oktay, 1973; Görür *et al*., l984). The southern margin of the Northern Neoteothys is inferred to be palaeogeographically irregular, with the Dinar units in the west being located in an embayment between the Geyik Dag-Hadim platform to the east and the Menderes-Bey Daglari platform to the west. To account for the slight lithostratigraphic differences, the Dinar units perhaps connected southward palaeogeographically through the Isparta Angle to the Southerly Neotethys (Robertson, l993). Assuming the in-sequence thrust model as in Figure 8.7 (a) the upper nappes could effectively restore as a westward extension of the Kirsehir-Nigde microcontinent (or satellite platforms). In Figure 8.7 (b) the Beysehir-Hoyran upper thrust sheets again fringed the Anatolide-Tauride continental margin as in the previous out-of-sequence thrust model, with the Beysehir-Hoyran ophiolites formed at a spreading centre within the Inner Tauride Ocean.

Additional evidence from the Izmir-Ankara-Erzincan suture zone to the north of the study area is needed to test fully the concept of an Inner Tauride ocean (Okay *et al.,* 2001). However, the extraordinary lateral continuity of the Beysehir-Hoyran Nappes over ca. 700 km, extending far to the southeast of the Kirsehir-Nigde Massif is consistent with the former existence of an Inner Tauride ocean, rather than requiring the nappes to be thrust >500km from the Ankara-Erzincan suture zone north of the Kirsehir Massif (Fig. 1.2). If this was the case then lateral correlations would be expected to be severely disrupted owing to irregular wrapping around the Kirsehir promontory, which is not the case. Additional evidence from recent work in the Ulukisla basin also supports the presence of an Inner Tauride Ocean (Clark, 2002). Thus, the favoured scenario for Mid-Jurassic palaeogeography of the northerly Neotethys is depicted in Fig. 8.7b.

8.2.8 Other possible models

Other factors need to be considered and examined before definitive conclusions can be drawn. So far each model reported in this thesis relies on initial Late Cretaceous northward-directed subduction and that emplacement of allochthonous units was by conventional thrust faulting mechanisms during Early Tertiary time. Even though the timing is well-constrained, the issue of whether the present configuration of tectonostratigraphic units could be assembled by other mechanisms needs to be addressed; therefore, this next section considers the possible viability of a number of different scenarios.

8.2.9 Southward subduction polarity during the Late Cretaceous

Each preceeding model implies that when subduction was initiated in the Late Cretaceous, the direction of the downgoing slab was dipping northwards. An alternative model considers the viability and implication of a southward-subduction scenario. Figure 8.8 (a) shows the genesis of a SSZ-type ophiolite above a southward-dipping subduction zone. One implication of southwards subduction is that ophiolite obduction is most likely to be to the north, i.e. onto the Pontide margin (Fig. 8.8b). It is clear that ophiolite emplacement was directly onto the Hadim Nappe, where present (e.g. Beysehir area; section 2.5.1); thus, the Hadim Nappe would restore to a northern margin given southwards-subduction conditions. This clearly contradicts the field evidence.

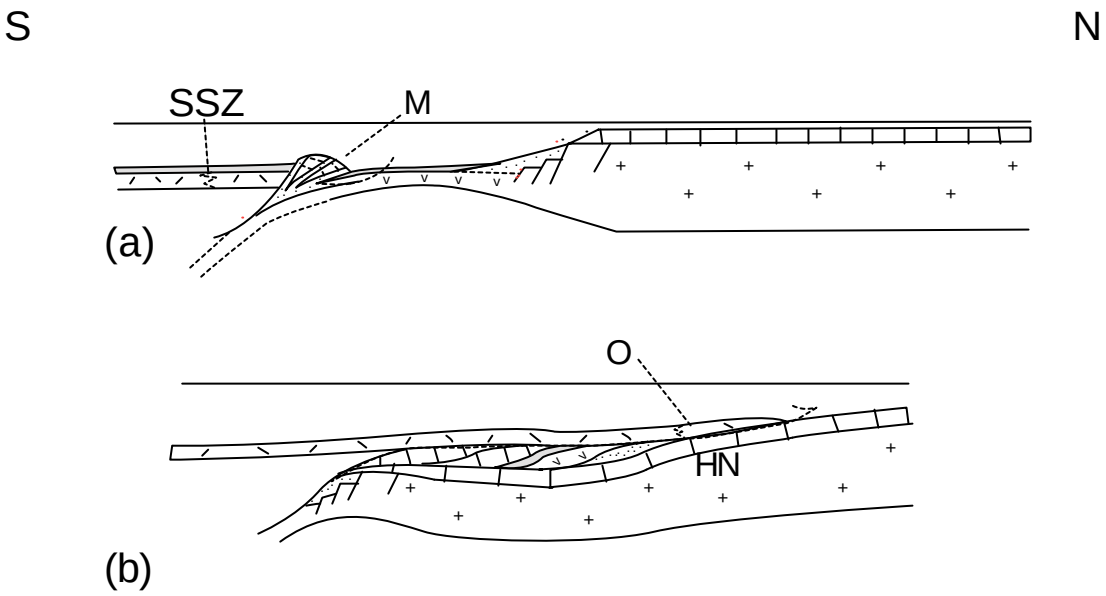

Fig. 8.8 Cartoon diagram showing Late Cretaceous **(a)** southwards subduction; **(b)** ophiolite emplacement onto northern margin. After genesis of a SSZ-type ophiolite (SSZ) and formation of Ophiolitic Melange (M) above a southwards dipping subduction-zone in Turonian? time, ophiolite obduction (O) onto Hadim Nappe (H) occurred during the Maastrichtian.

One of the main problems with the southwards-subduction model is that the Hadim Nappe is demonstrably part of the Menderes-Tauride block, with a closely related stratigraphy throughout Palaeozoic and Mesozoic time (e.g. Sections 2.4 and 4.5). It is extremely unlikely that the Hadim Nappe could restore to the Pontide margin in this manner. Regional evidence also discounts the widespread southward subduction model. Inception of a Coniacian-Campanian magmatic arc in the Pontides, ca. 150km north of the Izmir-Ankara suture, is highly indicative of northward subduction of the Neotethyan ocean (Okay *et al*., 2001). In addition, there are no structural data from Late Cretaceous accretionary terrains of central Anatolia to support southward subduction along the north margin of the Tauride-Anatolide carbonate platforms in the Late Cretaceous (Robertson *et al.*, 1996).

In summary, most local and regional evidence points to northward subduction during the Late Cretaceous.

8.2.10 Strike-slip terrain docking

This model considers the scenario that the Beysehir-Hoyran units accreted through dominantly strike-slip mechanisms. One such possible reconstruction is shown in Fig. 8.9. In this interpretation the allochthonous units would still restore to a position in the Neotethyan ocean northwards of the Menderes-Tauride block, as before. Early Tertiary oblique collision leads to transpressional deformation and the docking of allochthonous terranes along such a zone of oblique convergence. Transform faults may have initially played a role in the tectonic evolution of the Beysehir-Hoyran Nappes (e.g. intra-oceanic transforms), but the pervasive evidence for low-angle thrust faulting on all scales across the entire B-H Nappes indicates that any strike-slip influence has played a minor part. Regional evidence also downplays the role of strike-slip mechanisms in closure of the Neotethyan ocean (e.g. Lycian Nappes; Collins, 1997; Ulukisla basin, Clark, 2002); thus, this model can largely be discounted on all of these grounds.

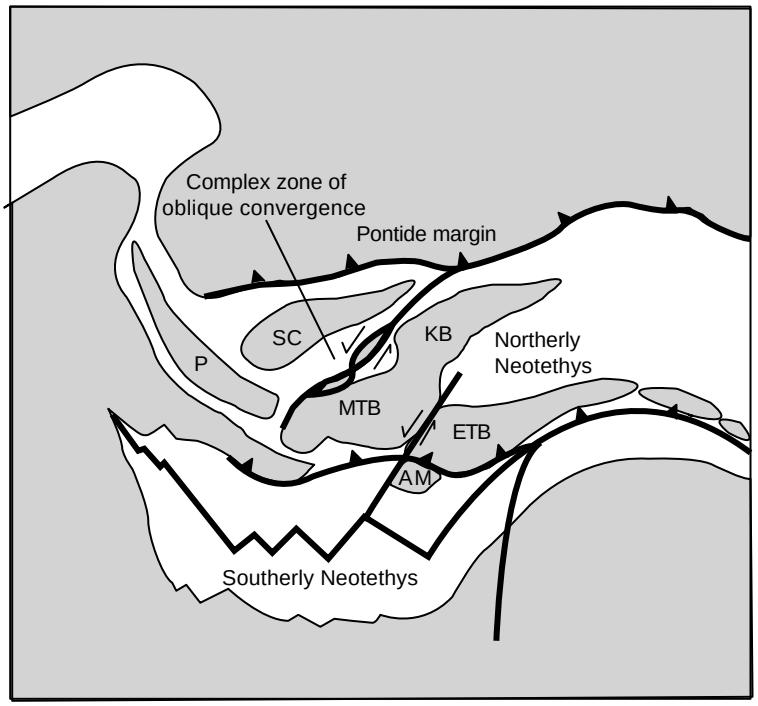

Fig. 8.9 Late Eocene Palaeotectonic map of the Eastern Mediterranean (after Robertson & Dixon, 1984). The Inner Tauride Ocean has closed during the suturing of the Kirsehir (KB) and Menderes-Tauride (MTB) blocks. The Eastern Tauride block (ETB) is separated from the Menderes-Tauride block by strike-slip motion (as in Robertson & Dixon, 1984). In this model the northern margin of the newly sutured Tauride-Kirsehir block is a complex zone of oblique convergence along which the B-H allochthon accreted.

8.3 Favoured model for the evolution of the B-H Nappes

Drawing together all the lines of evidence presented in this thesis, the following section summarises the Mesozoic to Early Tertiary tectonic evolution of the B-H Nappes assuming out-of-sequence thrusting from an Inner Tauride Ocean located north of the Tauride carbonate platforms.

8.3.1 Triassic-Cretaceous: Rift/passive margin phase.

The northern margin of Gondwana rifted in Permo-Triassic time, as represented by the autochthonous Taurus carbonate platform. During the Mid-Triassic, bordering the Tauride microcontinent, siliciclastic and carbonate turbidites accumulated in proximal slope settings. More distal siliciclastic sediments were associated with intermediate-composition volcanics, volcaniclastic sediments and tuffs, which became more acidic progressively as rifting continued. A thick volcanic pile built up before post-rift subsidence began in Late Triassic (Carnian-Norian) time. Pelagic sediments then blanketed the marginal basin areas. In more outboard locations carbonate platform conditions persisted until Mid-Jurassic time when subsidence was recorded by a condensed Ammonitico Rosso succession across most of the outboard locations. Locally conditions deepened and radiolarian chert accumulated in Late Jurassic time; however, this could be a function of increased productivity of siliceous microorganisms during this time (Jenkyns & Winterer, 1979). Regionally, pelagic conditions persisted through to the Late Cretaceous.

8.3.2 Latest Cretaceous: Intra-oceanic subduction, accretion and trench/passive margin collision.

Intra-oceanic thrusting probably began in the Late Cretaceous, as shown by metamorphic sole ages of 88 Ma beneath the Beysehir peridotite (Çelik, pers. comm, 2001). This was followed by northward-dipping intra-oceanic subduction. Along the leading edge of this subduction zone an accretionary complex developed. During subduction, Neotethyan oceanic crust, oceanic sediments and seamounts were detached and incorporated into the overlying accretionary wedge. An unknown amount of oceanic crust was consumed before marginal units bordering the autochthonous Tauride carbonate platform, represented now by the B-H Nappes, were incorporated wholesale into the accretionary prism. In the favoured out-of sequence thrust interpretation (Figs. 8.4 and 8.7b) the ophiolites and locally assembled broken formation were emplaced southwards along the length of the Anatolide-Tauride continental margin edge (i.e. Bolkar Dag and Hadim Nappe) in latest Cretaceous (Campanian-Maastrichtian) time. Meanwhile sedimentation in the Geyik Dag to the south continued into the Early Tertiary, indicating that the ophiolite was not emplaced far south during initial convergence. Ophiolite obduction in this case was probably related to trench/passive margin collision, as for other Late Cretaceous Tethyan ophiolites, e.g. Pozanti-Karsanti ophiolite, Polat & Casey, 1995; Oman ophiolite, Robertson 1987).

8.3.3 Early Tertiary 'hard collision'

During the Late Eocene, related to suture tightening and regional final closure of the Northern Neotethys, the former carbonate platform edge was detached and thrust southwards as the Hadim Nappe and Bolkar Dag Unit together with their cover of previously assembled allochthonous units. Sited in a former palaeogeographical embayment further west, the Late Cretaceous Dinar thrust sheets were merely re-thrust some distance further south over the relatively autochthonous carbonate platform without detaching large carbonate platform slices.

The Late Eocene thrusting possibly relates to "hard collision" that accompanied regional suturing of the Northern Neotethys to form the Ankara-Izmir-Erzincan Zone. This zone has been shown to be a tectonically disrupted Neotethyan suture between Eurasia, to the north, and the Tauride block, to the south (Sengör & Yilmaz, 1981; Robertson & Dixon, 1984).

Regionally, initial collision is inferred to have started in the Palaeocene (Okay *et al.*, 2001), although no evidence is recorded in the B-H Nappes until Late Eocene times. The boundaries between regional ophiolite obduction (latest Maastrichtian-Palaeocene) and initial collision (Palaeocene-Early Miocene) are not clear (Okay *et al.*, 2001), and vary from area to area. In this respect it is clear that the margins of the Neotethyan ocean were irregular, with varying positions of microcontinental units causing this observed diachronous collision.

The presence of an Oligo-Miocene unconformable cover of the Dinar units shows that this deformation was soon over, whereas, by contrast, a similar southward re-thrusting of the Lycian Nappes, beginning in Late Eocene time (Collins & Robertson, l998) was not completed until Late Miocene time (Poisson, 1977).

Chapter 9

9.CONCLUSIONS

9.1 Comparisons within the Eastern Mediterranean

The Beysehir-Hoyran Nappes effectively record the Mesozoic-Early Tertiary evolution of the northern margin of the Anatolian-Tauride microcontinent across an area spanning most of the Central Taurides of Southern Turkey. Discrete tectonic phases including initial rifting, passive margin subsidence, subduction/accretion and suturing are all documented.

Contemporaneous Neotethyan units along strike from the B-H Nappes indicate evolution of the Northern margin of the Anatolide-Tauride block varied considerably within relatively small distances. To the west, the adjacent Lycian Nappes possess a greater structural thickness, with the present outcrop restoring as proximal to distal units depending on closeness to the suture zone. A major difference is the predominance of marginal (e.g. slope) units preserved within the thrust sheets (Collins, 1997). In contrast, the B-H Nappes preserve mostly off-margin and oceanic units. The only marginal unit to be preserved in the B-H Nappes, the Korualan Unit, is restricted to one outcrop area.

Further east along strike, allochthonous Neotethyan units consist of the Pozanti-Karsanti ophiolite which was emplaced directly onto the Bolkar Dag carbonate platform in pre-Maastrichtian time as evidenced by transgressive Maastrichtian limestone in the Ulukisla area (Dermitasli *et al*., 1984; Clark, 2002); other off-margin units were not preserved. Closure of the Inner Tauride seaway occurred in the Maastrichtian, with the Early Tertiary Ulukisla basin recording the final tectonic evolution of Neotethys in the area (Clark, 2002).

In Greece, contemporary units are found in the less well known, fragmentary Vardar Zone (Robertson, 1996) and the well-studied Pindos Zone (Jones, 1990; Roberstson, *et al.,* 1991; Degnan, 1992).

The southern margin of the Anatolide-Tauride microcontinent and units of southerly Neotethys are variably preserved in the Antalya Complex, which have been emplaced by a combination of high angle strike-slip and low-angle thrust mechanisms (Woodcock & Robertson, 1982; Waldron, 1984; Robertson *et al*., 1991). Similar southerly Neotethyan units are preserved in Cyprus as the Mamonia Complex, which is interpreted as a tectonized and collapsed passive margin sequence that formed along the northern margin of Gondwanaland (Swarbrick, 1979, 1980; Swarbrick & Robertson, 1980; Malpas *et al.,* 1993). These preserved allochthonous units share similarities with the B-H Nappes, being preserved as broken formation and melange; however, the Mamonia complex is an order of magnitude smaller than the B-H Nappes outcrop area and has an enigmatic source because of the

complex history involving both strike-slip and thrust mechanisms (Malpas *et al.*, 1993; Swarbrick, 1993).

The lateral continuity of the Beysehir-Hoyran Nappes, with little structural variation over ca. 700km, is an extraordinary feature that is unprecedented in the Eastern Mediterranean region. The high degree of flattening, with no major proximal or distal variations in the nappe stack is unique and testifies to the huge transport distance, ca. 100km-200km from the Izmir-Ankara-Inner Tauride suture zone. Previously the B-H-H Nappes were seen as a critical missing link in regional synthesis of the Eastern Mediterranean. This study has importantly not only filled this huge gap in the knowledge of Neotethys, but has also highlighted the role of out-of-sequence thrusting in continental collision zones, which has been rarely considered in the past. This study also documents the effects of subduction/accretion on marginal and off-margin units, an unusual situation on a global scale, as most Pacific subduction/accretion involves just oceanic units (e.g. Franciscan Melange, Western USA).

9.2 Major tectonostratigraphic events in the evolution of the Beysehir-Hoyran Nappes

Assuming the-of-sequence thrust model, this study infers the following tectonostratigraphic events:

1. The northern margin of Gondwana rifted in Triassic time, as represented by the Autochthonous Taurus carbonate platform and the Hadim Nappe. Siliciclastic and carbonate turbidites accumulated in proximal slope settings (Korualan Group; Bozkir area). Bordering rift siliciclastics and minor calc-turbidites (e.g lower Ihsaniye unit, Ermenek area) were inundated with intermediate-silicic composition volcanics, volcaniclastics and tuff, which accumulated in a deep-water basin undergoing background radiolarian hemipelagic sedimentation. Neritic carbonate platforms developed in a generally more outboard setting (e.g. Boyali-Tepe Unit; Beysehir area). Platforms and basinal units varied in scale and palaeogeographic location from west to east.

2. Rifting ended in Late Triassic time and was followed by post-rift subsidence. Pelagic deposition persisted in rift basins (e.g. Huglu Unit; Beysehir area), whereas neritic platforms subsided in Lower-Mid Jurassic time and were covered by calcareous pelagic sediments (including Ammonitico Rosso), above the CCD. Nodular radiolarian chert accumulated during Late Jurassic-Early Cretaceous time.

3. The ophiolite was generated above a N-dipping intra-oceanic subduction zone probably in Late Cretaceous time. The amphibolite facies metamorphic sole (Beysehir area) was formed by underplating of oceanic crust beneath young hot supra-subduction zone lithosphere.

4. The WPB and MORB-type volcanic blocks within the Ophiolitic Melange, together with radiolarian chert, pelagic carbonates and volcanogenic sediments represent a Late Cretaceous subduction/accretionary complex related to northward subduction of Neotethys.

5. Tectonic disruption of the higher Beysehir-Hoyran nappes within Late Cretaceous (Maastrichtian) ophiolite-derived matrix resulted from collision and accretion of the Tauride continental margin with the north-dipping subduction zone.

6. During the latest Cretaceous the accretionary prism and SSZ ophiolite were emplaced southwards onto the northern edge of the Tauride carbonate platform (future Hadim Nappe), while platform deposition continued on the Tauride platform, ca.150km further south (Geyik Dag).

7. Erosion of the emplaced ophiolite probably took place in Palaeocene times, although no trace of a cover sequence remains, unlike the Lycian Nappes.

8. During the Early Tertiary any remaining Northerly Neotethyan oceanic crust was subducted leading to final collision of the Tauride continental unit with the Eurasian margin during Late Eocene time. During Late Eocene collision, the Palaeozoic-Early Tertiary successions were detatched as the Hadim Nappe and Bolkar Dag Unit and were thrust up to 200 km southwards over a Lower-Middle Eocene siliciclastic foredeep, with the previously assembled (Upper Cretaceous) nappe stack riding above. Further west (Dinar area), the regional platform remained *in situ* and the Upper Cretaceous Ophiolitic Melange and ophiolite were thrust onto the Eocene siliciclastic foredeep, resulting in interlayering of latest Cretaceous and Early Tertiary melange units.

9. After collision, the Beysehir-Hoyran Nappes underwent Miocene and younger extensional tectonics (e.g. east of Bozkir area/Dinar area) and clockwise palaeotectonic rotation.

10. This study of the B-H-H fills a critical gap in the knowledge of the Eastern Mediterranean region and also highlights specific concepts that remained unknown and poorly documented based on studies of other areas in the Eastern Mediterranean and elsewhere.

Appendix 1:

Radiolarian Study

Appendix 1: Radiolarian Study

Until recently, biostratigraphical studies using siliceous microfauna have not been carried out in the Beysehir – Hoyran Nappes. A number of radiolarian chert sequences exist within the thrust sheets, which are presently undated and would benefit from this technique. So, in order to improve the stratigraphic control of a number of these key sequences chert samples were collected from strategic outcrops from the following units; (a) Boyali Tepe type section in the Beysehir area (Fig, 2.19) and (b) Radiolarian chert succession from the Huglu-type unit in the Ermenek area (Fig. 5.11).

Methodology

The collected samples were ribbon radiolarian cherts, which were usually highly siliceous and hard. The samples collected were initially checked in the field for the presence of radiolaria. They were then cut with a diamond saw into small cubes (approximately 1cm diameter), and placed into polythene beakers. Samples with excess carbonate present as veins or on surfaces were then bathed in a 10% solution of HCl acid, and left for several days until the reaction stopped and the carbonate was removed. Next, the samples were washed and placed in a solution of 4% HF acid for approximately 24 hours. At the end of this period the residue was washed through a fine sieve (70 mesh) and collected. The samples were replaced back into a 4% solution of HF and left for another 24 hours. This process was repeated a further 2 or 3 times depending on the amount of residue shed from each washing. The residue from each sample was then meticulously picked from a tray using a binocular microscope to aid radiolarian recognition. Commonly <1% of the residue yielded samples good enough for recognition. These specimens were placed onto metal stubs, gold coated using a sputter machine and studied under a Phillips XL 30 CP scanning electron microscope, at the Edinburgh Microscopy and Materials Analytical Centre (EMMAC). Images were taken of the radiolarian fauna using the secondary electron detector, under typical beam conditions of 20kv and a working distance of 10mm. These images have been collated and presented here as plates.

Results

Radiolarian identification and age determination was carried out by Dr. Taniel Danelian at the Laboratoire de Micropaléontologie, Université Pierre & Marie Curie (Paris VI). The data presented here suggests the Boyali Tepe radiolarian chert section (Plates 1-2) ranges from Oxfordian to Early Hauterivian in age, whilst the Ihsaniye section (Plate 3) is probably of Jurassic age (T. Danelian, pers. comm, 2001). Generally, the radiolarians extracted from the later section were poorly preserved and require further laboratory work to acquire a more precise age. Indeterminate radiolarians are also documented here in Plates 4 through 12.

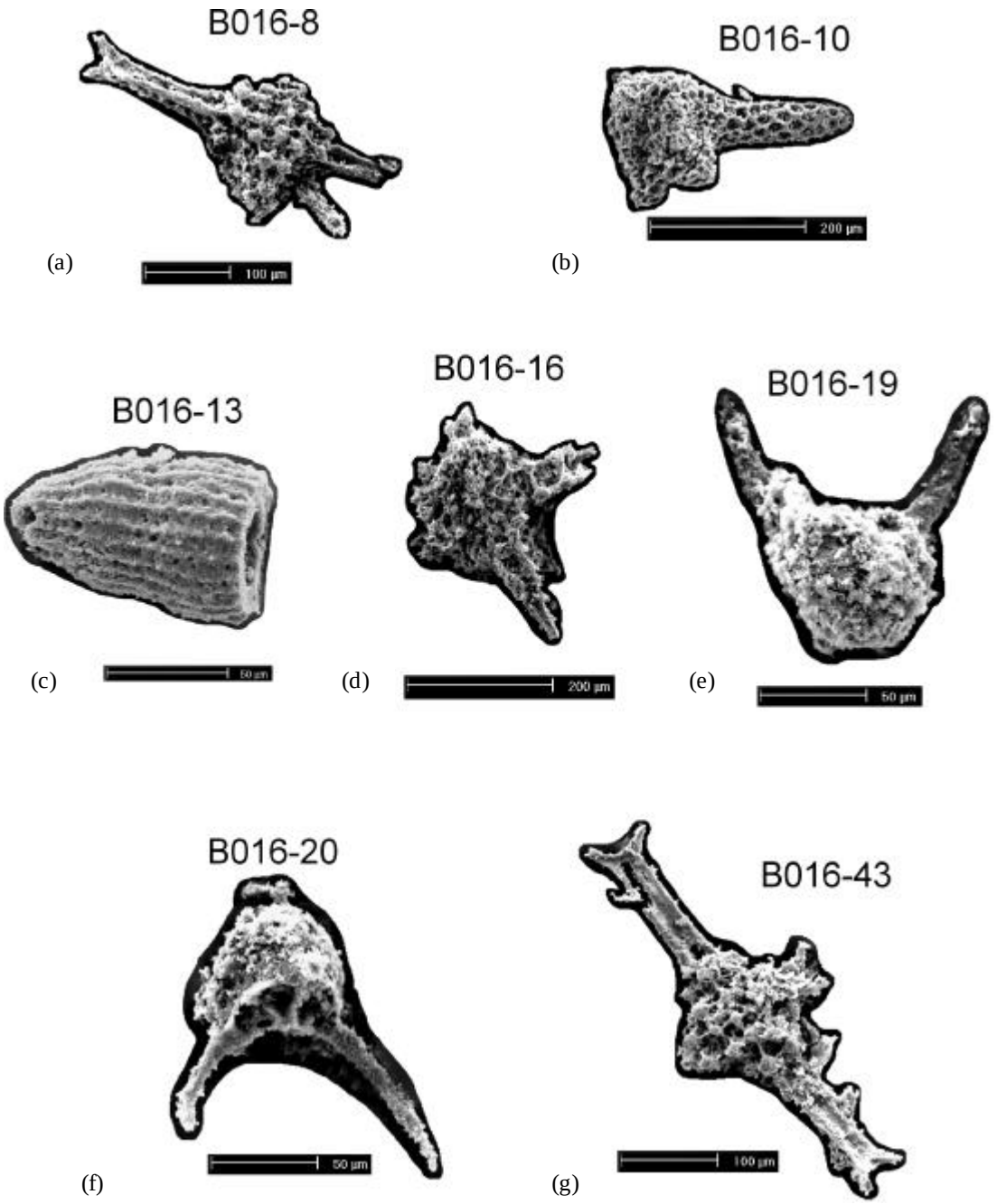

Plate 1 Identified radiolarians from the Boyali Tepe type section: chert sample BO16; (a) and (g) *Podocapsa amphitreptera*, (b) *Emiluvia hopsoni*, (c) *Emiluvia sp*., (d) *Archaeodictyomitra sp*., (e) and (f) *Saitoum sp*.

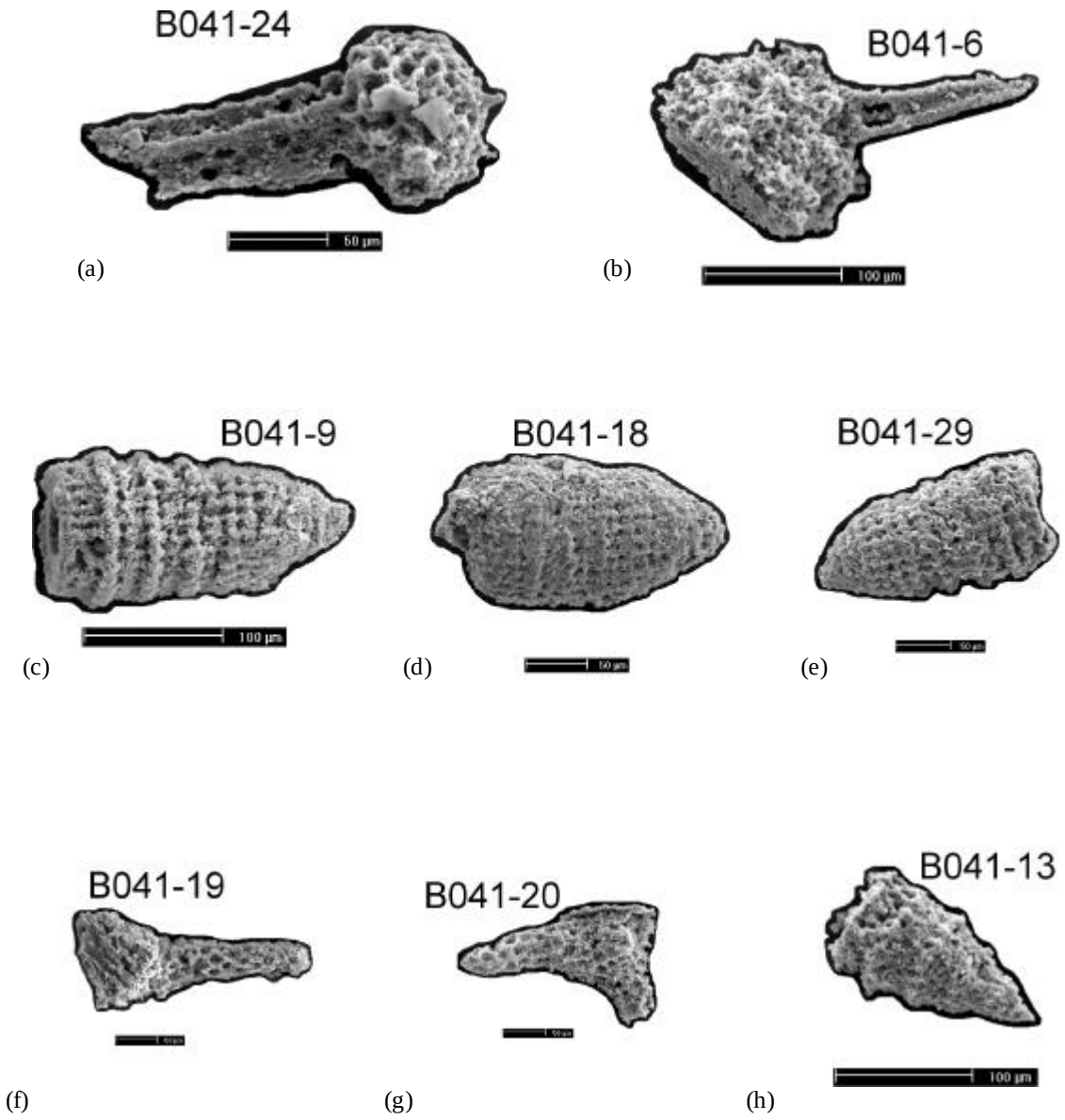

Plate 2 Radiolarians from the Boyali Tepe section: chert sample BO41; (a) *Tritrabinae sp*., (b) *Acaeniotyle sp*., (c) (d) and (e) *Archaeodictyomitra sp. cf. A. apiarium*, (f) and (g) *Podocapsa amphitreptera*, (h) *Parvicingula sp*.

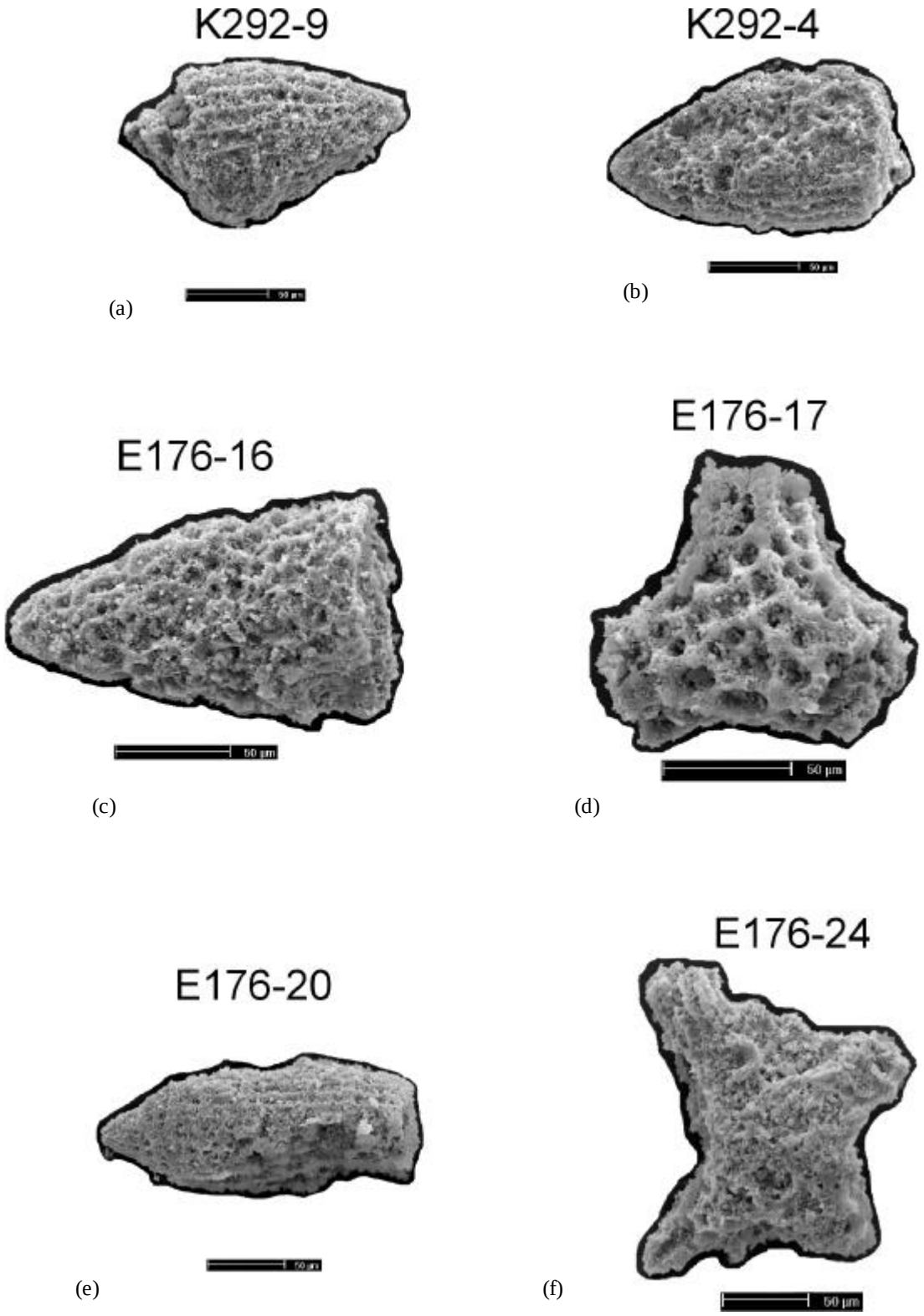

Plate 3 Radiolarians from the Ihsaniye section: chert sample K292 (a) and (b) *Archaeodictyomitridae sp*.; chert sample E176 (c) *Parvicingulidae sp*., (d) *Triatrbs sp*., (e) *Archaeodictyomitra sp. cf. A. apiarium*, and (f) *Emiluvia premyogii*.

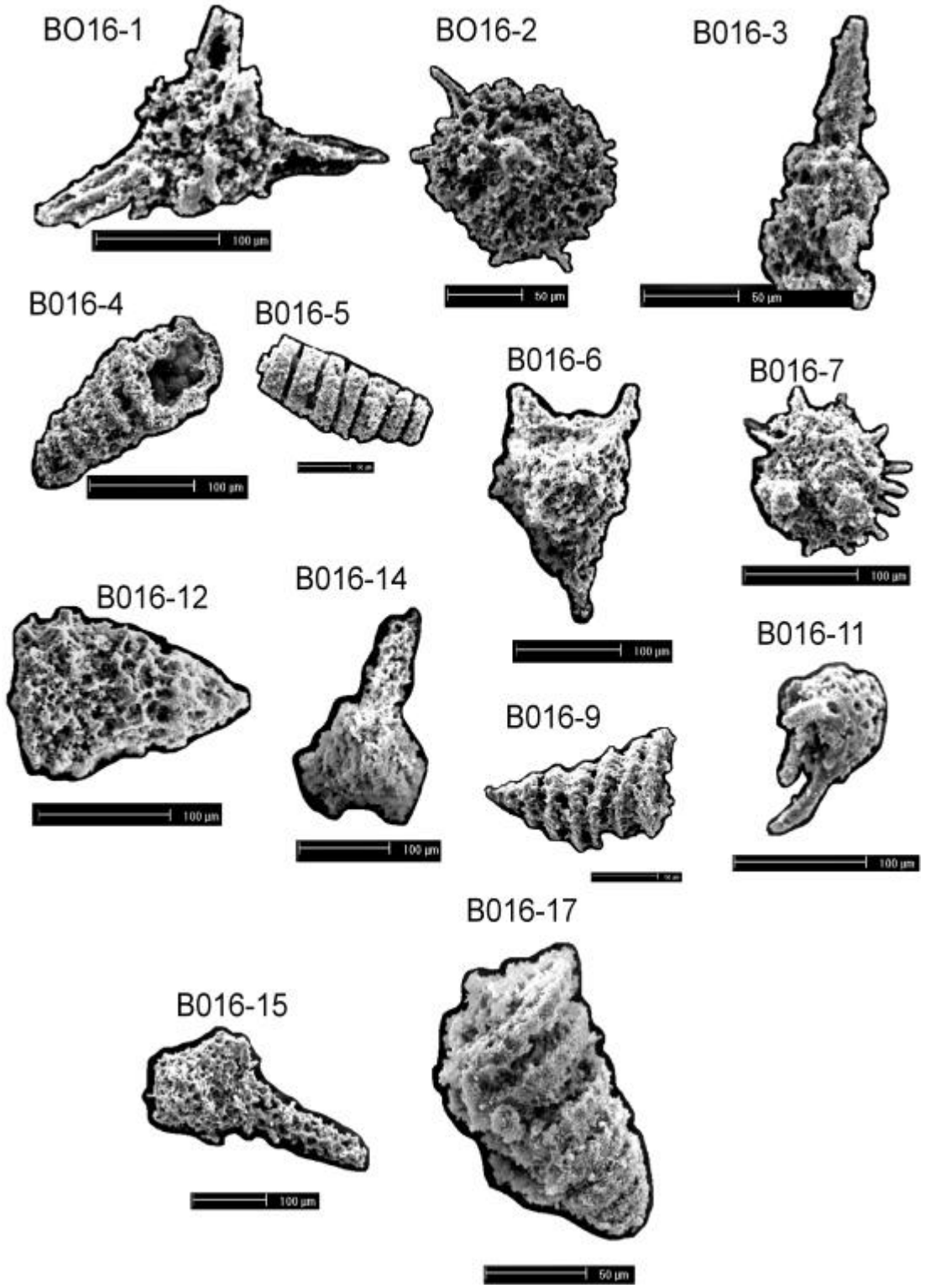

Plate 4 Indeterminate Jurassic and Cretaceous radiolarians from the Boyali Tepe type section; chert sample BO16

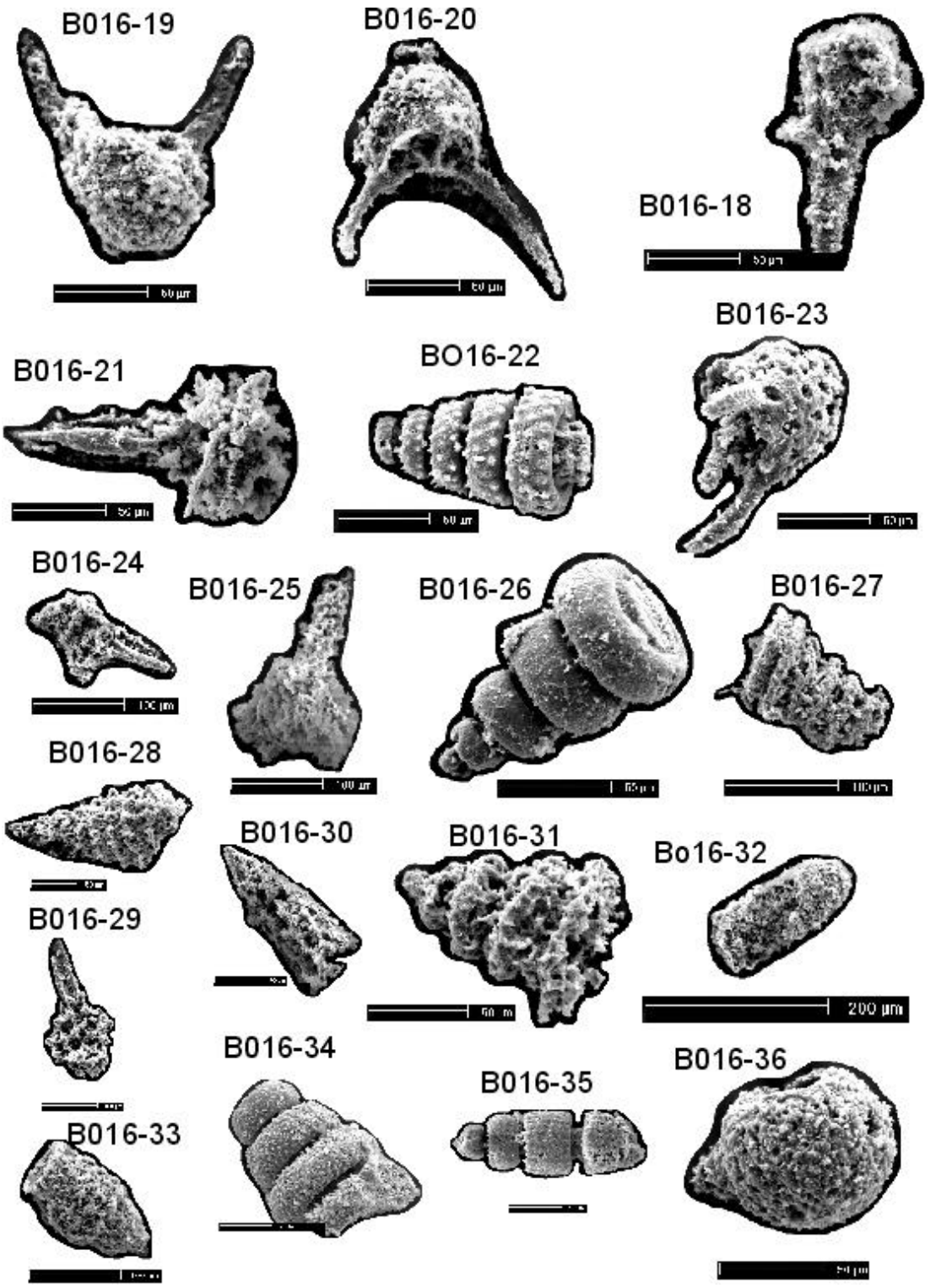

Plate 5 Indeterminate Jurassic and Cretaceous radiolarians from the Boyali Tepe type section; chert sample BO16.

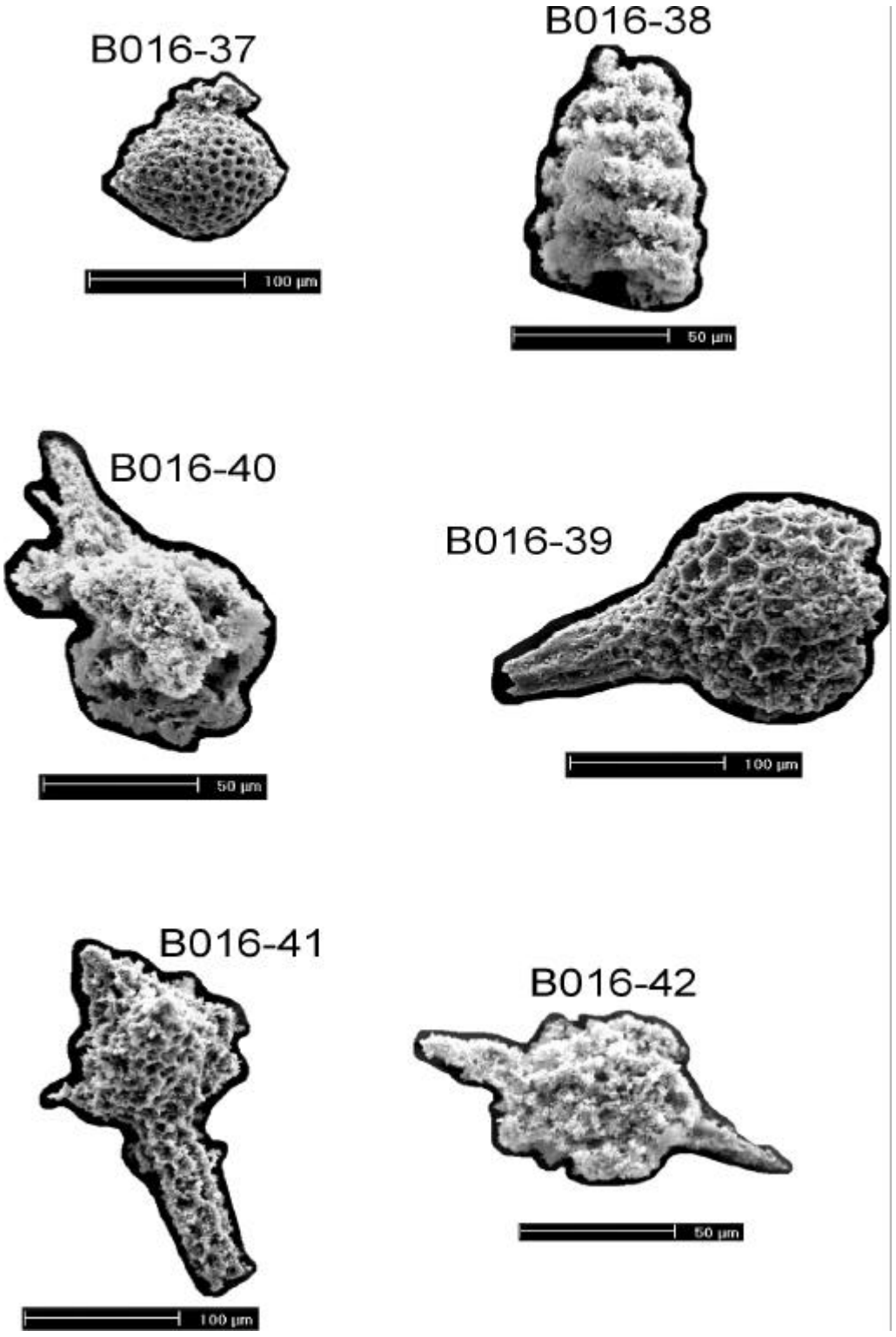

Plate 6 Indeterminate Jurassic and Cretaceous radiolarians from the Boyali Tepe type section; chert sample BO16.

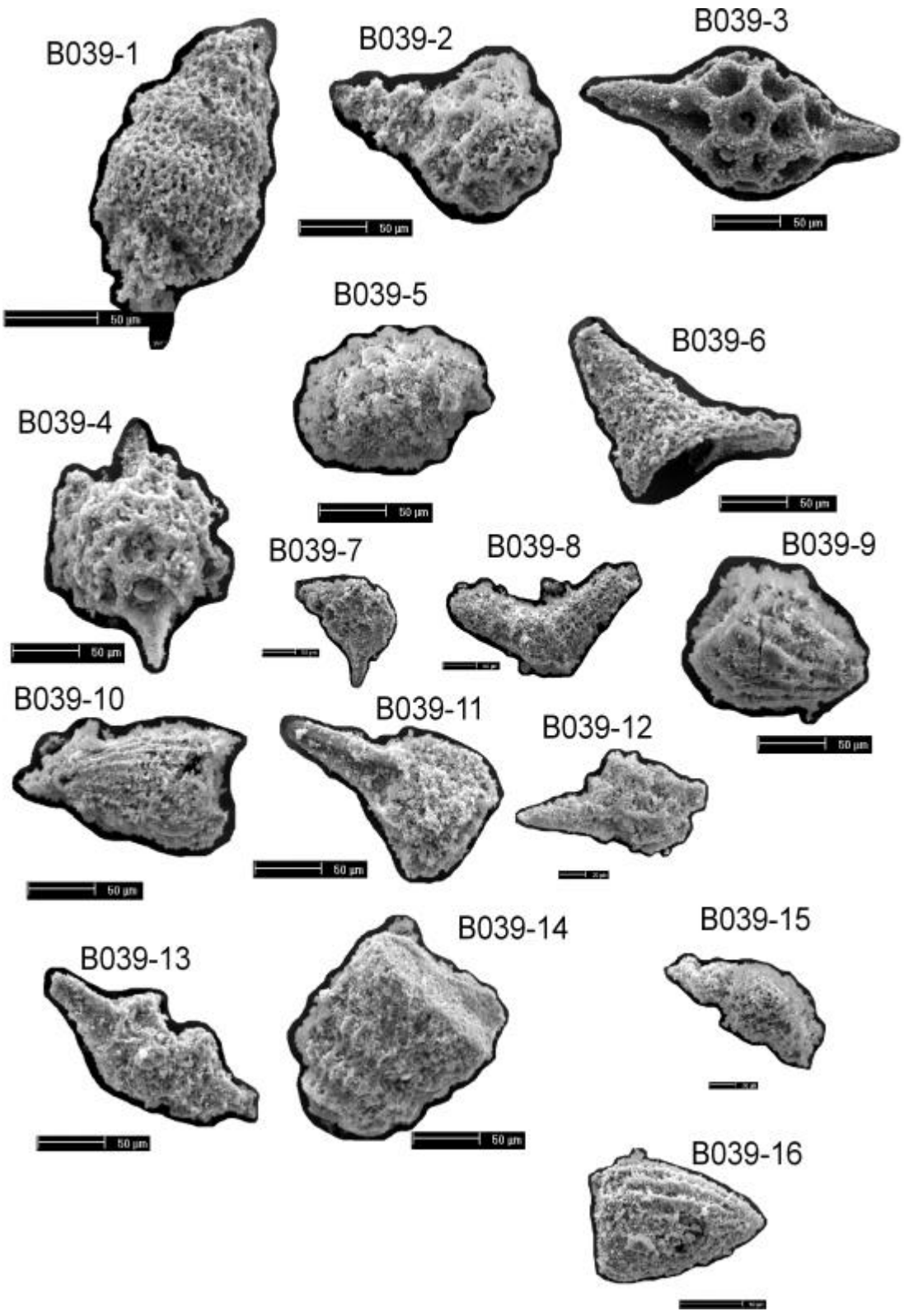

Plate 7 Indeterminate Jurassic and Cretaceous radiolarians from the Boyali Tepe type section; chert sample BO39.

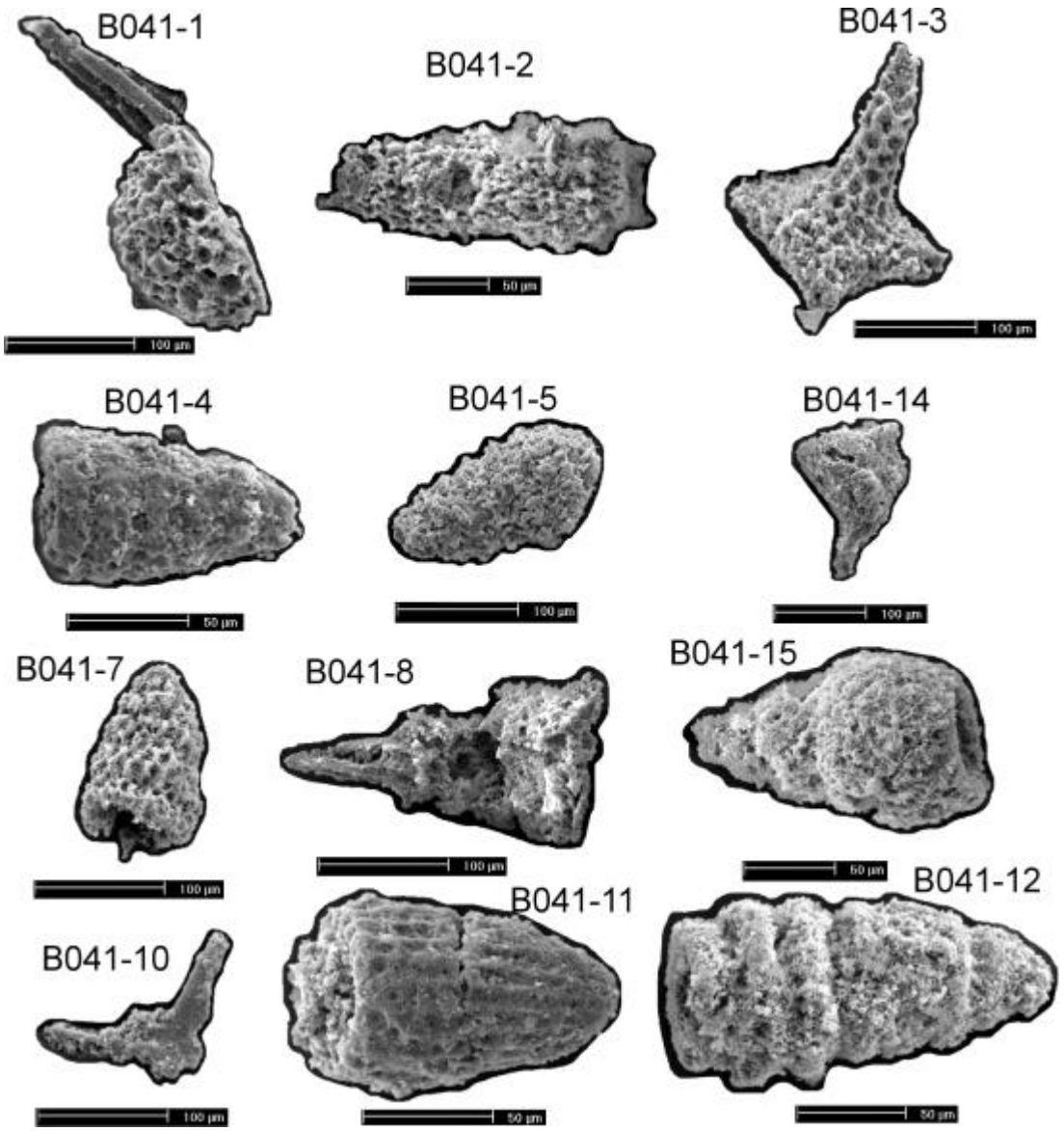

Plate 8 Indeterminate Jurassic and Cretaceous radiolarians from the Boyali Tepe type section; chert sample BO41.

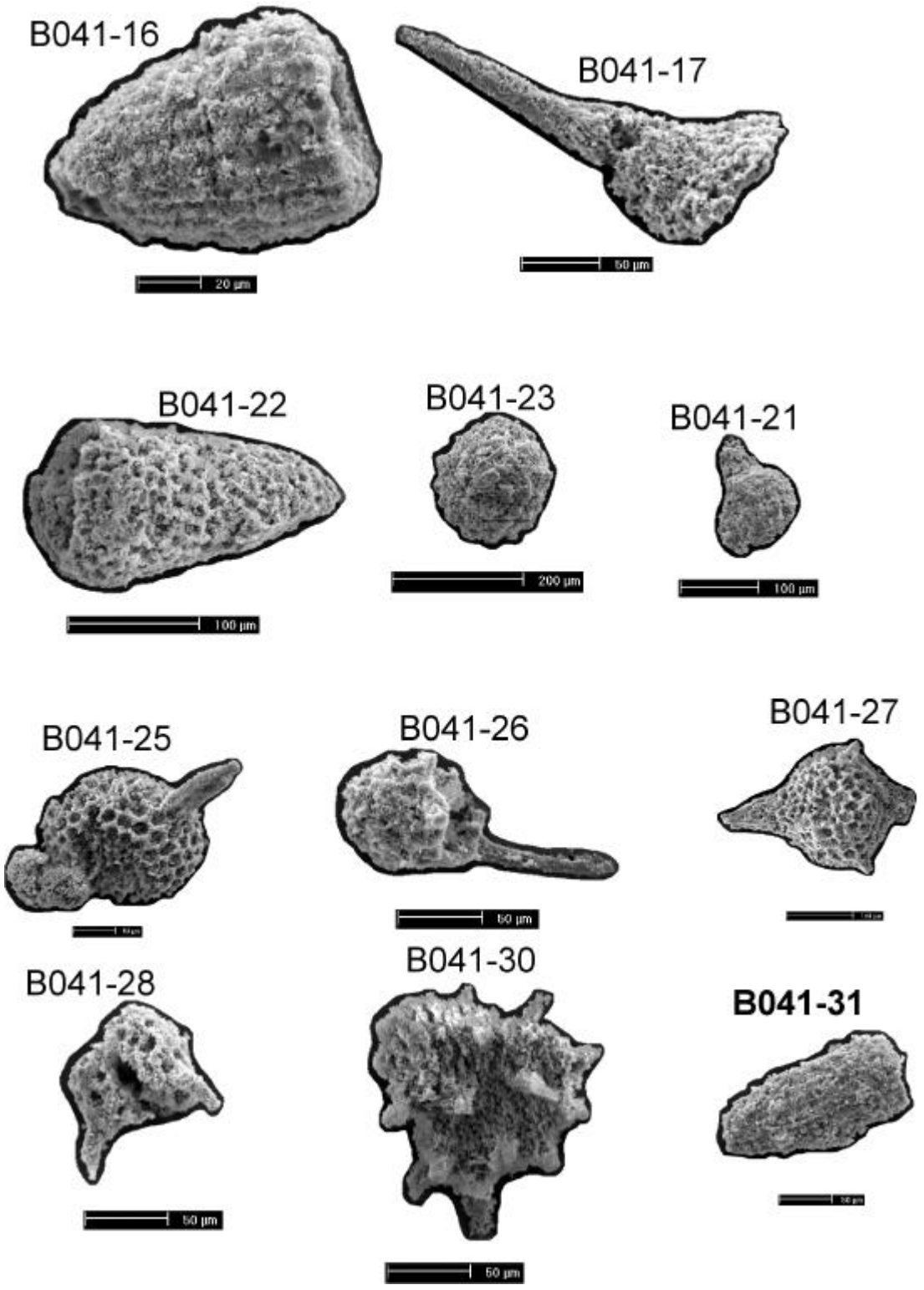

Plate 9 Indeterminate Jurassic and Cretaceous radiolarians from the Boyali Tepe type section; chert sample BO41.

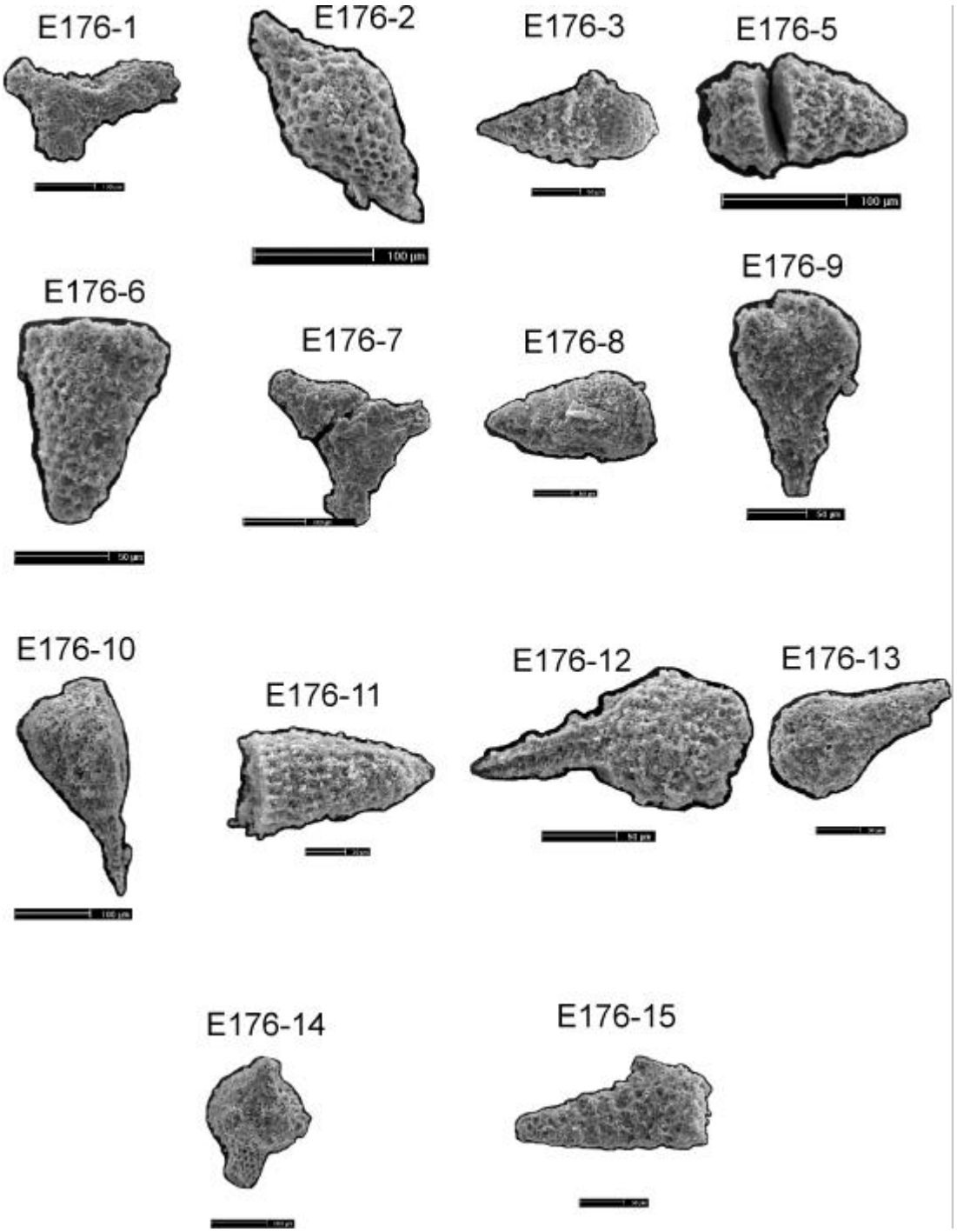

Plate 10 Indeterminate Jurassic radiolarians from the Ihsaniye section; chert sample E176.

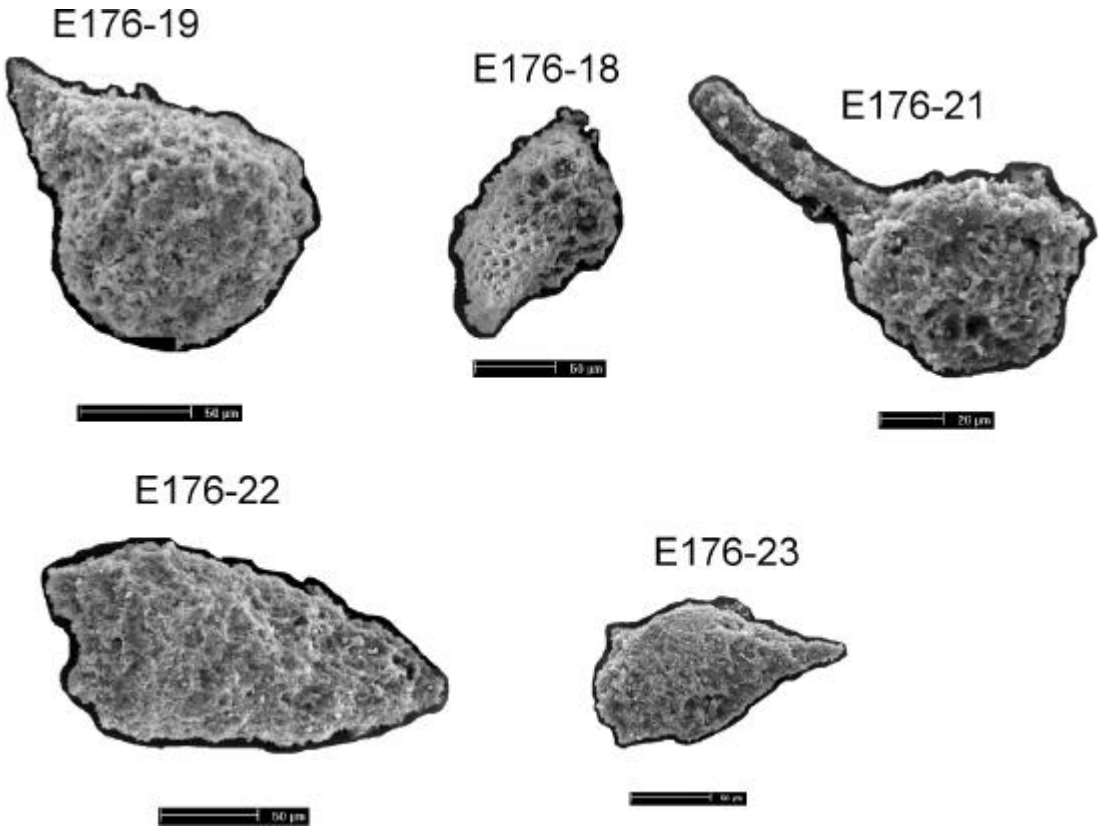

Plate 11 Indeterminate Jurassic radiolarians from the Ihsaniye section; chert sample E176.

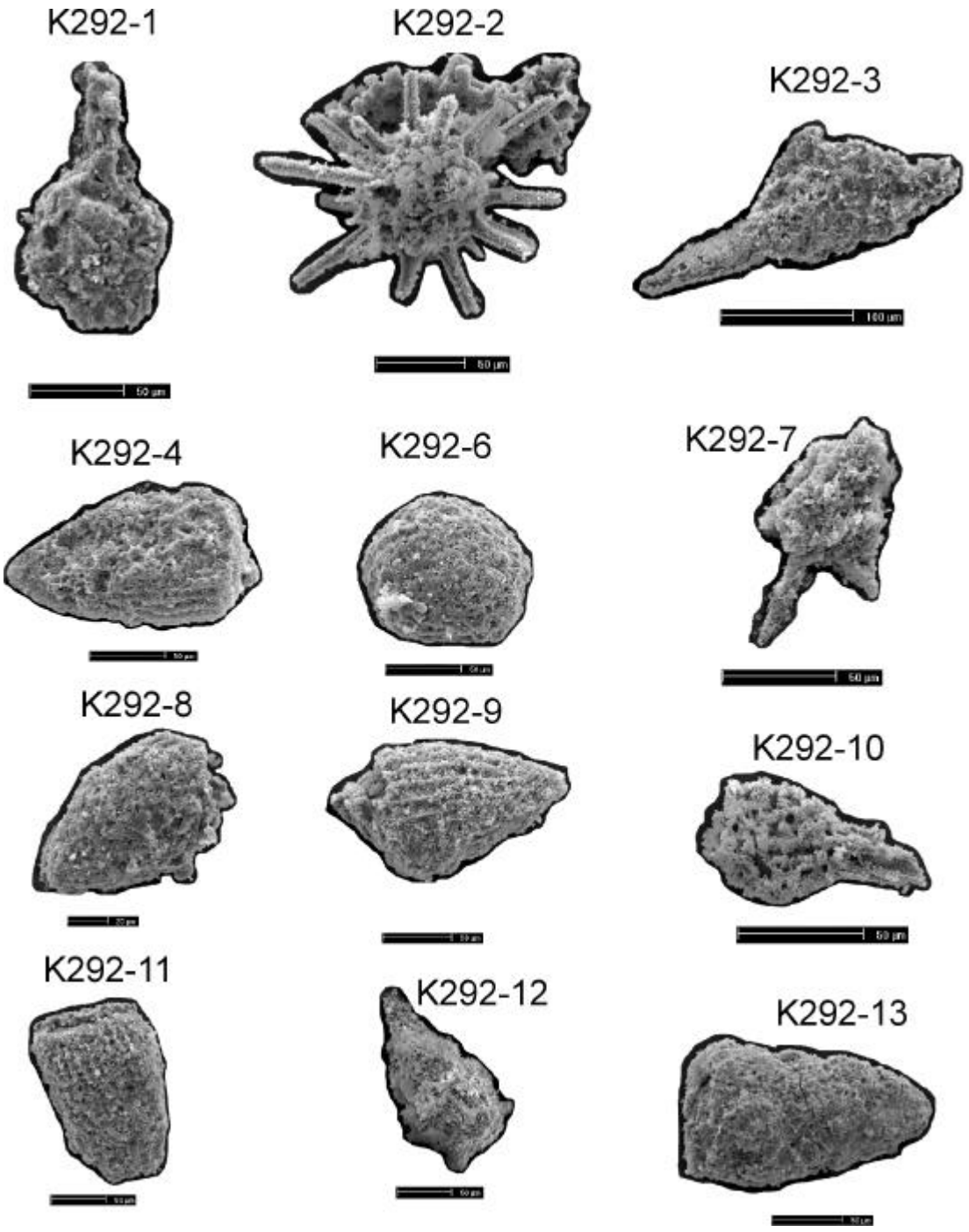

Plate 12 Indeterminate Jurassic radiolarians from the Ihsaniye section; chert sample K292.

Camlik area melange volcanics (recast to volatile free)

	TA 47	TA 62	TA 72	TA 75
Si02	49.79149	42.19364	53.3347	73.15135
Al203	15.71101	16.1016	15.76405	13.6484
Fe2O3	9.810259	14.17791	10.10174	1.537991
MgO	8.131776	7.64162	6.803001	0.478713
CaO	9.71643	10.21363	9.115199	1.731514
Na2O	5.640117	3.432883	3.010996	1.731514
K2O	0.330484	0.525029	0.794369	7.557547
TiO2	0.996664	3.791051	0.713185	0.346303
MnO	0.163678	0.249761	0.165451	0.052964
P2O5	0.072977	1.134021	0.03905	0.060094
LOI	4.08	5.91	2.69	1.82
Ti-O2	0.597414	2.27241	0.427493	0.207579
Ti ppm	5974.144	22724.1	4274.93	2075.787

	TA 47	TA 62	TA 72	TA 75
Nb	2.1	96.9	0.4	11.7
Zr	51.8	361.1	31.3	155.5
Y	22	45.3	17.8	22.4
Sr	101.4	897.2	307.5	279.8
Rb	6.5	15.7	10.7	146.3
La	-1.2	77.7	-2	24.1
Ce	7.5	163	-7.9	34.3
Nd	10.3	82.4	10.2	15.8
Zn	66.4	137.9	66.9	37.8
Cu	71.7	41.1	93.3	11.7
Ni	67.4	23.2	42.3	2.9
Cr	180.7	29.4	22.9	-4
V	272.4	154	278.6	30.9
Ba	37.9	228	69.6	737.8
Sc	35.9	13.1	38.6	5.1

Durak area melange volcanics (recast to volatile free)

	TA 138	TA 148b*	TA 139	TA 141a	TA 142	TA 143
Si02	75.97376	44.994	47.05361	74.01966	46.89528	49.10832
Al203	11.4329	10.57623	15.52946	1.10747	13.836	10.13764
Fe2O3	3.632694	4.729892	9.370846	9.639507	11.98615	4.236984
MgO	0.565086	1.632653	1.960567	0.565036	4.586759	1.879114
CaO	1.200807	29.14766	13.10368	13.93378	13.30593	26.8462
Na2O	5.489405	4.741897	6.003545	-0.0565	4.045868	4.536206
K2O	1.057518	0.328932	1.567346	0.00565	1.668109	0.278875
TiO2	0.61554	1.865546	1.880815	0.541304	3.052791	1.809695
MnO	0.082745	0.133253	0.09969	0.294949	0.167676	0.099342
P2O5	0.213925	0.857143	0.618077	0.079105	0.493293	0.761221
LOI	0.9	16.7	9.72	11.51	7.56	16.45
Ti-O2	0.368963	1.118235	1.127387	0.324465	1.829886	1.084757
TiO2 ppm	3689.633	11182.35	11273.87	3244.653	18298.86	10847.57

	TA 138	TA 148B*	TA 139	TA 141a	TA 142	TA 143
Nb	51.3	9.0	111.5	8.8	51.6	50.9
Zr	211.4	102.5	343.0	681.2	160.3	208.3
Y	22.4	33.5	32.6	23.4	25.0	20.3
Sr	241.3	79.0	785.0	152.9	457.3	219.0
Rb	2.2	17.1	27.5	0.1	19.6	2.0
La	48.7	19.6	73.6	19.8	31.4	44.3
Ce	101.1	37.9	142.3	49.6	74.8	92.6
Nd	48.7	21.4	62.2	23.2	37.1	43.6
Zn	118.7	75.6	136.3	16.4	116.2	91.4
Cu	18.2	5.3	10.2	7.2	88.9	13.8
Ni	10.5	4.2	23.0	6.9	61.2	12.4
Cr	11.9	8.5	12.6	23.6	70.5	12.6
V	131.8	76.9	18.4	13.3	296.5	116.2
Ba	333.5	627.7	269.2	330.8	331.3	1908.2
Sc	-8.7	14.3	-10.0	-5.8	21.9	-14.6

Dinar area melange volcanics (recast to volatile free)

	TA 257	TA 258	TA 259	TA 260
Si02	50.35986	58.30934	54.99281	55.54643
Al203	15.5254	14.61333	15.34826	15.63879
Fe2O3	10.37425	8.874949	8.393261	9.533094
MgO	6.827061	5.357877	5.208547	5.510518
CaO	9.777915	5.68696	7.879597	6.32119
Na2O	3.598602	6.334842	5.90713	6.157004
K2O	1.112482	0.204648	0.319499	0.08312
TiO2	1.612174	0.731181	1.074584	1.106208
MnO	0.163479	0.17174	0.13458	0.15803
P2O5	0.170677	0.06376	0.098623	0.107748
LOI	2.74	2.76	2.66	2.55
Ti-O2	0.96636	0.43828	0.644121	0.663077
TiO2 ppm	9663.596	4382.8	6441.208	6630.769

	TA 257	TA 258	TA 259	TA 260
Nb	4.6	0.6	2.0	1.7
Zr	114.2	34.0	60.7	61.9
Y	33.2	19.9	25.1	23.9
Sr	238.2	270.0	625.4	522.8
Rb	20.6	2.1	2.7	0.7
La	6.4	0.8	4.0	4.0
Ce	12.8	7.2	9.5	9.0
Nd	13.3	6.3	10.0	9.5
Zn	91.6	50.0	71.3	79.1
Cu	89.8	6.6	65.3	60.0
Ni	85.2	35.6	51.8	48.9
Cr	311.3	59.3	104.7	83.3
V	303.4	253.7	300.6	276.6
Ba	51.3	49.4	97.1	41.0
Sc	43.5	39.5	40.0	42.0

Hoyran area melange volcanics

	TA 251
Si02	55.54643
Al203	15.63879
Fe2O3	9.533094
MgO	5.510518
CaO	6.32119
Na2O	6.157004
K2O	0.08312
TiO2	1.106208
MnO	0.15803
P2O5	0.107748
LOI	4.14
Ti-O2	0.663077
TiO2 ppm	6630.769

	TA 251
Nb	1.5
Zr	97.7
Y	37.2
Sr	74.4
Rb	0.5
La	2.9
Ce	9.0
Nd	9.9
Zn	31.0
Cu	5.9
Ni	15.3
Cr	14.7
V	263.4
Ba	22.2
Sc	34.4

Sarkikaraagac area melange volcanics (recast to volatile free)

	TA 225	TA 226*	TA 227	TA 228	TA 229	TA 234	TA 236	TA 237*	TA 238	TA 240
Si02	62.82922	46.71827	51.34803	51.57355	51.48932	52.08186	51.87329	44.59148	51.49208	52.75837
Al203	18.99177	15.06708	15.47924	15.21271	15.34511	14.89211	14.1187	14.86766	14.57572	16.3625
Fe2O3	10.95679	9.081527	9.164531	9.041517	9.079704	10.66761	11.99025	8.193326	12.81973	11.35676
MgO	9.218107	7.585139	7.575602	7.473091	7.775267	7.496708	6.253579	5.719217	5.673975	5.516738
CaO	12.97325	20.08256	12.62942	12.54741	12.44864	10.70813	9.233404	17.67549	9.520909	9.490041
Na2O	4.506173	0.237358	2.942081	3.065095	2.999178	3.029075	3.41565	2.416571	3.420625	2.961727
K2O	0.207819	0.019608	0.133265	0.08611	0.115037	0.082059	0.306091	3.704258	0.279131	0.276358
TiO2	1.010288	0.832817	0.838544	0.819067	0.831964	1.017121	1.267946	1.943613	1.967113	1.441235
MnO	0.182099	0.149639	0.157868	0.159918	0.156122	0.152973	0.184465	0.301496	0.22026	0.190844
P2O5	0.082305	0.079463	0.069708	0.075859	0.070871	0.107385	0.145951	0.350978	0.063946	0.117843
LOI	2.8	3.1	2.45	2.45	2.64	1.29	1.3365	13.1	1.48	4.11
Ti-O2	0.605581	0.499202	0.502635	0.49096	0.498691	0.609677	0.760025	1.165029	1.179115	0.863896
TiO2 ppm	6055.809	4992.025	5026.353	4909.604	4986.909	6096.766	7600.248	11650.29	11791.15	8638.964

	TA 225	TA 226	TA 227	TA 228	TA 229	TA 234	TA 236	TA 237	TA 238	TA 240
Nb	0.6	0.8	0.9	0.9	0.7	3.0	4.3	23.3	10.9	1.2
Zr	47.3	50.3	48.1	51.5	47.0	61.8	79.3	159.0	43.8	85.2
Y	20.9	21.9	20.9	23.2	20.6	28.7	34.4	25.2	34.2	31.4
Sr	111.7	12.7	109.1	85.3	96.0	123.5	115.8	213.5	128.3	332.4
Rb	2.7	0.2	2.6	1.6	2.4	0.1	4.0	33.9	3.6	4.4
La	-0.4	5.3	1.7	3.1	3.1	3.0	3.8	18.4	-0.7	3.6
Ce	7.2	3.4	7.4	6.1	4.2	6.6	7.8	44.7	6.7	9.0
Nd	7.0	7.2	9.0	7.2	7.4	9.0	9.6	26.4	6.4	11.9
Zn	66.9	69.8	68.7	67.9	67.1	26.5	112.9	84.5	53.0	84.0
Cu	84.9	82.8	83.3	82.8	81.8	8.8	39.8	43.3	10.3	57.5
Ni	75.3	87.0	78.1	91.5	95.5	77.9	41.3	88.9	27.9	36.4
Cr	156.1	179.0	189.0	205.8	215.5	121.3	34.0	259.2	10.1	50.3
V	264.4	282.2	279.9	264.5	272.5	266.9	300.5	268.2	165.4	359.0
Ba	46.0	10.2	81.3	65.9	54.2	157.9	82.9	305.3	47.3	25.5

Sarkikaraagac area melange volcanics (recast to volatile free)

	TA 227	TA 228	TA 229	TA 234	TA 236	TA 237*	TA 238	TA 240
Si02	51.34803	51.57355	51.48932	52.08186	51.87329	44.59148	51.49208	52.75837
Al203	15.47924	15.21271	15.34511	14.89211	14.1187	14.86766	14.57572	16.3625
Fe2O3	9.164531	9.041517	9.079704	10.66761	11.99025	8.193326	12.81973	11.35676
MgO	7.575602	7.473091	7.775267	7.496708	6.253579	5.719217	5.673975	5.516738
CaO	12.62942	12.54741	12.44864	10.70813	9.233404	17.67549	9.520909	9.490041
Na2O	2.942081	3.065095	2.999178	3.029075	3.41565	2.416571	3.420625	2.961727
K2O	0.133265	0.08611	0.115037	0.082059	0.306091	3.704258	0.279131	0.276358
TiO2	0.838544	0.819067	0.831964	1.017121	1.267946	1.943613	1.967113	1.441235
MnO	0.157868	0.159918	0.156122	0.152973	0.184465	0.301496	0.22026	0.190844
P2O5	0.069708	0.075859	0.070871	0.107385	0.145951	0.350978	0.063946	0.117843
LOI	2.45	2.45	2.64	1.29	1.3365	13.1	1.48	4.11
Ti-O2	0.502635	0.49096	0.498691	0.609677	0.760025	1.165029	1.179115	0.863896
TiO2 ppm	5026.353	4909.604	4986.909	6096.766	7600.248	11650.29	11791.15	8638.964

Nb	TA 227	TA 228	TA 229	TA 234	TA 236	TA 237	TA 238	TA 240
Zr	0.9	0.9	0.7	3.0	4.3	23.3	10.9	1.2
Y	48.1	51.5	47.0	61.8	79.3	159.0	43.8	85.2
Sr	20.9	23.2	20.6	28.7	34.4	25.2	34.2	31.4
Rb	109.1	85.3	96.0	123.5	115.8	213.5	128.3	332.4
La	2.6	1.6	2.4	0.1	4.0	33.9	3.6	4.4
Ce	1.7	3.1	3.1	3.0	3.8	18.4	-0.7	3.6
Nd	7.4	6.1	4.2	6.6	7.8	44.7	6.7	9.0
Zn	9.0	7.2	7.4	9.0	9.6	26.4	6.4	11.9
Cu	68.7	67.9	67.1	26.5	112.9	84.5	53.0	84.0
Ni	83.3	82.8	81.8	8.8	39.8	43.3	10.3	57.5
Cr	78.1	91.5	95.5	77.9	41.3	88.9	27.9	36.4
V	189.0	205.8	215.5	121.3	34.0	259.2	10.1	50.3
Ba	279.9	264.5	272.5	266.9	300.5	268.2	165.4	359.0
Sc	81.3	65.9	54.2	157.9	82.9	305.3	47.3	25.5

Karaman area melange volcanics (recast to volatile free)

	TA 303	TA 307	TA 308	TA 309	TA 309b
Si02	51.48932	52.08186	51.87329	44.59148	51.49208
Al203	15.34511	14.89211	14.1187	14.86766	14.57572
Fe2O3	9.079704	10.66761	11.99025	8.193326	12.81973
MgO	7.775267	7.496708	6.253579	5.719217	5.673975
CaO	12.44864	10.70813	9.233404	17.67549	9.520909
Na2O	2.999178	3.029075	3.41565	2.416571	3.420625
K2O	0.115037	0.082059	0.306091	3.704258	0.279131
TiO2	0.831964	1.017121	1.267946	1.943613	1.967113
MnO	0.156122	0.152973	0.184465	0.301496	0.22026
P2O5	0.070871	0.107385	0.145951	0.350978	0.063946
LOI	1.29	3.21	2.49	0.97	1.18
Ti-O2	0.498691	0.609677	0.760025	1.165029	1.179115
TiO2 ppm	4986.909	6096.766	7600.248	11650.29	11791.15

	TA 303	TA 307	TA 308	TA 309	TA 309b
Nb	19.8	11.6	11.8	8.6	8.1
Zr	267.9	111.3	121.6	127.4	118.8
Y	30.5	22.1	23.7	31.9	30.1
Sr	22.3	328.7	345.2	43.9	50.1
Rb	74.2	8.9	3.6	3.3	12.3
La	45.4	11.2	10.6	19.1	17.5
Ce	79.0	25.6	24.8	39.4	39.5
Nd	35.4	17.6	17.5	23.1	21.2
Zn	51.8	58.5	67.1	3.7	7.2
Cu	4.1	61.6	85.8	-2.6	-1.8
Ni	3.5	100.9	71.5	15.1	11.8
Cr	9.0	262.8	245.6	16.7	14.4
V	1.8	223.1	232.0	24.2	23.5
Ba	189.8	164.9	93.8	43.7	88.4
Sc	4.5	31.4	35.3	9.8	9.0

Huglu-type unit volcanics- Ermenek area (recast to volatile free)

	TA 120	TA 158	TA 159	TA 160	TA 161b	TA 165	TA 166	TA 166c	TA 178a	TA 178b
Si02	73.09	65.47	65.64	73.01	75.59	76.89	65.33	65.31	72.18	71.96
Al203	13.52	14.80	14.81	13.00	12.13	10.83	14.58	14.48	12.88	12.84
Fe2O3	2.37	7.43	7.59	3.64	4.07	3.19	7.57	7.61	4.65	4.76
MgO	1.30	2.15	2.29	1.64	1.55	0.65	2.17	2.09	0.78	0.86
CaO	2.86	2.20	1.22	0.66	0.57	0.36	2.26	2.19	1.29	1.38
Na2O	0.28	6.65	6.77	2.63	4.43	0.52	5.66	5.58	5.47	5.42
K2O	5.66	0.11	0.11	5.22	1.63	7.28	1.85	1.82	2.06	1.93
TiO2	0.26	0.83	0.78	0.35	0.41	0.33	0.77	0.77	0.68	0.69
MnO	0.03	0.12	0.15	0.09	0.10	0.06	0.14	0.13	0.12	0.14
P2O5	0.04	0.27	0.25	0.14	0.07	0.07	0.25	0.25	0.23	0.22
LOI	6.89	3.01	2.17	1.86	4.49	1.47	1.85	1.92	0.87	0.92
Ti-O2	0.16	0.50	0.47	0.21	0.25	0.20	0.46	0.46	0.41	0.41

	TA 120	TA 158	TA 159	TA 160	TA 161b	TA 165	TA 166	TA 166c	TA 178a	TA 178b
Nb	20.4	12.2	11.9	12.4	9.3	13.6	11.3	11.4	10.3	10.1
Zr	259.4	137.6	132.3	148.4	770.5	135.6	126.9	128.3	114.4	113.7
Y	29.6	37.5	34.5	39.3	23.6	25.8	34.8	36.1	35.2	34.9
Sr	700.1	76.3	57.6	93.0	137.4	20.3	186.2	188.0	142.5	134.1
Rb	136.1	2.2	1.9	91.4	0.2	130.3	29.4	29.1	34.0	31.1
La	43.5	27.8	18.2	23.1	20.8	13.1	24.1	23.1	18.8	21.8
Ce	83.7	61.2	39.5	54.5	53.6	31.5	46.2	50.9	37.5	38.9
Nd	34.8	29.7	22.8	29.6	23.6	12.2	24.9	26.2	22.1	22.2
Zn	56.0	198.9	137.7	45.2	15.2	57.8	97.3	95.1	94.7	96.4
Cu	6.9	10.7	15.6	14.9	11.5	6.8	14.5	14.1	11.1	11.0
Ni	4.9	2.8	3.3	8.7	8.4	4.2	5.9	5.8	5.2	4.4
Cr	10.2	10.1	10.3	12.5	30.2	9.9	11.8	8.6	10.1	10.8
V	0.4	97.4	101.7	1.7	10.8	2.0	95.7	98.6	89.8	84.4
Ba	724.5	85.1	44.3	546.3	160.8	1188.0	388.7	389.4	568.9	534.2
Sc	0.6	30.8	27.8	7.9	-4.0	7.2	24.1	26.3	17.6	20.3

Huglu-type unit volcanics- Ermenek area (recast to volatile free)

TA 182	TA 182b	TA 201a	TA 201b	TA 203a	TA 205a*	TA 205b	TA 205c	TA 206a	TA 206	TA 208a	TA 208b	TA 296
65.93	65.91	75.64	75.13	62.69	65.20	69.25	70.61	79.31	78.57	64.90	65.23	80.02
14.58	14.64	11.84	12.14	18.33	15.14	13.89	14.29	13.54	11.63	14.30	14.34	10.94
7.17	7.36	2.76	2.73	4.50	6.69	5.31	4.48	2.60	1.82	7.89	7.89	1.38
2.07	2.09	0.61	0.57	1.11	2.46	1.97	1.35	0.78	0.54	2.09	2.10	0.61
1.37	1.33	2.65	2.80	1.61	1.52	1.64	0.94	0.15	0.13	1.72	1.72	1.21
5.78	5.76	4.32	4.43	7.29	5.58	4.46	6.11	1.34	2.43	5.99	5.96	0.32
1.63	1.60	2.10	2.06	3.78	2.86	3.78	1.70	7.83	5.05	1.65	1.64	5.37
0.78	0.78	0.23	0.23	0.36	0.44	0.36	0.31	0.19	0.15	0.77	0.76	0.16
0.17	0.18	0.07	0.07	0.16	0.21	0.16	0.14	0.01	0.01	0.14	0.14	0.01
0.25	0.25	0.02	0.03	0.09	0.10	0.09	0.08	0.04	0.03	0.25	0.25	0.02
2.37	2.38	5.15	4.79	4.36	4.01	3.05	4.20	7.44	2.83	1.74	1.96	3.40
0.46	0.47	0.14	0.14	0.22	0.26	0.22	0.19	0.11	0.09	0.46	0.46	0.10

TA 182	TA 182b	TA 201a	TA 201b	TA 203a	TA 205a	TA 205b	TA 205c	TA 206a	TA 206	TA 208a	TA 208b	TA 296
11.6	11.1	19.5	19.6	59.5	11.6	10.8	12.0	13.5	11.7	11.5	11.4	15.3
128.6	127.3	182.2	179.7	350.6	145.2	135.5	155.1	182.8	160.8	128.1	127.8	136.7
37.3	36.4	39.1	39.7	44.0	28.3	24.1	31.7	27.1	25.8	35.4	34.0	22.3
59.8	59.5	43.4	50.1	59.2	47.5	58.3	76.6	31.1	22.5	173.0	115.6	945.1
23.3	22.5	59.4	56.7	115.4	77.8	88.6	56.2	234.6	177.8	20.0	27.3	104.5
18.5	18.1	38.8	39.6	64.8	22.6	20.9	26.2	35.4	31.3	25.5	22.4	32.4
34.4	34.7	78.5	81.9	134.0	44.9	43.3	53.2	73.2	63.1	50.3	49.1	56.5
22.7	21.1	34.8	37.8	51.0	23.5	19.2	24.9	27.3	24.5	26.1	23.8	23.2
98.0	101.2	74.0	72.0	124.0	96.9	69.3	75.0	55.3	36.7	90.6	95.0	30.7
17.3	14.1	11.1	11.0	11.3	64.6	50.2	43.0	6.9	-0.2	13.5	11.3	9.1
7.7	4.4	4.6	4.3	3.5	9.6	8.4	6.6	5.1	4.9	4.5	3.5	3.2
9.5	12.3	7.7	8.8	11.4	30.4	26.2	16.8	10.6	7.9	11.6	11.1	11.1
93.7	93.8	0.0	0.0	10.7	93.4	80.6	47.8	1.7	0.0	91.6	95.9	0.0
309.1	313.0	142.8	147.1	338.6	349.9	412.6	186.3	1103.6	390.8	301.4	394.2	1243.4
25.2	25.6	3.5	5.8	1.7	19.7	16.0	11.6	-2.9	-2.3	24.1	23.6	-3.8

Huglu-type unit volcanics- Ermenek area (recast to volatile free)

	TA 148a*	TA 148b	TA 151	TA 172
Si02	61.63	59.32	74.18	55.09
Al203	16.97	16.50	11.94	16.18
Fe2O3	8.00	7.96	3.51	8.10
MgO	3.21	3.21	0.87	3.34
CaO	3.06	2.94	0.51	8.12
Na2O	5.98	5.76	0.15	7.35
K2O	3.90	3.87	8.59	0.21
TiO2	0.57	0.56	0.37	0.64
MnO	0.12	0.12	0.05	0.14
P2O5	0.15	0.15	0.05	0.12
LOI	5.67	2.78	1.65	6.53
Ti-O2	0.34	0.34	0.22	0.39

Huglu-type unit volcanics- Beysehir area (recast to volatile free)

	TA 30	TA 100	TA 117	TA 118*	TA 282	TA 283	TA 136
Si02	75.77	78.28	74.81	68.74	64.55	69.23	45.74
Al203	12.93	10.55	14.25	9.83	17.78	15.60	16.02
Fe2O3	2.46	1.82	2.28	2.00	4.08	3.34	14.35
MgO	0.47	0.63	1.30	0.55	2.30	1.75	6.54
CaO	0.25	0.49	4.42	9.72	0.78	0.55	6.29
Na2O	5.53	0.29	0.26	0.35	6.26	4.47	5.09
K2O	2.33	7.97	2.04	7.35	4.19	5.16	0.65
TiO2	0.29	0.20	0.31	0.26	0.27	0.21	4.42
MnO	0.03	0.03	0.01	0.15	0.13	0.12	0.20
P2O5	0.04	0.03	0.04	0.06	0.06	0.04	0.72
LOI	4.58	1.66	10.33	7.02	4.12	3.38	7.60
Ti-O2							2.65

	TA 148a	TA 148b	TA 151	TA 172
Nb	11.3	11.3	16.1	8.8
Zr	108.0	108.1	165.6	91.8
Y	20.1	19.8	41.0	23.5
Sr	68.8	68.1	18.9	110.2
Rb	64.1	65.8	173.2	3.8
La	20.6	23.7	25.9	24.0
Ce	40.3	41.9	47.2	43.7
Nd	17.2	17.3	24.6	20.8
Zn	77.0	78.1	36.8	85.6
Cu	64.5	67.1	6.1	76.0
Ni	16.1	15.1	3.9	17.0
Cr	35.3	33.6	12.5	47.1
V	161.2	165.3	3.3	199.9
Ba	537.8	569.1	682.0	117.9
Sc	25.8	24.8	11.7	28.8

	TA 30	TA 100	TA 117	TA 118	TA 282	TA 283	TA 136
Nb	16.7	9.5	20.6	13.0	31.4	27.7	82.2
Zr	207.7	127.3	279.0	181.2	270.6	239.7	293.5
Y	31.8	13.3	35.9	27.4	37.0	32.3	28.1
Sr	38.4	20.6	4232.7	44.0	33.7	25.0	257.0
Rb	79.1	151.9	91.2	136.9	119.7	118.2	6.5
La	30.1	15.3	43.6	36.4	35.6	31.7	58.0
Ce	57.5	26.6	90.4	65.6	79.9	71.3	117.0
Nd	30	14.5	35.0	26.8	33.5	29.1	58.6
Zn	55	23.3	59.9	42.1	112.0	84.2	121.9
Cu	3.3	8.0	12.6	13.8	16.4	7.6	16.9
Ni	1.2	6.2	2.4	5.2	6.2	4.4	7.0
Cr	-6.6	10.4	9.1	10.5	12.4	12.5	7.8
V	8.5	13.2	0.0	9.6	35.2	20.2	328.1
Ba	321.4	210.4	2012.7	239.1	237.2	301.1	317.3
Sc	5.5	1.0	2.4	-1.3	5.4	2.1	11.8

Peridotite (recast to volatile free)

	TA 22a	TA 022b	TA 34	TA 71	TA 112	TA 133	TA 276
Si02	78.30412	74.83684	68.77515	64.5912	69.25936	38.80675	0
Al203	10.54837	14.25782	9.835783	17.79415	15.60381	0.545245	0
Fe2O3	1.82079	2.275897	2.001593	4.080653	3.344412	8.388382	0
MgO	0.630665	1.305294	0.548824	2.306456	1.749863	43.09531	0
CaO	0.488256	4.417917	9.728171	0.782734	0.548774	0.524274	0
Na2O	0.294988	0.256596	0.355121	6.261871	4.473022	-0.41942	0
K2O	7.969769	2.043844	7.352087	4.188148	5.160542	-0.00105	0
TiO2	0.20344	0.021687	0.023057	0.011384	0.012782	0.012583	0.010597
MnO	0.02543	0.013388	0.153886	0.128368	0.115967	0.120583	0
P2O5	0.031533	0.039047	0.058111	0.064706	0.042452	0.004194	0
LOI	9.07	12.39	13.26	12.16	6.12	4.63	5.63

	TA 22a	TA 022b	TA 34	TA 71	TA 112	TA 133	TA 276
Nb		0.3	0.4	0.2	0.1	0.1	0.2
Zr		2.4	-5.3	-5.6	2.2	2.3	2.6
Y		0.2	0.7	0.5	0.2	0.3	0.7
Sr		-1.8	6.3	6.6	-2.4	-1.7	-1.3
Rb		0.4	-0.1	0.6	0.3	-0.1	0.2
La		2.3	-0.6	4.6	1.6	1.8	0.7
Ce		-0.1	-15.5	-10.6	-2.7	-2.2	-2.3
Nd		3.5	2.2	1.2	3.8	3.0	2.7
Zn		49.3	37.6	37.6	45.1	48.6	49.8
Cu		0.0	4.1	2.6	-2.0	1.6	1.1
Ni		2718.4	2380.5	2381.5	2529.7	2575.3	2600.7
Cr		2240.0	2726.8	2206.1	2041.1	2243.8	2398.2
V		20.6	28.3	25.6	10.4	24.1	30.1
Ba		10.2	5	11.8	14.1	10.9	4.9
Sc		5.9	6	8.6	0.7	5.8	2.6
Th			-0.2	0.6			
Pb			1.7	1.6			
				258			

Electron microprobe data chromite analysis data

	Sample	Na2O	SiO2	K2O	FeO	MgO	Al2O3	CaO	MnO	TiO2	Cr2O3	NiO	Total
Chromite	112	0.024	0.035	0.005	24.055	8.02	12.412	0.018	0.381	0.015	51.052	0.031	96.048
Chromite	112	0.012	0.047	0.005	24.122	8.067	12.486	0.015	0.414	0.018	53.233	0	98.419
Chromite	112	0	0.08	0.001	24.969	7.327	11.759	0.009	0.438	0.013	53.904	0	98.5
Chromite	112	0.011	0.104	0.003	27.233	5.937	11.904	0.011	0.475	0.011	51.121	0.036	96.846
Chromite	112	0.005	0.064	0.003	27.164	5.909	12.436	0.013	0.458	0.007	51.008	0.003	97.07
Chromite	112	0	0.034	0.006	22.215	9.417	10.106	0.01	0.333	0.064	57.194	0.042	99.421
Chromite	112	0	0.01	0.011	21.366	9.89	9.287	0.002	0.369	0.02	58.908	0.009	99.872
Chromite	112	0.009	0.016	0.009	23.637	8.449	9.962	0.001	0.394	0.027	56.961	0.038	99.503
Chromite	112	0.006	0.043	0.011	21.925	9.539	9.52	0.004	0.345	0.025	57.867	0.032	99.317
Chromite	20h	0.006	0.049	0.008	22.857	12.066	25.934	0.202	0.266	0.84	35.356	0.035	97.619
Chromite	20h	0.006	0.077	0.007	24.117	11.27	27.591	0.013	0.283	0.566	33.912	0.035	97.877
Chromite	20h	0.009	0.057	0.001	23.507	11.523	24.812	0.014	0.276	0.732	36.577	0.028	97.536
Chromite	20h	0.016	0.048	0	24.736	10.629	23.084	0.015	0.308	0.814	37.837	0.053	97.54
Chromite	20h	0.005	7.564	0.01	19.842	14.589	20.018	0.068	0.237	0.68	29.985	0.021	93.019
Chromite	20h	0	0.055	0.01	26.314	9.942	23.282	0.011	0.312	0.822	36.301	0.026	97.075
Chromite	20h	0	0.066	0.006	22.932	12.085	27.976	0.014	0.251	0.704	33.37	0.047	97.451
Chromite	276	0.018	0.025	0.01	14.931	10.545	16.628	0.015	0.273	0.003	38.576	0.018	81.042
Chromite	276	0	0.014	0.011	17.19	12.989	26.51	0	0.26	0	42.343	0.026	99.343
Chromite	276	0.008	0.054	0	17.413	12.593	27.212	0.024	0.265	0	40.914	0	98.483
Chromite	276	0.01	0.077	0.007	17.803	13.019	29.548	0.017	0.243	0	37.042	0.042	97.808
Chromite	276	0	0.036	0.003	17.716	12.812	26.612	0	0.249	0.007	41.347	0.026	98.808
Chromite	112	0	0.045	0.002	21.782	9.566	10.389	0.002	0.356	0.016	57.363	0.021	99.542
Chromite	112	0	0.081	0.015	24.294	8.399	15.954	0.011	0.344	0.018	48.201	0.053	97.37
Chromite	112	0.026	0.056	0.007	23.961	8.214	11.75	0.018	0.376	0.021	54.335	0	98.764
Chromite	112	0	0.071	0.007	24.375	8.325	12.271	0.019	0.4	0.007	53.072	0.031	98.578
Chromite	112	0	0.134	0.001	23.899	8.704	11.833	0.032	0.328	0.016	53.761	0.02	98.728

	Sample	Na2O	SiO2	K2O	FeO	MgO	Al2O3	CaO	MnO	TiO2	Cr2O3	NiO	Total
Chromite	133	0	0.041	0	17.176	13.036	28.082	0.043	0.272	0.002	40.149	0.012	98.813
Chromite	133	0	0.038	0.001	16.896	13.712	29.15	0.019	0.268	0.002	39.479	0.008	99.573
Chromite	133	0.009	0.038	0	17.624	12.566	25.046	0.026	0.269	0.001	43.368	0.017	98.964
Chromite	133	0.002	0.048	0.014	18.073	12.504	27.672	0.002	0.248	0	39.9	0.024	98.487
Chromite	133	0.005	0.043	0.012	17.16	13.021	28.449	0.012	0.249	0	39.599	0.008	98.558
Chromite	21h	0.014	0.048	0.001	24.247	10.762	24.416	0.072	0.318	0.54	37.608	0.042	98.068
Chromite	21h	0.047	0.042	0.009	24.457	10.812	24.821	0.032	0.302	0.502	37.614	0.004	98.642
Chromite	21h	0.043	0.063	0.003	25.906	9.676	22.843	0.015	0.32	0.405	38.553	0.04	97.867
Chromite	21h	0.012	0.062	0	23.643	10.931	26.343	0.02	0.287	0.288	36.797	0.006	98.389
Chromite	21h	0.01	0.029	0.001	24.071	11.428	25.794	0.016	0.286	0.713	36.053	0.024	98.425
Chromite	21h	0.007	0.027	0	23.495	11.257	25.358	0.02	0.286	0.278	37.194	0.021	97.943
Chromite	21h	0.017	0.042	0.001	23.877	11.068	26.124	0.009	0.296	0.392	36.188	0.02	98.034
Chromite	22b	0.014	0.06	0	22.085	11.203	26.049	0.026	0.308	0.013	37.75	0.051	97.559
Chromite	22b	0.015	0.074	0.008	28.248	8.596	17.418	0.015	0.358	0.015	41.915	0.043	96.705
Chromite	22b	0.048	0.144	0.005	31.674	7.362	18.815	0	0.38	0.026	38.528	0.05	97.032
Chromite	22b	0.015	0.072	0.003	29.063	8.928	19.772	0.014	0.338	0.041	39.139	0.031	97.416
Chromite	22b	0.014	0.047	0.002	24	9.837	20.522	0.01	0.305	0.039	42.724	0.038	97.538
Chromite	22b	0.011	0.067	0	22.154	11.031	17.382	0.017	0.293	0.052	47.835	0.03	98.872
Chromite	22b	0.026	0.027	0.005	21.984	10.885	16.189	0.007	0.325	0.031	49.522	0.03	99.031
SPINEL?	13h	0.018	3.881	0	45.66	8.624	2.753	0.378	5.575	0.27	22.483	0.05	89.692
SPINEL?	13h	0.023	0.044	0.001	15.26	16.882	42.99	0.015	0.165	0.025	21.942	0.018	97.365
Chromite	13h	0.021	0.023	0.009	14.347	17.658	41.599	0.017	0.175	0.108	25.06	0.18	99.197
Chromite	13h	0	0.026	0.009	14.184	17.649	41.707	0.003	0.189	0.126	24.517	0.195	98.605
Chromite	13h	0.004	0.053	0.003	14.013	17.838	41.35	0.02	0.18	0.128	24.806	0.17	98.565
Chromite	13h	0.005	0.039	0	14.627	17.268	40.262	0.003	0.156	0.136	26.359	0.156	99.197
Chromite	13h	0	0.029	0.006	15.015	17.251	41.861	0.011	0.186	0.117	24.034	0.19	98.605
Chromite	13h	0.001	0.031	0.001	14.834	17.05	40.638	0.014	0.181	0.128	25.729	0.214	98.565
Chromite	13h	0.025	0.044	0.005	14.818	17.075	40.879	0.018	0.155	0.112	25.638	0.182	99.011
Chromite	13h	0	0.05	0	15.405	16.839	40.482	0	0.165	0.11	25.861	0.162	98.7
Chromite	13h	0.007	0.047	0	17.135	15.234	38.337	0.01	0.165	0.077	26.555	0.162	98.821
Chromite	13h	0	0.043	0.001	19.184	13.482	28.235	0.011	0.254	0.215	37.866	0.124	98.951
Chromite	13h	0	0.035	0.008	18.447	13.659	25.879	0.015	0.226	0.32	40.465	0.105	99.074
Chromite	13h	0.005	0.056	0.004	19.636	13.202	28.664	0.013	0.253	0.213	37.194	0.105	97.729
Chromite	13h	0.006	0.066	0.004	19.713	13.15	29.714	0.016	0.254	0.164	35.291	0.102	99.415
Chromite	13h	0	0.042	0.004	16.513	15.691	37.143	0	0.181	0.101	29.288	0.154	99.159

	Sample	Na2O	SiO2	K2O	FeO	MgO	Al2O3	CaO	MnO	TiO2	Cr2O3	NiO	Total
Chromite	133	25	0.048	0.047	0.012	17.932	12.025	25.595	0.024	0.282	0.041	42.566	0.05
Chromite	133	26	0	0.06	0.004	16.056	14.821	36.643	0.019	0.22	0.045	31.101	0.088
Chromite	133	29	0.024	0.026	0.011	16.445	12.6	21.989	0.015	0.281	0.046	47.851	0.047
Chromite	133	30	0	0.029	0.006	17.44	11.834	20.421	0.015	0.309	0.063	49.097	0.044
Chromite	133	31	0.005	0.968	0.002	17.764	13.243	27.703	0.023	0.279	0.028	37.784	0.083
Chromite	133	33	0.03	0.066	0.014	17.577	12.251	26.43	0.012	0.3	0.047	41.715	0.09
Chromite	20h	36	0.002	0.031	0.009	18.919	12.96	26.369	0.007	0.235	0.672	39.68	0.096
Chromite	20h	37	0.034	0.037	0.004	18.26	13.525	25.692	0.024	0.27	0.767	40.464	0.152
Chromite	20h	38	0	0.024	0.004	18.322	13.68	25.617	0.009	0.251	0.752	40.446	0.09
Chromite	20h	42	0.003	0.029	0.004	20.073	12.327	24.811	0.004	0.261	0.633	40.562	0.104
Chromite	20h	45	0.017	0.026	0.011	18.538	13.293	25.543	0.023	0.275	0.731	40.284	0.111
Chromite	20h	46	0	0.036	0.01	19.567	12.184	24.964	0.008	0.277	0.425	40.29	0.114
Chromite	22a	47	0.014	0.042	0.016	23.227	10.422	16.114	0.017	0.391	0.088	49.226	0.094
Chromite	22a	49	0	0.049	0.01	24.339	9.866	19.451	0.027	0.32	0.047	44.503	0.093
Chromite	22a	50	0.037	0.061	0.003	27.889	9.116	18.438	0.025	0.343	0.089	42.832	0.095
Chromite	22a	51	0.017	0.056	0	25.293	9.455	21.08	0.019	0.342	0.058	42.009	0.107
Chromite	22a	52	0.01	0.049	0.007	21.577	10.922	15.282	0.005	0.321	0.083	50.953	0.086

Calculation of Mg/Cr ratios for Fig. 6.22b (after Dick & Bullen, 1984)

Sample	Cr	Al	Mg	Fe	Mg*100	Mg+Fe	Mg*100/(Mg+Fe)	Cr*100	Cr+Al	Cr*100/Cr+Al
13h	1.088065	0.097609	0.386762	1.148818	38.67623	1.535581	25.18671	108.8065	1.185674	91.76766
13h	0.852841	1.224169	0.608066	0.308362	60.80657	0.916428	66.35172	85.28411	2.07701	41.06101
13h	0.944427	1.148556	0.616685	0.281102	61.66852	0.897787	68.6895	94.44271	2.092983	45.1235
13h	0.93063	1.159846	0.620818	0.279913	62.08182	0.900731	68.9238	93.063	2.090476	44.5176
13h	0.940031	1.148002	0.626421	0.276078	62.64209	0.902499	69.40963	94.0031	2.088033	45.01992
13h	0.992447	1.110594	0.602497	0.286318	60.2497	0.888815	67.78657	99.24466	2.103041	47.19103
13h	0.915879	1.168701	0.609201	0.297476	60.92014	0.906677	67.19053	91.58788	2.08458	43.9359
13h	0.973945	1.127005	0.598095	0.291934	59.80955	0.890029	67.19952	97.39449	2.100949	46.35737
13h	0.969103	1.132057	0.59811	0.291199	59.81104	0.88931	67.25558	96.91035	2.10116	46.12231
13h	0.977832	1.121406	0.590024	0.302828	59.00245	0.892852	66.08311	97.78323	2.099238	46.58034
13h	0.977832	1.121406	0.590024	0.302828	59.00245	0.892852	66.08311	97.78323	2.099238	46.58034
13h	1.396951	0.763135	0.460915	0.367947	46.09149	0.828862	55.60814	139.6951	2.160086	64.67108
13h	1.480332	0.6936	0.463056	0.350849	46.30557	0.813905	56.89311	148.0332	2.173932	68.09469
13h	1.37844	0.778276	0.453408	0.37834	45.34082	0.831749	54.51265	137.844	2.156716	63.91384
13h	1.326855	0.81847	0.458163	0.385325	45.8163	0.843488	54.31767	132.6855	2.145325	61.84869
13h	1.100567	1.022552	0.546402	0.322602	54.64015	0.869004	62.87677	110.0567	2.123119	51.83726

Calculation of Mg/Cr ratios for Fig. 6.22b (after Dick & Bullen, 1984)

Sample	Cr	Al	Mg	Fe	Mg*100	Mg+Fe	$Mg*100/(Mg+Fe)$	Cr*100	Cr+Al	$Cr*100/Cr+Al$
20h	1.357402	0.729452	0.429283	0.456225	42.92826	0.885508	48.47869	135.7402	2.086854	65.04538
20h	1.31104	0.781469	0.403758	0.484731	40.37581	0.888489	45.44323	131.104	2.09251	62.65397
20h	1.403119	0.697316	0.409625	0.468812	40.96251	0.878437	46.63115	140.3119	2.100435	66.80133
20h	1.453897	0.649845	0.378481	0.494153	37.84809	0.872634	43.37226	145.3897	2.103742	69.11004
20h	29.985	20.018	14.589	19.842	1458.9	34.431	42.3717	2998.5	50.003	59.9664
20h	1.416975	0.665803	0.359627	0.534005	35.96267	0.893632	40.24329	141.6975	2.082778	68.03294
20h	1.29149	0.793236	0.433427	0.461415	43.34273	0.894842	48.43617	129.149	2.084727	61.95011
20h	1.463499	0.712519	0.442956	0.362772	44.29558	0.805728	54.97587	146.3499	2.176018	67.25584
20h	1.481573	0.689182	0.458909	0.347592	45.89085	0.8065	56.90121	148.1573	2.170755	68.2515
20h	1.480704	0.687073	0.464102	0.348723	46.41019	0.812825	57.09742	148.0704	2.167776	68.30519
20h	1.500728	0.672525	0.422644	0.386109	42.26439	0.808753	52.25874	150.0728	2.173253	69.05444
20h	1.482334	0.6886	0.453285	0.354643	45.32846	0.807927	56.10463	148.2334	2.170934	68.28092
20h	1.502406	0.682002	0.421031	0.37934	42.10314	0.800372	52.60449	150.2406	2.184408	68.77861
21h	1.435414	0.682737	0.380649	0.481138	38.06489	0.861787	44.16972	143.5414	2.118151	67.76732
21h	1.427679	0.690211	0.380296	0.482613	38.0296	0.862909	44.07139	142.7679	2.117891	67.41043
21h	1.479122	0.642068	0.344014	0.516727	34.40141	0.860741	39.96722	147.9122	2.121189	69.73078
21h	1.399629	0.734087	0.385297	0.467539	38.52966	0.852836	45.17829	139.9629	2.133717	65.59584
21h	1.37631	0.721399	0.404278	0.477731	40.42776	0.882009	45.836	137.631	2.097709	65.61016
21h	1.417044	0.707794	0.397436	0.465372	39.74364	0.862809	46.0631	141.7044	2.124838	66.68949
21h	1.38484	0.732414	0.392499	0.475039	39.24993	0.867539	45.24286	138.484	2.117254	65.40737

Calculation of Mg/Cr ratios for Fig. 6.22b (after Dick & Bullen, 1984)

Sample	Cr	Al	Mg	Fe	Mg*100	Mg+Fe	Mg*100/(Mg+Fe)	Cr*100	Cr+Al	Cr*100/Cr+Al
22a	1.777066	0.426181	0.348654	0.43593	34.8654	0.784584	44.43807	177.7066	2.203247	80.65668
22a	1.651942	0.528968	0.339376	0.469703	33.93762	0.809079	41.94599	165.1942	2.18091	75.74554
22a	1.613577	0.508882	0.318244	0.546222	31.8244	0.864466	36.81395	161.3577	2.122459	76.02395
22a	1.581948	0.58157	0.329948	0.495182	32.99484	0.825131	39.98742	158.1948	2.163518	73.11923
22a	1.824782	0.400962	0.362475	0.401742	36.24749	0.764217	47.43091	182.4782	2.225744	81.98526
22b	1.434452	0.725174	0.394492	0.436296	39.4492	0.830788	47.48407	143.4452	2.159626	66.42133
22b	1.62013	0.493243	0.307901	0.567653	30.79012	0.875554	35.16644	162.013	2.113372	76.66088
22b	1.52129	0.544279	0.26938	0.65021	26.93805	0.91959	29.29354	152.129	2.06557	73.64992
22b	1.519235	0.562274	0.321147	0.586503	32.11472	0.90765	35.38225	151.9235	2.081509	72.98721
22b	1.610308	0.566681	0.343585	0.470287	34.3585	0.813872	42.2161	161.0308	2.176988	73.96951
22b	1.738154	0.462726	0.371443	0.418513	37.14429	0.789956	47.02069	173.8154	2.20088	78.9754
22b	1.786754	0.427926	0.36394	0.412371	36.39398	0.776311	46.88069	178.6754	2.214679	80.67776
112	1.905747	0.33945	0.277435	0.466845	27.74352	0.74428	37.27564	190.5747	2.245198	84.88105
112	1.931506	0.33191	0.271245	0.455033	27.12451	0.726278	37.34726	193.1506	2.263416	85.33588
112	1.95817	0.312955	0.246655	0.471569	24.66552	0.718224	34.34236	195.817	2.271124	86.22027
112	1.920545	0.327642	0.206694	0.531907	20.66935	0.7386	27.9845	192.0545	2.248187	85.42638
112	1.912342	0.341578	0.205294	0.529463	20.52939	0.734757	27.94037	191.2342	2.25392	84.84516
112	2.015716	0.26094	0.307557	0.407043	30.75573	0.7146	43.03909	201.5716	2.276655	88.53847
112	2.049995	0.236775	0.31894	0.38656	31.89404	0.7055	45.20771	204.9995	2.28677	89.64588
112	2.01904	0.2587	0.277528	0.435587	27.75283	0.713115	38.91776	201.904	2.27774	88.64227
112	2.034549	0.24522	0.310796	0.400767	31.07955	0.711562	43.67791	203.4549	2.279769	89.24365
112	2.015229	0.267392	0.311428	0.397837	31.1428	0.709265	43.90856	201.5229	2.282621	88.28575
112	1.794638	0.435183	0.28979	0.470256	28.97898	0.760046	38.12792	179.4638	2.229822	80.48349
112	1.956753	0.31001	0.274123	0.448617	27.41231	0.72274	37.9283	195.6753	2.266763	86.32366
112	1.924456	0.32599	0.279744	0.459517	27.97444	0.739262	37.84105	192.4456	2.250446	85.51443
112	1.93823	0.312546	0.290798	0.447953	29.0798	0.738751	39.36347	193.823	2.250776	86.11384

Calculation of Mg/Cr ratios for Fig. 6.22b (after Dick & Bullen, 1984)

Sample	Cr	Al	Mg	Fe	Mg*100	Mg+Fe	Mg*100/(Mg+Fe)	Cr*100	Cr+Al	Cr*100/Cr+Al
133	1.746663	0.532247	0.39014	0.322564	39.014	0.712704	54.74084	174.6663	2.27891	76.64468
133	1.409982	0.757381	0.457959	0.344636	45.79591	0.802595	57.05976	140.9982	2.167363	65.05519
133	1.528626	0.709558	0.416021	0.334864	41.60208	0.750885	55.40408	152.8626	2.238183	68.2976
133	1.470052	0.7533	0.44232	0.32696	44.23204	0.769281	57.49794	147.0052	2.223352	66.11873
133	1.435478	0.776517	0.462025	0.319396	46.20254	0.781421	59.1263	143.5478	2.211995	64.89518
133	1.572771	0.665451	0.422307	0.332288	42.23065	0.754595	55.96466	157.2771	2.238222	70.26876
133	1.471642	0.747742	0.427379	0.346557	42.73786	0.773935	55.2215	147.1642	2.219383	66.30859
133	1.455621	0.766148	0.44355	0.327941	44.35505	0.771492	57.49258	145.5621	2.221769	65.51629
276	1.689527	0.533543	0.427986	0.339979	42.79855	0.767964	55.72989	168.9527	2.22307	75.99971
276	1.532328	0.702848	0.435593	0.323415	43.55926	0.759008	57.38972	153.2328	2.235176	68.55513
276	1.501034	0.73141	0.428137	0.332129	42.81366	0.760266	56.31408	150.1034	2.232444	67.23725
276	1.385181	0.809509	0.451153	0.346115	45.11534	0.797268	56.58742	138.5181	2.19469	63.11509
276	1.510994	0.712489	0.433881	0.336588	43.38806	0.770469	56.31383	151.0994	2.223482	67.95618